SYSTEM MANUALS

of BASEMENT

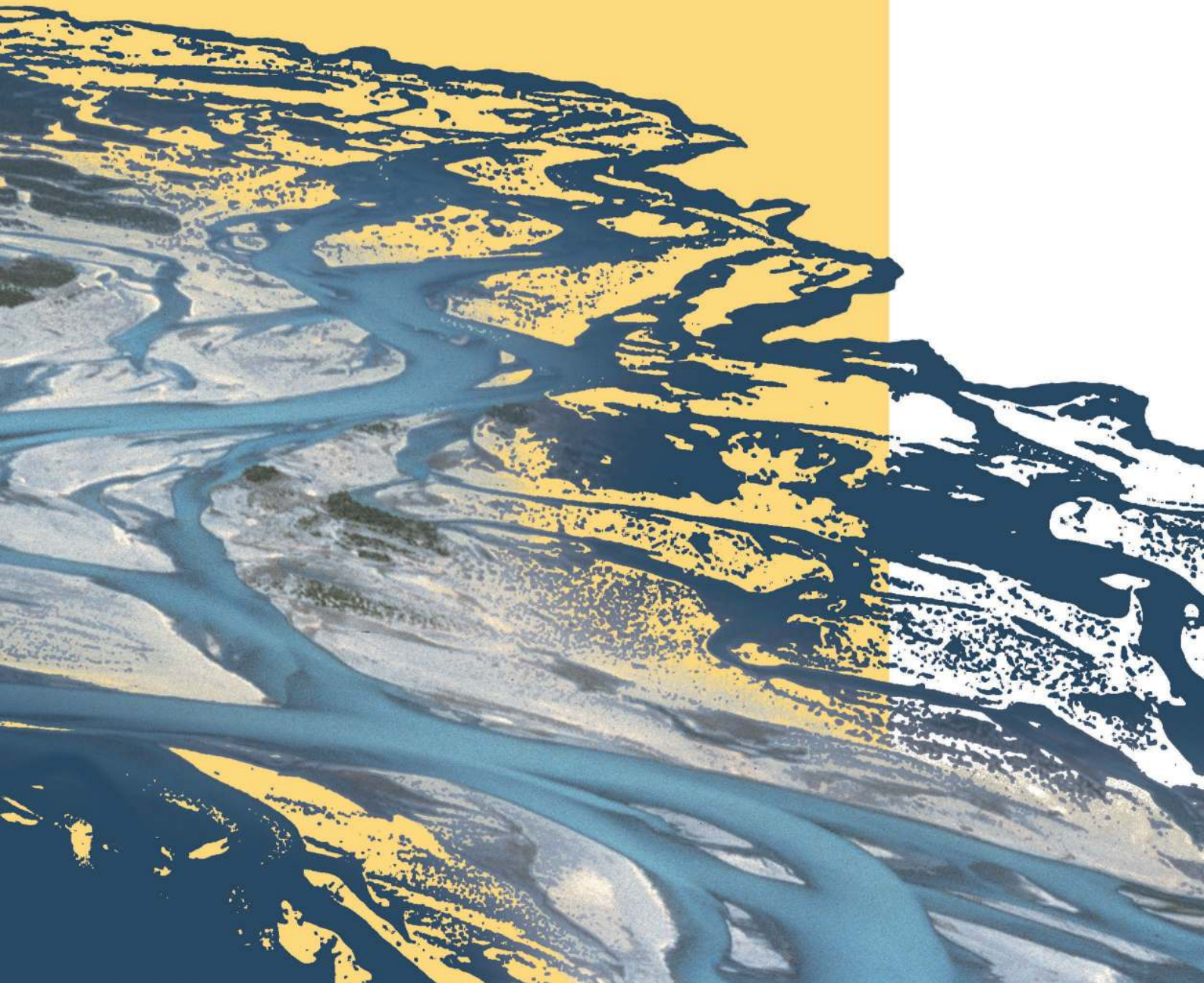

R

REFERENCE MANUAL

of BASEMENT

Contents

Preamble

VERSION 2.8.1

November, 2020

Credits

Project Team

Software Development, Documentation and Test (alphabetical)

M. Bürgler, MSc. ETH Environmental Eng.
F. Caponi, MSc. Environmental Eng.
Dr. D. Conde, MSc. Civil Eng.
E. Gerke, MSc. ETH Civil Eng.
S. Kammerer, MSc. ETH Environmental Eng.
Dr.techn. M. Weberndorfer, MSc.

Scientific Board

Prof. Dr. R. Boes, Director VAW, Member of Project Board
Dr. A. Siviglia, MSc, Scientific Adivisor
Dr. D. Vanzo, MSc. Environmental Eng., Scientific Adivisor
Dr. D. Vetsch, Dipl. Ing. ETH, Project Director

Former Project Members

See https://www.basement.ethz.ch/people

Cover Page Art Design

W. Thürig

Commissioned and co-financed by

Swiss Federal Office for the Environment (FOEN)

Contact

website: http://www.basement.ethz.ch
user forum: http://people.ee.ethz.ch/~basement/forum

Citation Advice

For System Manuals:

Vetsch D., Siviglia A., Bürgler M., Caponi F., Ehrbar D., Facchini M., Faeh R., Farshi D., Gerber M., Gerke E., Kammerer S., Koch A., Mueller R., Peter S., Rousselot P., Vanzo D., Veprek R., Volz C., Vonwiller L., Weberndorfer M. 2020. System Manuals of BASEMENT, Version 2.8.1 Laboratory of Hydraulics, Glaciology and Hydrology (VAW). ETH Zurich. Available from http://www.basement.ethz.ch. [date of access].

For Website:

BASEMENT – Basic Simulation Environment for Computation of Environmental Flow and Natural Hazard Simulation, 2020. http://www.basement.ethz.ch

For Software:

BASEMENT – Basic Simulation Environment for Computation of Environmental Flow and Natural Hazard Simulation. Version 2.8.1 © ETH Zurich, VAW, 2006-2020.

License

BASEMENT SOFTWARE LICENSE

between

ETH

Rämistrasse 101

8092 Zürich

Represented by Prof. Dr. Robert Boes

VAW

(Licensor)

and

Licensee

1. Definition of the Software

The Software system BASEMENT is composed of the executable (binary) file BASEMENT and its documentation files (System Manuals), together herein after referred to as "Software". Not included is the source code.

Its purpose is the simulation of water flow, sediment and pollutant transport and according interaction in consideration of movable boundaries and morphological changes.

2. License of ETH

ETH hereby grants a single, non-exclusive, world-wide, royalty-free license to use Software to the licensee subject to all the terms and conditions of this Agreement.

3. The scope of the license

a. Use

The licensee may use the Software:

- according to the intended purpose of the Software as defined in provision 1
- by the licensee and his employees
- for commercial and non-commercial purposes

The generation of essential temporary backups is allowed.

b. Reproduction / Modification

Neither reproduction (other than plain backup copies) nor modification is permitted with the following exceptions:

Decoding according to article 21 URG [Bundesgesetz über das Urheberrecht, SR 231.1)

If the licensee intends to access the program with other interoperative programs according to article 21 URG, he is to contact licensor explaining his requirement.
If the licensor neither provides according support for the interoperative programs nor makes

the necessary source code available within 30 days, licensee is entitled, after reminding the licensor once, to obtain the information for the above mentioned intentions by source code generation through decompilation.

c. Adaptation

On his own risk, the licensee has the right to parameterize the Software or to access the Software with interoperable programs within the aforementioned scope of the licence.

d. Distribution of Software to sub licensees

Licensee may transfer this Software in its original form to sub licensees. Sub licensees have to agree to all terms and conditions of this Agreement. It is prohibited to impose any further restrictions on the sub licensees' exercise of the rights granted herein.

No fees may be charged for use, reproduction, modification or distribution of this Software, neither in unmodified nor incorporated forms, with the exception of a fee for the physical act of transferring a copy or for an additional warranty protection.

4. Obligations of licensee

a. Copyright Notice

Software as well as interactively generated output must conspicuously and appropriately quote the following copyright notices:

Copyright by ETH Zurich / Laboratory of Hydraulics, Glaciology and Hydrology (VAW), 2006-2018

5. Intellectual property and other rights

The licensee obtains all rights granted in this Agreement and retains all rights to results from the use of the Software.

Ownership, intellectual property rights and all other rights in and to the Software shall remain with ETH (licensor).

6. Installation, maintenance, support, upgrades or new releases

a. Installation

The licensee may download the Software from the web page http://www.basement.ethz.ch or access it from the distributed CD.

b. Maintenance, support, upgrades or new releases

ETH doesn't have any obligation of maintenance, support, upgrades or new releases, and disclaims all costs associated with service, repair or correction.

7. Warranty

ETH does not make any warranty concerning the:

- warranty of merchantability, satisfactory quality and fitness for a particular purpose
- warranty of accuracy of results, of the quality and performance of the Software;
- warranty of noninfringement of intellectual property rights of third parties.

8. Liability

ETH disclaims all liabilities. ETH shall not have any liability for any direct or indirect damage except for the provisions of the applicable law (article 100 OR [Schweizerisches Obligationenrecht]).

9. Termination

This Agreement may be terminated by ETH at any time, in case of a fundamental breach of the provisions of this Agreement by the licensee.

10. No transfer of rights and duties

Rights and duties derived from this Agreement shall not be transferred to third parties without the written acceptance of the licensor. In particular, the Software cannot be sold, licensed or rented out to third parties by the licensee.

11. No implied grant of rights

The parties shall not infer from this Agreement any other rights, including licenses, than those that are explicitly stated herein.

12. Severability

If any provisions of this Agreement will become invalid or unenforceable, such invalidity or enforceability shall not affect the other provisions of Agreement. These shall remain in full force and effect, provided that the basic intent of the parties is preserved. The parties will in good faith negotiate substitute provisions to replace invalid or unenforceable provisions which reflect the original intentions of the parties as closely as possible and maintain the economic balance between the parties.

13. Applicable law

This Agreement as well as any and all matters arising out of it shall exclusively be governed by and interpreted in accordance with the laws of , excluding its principles of conflict of laws.

14. Jurisdiction

If any dispute, controversy or difference arises between the Parties in connection with this Agreement, the parties shall first attempt to settle it amicably.
Should settlement not be achieved, the Courts of Zurich-City shall have exclusive jurisdiction.
This provision shall only apply to licenses between ETH and foreign licensees

By using this software you indicate your acceptance.

(License version: 2018-05-31)

THIRD PARTY SOFTWARE

BASEMENT uses third party software. For instance, the BASEMENT executable directly links the following external libraries:

- CGNS
- HDF5
- Qt5 (non-cluster version only)
- Qwt (non-cluster version only)
- Shapelib
- TecIO
- VTK (non-cluster version only)

The libraries (and their dependencies) are included in the BASEMENT distribution if they are not provided by the operating system.

Please refer to `ThirdPartySoftwareLicenses.txt` in the distribution and/or the operating system documentation for the third party software licenses and copyright notices. The external libraries for Windows 10 have been built using `vcpkg` version 2020.07 (`HDF5` was compiled without `szip`).

1

Mathematical Models

1.1 Governing Flow Equations

1.1.1 Saint-Venant Equations

1.1.1.1 Introduction

The BASEchain module is based on the Saint Venant Equations (SVE) for unsteady one dimensional flow. The validity of these equations implies the following conditions and assumptions:

- Hydrostatic distribution of pressure: this is fulfilled if the streamline curvatures are small and the vertical accelerations are negligible
- Uniform velocity over the cross section and horizontal water surface across the section
- Small slope of the channel bottom, so that the cosine of the angle of the bottom with the horizontal can be assumed to be 1
- Steady-state resistance laws are applicable for unsteady flow.

The flow conditions at a channel cross section can be defined by two flow variables. Therefore, two of the three conservation laws are needed to analyze a flow situation. If the flow variables are not continuous, these must be the mass and the momentum conservation laws (Cunge et al., 1980).

1.1.1.2 Conservative Form of SVE

1.1.1.2.1 Mass Conservation

For the control volume illustrated in Figure 1.1, the conservation of mass is formulated assuming the mass density ρ is constant (incompressible flow). This leads basically to a

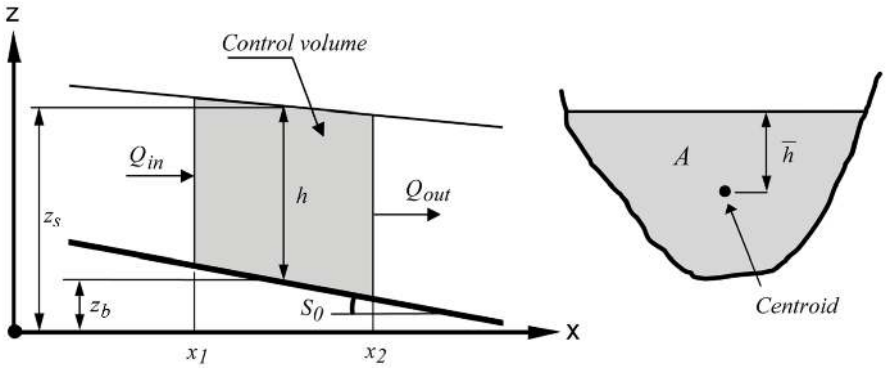

Figure 1.1 *Definition Sketch*

conservation of Volume. The temporal change in Volume equals the difference between inflowing and outflowing Volume (eq. 1.1).

$$\frac{\mathrm{d}}{\mathrm{d}t}\int_{x_1}^{x_2} A\,\mathrm{d}x + Q_{out} - Q_{in} - q_l(x_2 - x_1) = 0 \tag{1.1}$$

where:

A	$[m^2]$	wetted cross section area
Q	$[m^3/s]$	discharge
q_l	$[m^2/s]$	lateral discharge per meter of length (specific discharge)
V	$[m^3]$	volume
x	$[m]$	distance
t	$[s]$	time

Applying Leibnitz's rule and integrating with the mean value theorem

$$\frac{\mathrm{d}}{\mathrm{d}t}\int_{x_1}^{x_2} A\,\mathrm{d}x = \int_{x_1}^{x_2}\frac{\partial A}{\partial t}\,\mathrm{d}x = \frac{\partial A}{\partial t}(x_2 - x_1)$$

and then dividing by (x_2 - x_1) and making use of $\frac{Q_{out} - Q_{in}}{(x_2 - x_1)} = \frac{\partial Q}{\partial x}$, we obtain the differential form of the continuity equation:

$$\frac{\partial A}{\partial t} + \frac{\partial Q}{\partial x} - q_l = 0 \tag{1.2}$$

1.1.1.2.2 Momentum Conservation

Newton's second law of motion says: The change in momentum equals to the Sum of all external Forces. The momentum is defined as

$$p = m\,u$$

$$\frac{\mathrm{d}p}{\mathrm{d}t} = m\,a = \sum F$$

where:

p	$[kg\ m/s]$	momentum
m	$[kg]$	mass
u	$[m/s]$	velocity
a	$[m/s^2]$	acceleration
F	$[N]$	force

Making use of the Reynolds transport theorem (Chaudhry, 1993) and referring to the control volume in Figure 1.1 one obtains a conservative formulation for the left part of the momentum equation

$$\frac{\mathrm{d}p}{\mathrm{d}t} = \sum F = \frac{\mathrm{d}}{\mathrm{d}t}\int_{x_1}^{x_2} u\rho A\,dx + u_2\rho A_2 u_2 - u_1\rho A_1 u_1 - u_x\rho q_l(x_2 - x_1) \tag{1.3}$$

where:

u_x	$[m/s]$	velocity in x direction (direction of flow) of lateral sources
ρ	$[kg/m^3]$	mass density

Further simplification is achieved by applying Leibnitz's rule and writing $Q = A\,u$ and $Q/A = u$ resulting in:

$$\sum F = \int_{x_1}^{x_2} \rho\frac{\partial Q}{\partial t}\,\mathrm{d}x + \rho\frac{Q^2}{A}\bigg|_{out} - \rho\frac{Q^2}{A}\bigg|_{in} - u_x\rho q_l(x_2 - x_1) \tag{1.4}$$

Applying the mean value theorem $\int_{x_1}^{x_2} \rho\frac{\partial Q}{\partial t}\,\mathrm{d}x = \frac{\partial Q}{\partial t}(x_2 - x_1)\rho$

and dividing both sides by $\rho(x_2 - x_1)$ and by using

$$\left(\frac{Q^2}{A}\bigg|_{out} - \frac{Q^2}{A}\bigg|_{in}\right)\frac{1}{(x_2 - x_1)} = \frac{\partial}{\partial x}\left(\frac{Q^2}{A}\right)$$

leads to the following formulation:

$$\frac{\sum F}{\rho(x_2 - x_1)} = \frac{\partial Q}{\partial t} + \frac{\partial}{\partial x}\left(\frac{Q^2}{A}\right) - q_l u_x \tag{1.5}$$

For the determination of $\sum F$ all external forces acting on the control volume have to be considered. These are:

- the pressure force upstream and downstream of the control volume: $F_1 = -\rho g A_1\overline{h_1}$ and $F_2 = \rho g A_2\overline{h_2}$ (hydrostatic pressure is $p = \rho g h$, the force is then $F = pA$)
- the weight of water (gravitational force) in x-direction: $F_3 = \rho g\int_{x_1}^{x_2} AS_B\,\mathrm{d}x$
- and the frictional force: $F_4 = \rho g\int_{x_1}^{x_2} AS_f\,\mathrm{d}x$

where

S_B	$[-]$	bottom slope
S_f	$[-]$	friction slope
g	$[m/s^2]$	gravity

All these forces are now put into the sum of eq. 1.5. For the pressure forces, we get directly a differential form as

$$\frac{\sum F}{\rho(x_2 - x_1)} = \frac{\rho g A_2 \overline{h_2} - \rho g A_1 \overline{h_1}}{\rho(x_2 - x_1)} = g\frac{\partial}{\partial x}(A\overline{h})$$

For the gravitational force and the friction force, the mean value theorem is applied:

$$\int_{x_1}^{x_2} A(S_B - S_f)\,\mathrm{d}x = A(S_B - S_f)(x_2 - x_1)$$

This results in the following momentum equation:

$$\frac{\partial Q}{\partial t} + \frac{\partial}{\partial x}\left(\frac{Q^2}{A}\right) - q_l u_x = -g\frac{\partial}{\partial x}(A\overline{h}) + gA(S_B - S_f) \tag{1.6}$$

There is still an unknown $\overline{h}$ on the right hand side which should possibly be eliminated. Based upon geometrical considerations and using the Leibniz rule, the pressure Term can be expressed as the following not obvious relation. This can be proven mathematically even under the consideration that changes in the channel width are not negligible.

$$-g\frac{\partial}{\partial x}(A\overline{h}) = -gA\frac{\partial h}{\partial x} \tag{1.7}$$

Now, the unknown water depth h can be eliminated using the transformation

$$h = z_S - z_B \quad \text{and} \quad \frac{\partial h}{\partial x} = \frac{\partial z_S}{\partial x} - \frac{\partial z_B}{\partial x} = \frac{\partial z_S}{\partial x} + S_B$$

Inserting this into eq. 1.7, resp. eq. 1.6 leads to a formulation of the momentum equation where we have a term with the gradient of the water surface elevation z_S combining the pressure forces and the gravitational force. Note that the bottom slope S_B vanished.

$$\frac{\partial Q}{\partial t} + \frac{\partial}{\partial x}\left(\frac{Q^2}{A}\right) + gA\frac{\partial z_S}{\partial x} + gAS_f - q_l u_x = 0 \tag{1.8}$$

If only the cross sectional area where the water actually flows (and therefore contributes to the momentum balance) shall be used, and by introducing a factor β accounting for the velocity distribution in the cross section (Cunge et al. (1980)), eq. 1.9 is obtained:

$$\frac{\partial Q}{\partial t} + \frac{\partial}{\partial x}\left(\beta\frac{Q^2}{A_{red}}\right) + gA_{red}\frac{\partial z_S}{\partial x} + gA_{red}S_f - q_l u_x = 0 \tag{1.9}$$

where A_{red} [m^2] is the reduced area, i.e. the part of the cross section area where water flows.

If Strickler values are used to define the friction

$$\beta = \frac{A \sum_i k_{str_i}^2 h_i^{7/3} b_i}{\left(\sum_i k_{str_i} h_i^{5/3} b_i \right)^2} \tag{1.10}$$

If the equivalent roughness height is used

$$\beta = \frac{A \sum_i k_{s_i}^2 h_i^2 b_i}{\left(\sum_i k_{s_i} h_i^{3/2} b_i \right)^2} \tag{1.11}$$

1.1.1.3 Source Terms

With the given formulation of the flow equation there are 4 source terms:

For the continuity equation:

- The lateral in- or outflow q_l

For the momentum equation:

- The bed slope
$$W = gA \frac{\partial z_S}{\partial x} \tag{1.12}$$
- The bottom friction:
$$Fr = gA_{red} S_f \tag{1.13}$$
- The influence of lateral in- or outflow:
$$q_l u_x \tag{1.14}$$

However, in BASEchain, the influence of the lateral inflow on the momentum equation is neglected.

1.1.1.4 Closure Conditions

1.1.1.4.1 Determination of Friction Slope

The relation between the friction slope S_f and the bottom shear stress is:

$$\frac{\tau_B}{\rho} = gRS_f \tag{1.15}$$

As the unit of τ_B/ρ is the square of a velocity, a shear stress velocity can be defined as:

$$u_* = \sqrt{\frac{\tau_B}{\rho}} \tag{1.16}$$

The velocity in the channel is proportional to the shear flow velocity and thus:

$$u = c_f \sqrt{gRS_f} \tag{1.17}$$

where c_f is the dimensionless Chézy coefficient. It is defined as $c_f = C/\sqrt{g}$, where C is the Chézy coefficient [$m^{1/2}/s$].

If u is replaced by Q/A:

$$\frac{Q}{A} = c_f \sqrt{gRS_f} \tag{1.18}$$

results, with

$$S_f = \frac{Q|Q|}{gA^2 c_f^2 R} \tag{1.19}$$

Introducing the conveyance K :

$$K = \frac{Q}{\sqrt{S_f}} = A c_f \sqrt{Rg} \tag{1.20}$$

$$S_f = \frac{Q|Q|}{K^2} \tag{1.21}$$

The dimensionless friction coefficient c_f can be determined based on a power-law approach using Manning-Strickler friction coefficient k_{str} or based on log-law approach using equivalent sand roughness k_s of Nikuradse.

Power Friction Law

The power friction law according to Manning-Strickler is widely used in practice. Therfore channel roughness is defined using Strickler's k_{str} or Manning's n. For conversion a simple relation holds:

$$k_{str} = \frac{1}{n}$$

The dimensionless friction coefficient c_f is calculated as

$$c_f = \frac{k_{str} R^{1/6}}{\sqrt{g}} \tag{1.22}$$

Logarithmic Friction Laws

The following approaches are implemented to determine the coefficient c_f:

Chézy:

$$c_f = 5.75 \log\left(12\frac{R}{k_s}\right) \tag{1.23}$$

Yalin:

$$c_f = \frac{1}{\kappa} \ln\left(11\frac{R}{k_s}\right) \tag{1.24}$$

Bezzola:

This approach uses the roughness sublayer y_R as relevant roughness height. Usually for rivers $y_R \approx 1.0 d_{90}$ is a good approximation. This approach takes small relative roughness heights into account Bezzola (2002).

$$\begin{aligned} c_f &= 2.5\sqrt{1-\frac{y_R}{R}}\ \ln\left(10.9\frac{R}{y_R}\right), && \text{for} \quad \frac{R}{y_R} > 2 \\ c_f &= 1.25\sqrt{\frac{R}{y_R}}\ \ln\left(10.9\frac{R}{y_R}\right), && \text{for} \quad \frac{R}{y_R} \leq 2 \\ c_f &= 1.5, && \text{for} \quad \frac{R}{y_R} < 0.5 \end{aligned} \tag{1.25}$$

Darcy-Weissbach:

$$c_f = \sqrt{\frac{8}{f}} \quad \text{with} \quad f = \frac{0.24}{\log\left(\frac{12R}{k_s}\right)} \tag{1.26}$$

In the case where friction is determined based on the bed composition of the mobile bed, friction can be determined based on the local characteristic grain size d_{90}:

$$k_{str} = \frac{\text{factor}}{\sqrt[6]{d_{90}}} \quad \text{default value of factor} = 21.1 \tag{1.27}$$

or

$$k_s = \text{factor} \cdot d_{90} \quad \text{default value of factor} = 3 \tag{1.28}$$

The default values of the factors above correspond to a natural river bed with well graded bed material and exposed coarse components.

1.1.1.5 Boundary Conditions

At the upper and lower end of the channel it is necessary to know the influence of the region outside on the flow within the computational domain. The influenced area depends on the propagation velocity of a perturbation. The propagation velocity in standing water is

$$c = \sqrt{gh} \tag{1.29}$$

If a one dimensional flow is considered this propagation takes place in two directions: upstream ($-c$) and downstream ($+c$). These velocities must then be added to the flow velocities in the channel, giving the upstream (C_-) and downstream (C_+) characteristics:

$$C_- = \frac{\mathrm{d}x}{\mathrm{d}t} = u - c \tag{1.30}$$

$$C_+ = \frac{\mathrm{d}x}{\mathrm{d}t} = u + c \tag{1.31}$$

With these functions it is possible to determine which region is influenced by a perturbation and which region influences a given point after a given time.

In particular it can be said that if $c < u$ the information will not be able to spread in upstream direction, thus the condition in a point cannot influence any upstream point, and a point cannot receive any information from downstream. This is the case for a supercritical flow.

In contrast, if $c > u$, which is the case for sub-critical flow, the information spreads in both directions, upstream and downstream. This fact substantiates the necessity and usefulness of information at the boundaries. As there are two equations to solve, two variables are needed for the solution.

If the flow conditions are sub-critical, the flow is influenced from downstream. Thus at the inflow boundary one condition can be taken from the flow region itself and only one additional boundary condition is needed. At the outflow boundary, the flow is influenced from outside and so one boundary condition is needed.

If the flow is supercritical, no information arrives from downstream. Therefore, two boundary conditions are needed at the inflow end. In contrast, as it cannot influence the flow within the computational domain, it is not useful to have a boundary condition at the downstream end.

Table 1.1 *Number of needed boundary conditions*

Flow type	Inflow	Outflow
Sub critical flow ($Fr < 1$)	1	1
Supercritical flow ($Fr > 1$)	2	0

At the inflow boundary the given value is usually Q. If the flow is supercritical the second variable A is determined by a flow resistance law (slope is needed!).

At the outflow boundary there are several possibilities to provide the necessary information at the boundary:

- determine an out flowing discharge by a weir or a gate;
- set the water surface elevation as a function of time;
- set the water surface elevation as a function of the discharge (rating curve).

1.1.2 Shallow Water Equations

1.1.2.1 Introduction

Mathematical models of the so-called *shallow water* type govern a wide variety of physical phenomena. For reasons of simplicity, the shallow water equations will from here on be abbreviated as SWE. An important class of problems of practical interest involves water flows with a free surface under the influence of gravity. It includes:

- Tides in oceans
- Flood waves in rivers
- Dam break waves

The validity of the SWE implies the following conditions and assumptions:

- Hydrostatic distribution of pressure: this is fulfilled if the vertical accelerations are negligible.
- Small slope of the channel bottom, so that the cosine of the angle between the bottom and the horizontal can be assumed to be 1.
- Steady-state resistance laws are applicable for unsteady flow.

A key assumption made in derivation of the approximate shallow water theory concerns the first aspect, the hydrostatic pressure distribution. Supposing that the vertical velocity acceleration of water particles is negligible, a hydrostatic pressure distribution can be assumed. This eventually allows for integration over the flow depth, which results in a non-linear initial value problem, namely the shallow water equations. They form a time-dependent two-dimensional system of non-linear partial differential equations of hyperbolic type.

There are two approaches for the derivation of shallow water equations:

- Integrating the three-dimensional system of Navier-Stokes equations over flow depth
- Direct approach by considering a three-dimensional control volume

In the following the derivation of the depth integrated mass and momentum conservation equations from the Reynolds-averaged 3-D Navier-Stokes equation is briefly presented. Following boundary conditions are imposed:

1. At the top of water surface:

   Kinematic boundary condition (this condition describes that no flow across the water surface can take place):

$$w_s = \frac{\partial z_S}{\partial t} + u_s \frac{\partial z_S}{\partial x} + v_s \frac{\partial z_S}{\partial y} \tag{1.32}$$

   Dynamic boundary condition:

$$\tau = (\tau_{Sx}, \tau_{Sy}) \quad \text{and} \quad \mathrm{P} = \mathrm{P}_{atm} \tag{1.33}$$

2. At the bottom of water body:

   Kinematic boundary condition (this condition describes that no flow through the bed surface can take place):

$$w_B = u_B \frac{\partial z_B}{\partial x} + v_B \frac{\partial z_B}{\partial y} \tag{1.34}$$

Derivation of mass conservation

The derivation makes use of Leibniz's integration rule, which is used here to remove the partial derivatives from the integral. It can be written generally as

$$\int_{z_B(x,y)}^{z_S(x,y)} \frac{\partial f(x,y,z)}{\partial x}\, dz = \frac{\partial}{\partial x} \int_{z_B(x,y)}^{z_S(x,y)} f(x,y,z)\, dz + f(x,y,z_B)\, \frac{\partial z_B}{\partial x} - f(x,y,z_S)\, \frac{\partial z_S}{\partial x}$$

The 3-D Reynolds-averaged mass conservation equation is integrated over the flow depth from the bed bottom z_B to the water surface z_S.

$$\int_{z_B}^{z_S} \left[\frac{\partial u}{\partial x} + \frac{\partial v}{\partial y} + \frac{\partial w}{\partial z} \right] dz = 0 \tag{1.35}$$

Applying Leibniz's rule on the first term, the velocity gradient in x-direction, leads to

$$\int_{z_B}^{z_S} \frac{\partial u}{\partial x}\, dz = \frac{\partial}{\partial x} \int_{z_B}^{z_S} u\, dz + u_B \frac{\partial z_B}{\partial x} - v_s \frac{\partial z_S}{\partial x}$$

whereas u_B, u_S and v_B, v_S are the velocities at the bottom and at the surface in x- and y-directions respectively. The second term of eq. 1.35 is treated analogous.

The third term can be evaluated exactly by applying the fundamental theorem of calculus. It results in the difference of the vertical velocity at the surface and the bottom:

$$\int_{z_B}^{z_S} \frac{\partial w}{\partial z}\, dz = w_S - w_B$$

Assembling these terms, one can identify and eliminate the kinematic boundary conditions as stated above.

$$\frac{\partial}{\partial x} \int_{z_B}^{z_S} u\, dz + \frac{\partial}{\partial y} \int_{z_B}^{z_S} v\, dz + \underbrace{u_B \frac{\partial z_B}{\partial x} + v_B \frac{\partial z_B}{\partial y} - w_B}_{=0} - \underbrace{u_S \frac{\partial z_S}{\partial x} - v_S \frac{\partial z_S}{\partial y} + w_S}_{= \frac{\partial z_S}{\partial t} = \frac{\partial h}{\partial t}} = 0$$

Evaluating the integrals over the depth as

$$\int_{z_B}^{z_S} u \, dz = \overline{u}h$$

finally leads to the depth integrated formulation of mass conservation:

$$\frac{\partial h}{\partial t} + \frac{\partial(\overline{u}h)}{\partial x} + \frac{\partial(\overline{u}h)}{\partial y} = 0$$

Derivation of momentum conservation

The Reynolds-averaged 3-D momentum equation in x-direction of the Navier-Stokes equation is integrated over the depth

$$\int_{z_B}^{z_S} \left[\frac{\partial u}{\partial t} + \frac{\partial u^2}{\partial x} + \frac{\partial uv}{\partial y} + \frac{\partial uw}{\partial z} \right] dz = \int_{z_B}^{z_S} \left[-\frac{1}{\rho}\frac{\partial p}{\partial x} + \frac{1}{\rho}\frac{\partial \tau_{xx}}{\partial x} + \frac{1}{\rho}\frac{\partial \tau_{xy}}{\partial y} + \frac{1}{\rho}\frac{\partial \tau_{xz}}{\partial y} \right] dz \quad (1.36)$$

whereas the momentum equation in y-direction can be treated in an analogous manner.

The first term, the time derivative of the x-velocity, is transformed with Leibniz's rule and integrated over the depth.

$$\int_{z_B}^{z_S} \frac{\partial u}{\partial t} \, dz = \frac{\partial}{\partial t} \int_{z_B}^{z_S} u \, dz + u_B \frac{\partial z_B}{\partial t} - u_S \frac{\partial z_S}{\partial t} = \frac{\partial \overline{u}h}{\partial t} + u_B \frac{\partial z_B}{\partial t} - u_S \frac{\partial z_S}{\partial t}$$

The Leibniz rule is also applied on the advective terms as follows:

$$\int_{z_B}^{z_S} \frac{\partial u^2}{\partial x} \, dz = \frac{\partial}{\partial x} \int_{z_B}^{z_S} u^2 \, dz + u_B^2 \frac{\partial z_B}{\partial x} - u_S^2 \frac{\partial z_S}{\partial x} \quad , \quad \int_{z_B}^{z_S} \frac{\partial uv}{\partial y} \, dz = \frac{\partial}{\partial y} \int_{z_B}^{z_S} uv \, dz + u_B v_B \frac{\partial z_B}{\partial y} - u_S v_S \frac{\partial z_S}{\partial y}$$

And the fundamental theorem of calculus allows the evaluation of the fourth term on the left hand side.

$$\int_{z_B}^{z_S} \frac{\partial uw}{\partial z} dz = u_S w_S - u_B w_B$$

All terms of the left hand side of eq. 1.36 now can be assembled, and again, the kinematic boundary conditions are identified and can be eliminated. The left hand side is reduced to three remaining terms.

$$\overline{u}h + \frac{\partial}{\partial x} \int_{z_B}^{z_S} u^2 \, dz + \frac{\partial}{\partial y} \int_{z_B}^{z_S} uv \, dz + u_B \underbrace{\left(\frac{\partial z_B}{\partial t} + u_B \frac{\partial z_B}{\partial x} + v_B \frac{\partial z_B}{\partial x} - w_B \right)}_{=0} -$$

$$u_S \underbrace{\left(\frac{\partial z_S}{\partial t} + u_s \frac{\partial z_S}{\partial x} + v_S \frac{\partial z_S}{\partial y} + w_S \right)}_{=0}$$

With the assumption of a hydrostatic pressure distribution, the pressure term on the right hand side can be evaluated. Furthermore, the water surface elevation is replaced by the bottom elevation and the depth.

$$\frac{1}{\rho} \int_{z_B}^{z_S} \frac{\partial p}{\partial x} \, dz = gh \frac{\partial z_S}{\partial x} = gh \left(\frac{\partial z_B}{\partial x} + \frac{\partial h}{\partial x} \right)$$

The depth integration of the first two shear stresses of the right hand side yields the depth integrated viscous and turbulent stresses, which require additional closure conditions to be evaluated.

$$\frac{1}{\rho} \int_{z_B}^{z_S} \frac{\partial \tau_{xx}}{\partial x} \, dz + \frac{1}{\rho} \int_{z_B}^{z_S} \frac{\partial \tau_{yx}}{\partial y} \, dz = \frac{1}{\rho} \frac{\partial \overline{\tau}_{xx} h}{\partial x} + \frac{1}{\rho} \frac{\partial \overline{\tau}_{xy} h}{\partial y}$$

The third shear stress term can be integrated over the depth and introduces the bottom and surface shear stresses at the domain boundaries, which again need additional closure conditions. The surface shear stresses τ_{Bx}, e.g. due to wind flow over the water surface, are neglected from here on.

$$\frac{1}{\rho} \int_{z_B}^{z_S} \frac{\partial \tau_{zx}}{\partial z} \, dz = \frac{1}{\rho} (\tau_{Sx} - \tau_{Bx})$$

Putting the terms together one obtains

$$\frac{\partial \overline{u} h}{\partial t} + \frac{\partial}{\partial x} \int_{z_B}^{z_S} u^2 \, dz + \frac{\partial}{\partial y} \int_{z_B}^{z_S} uv \, dz + gh \frac{\partial h}{\partial x} = -gh \frac{\partial z_B}{\partial x} - \frac{1}{\rho} \tau_{Bx} + \frac{1}{\rho} \frac{\partial \overline{\tau}_{xx} h}{\partial x} + \frac{1}{\rho} \frac{\partial \overline{\tau}_{xy} h}{\partial y}$$

The depth integrals of the advective terms still need to be solved. By dividing the velocities in a mean velocity $\overline{u}$ and a deviation from the mean u', similar to the Reynolds averaging procedure, the advective terms can be evaluated as follows. The depth integration introduces new dispersion terms, which describe the effects of the non-uniformity of the velocity distribution.

$$u = \overline{u} + u' \Rightarrow \frac{\partial}{\partial x} \int_{z_B}^{z_S} u^2 \, dz = \frac{\partial \overline{u}^2 h}{\partial x} + \frac{\partial \overline{u'u'} h}{\partial x} = \frac{\partial \overline{u}^2 h}{\partial x} + \frac{1}{\rho} \frac{\partial D_{xx} h}{\partial x}$$

In the end, after dividing the equations by the water depth, the depth integrated x-momentum equation of the SWE is obtained in the following formulation:

$$\frac{\partial \overline{u}}{\partial t} + \overline{u} \frac{\partial \overline{u}}{\partial x} + \overline{v} \frac{\partial \overline{u}}{\partial y} + g \frac{\partial h}{\partial x} = -g \frac{\partial z_B}{\partial x} - \frac{1}{\rho h} \tau_{Bx} + \frac{1}{\rho h} \frac{\partial [h(\overline{\tau}_{xx} + D_{xx})]}{\partial x} + \frac{1}{\rho h} \frac{\partial [h(\overline{\tau}_{xy} + D_{yx})]}{\partial y}$$

Shallow Water Equations

Conclusive, as shown before, the complete set of SWE is derived in the form:

$$\frac{\partial h}{\partial t} + \frac{\partial(\overline{u}h)}{\partial x} + \frac{\partial(\overline{v}h)}{\partial y} = 0 \tag{1.37}$$

$$\frac{\partial \overline{u}}{\partial t} + \overline{u}\frac{\partial \overline{u}}{\partial x} + \overline{v}\frac{\partial \overline{u}}{\partial y} + g\frac{\partial h}{\partial x} = -g\frac{\partial z_B}{\partial x} - \frac{1}{\rho h}\tau_{Bx} + \frac{1}{\rho h}\frac{\partial[h(\overline{\tau}_{xx} + D_{xx})]}{\partial x} + \frac{1}{\rho h}\frac{\partial[h(\overline{\tau}_{xy} + D_{yx})]}{\partial y} \tag{1.38}$$

$$\frac{\partial \overline{v}}{\partial t} + \overline{u}\frac{\partial \overline{v}}{\partial x} + \overline{v}\frac{\partial \overline{v}}{\partial y} + g\frac{\partial h}{\partial y} = -g\frac{\partial z_B}{\partial y} - \frac{1}{\rho h}\tau_{By} + \frac{1}{\rho h}\frac{\partial[h(\overline{\tau}_{yx} + D_{yx})]}{\partial x} + \frac{1}{\rho h}\frac{\partial[h(\overline{\tau}_{yy} + D_{yy})]}{\partial y} \tag{1.39}$$

where:

h	$[m]$	water depth
g	$[m/s^2]$	gravity acceleration
P	$[Pa]$	pressure
$\overline{u}$	$[m/s]$	depth averaged velocity in x direction
u_S	$[m/s]$	velocity in x direction at water surface
u_B	$[m/s]$	velocity in x direction at bottom (usually equal zero)
$\overline{v}$	$[m/s]$	depth averaged velocity in y direction
v_S	$[m/s]$	velocity in y direction at water surface
v_B	$[m/s]$	velocity in y direction at bottom (usually equal zero)
w_S	$[m/s]$	velocity in z direction at water surface
w_B	$[m/s]$	velocity in z direction at bottom (usually equal zero)
z_B	$[m]$	bottom elevation
z_S	$[m]$	water surface elevation
τ_{Sx}, τ_{Sy}	$[N/m^2]$	surface shear stress in x- and y direction (here neglected)
τ_{Bx}, τ_{By}	$[N/m^2]$	bed shear stress in x- and y direction
$\overline{\tau}_{xx}, \overline{\tau}_{xy}, \overline{\tau}_{yx}, \overline{\tau}_{yy}$	$[N/m^2]$	depth averaged viscous and turbulent stresses
$D_{xx}, D_{xy}, D_{yx}, D_{yy}$	$[N/m^2]$	momentum dispersion terms

For brevity, the over bars indicating depth averaged values will be dropped from here on.

1.1.2.2 Closure Conditions

1.1.2.2.1 Turbulence

The turbulent and viscous shear stresses can be quantified in accordance with the Boussinesq eddy viscosity concept, which can be expressed as

$$\tau_{xx} = 2\rho\nu\frac{\partial u}{\partial x} \quad , \quad \tau_{yy} = 2\rho\nu\frac{\partial v}{\partial y} \quad , \quad \tau_{xy} = \rho\nu\left(\frac{\partial u}{\partial y} + \frac{\partial v}{\partial x}\right) \tag{1.40}$$

If the flow is dominated by the friction forces, the total viscosity is the sum of the eddy viscosity (quantity due to turbulence modelling) and molecular viscosity (kinematic viscosity of the fluid): $v = v_t + v_m$.

Turbulent eddy viscosity may be dynamically calculated as $v_t = \kappa u_* h/6$ with the friction velocity $u_* = \sqrt{\tau_B/\rho}$.

The molecular viscosity is a physical property of the fluid and is constant due to the assumption of an isothermal fluid.

1.1.2.2.2 Bed Shear Stress

The bed shear stresses are related to the depth–averaged velocities by the quadratic friction law

$$\tau_{Bx} = \rho \frac{|\boldsymbol{u}|u}{c_f^2} \quad ; \quad \tau_{By} = \rho \frac{|\boldsymbol{u}|v}{c_f^2} \tag{1.41}$$

in which $|\boldsymbol{u}| = \sqrt{u^2 + v^2}$ is the magnitude of the velocity vector. The friction coefficient c_f can be determined by any friction law.

1.1.2.2.3 Momentum Dispersion

The momentum dispersion terms account for the dispersion of momentum transport due to the vertical non-uniformity of flow velocities.

At the moment the momentum dispersion terms are not explicitly modelled here. Usually, in straight channels, these dispersive effects can be accounted for by adapting the turbulent viscosity in the determination of the turbulent stresses (Wu, 2007).

1.1.2.3 Conservative Form of SWE

Various forms of SWE can be distinguished with their primitive variables. The proper choice of these variables and the corresponding set of equations plays an extremely important role in numerical modelling. It is well known that the conservative form is preferred over the non-conservative one if strong changes or discontinuities in a solution are to be expected. In flooding and dam break problems, this is usually the case.

Bechteler et al. (1993) showed that the equation sets in conservative form, with (h, uh, vh) as independent and primitive variables produce best results. The conservative form can be derived by multiplying the continuity equation with u and v and adding to momentum equations in x and y direction respectively. This set of equations can be written in the following form:

$$\boldsymbol{U}_t + \nabla(\boldsymbol{F}, \boldsymbol{G}) + \boldsymbol{S} = 0 \tag{1.42}$$

where $U, F(U), G(U)$ and S are the vectors of conserved variables, fluxes in the x and y directions and sources respectively, given by:

$$\boldsymbol{U} = \begin{pmatrix} h \\ uh \\ \nu h \end{pmatrix} \tag{1.43}$$

$$\boldsymbol{F} = \begin{pmatrix} uh \\ u^2h + \frac{1}{2}gh^2 - \nu h\frac{\partial u}{\partial x} \\ u\nu h - \nu h\frac{\partial u}{\partial y} \end{pmatrix} \quad ; \quad \boldsymbol{G} = \begin{pmatrix} \nu h \\ u\nu h - \nu h\frac{\partial \nu}{\partial x} \\ \nu^2h + \frac{1}{2}gh^2 - \nu h\frac{\partial \nu}{\partial y} \end{pmatrix} \tag{1.44}$$

$$\boldsymbol{S} = \begin{pmatrix} 0 \\ gh(S_{fx} - S_{Bx}) \\ gh(S_{fy} - S_{By}) \end{pmatrix} \tag{1.45}$$

where ν is the total viscosity.

1.1.2.4 Source Terms

The eq. 1.45 has two source terms: the bed shear stress ($\tau_B/\rho = ghS_f$) and the bed slope term (ghS_B). The viscous stresses in the flux of eq. 1.44 are also treated as flux term.

The bed shear stress is the most important physical parameter besides water depth and velocity field of a hydro- and morphodynamic model. It causes the turbulence and is responsible for sediment transport and has a non-linear effect of retarding the flow. When the effect of turbulence grows, the effect of molecular viscosity becomes relatively smaller, while viscous boundary layer near a solid boundary becomes thinner and may even appear not to exist. It means that the bed stress (friction) is equal to the bed turbulent stress.

However, bed stress is usually estimated by using an empirical or semi-empirical formula since the vertical distribution of velocity cannot be readily obtained.

In the one dimensional system of equations the term bed stress can be expressed as gRS_f, where S_f denotes the energy slope. Assuming that the frictional force in a two dimensional unsteady open flow can be estimated by referring to the formulas for one dimensional flows in open channel it can be written:

$$S_f = \frac{u|u|}{gc_f^2 R} \tag{1.46}$$

where u = velocity; c_f = friction coefficient; R = hydraulic radius. It can be easily seen that the above formula can be approximately generalized to the two dimensional system. In one-dimensional flows it is not distinguished between bottom and lateral (side wall) friction, while in two dimensional flows it is often taken a unit width channel ($R = h$). For the two dimensional system the eq. 1.46 has the following forms

$$S_{fx} = \frac{u\sqrt{u^2+v^2}}{gc_f^2 R} \quad ; \quad S_{fy} = \frac{v\sqrt{u^2+v^2}}{gc_f^2 R} \tag{1.47}$$

The coefficient c_f can be calculated by different empirical approaches as in the one dimensional system, e.g. using the Manning or Strickler coefficients. See Section 1.1.1.4 for

further details on the determination of the friction coefficient c_f . If the friction value is calculated from the bed composition, the d_{90} diameter of the mixture is determined. In case of single grain simulations the d_{90} diameter is estimated by $d_{90} = 3 \cdot d_{mean}$.

The bed stress terms need additional closures equation (see Section 1.1.2.2.2) to be determined. Bed slope terms represent the gravity forces

$$S_{B,x} = -\partial z_B/\partial x \quad ; \quad S_{B,y} = -\partial z_B/\partial y \tag{1.48}$$

The viscous fluxes are treated as source terms (The superscript 'd' refers to the diffusion)

$$\boldsymbol{S}_d = \frac{\partial \boldsymbol{F}^d}{\partial x} + \frac{\partial \boldsymbol{G}^d}{\partial y}$$

where the diffusive fluxes read

$$\boldsymbol{F}^d = \begin{pmatrix} 0 \\ \nu h \dfrac{\partial u}{\partial x} \\ \nu h \dfrac{\partial \nu}{\partial x} \end{pmatrix}$$

,

$$\boldsymbol{G}^d = \begin{pmatrix} 0 \\ \nu h \dfrac{\partial u}{\partial y} \\ \nu h \dfrac{\partial \nu}{\partial y} \end{pmatrix}$$

The total viscosity ν is the sum of the kinematic viscosity and turbulent eddy viscosity. The kinematic viscosity is a physical property of the fluid and is set to a constant value.

The turbulent eddy viscosity can either be set to a constant value or calculated dynamically as Turbulent eddy viscosity may be dynamically calculated as $\nu_t = \kappa u_* h/6$ with the friction velocity $u_* = \sqrt{\tau_B/\rho}$.

1.1.2.5 Boundary Conditions

SWE provide a model to describe dynamic fluid processes of various natural phenomena and find therefore widespread application in science and engineering. Solving SWE needs the appropriate boundary conditions like any other partial differential equations. In particular, the issue of which kind of boundary conditions are allowed is still not completely understood (Agoshkov et al., 1994). However several sets of boundary conditions of physical interest that are admissible from the mathematical viewpoint will be discussed here.

The physical boundaries can be divided into two sets: one *closed* (Γ_c), the other *open* (Γ_o) (Figure 1.2). The former generally expresses that no mass can flow through the boundary. The latter is an imaginary fluid-fluid boundary and includes two different inflow and outflow types.

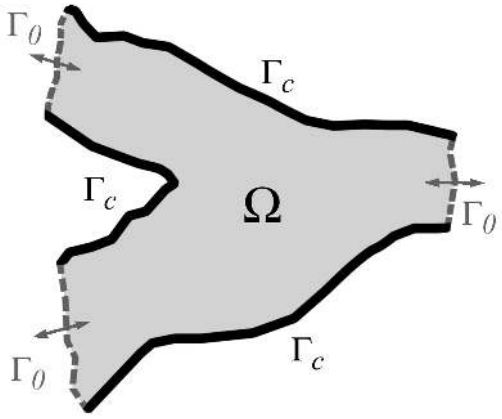

Figure 1.2 *Computational Domain and Boundaries*

1.1.2.5.1 Closed Boundary

The following relations are often described on the closed boundary, say Γ_c :

$$\rho \boldsymbol{u} \cdot \boldsymbol{n} = 0 \quad \frac{\partial \boldsymbol{u}}{\partial \boldsymbol{n}} = 0 \tag{1.49}$$

where

$\boldsymbol{n}$	$[m]$	the normal (directed outward) unit vector on Γ_c
$\boldsymbol{u}$	$[m/s]$	velocity vector $= (u, v)$

1.1.2.5.2 Open Boundary

The number of boundaries of a partial differential equations system depends on the type of the system. From the mathematical point of view, the SWE establish a quasi-linear hyperbolic differential equations system. If the temporal derivatives vanish, the system is elliptical for $F_r \leq 1.0$ and hyperbolical for $F_r \geq 1.0$, where F_r is Froude number.

On the open boundary (Γ_o) the two types inflow and outflow can be respectively distinguished as follows:

$$\Gamma_{in} = (x \in \Gamma_o; \boldsymbol{u} \cdot \boldsymbol{n} < 0) \tag{1.50}$$

$$\Gamma_{out} = (x \in \Gamma_o; \boldsymbol{u} \cdot \boldsymbol{n} > 0) \tag{1.51}$$

Based on the behaviour of the system of equations, the theoretical number of open boundary conditions is listed in Table 1.2 (Agoshkov et al., 1994) (Beffa, 1994):

Table 1.2 *The Correct Number of Boundary Conditions in SWE*

Flow type	Inflow	Outflow
Sub critical flow ($Fr < 1$)	2	1
Supercritical flow ($Fr > 1$)	3	0

However in practical application of boundary conditions, the number of the implemented conditions is often higher or lower than the theoretical criteria (Nujić, 1998).

1.2 Sediment and Pollutant Transport

1.2.1 Fundamentals of Sediment Motion

1.2.1.1 Threshold Condition for Sediment Transport

1.2.1.1.1 Determination of the Critical Shear Stress

The critical shear stress $\tau_{B_{cr}} = \theta_{cr}(\rho_s - \rho)gd_g$ is the threshold for incipient motion of grain class g where the critical Shields parameter θ_{cr} is a function of the shear Reynolds number Re^* (Shields, 1936). The critical Shields parameter θ_{cr} can be set to a constant value, e.g. Meyer-Peter and Müller (1948) proposed a constant Shields parameter of 0.047 for fully turbulent flow ($Re^* > 10^3$). Furthermore, θ_{cr} can be dynamically determined from a transformed Shields diagram as a function of the dimensionless grain diameter D^* ($\theta_{cr} = f(D^*)$) (Figure 1.3).

An approximation of the original Shields diagram was proposed by van Rijn (1984a):

$$\begin{array}{lll} \theta_{cr} = 0.24(D^*)^{-1} & for & 1 \leq D^* \leq 4 \\ \theta_{cr} = 0.14(D^*)^{-0.64} & for & 4 < D^* \leq 10 \\ \theta_{cr} = 0.04(D^*)^{-0.1} & for & 10 < D^* \leq 20 \\ \theta_{cr} = 0.013(D^*)^{0.29} & for & 20 < D^* \leq 150 \\ \theta_{cr} = 0.055 & for & D^* > 150 \end{array} \tag{1.52}$$

where the dimensionless grain diameter D^* is defined as

$$D^* = \left(\frac{(\rho_s - \rho)g}{\rho v^2}\right)^{1/3} d \tag{1.53}$$

Another explicit formulation of the Shields curve was proposed by Yalin and Silva (2001):

$$\theta_{cr} = 0.13D^{*-0.392}\exp(-0.015D^*) + 0.045\,(1 - \exp(-0.068D^*)) \tag{1.54}$$

1.2.1.1.2 Influence of Local Slope on Incipient Motion

The investigations on incipient motion by Shields were made for almost horizontal bed. In the case of sloped bed in flow direction or transverse to it, the stability of grains can either be reduced or increased due to gravity. One approach to consider the effects of local slopes on the threshold for incipient motion is to correct the critical shear stresses for incipient motion. Here k_β and k_γ are correction factors for slope in flow direction and in transversal direction and $\tau_{B_{cr},Shields}$ is the critical shear stress for almost horizontal bed as derived by Shields. The corrected critical shear stress then is determined as

$$\tau_{B_{cr}} = k_\beta k_\gamma \tau_{B_{cr},Shields} \tag{1.55}$$

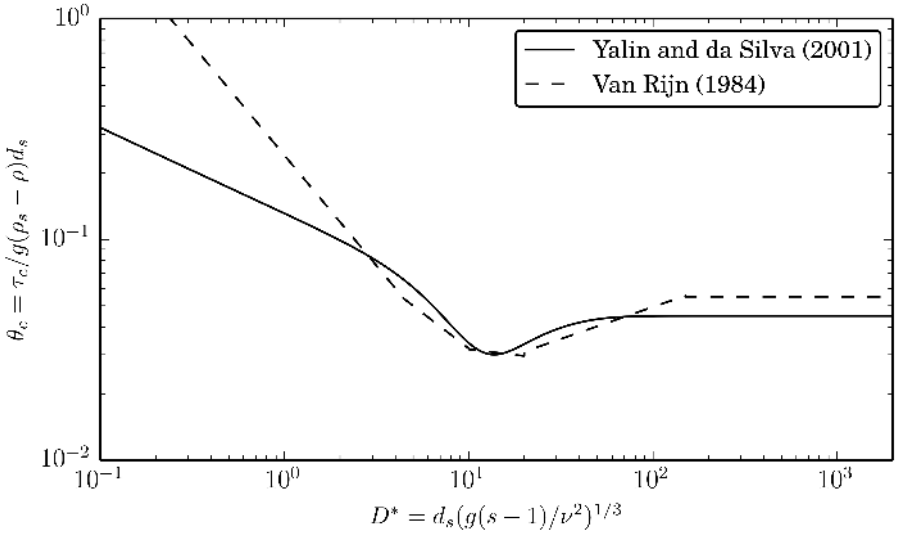

Figure 1.3 *Transformed Shields diagram to determine critical Shields parameter*

The correction factors are calculated as suggested by van Rijn (1989):

$$k_\beta = \begin{cases} \dfrac{sin(\gamma - \beta)}{sin\gamma} & \text{if slope} < 0 \\ \dfrac{sin(\gamma + \beta)}{sin\gamma} & \text{if slope} > 0 \end{cases}$$
$$k_\gamma = \left\{ \; cos\delta\sqrt{1 - \frac{tan^2\delta}{tan^2\gamma}} \right. \tag{1.56}$$

where β is the angle between the horizontal and the bed in flow direction, δ is the slope angle transversal to the flow direction and γ is the angle of repose of the sediment material.

Furthermore, Chen et al. (2010) proposed a correction $k = k_\beta k_\gamma$ as follows

$$k = \frac{\tau_{B_{cr}}}{\tau_{B_{cr},Shields}} = \frac{1}{\tan\gamma}\left(\cos^2\left(\frac{\pi}{2} - \beta\right) - 1 + \frac{1}{(1 + \tan^2\beta + \tan^2\gamma)} + \frac{\tan^2\gamma}{(1 + \tan^2\beta + \tan^2\gamma)}\right)^{0.5} + \cos\left(\frac{\pi}{2} - \beta\right) \tag{1.57}$$

1.2.1.2 Influence of Bed Forms on Bottom Shear Stress

In presence of bed forms, like ripples, sand dunes or gravel banks, additional friction losses can occur due to complex flow conditions around these bed forms and the formation of turbulent eddies. In such cases the dimensionless bottom shear stress θ determined from

the present flow conditions can differ from the effective dimensionless bottom shear stress θ', which is relevant for the transport of the sediment particles. It is usually assumed that the determination of the effective shear stress should be based upon the grain friction losses only and should exclude additional form losses, to prevent too large sediment transport rates. Therefore a reduction factor μ is introduced for the determination of the effective bottom shear stress θ' from the bottom shear stress θ as

$$\mu = \frac{\tau'_B}{\tau_B} = \frac{\theta'}{\theta} \quad \text{with} \quad \begin{cases} \mu = 1.0 & \text{(no bed forms)} \\ \mu < 1.0 & \text{(bed forms)} \end{cases} \tag{1.58}$$

This reduction factor (also called "ripple factor") can be given a constant value if the bed forms are distributed uniformly over the simulation domain. After Jäggi this factor should be set between 0.8 and 0.85. If there are no bed forms present one can consider that $\theta' = \theta$, i.e. μ=1.0. Generally can be said, the larger the form resistance, the smaller becomes the reduction factor μ.

Another approach is to calculate the reduction factor by introducing a reduced energy slope J', compared to the energy slope J, due to the presence of the bed forms as done by Meyer-Peter and Müller. This approach is in particular suitable if ripples are present at the river bed and finally leads to the following estimation of the reduction factor.

$$\mu = \left(\frac{k_{str}}{k'_{str}}\right)^{3/2} \tag{1.59}$$

Here, k'_{str} corresponds to the definition of the Strickler coefficient for experiments with Nikuradse-roughness (Jäggi, 1995) and can be calculated from the grain sizes using the d90 diameter as detailed in section Section 1.1.1.4. k_{str} is the calibrated Strickler coefficient used in the hydraulic calculations which includes the form friction effects.

1.2.1.3 Bed Armouring

In morphological simulations with fractional sediment transport the forming or destroying of bed armouring layers can be simulated by modelling sorting effects without special features.

But there are also some types of protection layers which need a special treatment, like e.g. grass layers or geotextiles. Furthermore, for single grain simulations the bed material sorting effects cannot be captured and therefore a special treatment is needed if effects of bed armouring shall be considered.

The effects of such a protection layer can be considered using two methods:

- A critical shear stress $\tau_{cr,start}$ of the protection layer can be specified, which must be exceeded at least once before erosion of the substrate can take place. This method is suited for simulations with one or multiple grain classes. Start of erosion: $\tau_B > \tau_{cr,start}$
- Another approach is to define the d90 grain diameter of the bed armouring layer. The dimensionless critical shear stress $\theta_{cr,armour}$ of this bed armour is then estimated as

$$\theta_{cr,armour} = \theta_{cr} \left(\frac{d_{90}}{d} \right)^{2/3}$$

where d_{90} is the specified d90 grain diameter of the bed armour and d and θ_{cr} are the diameter and critical shear stress of the substrate. But be aware that in case the bed armour is eroded once, it cannot be built up again using this approach in single grain computations.

If sediment has accumulated above the protection layer, the armouring condition is not applied until this sediment is totally eroded.

1.2.1.4 Settling Velocities of Particles

The settling velocity w of sediment particles is an important parameter to determine which particles are transported as bed load or as suspended load. Many different empirical or semi-empirical relations for the determination of settling velocities in dependence of the grain diameter have been suggested in literature.

Approach of van Rijn

The sink rate can be determined against the grain diameter after van Rijn (1984b).

$$w = \frac{(s-1)gd^2}{18\nu} \quad for \quad 0.001 < d \leq 0.1 \quad mm \tag{1.60}$$

$$w = \frac{10\nu}{d} \left(\sqrt{1 + \frac{0.01(s-1)gd^3}{\nu^3}} - 1 \right) \quad for \quad 0.1 < d \leq 1 \quad mm \tag{1.61}$$

$$w = 1.1\sqrt{(s-1)gd} \quad for \quad d \geq 1 \quad mm \tag{1.62}$$

d is the diameter of the grain, ν is the kinematic viscosity and $s = \rho_S/\rho$ the specific density.

Approach of Wu and Wang

A newer approach for the computation of the sink velocity is the one of Wu et al. (2000):

$$w = \frac{M\nu}{Nd} \left[\sqrt{\frac{1}{4} + \left(\frac{4N}{3M^2} (D^*)^3 \right)^{1/n}} - \frac{1}{2} \right]^n \tag{1.63}$$

where:
$M = 53.5e^{-0.65S_p}$
$N = 5.65e^{-2.5S_p}$
$n = 0.7 + 0.9S_p$

S_p is the Corey shape factor, with a value for natural sediments of about 0.7 (0.3 - 0.9).

Approach of Zhang

The Zhang formula (Zhang, 1961) is based on many laboratory data and was developed for naturally worn sediment particles. It can be used in a wide range of sediment sizes in the laminar as well turbulent settling region (Wu, 2007).

$$w = \sqrt{\left(13.95\frac{\nu}{d}\right)^2 + 1.09(s-1)gd} - 13.95\frac{\nu}{d} \tag{1.64}$$

1.2.1.5 Bed load Propagation Velocity

The propagation velocity of sediment material is an important parameter to characterize the bed load transport in rivers. In some numerical approaches for morphological simulations this velocity is a useful input parameter.

Several empirical investigations have been made to measure the velocity of bed load material in experimental flumes. One recent approach for the determination of the propagation velocity is the semi-empirical equation based on probability considerations by Zhilin Sun and John Donahue (Sun and Donahue, 2000) as

$$u_B = 7.5(\sqrt{\theta'} - C_0\sqrt{\theta_{cr}})\sqrt{(s-1)gd} \tag{1.65}$$

where θ' is the dimensionless effective bottom shear stress and θ_{cr} is the critical Shields parameter for incipient motion for a grain of diameter d. Furthermore, C_0 is a coefficient less than 1 and s is specific density of the bedload material. As can be seen, the propagation velocity will increase if the difference of the actual shear stress and the criticial shear stress enlarges as well as in the case of larger grain diameters.

1.2.2 Suspended Sediment and Pollutant Transport

1.2.2.1 One Dimensional Advection-Diffusion-Equation

For a channel with irregular cross section area A (Figure 1.1) the following advection-diffusion equation for to the number of pollutant species or grain size classes ng holds:

$$\frac{\partial(AC_g)}{\partial t} + \frac{\partial(QC_g)}{\partial x} - \frac{\partial}{\partial x}\left(A\Gamma\frac{\partial C_g}{\partial x}\right) - S_g - Sl_g = 0 \quad for \quad g = 1, ..., ng \tag{1.66}$$

Introducing the continuity equation $\frac{\partial A}{\partial t} + \frac{\partial Q}{\partial x} = 0$ in eq. 1.66 one becomes:

$$A\frac{\partial(C_g)}{\partial t} + Q\frac{\partial(C_g)}{\partial x} - \frac{\partial}{\partial x}\left(A\Gamma\frac{\partial C_g}{\partial x}\right) - S_g - Sl_g = 0 \quad for \quad g = 1, ..., ng \tag{1.67}$$

1.2.2.2 Two Dimensional Advection-Diffusion-Equation

According to the number of pollutant species or grain size classes, ng advection-diffusion equations for transport of the suspended material are provided as follows:

$$\frac{\partial}{\partial t}C_g h + \frac{\partial}{\partial x}\left(C_g q - h\Gamma\frac{\partial C_g}{\partial x}\right) - \frac{\partial}{\partial y}\left(C_g r - h\Gamma\frac{\partial C_g}{\partial y}\right) - S_g - Sl_g = 0 \quad for \quad g = 1, ..., ng \tag{1.68}$$

where C_g is the concentration of each grain size class and Γ is the eddy diffusivity.

1.2.2.3 Source Terms

For both suspended sediment and pollutant transport there can be a local sediment or pollutant source: Sl_g given by a volume.

For suspended sediment transport an additional source term S_g representing the exchange with the bed has to be considered. This term appears also in the bed load equations if they are applied in combination with suspended load.

This term is calculated by the difference between the deposition rate q_d and the suspension (entry) rate q_{e_k}.

$$S_g = q_{e_g} - q_{d_g} \tag{1.69}$$

The deposition rate is expressed as convection flux of the sink rate:

$$q_{d_g} = w_g C_{d_g} \tag{1.70}$$

w_g is the sink rate of grain class g and C_{d_g} its concentration near the bed. According to a suggestion of Bennett and Nordin (1977), the suspension entry is formulated in line with the deposition rate employing empirical relations:

$$q_{e_g} = w_g \beta_g C_{e_g} \tag{1.71}$$

The outcome of this is:

$$S_g = w_g(\beta_g C_{e_g} - C_{d_g}) \tag{1.72}$$

The sink rate w_g can be determined against the grain diameter after one of the relations given in Section 1.2.1.4

The reference concentration for the suspension entry can be calculated as follows after van Rijn (1984b):

$$C_{e_g} = 0.015 \frac{d_g}{a} \frac{T_g^{1.5}}{(D^*)_g^{0.3}} \tag{1.73}$$

where:

T_g	is the dimensionless characteristic number for the bottom shear stress of grain class g.
a	is the reference height above the mean bed bottom.
D_g^*	is the dimensionless diameter of grain class g.

Another approach is the one of Zyserman and Fredsøe (1994):

$$C_{e_g} = \frac{0.331(\theta' - 0.045)^{1.75}}{1 + 0.72(\theta' - 0.045)^{1.75}} \tag{1.74}$$

with the dimensionless effective bottom shear stress

$$\theta' = u_*^2/[(s-1)gd] \tag{1.75}$$

The reference concentration for the deposition rate is calculated after Lin (1984):

$$C_{d_g} = \left(3.25 + 0.55 \ln\left(\frac{w_g}{\kappa u_*}\right)\right) C_g \tag{1.76}$$

where:

C_g is the mean concentration over depth of suspended particles of grain class g,
u_* is the shear velocity,
κ the Von Karmann constant.

Another approach is the one of Minh Duc (1998):

$$\alpha_c = \frac{(h-\delta)}{\int_\delta^h \left(\frac{h-z}{z}\frac{\delta}{h-\delta}\right)^{\omega/\kappa U_*} dz}$$

The erosion and deposition rates can also be computed using critical shear stresses, as does Xu (1998).

$$q_d = \begin{cases} \omega_s C_a \left(1 - \dfrac{\tau}{\tau_{c,S}}\right) & \tau < \tau_{c,S} \\ 0 & \tau \geq \tau_{c,S} \end{cases}$$

$$\tau_{c,S} = \frac{\rho_s - \rho}{\rho_s} \frac{gh\omega_s C_k}{T_k U}$$

T_k is a calibration parameter which has been suggested to take a value of 0.0018 by Westrich and Juraschek (1985). The reference concentration C_a can be determined after van Rijn (1984b) (eq. 1.73) or Zyserman and Fredsøe (1994) (eq. 1.74). Alternatively, C_a can be set to the actual depth-averaged concentration C_k.

$$q_e = \begin{cases} M\left(\dfrac{\tau}{\tau_{c,E}} - 1\right)^n & \tau > \tau_{c,E} \\ 0 & \tau \leq \tau_{c,E} \end{cases}$$

With $\tau_{c,E} = \rho u_{*cr}^2$. M and n are calibration parameters.

1.2.3 Bed Load Transport

1.2.3.1 One Dimensional Bed Load Transport

1.2.3.1.1 Component of the Bed Load Flux

The bed load flux for the one-dimensional case consists of one single component for each grain size, namely the specific bed load flux in stream wise direction q_{B_g}.

1.2.3.1.2 Evaluation of Bed Load Transport due to Stream Forces

In the one-dimensional case, the total specific bed load flux due to stream forces is evaluated as follows:

$$q_{B_g} = \beta_g q_B(\xi_g) \tag{1.77}$$

Details about the transport laws for evaluation of q_B with or without the consideration of the hiding factor ξ_g can be found in Section 1.2.3.4.

1.2.3.1.3 Bed Material Sorting

For each fraction g a mass conservation equation can be written, the so called "bed-material sorting equation":

$$(1-p)\frac{\partial}{\partial t}(\beta_g \cdot h_m) + \frac{\partial q_{B_g}}{\partial x} + s_g - sf_g - sl_{B_g} = 0 \quad for \quad g = 1, ..., ng \tag{1.78}$$

where p = porosity of bed material (assumed to be constant), q_{B_g} = total bed load flux per unit width, sf_g = specific flux through the bottom of the active layer due to its movement and sl_{B_g} = source term per unit width to specify a local input or output of material (e.g. rock fall, dredging). The term s_g describes the exchange per unit width between the sediment and the suspended material (see Section 1.2.2.3).

1.2.3.1.4 Global Mass Conservation

Finally, the global bed material conservation equation is obtained by adding up the masses of all sediment material layers between the bed surface and a reference level for all fractions (Exner-equation) directly resulting in the elevation change of the actual bed level:

$$(1-p)\frac{\partial z_B}{\partial t} + \sum_{g=1}^{ng}\left(\frac{\partial q_{B_g}}{\partial x} + s_g - sl_{B_g}\right) = 0 \tag{1.79}$$

1.2.3.2 Two Dimensional Bed Load Transport

1.2.3.2.1 Components of the Bed Load Flux

The specific bed load flux in x direction is composed of three parts (an analogous relation exists in y direction):

$$q_{B_g,x} = q_{B_g,xx} + q_{B_g,xlateral} + q_{B_g,xgrav} \tag{1.80}$$

where (quantities per unit width) $q_{B_g,xx}$ = bed load transport due to flow in x direction, $q_{B_g,xlateral}$ = lateral transport in x-direction (due to bed load transport in y direction on sloped bed), $q_{B_g,xcurv}$ = transport due to curvature effect in x-direction, and $q_{B_g,xgrav}$ = pure gravity induced transport (e.g. due to collapse of a side slope).

1.2.3.2.2 Evaluation of Equilibrium Bed Load Transport

In the two-dimensional case, bed load transport is evaluated as follows

$$q_{B_g,xx} = \beta_g q_B(\xi_g) \cdot \boldsymbol{e}_x \tag{1.81}$$

The specific bed load discharge q_{B_g} of the g^{th} grain class has to be evaluated by a suitable transport law. Approaches for the bed load discharge $q_{B_g}(\xi_g)$ with or without the consideration of a hiding factor ξ_g are discussed in Section 1.2.3.4.

1.2.3.2.3 Bed Load Direction due to Lateral Bed Slope

Empirical bed load formulas were originally derived for situations where bed slope equals flow direction. However, in case of lateral bed slope with respect to flow direction, bed load direction differs from flow direction due to gravitational influence on the bed material, e.g. moving sediment particle on riverbank. Therefore, bed load direction is corrected for lateral bed slope based on the following approach (e.g. see Ikeda (1982); Talmon et al. (1995)):

$$\tan\varphi_b = -N_l \left(\frac{\tau'_{B_{cr,g}}}{\tau'_B} \right)^{\gamma} \vec{s} \cdot \vec{n}_q \tag{1.82}$$

where: φ_b = bed load direction with respect to the flow vector $\vec{q}$, N_l = lateral transport factor ($1.2 \leq N_l \leq 2.4$), γ = lateral transport exponent (default $\gamma = 0.5$), $\vec{s}$ = bed slope (positive uphill, negative downhill), $\vec{n}_q$ = is the unit vector perpendicular to $\vec{q}$ pointing in downhill direction ($\vec{s} \cdot \vec{n}_q < 0$) , τ'_B = dimensionless bed shear stress, and $\tau'_{B_{cr,g}}$ = dimensionless critical shear stress of the individual grain class.

1.2.3.2.4 Bed Load Direction due to Curvature Effect

Due to the presence of geometrical curvatures in rivers, the bed load direction may deviate from the depth averaged flow direction. Due to the three dimensional spiral flow motion, the bed load direction tends to point towards the inner side of the curve (Figure 1.4). This curvature effect is taken into account according to an approach proposed by Engelund (1974) , where the deviation angle φ_b (positive counterclockwise and vice versa) from the main flow direction is determined as

$$\tan\varphi_b = N_* \frac{h}{R} \tag{1.83}$$

where h denotes the water depth, N_* denotes a curvature factor, and R denotes the radius of the river bend (positive for curvature in counterclockwise direction and vice versa).

Note that the curvature factor N_* mainly depends on bed roughness. Therefore, $N_* \approx 7$ for natural streams (Engelund, 1974), and values up $N_* \approx 11$ for laboratory channels (Rozovskii, 1957).

1.2.3.2.5 Gravitational Bank Collapse

Gravitational induced riverbank or sidewall failures are significant aspects concerning erosion and transport modelling. Such processes may play an important role in many

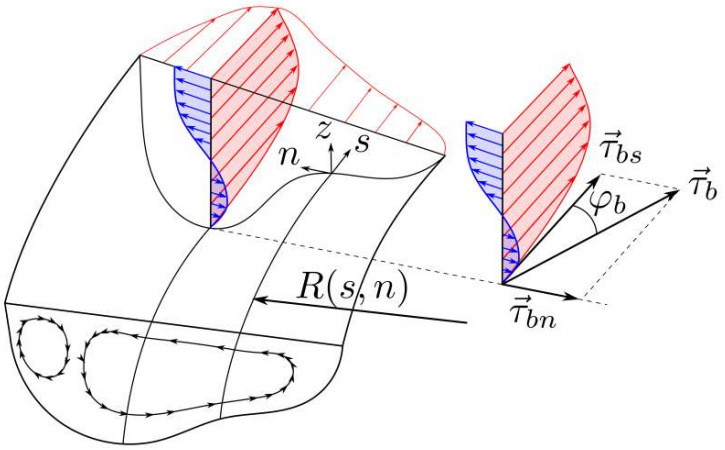

Figure 1.4 *Effect of spiral motion in river bend on bed shear stress τ_b with deviation angle from main flow direction φ_b, adapted from Blanckaert (2011)*

situations, such as meandering streams, river widenings or failures of erodible embankment structures due to overtopping waters. Such slope failure processes take place mostly discontinuous and can deliver significant contributions to the total sum of transported material.

The modes of slope failures can differ largely (falls, topples, slides, etc.) and depend on the soil material, the degree of soil compaction and the pore pressures within the soil matrix. Here, a simplified, geometric approach is applied to be able to consider some aspects of this purely gravitational induced transport.

This approach is based on the idea that a slope is flattened if its angle α becomes steeper than a given critical slope angle γ_{crit} .

$$q_{B_g,xgrav} = \begin{cases} 0 & \text{if } (\alpha \leq \gamma_{crit}) \\ f(\alpha, \gamma_{crit}) & \text{if } (\alpha > \gamma_{crit}) \end{cases} \tag{1.84}$$

The sliding material is moved from the sediment element with higher elevation to the lower situated element. Three characteristic critical slope angles are defined in this approach to have some flexibility in modelling the complex geotechnical aspects. The critical angles can be characterized as:

- critical angle for dry or partially saturated bank material which may greatly exceed the material's angle of repose (up to nearly vertical walls) due to negative pore pressures,
- critical angle for fully saturated and over flown material which is in the range of the material's angle of repose and
- a critical angle for deposited, not-compacted material.

A more physically based geotechnical approach, which takes into account more geotechnical considerations, is planned to be implemented in the future.

1.2.3.2.6 Bed Material Sorting

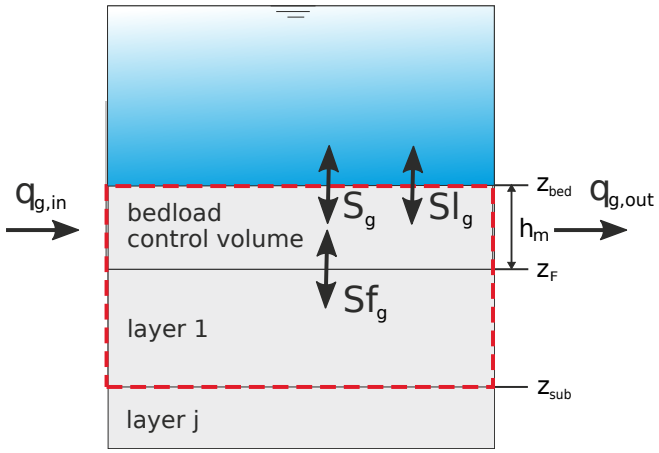

Figure 1.5 *Definition sketch of overall control volume (red) of bed material sorting equation*

The change of volume of a grain class g is balanced over the bed load control volume V_g and the underneath layer volume V_{sub_g} , as it is illustrated in Figure 1.5.

Depending on the bedload in- and outflows, the composition of the grain fractions in the bedload control volume can change. Futhermore three source terms are distinguished:

- External sediment sources or sinks can be specified (Sl_g).
- An exchange of sediment with the water column can take place (S_g).
- The movement of the bedload control volume bottom Z_F can lead to changes of the grain compositions within the bedload control volume and the underneath soil layer (Sf_g). (This is a special kind of source term, because it does not change the overall grain volume within the control volume indicated in Figure 1.5. It is not related with a physical movement of particles.)

For each grain class g a mass conservation equation can be written, the so called "bed-material sorting equation", which is used to determine the grain fractions β_g at the new time level

$$\frac{\partial V}{\partial t} = (1-p)\left[\underbrace{\frac{\partial(\beta_g \cdot h_m)}{\partial t}}_{\text{change of grain volume in bedload control volume}} + \underbrace{\frac{\partial(\beta_{sub_g} \cdot (z_F - z_{sub}))}{\partial t}}_{\text{change of grain volume in layer 1}=sf_g}\right]$$

$$= \underbrace{-\frac{\partial q_{B_g,x}}{\partial x} - \frac{\partial q_{B_g,y}}{\partial y}}_{\text{fluxes over boundary}} \underbrace{-s_g + sl_{Bg}}_{\text{source terms}}$$

Rearranging this sorting equation leads to following formulation which is used from here on

$$(1-p)\frac{\partial}{\partial t}(\beta_g \cdot h_m) + \frac{\partial q_{B_g,x}}{\partial x} + \frac{\partial q_{B_g,y}}{\partial y} + s_g - sf_g - sl_{B_g} = 0 \qquad for \quad g = 1, ..., ng \tag{1.85}$$

where h_m = thickness of bedload control volume, p = porosity of bed material (assumed to be constant), $(q_{B_g,x}, q_{B_g,y})$ = components of total bed load flux per unit width, sf_g = flux through the bottom of the bedload control volume due to its movement and sl_{B_g} = source term to specify a local input or output of material (e.g. rock fall, dredging).

1.2.3.2.7 Global Mass Conservation

The global bed material conservation equation, which is often called Exner-equation, is obtained by adding up the masses of all sediment material layers between the bed surface and a reference level. This is done for all grain fractions and directly results in the elevation change of the actual bed level z_B:

$$(1-p)\frac{\partial z_B}{\partial t} + \sum_{g=1}^{ng}\left(\frac{\partial q_{B_g,x}}{\partial x} + \frac{\partial q_{B_g,y}}{\partial y} + s_g - sl_{B_g}\right) = 0 \tag{1.86}$$

1.2.3.3 Sublayer Source Term

The bottom elevation of the bed load control volume z_F is identical to the top level of the underneath layer. If z_F moves up, sediment flows into this underneath layer and leads to changes in its grain compositions. The exchange of sediment particles between the bed load control volume and the underlying layer is expressed by the source term:

$$s_{f_g} = -(1-p)\frac{\partial}{\partial t}((z_F - z_{sub})\beta_{sub_g}) \tag{1.87}$$

1.2.3.4 Closures for Bed Load Transport

In the following a variety of bed load transport formulas are listed which are implemented to calculate the transport capacity. For practical purposes usually a calibration of the used formula is needed and several parameters can be adjusted by the user.

1.2.3.4.1 Meyer-Peter and Müller (MPM & MPM-Multi)

The bed load transport formula of Meyer-Peter and Müller (Meyer-Peter and Müller, 1948) can be written as follows:

$$q_{B_g} = \alpha\sqrt{(s-1)gd_g^3}\,(\theta_g - \theta_{cr,g})^m \tag{1.88}$$

Herein, α denotes the bed load factor (orginally $\alpha = 8$), m the bed load exponent (orginally $m = 1.5$), q_{B_g} is the specific bed load transport rate of grain class g, θ_g is the effective dimensionless shear stress for grain class g, $\theta_{cr,g}$ is the critical dimensionless shear stress for grain class g , d_g is the diameter of the grain class g, $s = \rho_s/\rho$ and g stands for the gravitational acceleration. Note that by adjusting α to 4.93 and m to 1.6, the bed load formula can be adapted accoring to Wong and Parker (2006).

Meyer-Peter and Müller observed in their experiments that the fist grains moved already for $\theta_{cr} = 0.03$. But as their experiments took place with steady conditions they used a value for which already 50% of the grains where moving. They proposed the value of 0.047.

However for very unsteady conditions one should use values for which the grains really start to move (Fäh, 1997) like the values given by the shields diagram.

The formula of Meyer-Peter and Müller is applicable in particular for coarse sand and gravel with grain diameters above 1 mm (Malcherek, 2001).

The original bed load transport formula is intended for single grain simulations. But an extension of the MPM-Formula for fractional transport is implemented in the program and called MPM-Multi. It uses the hiding function ξ_g proposed by Ashida and Michiue (1971):

$$\xi_g = \begin{cases} [\log(19)/\log(19 d_g/d_m)]^2 & d_g/d_m \geq 0.4 \\ d_m/d_g & d_g/d_m < 0.4 \end{cases} \tag{1.89}$$

d_g is the grain size diameter of grain class g and d_m the mean diameter of the grain mixture. The dimensionless critical shear stress of grain class becomes:

$$\theta_{cr,g} = \theta_{cr,ref} \xi_g, \tag{1.90}$$

where $\theta_{cr,ref}$ usually is assigned to a fix value (e.g. $\theta_{cr,ref} = 0.047$) or the critical Shields paramter of the mean grain size.

1.2.3.4.2 Ashida and Michiue

The bed load formula for non-uniform sediments according to Ashida and Michiue (Ashida and Michiue, 1971) reads

$$q_{B_g} = 17\sqrt{(s-1)g d_g^3}\,(\theta_g - \xi_g \theta_{cr,ref})(\sqrt{\theta_g} - \sqrt{\xi_g \theta_{cr,ref}}) \tag{1.91}$$

where q_{B_g} is the specific bed load transport rate of grain class g, θ_g is the dimensionless shear stress for grain class g, $\theta_{cr,ref}$ is the reference critical dimensionless shear stress (Ashida and Michiue (1971) proposed $\theta_{cr,ref} = 0.05$), d_g is the diameter of the grain class g, $s = \rho_s/\rho$, g is the gravitational acceleration, and ξ_g is the hiding function according to eq. 1.89.

1.2.3.4.3 Parker

Parker extended his empirical substrate-based bed load relation for gravel mixtures (G. Parker, 1990, Parker et al. (1982)), which was developed solely with reference to field data and suitable for near equilibrium mobile bed conditions, into a surfaced-based relation. The new relation is proper for non-equilibrium processes.

Based on the fact that the rough equality of bed load and substrate size distribution is attained by means of selective transport of surface material and the surface material is the source for bed load, Parker has developed the new relation based on the surface material. An important assumption in deriving the new relation is suspension cut-off size. Parker supposes that during flow conditions at which significant amounts of gravel are moved, it is commonly (but not universally) found that the sand moves essentially in suspension (1 to 6 mm). There for Parker has excluded sand from his analysis. In his free access Excel file, he has explicitly emphasised that the formula is valid only for the size larger than 2 mm. Regarding to the Oak Creek data, the original relation predicted 13% of the bed load as sand. For consistency it has to be corrected for the exclusion of sand and finer material.

$$W_{si}^{*} = 0.00218\, G[\xi_s \omega \phi_{sg0}] \quad ; \quad W_{si}^{*} = \frac{Rgq_{bi}}{(\tau_B/\rho)^{3/2} F_i} \tag{1.92}$$

where:

$$\xi_s = \left(\frac{d_i}{d_g}\right)^{-0.0951} \quad ; \quad \phi_{50} = \frac{\tau_{sg}^{*}}{\tau_{rsg0}^{*}} \quad ; \quad \tau_{sg}^{*} = \frac{\tau_B}{\rho R g d_g} \quad ; \quad \tau_{rsg0}^{*} = 0.0386$$

$$\omega = 1 + \frac{\sigma}{\sigma_0(\phi_{sg0})}[\omega_0(\phi_{sg0}) - 1] \quad ; \quad \sigma = \sum F_i \left[\frac{\ln(d_i/d_g)}{\ln(2)}\right]^2 \quad ; \quad d_g = e^{\sum F_i \ln(d_i)}$$

ξ_s is a "reduced" hiding function and differs from the one of Einstein. The Einstein hiding factor adjusts the mobility of each grain d_i in a mixture relative to the value that would be realized if the bed were covered with uniform material of size d_i. The new function adjusts the mobility of each grain di relative to the d_{50} or d_g , where d_g denotes the surface geometric mean size.

Although the above formulation does not contain a critical shear stress, the reference shear stress τ_{rsg0}^{*} makes up for it, in that transport rates are exceedingly small for $\tau_{sg}^{*} < \tau_{rsg0}^{*}$. Regarding to the fact that parker's relation is based on field data and field data are often in case of low flow rates, the relation calculates low bed load rates (Marti, 2006).

If this transport formula is used in combination with a local slope correction of the reference shear stress (see Section 1.2.1.1.2) attention must be paid that τ_{rsg0}^{*} may not become too small or even zero. Since this value is in the denominator of the transport formula, such situations may lead to numerical instabilities. To avoid these problems a minimum value is enforced:

$$\tau_{rsg0}^{*} = min(\tau_{rsg0}^{*,min}, \tau_{rsg0}^{*})$$

1.2.3.4.4 Wilcock and Crowe

Wilcock and Crowe developed a sediment transport model for sand/gravel mixtures (Wilcock, 2003), similar to Parker's model (G. Parker, 1990), and it was developed with a large experimental results dataset. It reference fractional transport rates to the size distribution of the bed surface, rather than the subsurface, making the model explicit and capable of predicting transient conditions. The hiding function incorporated in the model resolves discrepancies obvserved among earlier hiding functions implemented in other transport models, such as the Oak Creek and the Cambridge ones (A.J. Parker G.; Sutherland, 1990). Wilcock and Crowe model (Wilcock, 2003) uses the full grain size distribution of the bed surface, including sand, incorporating a non-linear effect of sand content on gravel transport rate.

$$W_{si}^{*} = G(\phi_i) \quad ; \quad W_{si}^{*} = \frac{Rgq_{bi}}{(\tau_B/\rho)^{3/2} F_i} \tag{1.93}$$

where:

$$G(\phi_i) = \begin{cases} 0.002\,\phi_i^{7.5} & \phi_i < 1.35 \\ 14\left(1 - \dfrac{0.894}{\phi_i^{0.5}}\right)^{4.5} & \phi_i \geq 1.35 \end{cases}$$

and:

$$\phi_i = \frac{\tau^*_{sg}}{\tau^*_{ssrg}} \frac{d_i}{d_g}^{-b} \quad ; \quad \tau^*_{ssrg} = \frac{\tau_B}{\rho R g d_g}$$
$$\tau^*_{ssrg} = 0.021 + 0.015 exp(-20F_s) \quad ; \quad b = \frac{0.67}{1 + exp(1.5 - \dfrac{d_i}{d_g})}$$

The non-linear effect of sand content F_s on gravel transport is taken into account in τ^*_{ssrg}. Wilcock and Crowe (Wilcock, 2003) have shown that increasing sand content in the bed active layer of a gravel-bed stream increases the surface gravel mobility. This effect is captured in their relationship between τ^*_{ssrg} (a surrogate for a critical Shields number) and the fraction sand in the active layer F_s. Note that τ^*_{ssrg} decreases as F_s increases, causing an increase of ϕ_i and in turn of the fraction bedload q_{bi}.

1.2.3.4.5 Hunziker (MPM-H)

Hunziker (1995) proposed a bed load formula for fractional bed load transport of graded sediment:

$$q_{Bg} = 5\beta_g[\xi_g(\theta'_{dms} - \theta_{cdms})]^{3/2}\sqrt{(s-1)g d^3_{ms}} \tag{1.94}$$

where θ'_{dms} denotes the Shields parameter of the mean grain size of the surface bed material d_{ms} according to eq. 1.95, ξ_g denotes the hiding function applied on the excess shear stress $(\theta'_{dms} - \theta_{cdms})$.

$$\theta'_{dms} = \frac{\tau'_b}{\rho_w\,(s-1)\,d_{ms}} \tag{1.95}$$

Note that due to the correction of the excess shear stress $(\theta'_{dms} - \theta_{cdms})$, the transport formula is based on the concept of "equal mobility", i.e. all grain classes start to move at same flow condition. The critical Shields parameter θ_{cdms} of the mean grain size diameter is determined according to

$$\theta_{cdms} = \theta_{ce}\left(\frac{d_{mo}}{d_{ms}}\right)^{0.33} \tag{1.96}$$

where θ_{ce} denotes the critical Shields parameter for incipient motion for uniform bed material. Two sediment layers are distinguished: the upper mixing layer which is in interaction with the flow and a subsurface layer below. Here, d_{ms} denotes the mean grain size diameter of surface bed material and d_{mo} denotes the mean grain size diameter of subsurface bed material. This relation (d_{ms}/d_{mo}) can be approximated as a function of the Shields parameter of the mean grain size of the surface bed material as

$$\frac{d_{ms}}{d_{mo}} = 0.0163\theta'^{-1.45}_{dms} + 0.6 \tag{1.97}$$

Finally, the hiding function is determined as

$$\xi_g = \left(\frac{d_g}{d_{ms}}\right)^{-\alpha} \tag{1.98}$$

where α is an empirical parameter depending on the Shields parameter (see also Hunziker and Jaeggi (2002)) according to eq. 1.99, which is limited to a range between -0.4 and 2.0.

$$\alpha = 0.011\theta'^{-1.5}_{dms} - 0.3 \tag{1.99}$$

1.2.3.4.6 Rickenmann

Experiments for bed load transport in gravel beds were performed at VAW ETH Zurich for bed slopes of 0.0004-0.023 by Meyer-Peter and Müller (1948) and for bed slopes of 0.03-0.2 by Smart and Jaeggi (1983) and by Rickenmann (1990). Rickenmann (1991) developed the following bed load transport formula for the entire slope range using 252 of these experiments.

$$\Phi_B = 3.1\left(\frac{d_{90}}{d_{30}}\right)^{0.2}\theta'^{0.5}(\theta' - \theta_{cr})Fr^{1.1}(s-1)^{-0.5} \tag{1.100}$$

$$q_B = \Phi_B((s-1)gd_m^3)^{0.5} \tag{1.101}$$

θ' is the dimensionless shear stress, θ_{cr} the dimensionless shear stress at the beginning of bed load transport, $s = \rho_s/\rho$ the sediment density coefficient, Fr the Froude number and d_m the mean grain size.

1.2.3.4.7 Smart and Jäggi (for single grain and multiple grain classes)

Experiments for bed load transport in gravel beds were performed at VAW ETH Zurich for bed slopes of 0.0004-0.023 by Meyer-Peter and Müller (1948) and for bed slopes of 0.03-0.2 by Smart and Jaeggi (1983) and by Rickenmann (1990). Smart and Jäggi developed a bed load transport formula for steep channels using their own experimental results and the results of Meyer-Peter and Müller.

$$q_B = \frac{4}{s-1}\left(\frac{d_{90}}{d_{30}}\right)^{0.2} J^{0.6}Ru(J - J_{cr}) \tag{1.102}$$

where s is the sediment density coefficient ($s = \rho_s/\rho$), R is the hydraulic radius, u is the velocity, J is the slope and J_{cr} is the critical slope for the initiation of the bed load transport, which is calculated as

$$J_{cr} = \frac{\theta_{cr}(s-1)d_m}{R} \tag{1.103}$$

where θ_{cr} is the critical shields parameter (for the initiation of motion) and d_m is the mean grain size. In order to account for the gravitational influence of the local bed slope Smart and Jaeggi (1983) proposed the following reduction of the critical shields parameter:

$$\theta_{cr} = \theta_{cr,Ref}(\cos(\arctan J))\left(1 - \frac{J}{\tan\psi}\right) \tag{1.104}$$

where J is the local bed slope, ψ the angle of repose and $\theta_{cr,Ref}$ the critical reference shields parameter for the medium grain size defined by the user (Smart and Jaeggi (1983) propose a value of 0.05).

The Smart & Jäggi transport formula is extended to multiple grain classes by applying the original equation to the individual grain classes according to the following approach:

$$q_{B,g} = \frac{4}{s-1}\left(\frac{d_{90}}{d_{30}}\right)^{0.2} J^{0.6} Ru(J - J_{cr,g}) \tag{1.105}$$

Compared to the original eq. 1.102 the transport rate for each grain class $q_{B,i}$ is calculated with the critical slope $J_{cr,g}$ for the initiation of motion of the grain class i according to

$$J_{cr,g} = \frac{\theta_{cr,g}(s-1)d_i}{R}$$

where $\theta_{cr,g}$ is the critical shields parameter for grain class g, d_g is the diameter of the grain class g.

With the term $\alpha = (d_{90}/d_{30})^{0.2}$ the original equation intends to account for the influence of the grain class distribution. According to Smart and Jaeggi (1983) this term is in the range of $1.06 \leq \alpha \leq 1.53$. If this term is to be neglected Smart and Jaeggi (1983) recommend substituting $\alpha = 1.05$. The influence of the grain class distribution is considered in the hiding and exposure approach according to Ashida and Michue (Ashida and Michiue, 1971; Parker, 2008) in eq. 1.106 and eq. 1.107.

$$\zeta_g = \begin{cases} 0.85\left(\dfrac{d_g}{d_m}\right)^{-1} & \text{for} \quad \dfrac{d_g}{d_m} \leq 0.4 \\ \left(\dfrac{\log(19)}{\log\left(19\dfrac{d_g}{d_m}\right)}\right)^2 & \text{for} \quad \dfrac{d_g}{d_m} > 0.4 \end{cases} \tag{1.106}$$

$$\theta_{cr,g} = \zeta_g \theta_{cr} \tag{1.107}$$

The critical shields parameter θ_{cr} is calculated according to eq. 1.104.

1.2.3.4.8 Wu

Wu et al. (2000) developed a transport formula for graded bed materials based on a new approach for the hiding and exposure mechanism of non-uniform transport. The hiding and exposure factor is assumed to be a function of the hidden and exposed probabilities, which are stochastically related to the size and gradation of bed materials. Based on this concept, formulas to calculate the critical shear stress of incipient motion and the fractional

bed-load transport have been established. Different laboratory and field data sets were used for these derivations.

The probabilities of grains d_g hidden and exposed by grains d_i is obtained from

$$p_{hid_g} = \sum_{i=1}^{ng} \beta_i \frac{d_i}{d_g + d_i}, \quad p_{exp_g} = \sum_{i=1}^{ng} \beta_i \frac{d_g}{d_g + d_i} \tag{1.108}$$

The critical dimensionless shields parameter for each grain class g can be calculated with the hiding and exposure factor η_g and the shields parameter of the mean grain size θ_{cr_m} as

$$\theta_{cr_g} = \theta_{cr_m} \underbrace{\left(\frac{p_{exp_g}}{p_{hid_g}} \right)^m}_{\eta_g} \tag{1.109}$$

The transport capacity now can be determined with Wu's formula in dimensionless form as

$$\Phi_{B_g} = 0.0053 \left[\frac{\theta'}{\theta_{cr_g}} - 1 \right]^{2.2} \tag{1.110}$$

Finally the bed load transport rates calculates for each grain fraction as

$$q_{b_g} = \beta_g \sqrt{(s-1) g d_g^3}\, \Phi_{B_g} \tag{1.111}$$

As results of their data analysis the authors recommend to set $m = -0.6$ and $\theta_{cr_m} = 0.03$ to obtain best results.

If this transport formula is used in combination with a local slope correction of the critical shear stress (see Section 1.2.1.1.2) attention must be paid that θ_{cr_g} may not become too small or even zero. Since this critical dimensionless shear stress is in the denominator of the transport formula, such situations may lead to numerical instabilities. To avoid these problems a minimum value for θ_{cr_g} is enforced.

$$\theta_{cr_g} = min(\theta_{cr}^{min}, \theta_{cr_g})$$

1.2.3.4.9 Van Rijn

van Rijn (1984a) developed a bed load formula for grain sizes between 0.2 and 2 mm according to eq. 1.112.

$$q_B = 0.053 \sqrt{(s-1) g}\, \frac{d_{50}^{1.5} T^{2.1}}{D_*^{0.3}} \tag{1.112}$$

Here D^* is the dimensionless grain diameter according to eq. 1.53 and T is the non-dimensional excess bed shear stress or the transport stage number, defined as

$$T = (u_* / u_{*cr})^2 - 1 \tag{1.113}$$

where u_* is the effective bed shear velocity determined as

$$u_* = u\sqrt{g}/C'_h \tag{1.114}$$

with $C'_h = 18\log(4h/d_{90})$.

u_{*cr} is the critical bed shear velocity, u is the mean flow velocity, h is the water depth, d_{50} and d_{90} are characteristic grain diameters of the bed material.

1.2.3.4.10 Engelund and Hansen

Engelund and Hansen (1972) proposed a bed load transport formula for uniform bed material

$$q_B = 0.05\sqrt{(s-1)g}\; c_f^2\theta^{2.5}d_f^{1.5} \tag{1.115}$$

where d_f denotes the mean fall diameter of the bed material and θ the Shields parameter. Note that this rather simple bed load formula does not consider critical Shields parameter.

1.2.3.4.11 Power Law

The power law bed load formula is a very simple approach. Therfore, no critical shear stress is taken into account and bed load transport only depends on the flow velocity u.

$$q_b = au^b \tag{1.116}$$

Coefficient a and exponent b are used as calibration parameter.

1.2.3.5 Abrasion in 1D

The reduction of the grain diameters by mechanical stress can be described by the approach of Sternberg (1875). It postulates, that the mass loss dM of a grain, which is transported over a distance of dx, is proportional to the achieved work $M \cdot g \cdot dx$. If the equation $(-dM = c \cdot M \cdot dx)$ is integrated over the distance from x_0 to x (where the mass of the grain at x_0 is M_0) one obtains the relation for the reduction of the mass of the grain:

$$M(x) = M_0 e^{-c(x-x_0)} \tag{1.117}$$

The abrasion coefficient of Sternberg c is determined empirically.

1.2.3.6 Sediment Boundary Conditions

The necessity of hydraulic boundary conditions for SWE and Saint-Venant equation were explained in Section 1.1.1.5 and Section 1.1.2.5 respectively. In case of bed load transport, boundary conditions are also needed to solve the bed load transport formula and calculate the transport capacity. Boundary conditions are defined upstream and downstream of the channel (i.e. at the inflow and outflow cross section). If no boundary condition is defined, a wall is assumed at the boundary and sediment transport will not occur.

1.2.3.6.1 Upstream boundary condition

The bed load input type is given by the upstream boundary condition. Three types of upstream boundary condition are available:

- sediment_discharge: based on a sediment hydrograph describing the bed load inflow at an upstream boundary in time.
- transport_capacity: based on a given mixture, the sediment inflow is calculated for every element by calculating the equilibrium transport capacity. In this case, it is required that the sediment inflow is defined on edges and an inflow hydrograph (set as hydraulic boundary condition) has to be defined.
- IOUp: this upstream boundary condition grants a constant bed level at the inflow. The same amount of sediment leaving the first computational cell in flow direction enters the cell from the upstream bound.

1.2.3.6.2 Downstream boundary condition

The IODown is the only downstream boundary condition available for sediment transport. It corresponds to the definition of IOup, where all sediment entering the last computational cell will leave the cell over the downstream boundary.

1.2.4 Enforced Bed Movement

In case the effect of bed movements on hydraulic variables want to be investigated, we can enforce grid nodes to move vertically with time. The movements are user defined, thus they are not coupled to any morphological calculations. These changes in the nodal elevation can be regarded as *enforced erosion or aggradation*.

The elevation update of the moving nodes is done right after the calculation of the hydraulic variables. The water depth and flow velocities are not touched, i.e. no change in the mass or impulse balance. Moving node(s) simply leads to a changed water surface in the next time step.

$$w_{S,t+1}^{forced} = z_{B,t}^{forced} + h_t \tag{1.118}$$

1.2.5 Random Bed Perturbation

Random bed perturbation can be applied to the bed topography during morphological simulations. Therefore, bed elevation is perturbed by

$$z_b^t = z_b^{t-1} + \varepsilon \tag{1.119}$$

where z_b^{t-1} denotes the bed elevation from the previous time step and ε is the perturbation offset. Bed perturbation is applied on all cells using randomly $-\varepsilon$, $+\varepsilon$, or zero.

1.3 Sub-surface flow

1.3.1 Introduction

Seepage analysis is an important part of geotechnical engineering and is, for example, required for design and stability evaluations of earth embankment structures. Solving the Richard's equation accounts for the flow in the saturated zone as well as in the unsaturated zone and allows for an accurate modelling of water infiltration into the soil.

Empirical constitutive models consisting of a retention curve and a relative hydraulic conductivity function allow for approximating the multi-phase flow in the unsaturated zone with a single partial differential equation. Thereby the assumption is made that the air phase is always continuous and at atmospheric pressure, which is often said to be accurate enough for most practical applications (Lam et al., 1987).

1.3.2 Governing equations

The Richard's equation is a non-linear partial differential equation, which can be formulated in form of an advection-diffusion equation. The soil moisture content θ [-] in the equation is defined as the effective water saturation $\theta = (\theta_0 - \theta_R)/(\theta_S - \theta_R)$, with θ_0 = water content, θ_R = residual water content and θ_S = saturated water content (=porosity). The other main variable is the pore pressure of the water within the embankment body which is described in a pressure head formulation as $h = p/(\rho g)$ [L].

The 3-D Richard's equation is applied in a moisture formulation for θ as primary variable as

$$\begin{aligned} &\frac{\partial \theta}{\partial t} - \nabla(K \nabla z) - \nabla(D\theta) = Q \\ &D = K \frac{\partial h}{\partial \theta} \end{aligned} \tag{1.120}$$

It is implemented also in a mixed moisture and pressure head formulation for θ and h as

$$\begin{aligned} &\frac{\partial \theta}{\partial t} - \nabla(K \nabla z) - \nabla(D \nabla h) = Q \\ &D = K \end{aligned} \tag{1.121}$$

where D is a diffusivity and K is the soil conductivity which is calculated as $K = k_r(\theta) k_f$, being the product of the dimensionless relative conductivity k_r [-] and the hydraulic soil conductivity k_f [L/T].

These formulations of the Richard's equation are made dimensionless for the computations using the cell size Δx as length scale and $\Delta x/\Delta t$ as velocity scale, leading to a "mesh speed" of c=1 in the model.

1.3.3 Constitutive relationships

Empirical closures for the retention curve $h = f(\theta)$ and the relative permeability function $k_r = f(\theta)$ are required to close Richard's equation. The retention function in soil sciences describes how much water is retained in the soil by the capillary pressure and can be seen as a description of the pore distributions of the soil. The relative conductivity function describes the water mobility within the unsaturated zone depending on the moisture contents. It equals 1.0 in the saturated zone and reduces to smaller values in the unsaturated zone, mainly due to longer flow paths. Two different empirical relationships are employed here, the approach after Brooks and Corey (1964) and Mualem (1976) (BCM) and a modified version of the van Genuchten (1980) and Mualem model (VGM).

For the BCM model the following relations are used

$$\begin{aligned} h(\theta) &= h_s \theta^{-1/\lambda} \\ k_r &= (h/h_S)^{-(4\lambda+2)} \\ \frac{\partial h}{\partial \theta} &= -\frac{h_S}{\lambda}\theta^{-1/\lambda-1} \end{aligned} \tag{1.122}$$

with λ [-] being a soil parameter.

For the modified VGM model the functions and derivate are as follows

$$\begin{aligned} h(\theta) &= \frac{-1}{\alpha}\left[-\varkappa\left(\frac{\beta}{\theta}\right)\right]^{1/n} \\ k_r &= \sqrt{\theta}\left(\frac{1-\varkappa^m\theta/\beta}{1-\varkappa^m 1/\beta}\right)^2 \\ \frac{\partial h}{\partial \theta} &= \frac{1-m}{\beta m\alpha}\frac{\theta^{-1/m-1}}{\beta} - \varkappa\left(\frac{\beta}{\theta}\right)^{-m} \end{aligned} \tag{1.123}$$

with $\varkappa(x) = 1 - x^{1/m}$ and $m = 1 - 1/n$. The empirical constants α [1/L] and n [-] describe the soil properties. The modified Version of the VGM model is used instead of the original VGM model in order to prevent infinite slopes $\partial h/\partial\theta$ at the transition to the saturated zone.

Following Ginzburg, the primary variable θ is used for the unsaturated zone as well as for the saturated zone. Therefore the retention curve $h(\theta)$, which is defined for the unsaturated zone only, is extrapolated linearly into the saturated zone as

$$h(\theta) = (\theta - 1)\left.\frac{\partial h}{\partial \theta}\right|_{\theta=1} + h_S \quad \theta \geq 1 - 0 \tag{1.124}$$

with $\partial h/\partial\theta$ being the gradient of the retention curve at the transition to the saturated zone ($\theta = 1.0$) and h_S [L] being the air entry pressure head, at which air can enter the pores when the soil is drained (= measure of the largest pore sizes).

This approach has the advantage that no special treatment and no change of variables regarding the saturated/unsaturated zones are necessary. However, it leads to an artificial

compressibility error in unsteady simulations. This error is neglected here, but can be mitigated in principle using sub-iterations (Ginzburg et al., 2004).

1.4 Morphodynamics and Vegetation

1.4.1 Introduction

Vegetation, as main biotic component of riverine environments, has a key role on shaping river morphology at a wide range of spatial and temporal scales. Above-ground biomass (plant canopy) affects the flow field altering turbulence structure and hydraulic roughness, while below-ground biomass (plant roots) modify sediment properties increasing the soil cohesion. Morphodynamic processes in turn affect vegetation survival mainly by causing burial and uprooting.

The hydrological regimes plays also an important role on the spatial distribution of vegetation by controlling seed dispersal and ensuring water and nutrients for plant growth. In riparian systems, the water table level usually represents the main source of water determining, in combination with the fluvial disturbance, a strong control on plant species distribution and composition on the elevation gradient. As a result, each species is characterized by a specific range of elevations in which its optimal conditions are met. The timescale at which vegetation reaches its equilibrium value may vary across environments and among species, allowing for the co-existence of vegetation patterns with different biomass densities.

1.4.2 Mathematical model

The mathematical model accounting for the main feedback between river morphodynamics and vegetation and implemented in BASEMENT has been developed by a joint research between the Laboratory of Hydraulics, Hydrology and Glaciology (VAW) at ETH Zurich and the Department of Civil, Environmental and Mechanical Engineering at University of Trento (Italy). Model and results are presented in Bertoldi et al. (2014). This approach is built upon three main cornerstones that describe:

- the vegetation biomass dynamics depending on species-specific parameters;
- the feedback mechanisms between river morphodynamic processes and vegetation;
- the mean water table level (groundwater) computed by adopting a simple spatial interpolation method.

1.4.3 Vegetation dynamics

In Figure 1.6, the blue line represents the water discharge through time and the dotted brown line corresponds to the discharge at which the Shields parameter θ reaches its critical value θ_{cr}, needed for the onset of sediment transport. Vegetation growth ($\frac{\partial B}{\partial t} > 0$) is enabled only during the time frame T_v, where $\theta \leq \theta_{cr}$, while is inhibited during T_m, in which sediment transport takes place ($\theta > \theta_{cr}$). During T_m, if uprooting occurs, vegetation biomass is assumed to instantaneously decrease to $B = 0$, otherwise it does not change until the beginning of subsequent vegetation growth phase (T_v).

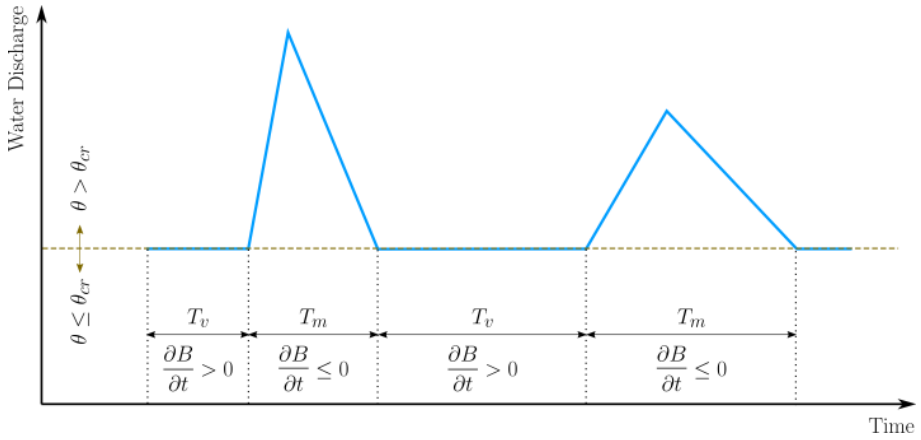

Figure 1.6 *Schematic illustration of the time frame concept used in the vegetation module.*

Vegetation is described with a dimensionless biomass density B in which both above-ground and below-ground are lumped. Within each computational cell a value of B is defined with respect to a reference dimensional value B_{max} [kg m^{-2}], representing its maximum carrying capacity. Following Marani et al, we can define an equilibrium biomass B_{eq}, normalized by its maximum, as

$$B_{eq} = \frac{1}{exp[\lambda_1(z - z_0)] + exp[-\lambda_2(z - z_0)]} \tag{1.125}$$

in which z is the bed elevation, the parameters λ_1 and λ_2 define the rate at which vegetation fitness diminishes away from it maximum, while z_0 represents the optimal elevation above the mean water table level z_w. If $\lambda_1 = \lambda_2$, B_{eq} represents a bell-shaped function with its maximum at the elevation $z_w + z_0$, such as $B_{eq}(z_w + z_0) = B_{max}$. Adopting different values of the parameters λ_1, λ_2 and z_0 correspond to modeling different species or type of vegetation that are adapted to grow in specific range of elevations. For instance, specialized vegetation would have higher values of $\lambda_{1,2}$, while species with greater tolerance to drought can be characterized by higher value of z_0 (more distant to the mean water level z_w).

Vegetation growth is governed by a logistic differential equation (non-linear ordinary differential equation)

$$\frac{dB}{dt} = \sigma B(t)\left[1 - \frac{B(t)}{B_{eq}(z)}\right] \tag{1.126}$$

where σ represents the vegetation grow rate [s^{-1}]. The timescale of vegetation growth is significantly higher when compared to the morphological timescale. The time needed for a riparian species to reach its maximum expansion (i.e. $B = B_{max}$), under optimal conditions, ranges from years to decades, while the timescale at which bed level changes occur, for example during a flood event, ranges from hours to days. In addition, rivers often experience only a few events that causes riverbed changes during the year. To allow for computationally feasible simulations while including all those timescales, vegetation dynamics and morphodynamic processes have been decoupled. Vegetation growth is enabled during the time frame (T_v) in which morphological changes do not occur (e.g. during low flow period), whereas it is inhibited during high flows, where sediment transport and morphodynamic processes take place (time frame T_m, see Figure 1.6). Since during T_v

riverbed does not change, we can significantly reduce computational time by decreasing T_v and increasing the grow rate of vegetation (σ), without affecting hydro-morphodynamic processes.

From a computational point of view, eq. 1.126 is integrated by using a classical Euler method with an integration timestep that equals the timestep computed for morphodynamics.

1.4.4 Feedback

1.4.4.1 Vegetation effects on hydro-morphodynamics

Vegetation increases the hydraulic roughness depending on the abundance and type. By adopting the Manning-Strickler approach for calculation of the friction factor c_f, we assume

$$K_s = K_{s,g} + (K_{s,g} - K_{s,v})\frac{B}{B_{max}} \tag{1.127}$$

where K_s $[m^{1/3}\ s^{-1}]$ is the Strickler coefficient and $K_{s,g}$ and $K_{s,v}$ refer to the values attributed to the grain and the vegetation, respectively. $K_{s,v}$ is a lumped variable encompassing a variety of plant characteristics (e.g. stiffness, bending ability, crown area and leaves density) and different plant life stages.

The modifications of the flow field have a profound effect on sediment transport as well. In vegetated flows the friction factor incorporates not only the friction located at the bottom of the river but also the drag generated by the vegetation. Therefore we assume that the shear stresses τ_g, responsible for sediment transport, decreases as a function of the grain-related roughness $K_{s,g}$. Although this approach can be generalized to any transport formula, the model only accounts for the Meyer-Peter and Müller formula (no other formulas are allowed with vegetation module activated). In term of dimensionless shear stress θ (Shield parameter), it can be derived as

$$\frac{\theta}{\theta'} = \left(\frac{K_{s,g}}{K_{s,v}}\right)^2 \tag{1.128}$$

where θ' represents the effective dimensionless shear stress applied at the bottom of the river. Notably, this strategy is similar to the correction factor applied to limit sediment transport in case of bed forms with the Meyer-Peter and Müller formula.

The presence of vegetation also changes the sediment properties, increasing the sediment cohesion and reinforcing the soil matrix. This results in a reduction of the sediment mobility and a consequent modification of the threshold for the onset of sediment transport (in case of bed load). Similarly to the added roughness by the vegetation, this can be modeled as

$$\theta_{cr} = \theta_{cr,g} + (\theta_{cr,v} - \theta_{cr,g})\frac{B}{B_{max}} \tag{1.129}$$

in which θ_{cr} represents the critical value of the Shields number that has to be exceeded to have sediment transport. $\theta_{cr,v}$ is the value attributed in presence of vegetation, while $\theta_{cr,g}$ is the typical value for gravel. This effect is usually considered to be dependent on the below-ground vegetation biomass, i.e. plant roots, and its characteristics. Here, we

assume that the biomass density B is representative of the overall plant biomass, with no distinction between above-ground (plant canopy) and below-ground biomass.

1.4.4.2 Hydro-morphodynamic effects on vegetation

Hydro-morphological processes have a significant impact of vegetation distribution determining plant removal by uprooting, which occurs when the resistance provided by the plant roots equals the pull-out forces on the canopy. Recent studies suggest that plants are able to increase their resistance to uprooting by growing large root systems. Therefore, we assume that vegetation, during morphological phases (T_m), can be uprooted by flow erosion when the bed level changes Δz exceed a threshold value z_{upr}. The latter represents a lumped estimation of the rooting depth.

1.4.5 Range of the parameters used in previous works

Model parameters used in previous publications (Bertoldi et al. (2014), Li and Millar (2011), Zen et al. (2016)) are reported in Table 1.3.

Table 1.3 *Vegetation Parameters*

Parameter	Range [min, max]	References
λ_1 $[m^{-1}]$	[0, 6]	Bertoldi et al. (2014), Zen et al. (2016)
λ_2 $[m^{-1}]$	[0.4, 100]	Bertoldi et al. (2014), Zen et al. (2016)
z_0 $[m]$	[0.5, 1.25]	Bertoldi et al. (2014), Zen et al. (2016)
$K_{s,v}$ $[m^{1/3}s^{-1}]$	[9, 17]	Bertoldi et al. (2014), Zen et al. (2016), Li and Millar (2011)
$\theta_{cr,v}$ $[-]$	[0.055, 0.21]	Bertoldi et al. (2014), Zen et al. (2016), Li and Millar (2011)

1.4.6 Reconstruction of the position of the mean water table

The key assumption used for the calculation of the position of the mean water table is that the water table level z_w instantaneously match the river water stage, which holds for gravel bed substrates in proximity to the river. z_w is computed by using the Inverse Distance Weighting method (IDW), a popular deterministic model adopted in spatial interpolation. The basic assumption of the model is that the values of any given pair of points are related to each other, but their similarities are inversely related to the distance between their locations (Lu and Wong, 2008). IDW assumes that the unknown value of the variable in location $S_j = (x_j, y_j)$ can be estimated by the observed value at sample location $S_i = (x_i, y_i)$. Here, the unknown variable is represented by the water table elevation in dry cells, $\hat{z}_w$, while its observed value is the water surface elevation in submerged cells, z_w. Formally, given the number of known locations N, the model reads

$$\hat{z}_w(x_j, y_j) = \sum_{i=1}^{N} \alpha_i z_w(x_i, y_i) \tag{1.130}$$

where the estimated value $\hat{z}_w(x_j, y_j)$ is a linear combination of the weights α_i and the

known value $z_w(x_i, y_i)$. α_i can be written as

$$\alpha_i = \frac{d_{j,i}^{-\gamma}}{\sum_{i=1}^{N} d_{j,i}^{-\gamma}} \tag{1.131}$$

with

$$\sum_{i=1}^{N} \alpha_i = 1 \tag{1.132}$$

in which $d_{j,i}$ is the distance between S_i and S_j and γ a parameter used to account for the so-called distance-decay effect. IDW, in fact, assumes that the local influence of a know variable decreases with the distance ($d_{j,i}$), where greater weights α_i are given to the points closest to the location S_j. As such, γ measures the rate at which the weights decrease with the distance. If $\gamma = 0$, there is no decrease with the distance and the method results on a mean of the known variables, while at higher values only the immediate surrounding points from the location of the unknown variable affect the prediction.

Because of the decreasing similarities with the distance between any pair of points, to speed calculation, we can exclude the more distant points from the location of the unknown variable S_j. This is obtained by specifying a radius r [m] centered in such location, within which the algorithm searches the known values of the variable (z_w) for the interpolation. In addition, the search can be also limited by a specific number of points surrounding the prediction location (default = 3).

2

Numerics Kernel

2.1 General View

There is great improvement in the development of numerical models for free surface flows and sediment movement in the last decade. The presented number of publications about these subjects proves this clearly. The SWE and the sediment flow equation are a nonlinear, coupled partial differential equations system. A unique analytical solution is only possible for idealised and simple conditions. For practical cases, it is required to implement the numerical methods. A numerical solution arises from the discretisation of the equations. There are different methods to discretize the equations such as:

- Finite difference.....(FD)
- Finite volume.....(FV)
- Finite element.....(FE)
- Characteristic Method.....(CM)

It is normally distinguished between temporal and spatial discretisation of continuum equations. The latter can be undertaken on different forms of grids such as Cartesian, non-orthogonal, structured and unstructured, while the former is usually done by a FD scheme in time direction, which can be explicit or implicit. The explicit method is usually used for strong unsteady flows.

In FD methods the partial derivations of equations are approximated by using Taylor series. This method is particularly appropriate for an equidistant Cartesian mesh. In FV methods; the partial derivations of equations are not directly approximated like in FD methods. Instead of that, the equations are integrated over a volume, which is defined by nodes of grids on the mesh. The volume integral terms will be replaced by surface integrals using the Gauss formula. These surface integrals define the convective and diffusive fluxes through the surfaces. Due to the integration over the volume, the method is fully conservative. This is an important property of FV methods. It is known that in order to simulate discontinuous transition phenomena such as flood propagation, one must use conservative

numerical methods. In fact, 40 years ago Lax and Wendroff proved mathematically that conservative numerical methods, if convergent, do converge to the correct solution of the equations. More recently, Hou and LeFloch proved a complementary theorem, which says that if a non-conservative method is used, then the wrong solution will be computed, if this contains a discontinuity such as a shock wave (Toro, 2001).

The FE methods originated from the structural analysis field as a result of many years of research, mainly between 1940 and 1960. In this method the problem domain is ideally subdivided into a collection of small regions, of finite dimensions, called finite elements. The elements have either a triangular or a quadrilateral form (Figure 2.1) and can be rectilinear or curved. After subdivision of the domain, the solution of discrete problem is assumed to have a prescribed form. This representation of the solution is strongly linked to the geometric division of sub domains and characterized by the prescribed nodal values of the mesh. These prescribed nodal values must be determined in such way that the partial differential equations are satisfied. The errors of the assumed prescribed solution are computed over each element and then the error must be minimised over the whole system. One way to do this is to multiply the error with some weighting function $\omega(x, y)$, integrate over the region and require that this weighted-average error is zero. The finite volume method has been used in this study; therefore it is explained in more detailed.

In this chapter it will be reviewed how the governing equations comprising the SWE and the bed-updating equation, can be numerically approximated with accuracy. The first section studies the fundamentals of the applied methods, namely the finite volume method and subsequently the hydro- and morphodynamic models are discussed. In section on the hydrodynamic model, the numerical approximate formulation of the SWE, the flux estimation based on the Riemann problem and solver and related problems such as boundary conditions will be analyzed. In the section on morphodynamics, the numerical determination of the bed shear stress and the numerical treatment of bed slope stability will be discussed as well as numerical approximation of the bed-updating equation.

2.2 Methods for Solving the Flow Equations

2.2.1 Fundamentals

2.2.1.1 Finite Volume Method

The basic laws of fluid dynamics and sediment flow are conservation equations; they are statements that express the conservation of mass, momentum and energy in a volume enclosed by a surface. Conversion of these laws into partial differential equations requires sufficient regularity of the solutions.

This condition of regularity cannot always undoubtedly be guaranteed. The case of occurring of discontinuities is a situation where an accurate representation of the conservation laws is important in a numerical method. In other words, it is extremely important that these conservation equations are accurately represented in their integral form. The most natural method to achieve this is obviously to discretize the integral form of the equations and not the differential form. This is the basis of the finite volume (FV) method. Actually the finite volume method is in fact in the classification of the weighted residual method (FE) and hence it is conceptually different from the finite difference method. The weighted function is chosen equal unity in the finite volume method.

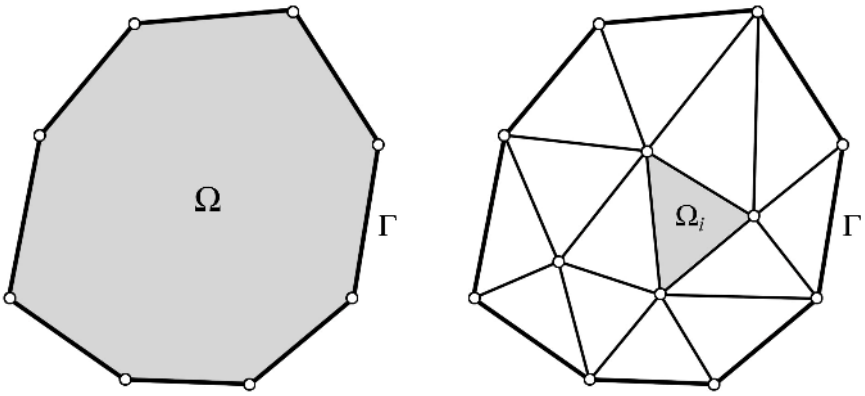

Figure 2.1 *Triangular Finite Elements of a Two-Dimensional Domain*

In this method, the flow field or domain is subdivided, as in the finite element method, into a set of non-overlapping cells that cover the whole domain on which the equations are applied. On each cell the conservation laws are applied to determine the flow variables in some discrete points of the cells, called nodes, which are at typical locations of the cells such as cell centres (cell centred mesh) or cell-vertices (cell vertex mesh) (Figure 2.2).

Obviously, there is basically considerable freedom in the choice of the cell shapes. They can be triangular, quadrilateral etc. and generate a structured or an unstructured mesh. Due to this unstructured form ability, very complex geometries can be handled with ease. This is clearly an important advantage of the method. Additionally the solution on the cell is not strongly linked to the geometric representation of the domain. This is another important advantage of the finite volume method in contrast to the finite element method.

2.2.1.2 The Riemann Problem

Formally, the Riemann problem is defined as an initial-value problem (IVP):

$$\left.\begin{aligned} &\mathbf{U}_t + \mathbf{F}_x(\mathbf{U}) = 0 \\ &\mathbf{U}(x,0) = \begin{cases} \mathbf{U}_L & \forall \quad x < 0 \\ \mathbf{U}_R & \forall \quad x > 0 \end{cases} \end{aligned}\right\} \tag{2.1}$$

Here eq. 1.36 and eq. 1.37 are considered for the x-split of SWE. The initial states $\mathbf{U}_L$, $\mathbf{U}_R$ at the left or right side of an triangle edge

$$\boldsymbol{U}_L = \begin{pmatrix} h_L \\ u_L h_L \\ \nu_L h_L \end{pmatrix}$$

$$\boldsymbol{U}_R = \begin{pmatrix} h_R \\ u_R h_R \\ \nu_R h_R \end{pmatrix}$$

are constant vectors and present conditions to the left of axes $x = 0$ and to the right $x = 0$, respectively (Figure 2.3).

There are four possible wave patterns that may occur in the solution of the Riemann

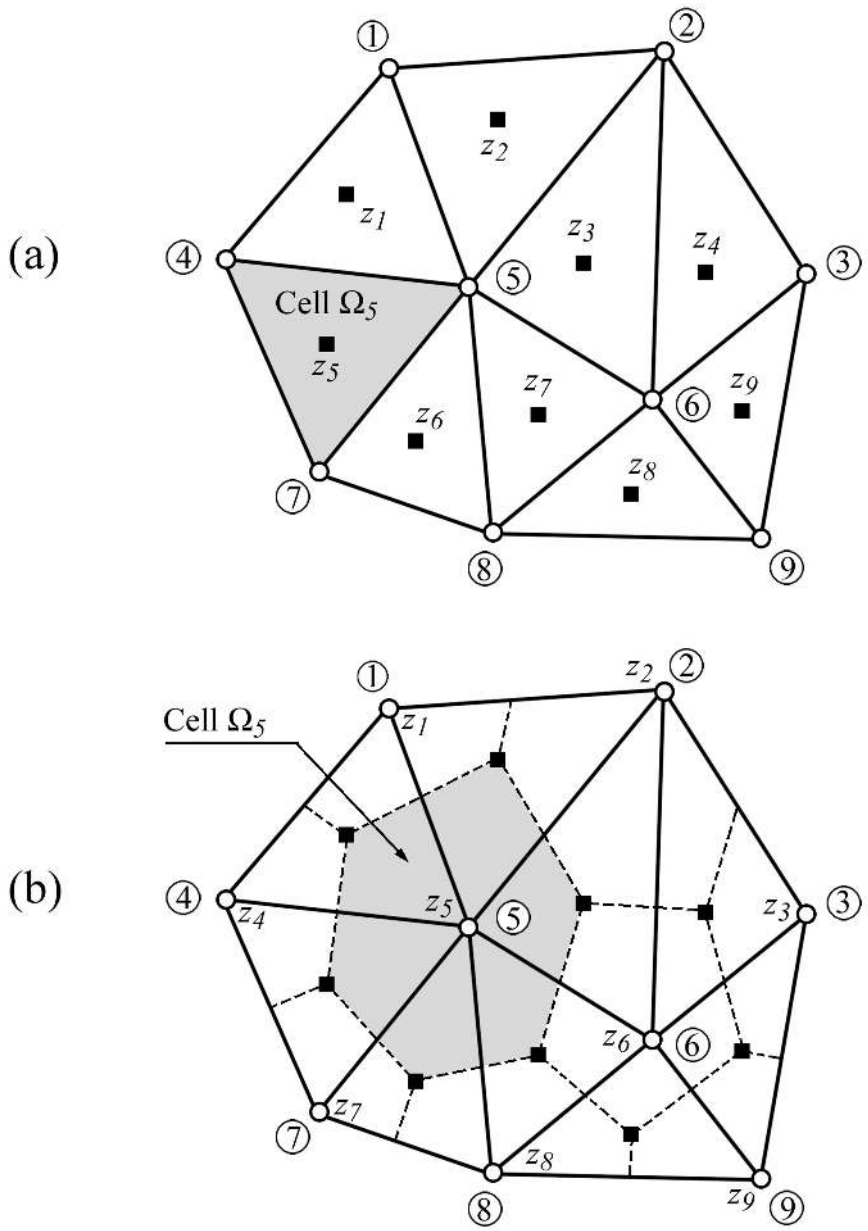

Figure 2.2 *Two-Dimensional Finite Volume Mesh: (a) Cell Centered mesh (b) Cell Vertex mesh*

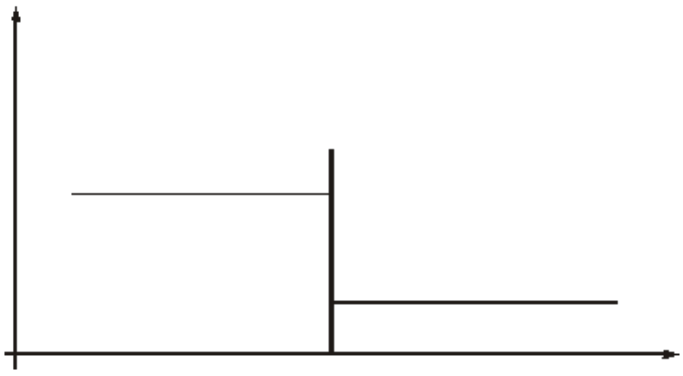

Figure 2.3 *Initial Data for Riemann Problem*

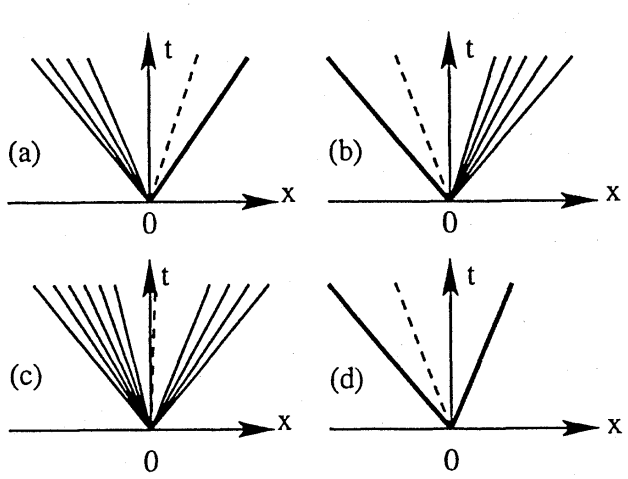

Figure 2.4 *Possible Wave Patterns in the Solution of Riemann Problem*

problem. These are depicted in Figure 2.4. In general, the left and right waves are shocks and rarefactions, while the middle wave is always a shear wave. A shock is a discontinuity that travels with Rankine-Hugoniot shock speed. A rarefaction is a smoothly varying solution which is a function of the variable x/t only and exists if the eigenvalues of $\boldsymbol{J} = \partial \boldsymbol{F}(\boldsymbol{U})/\partial \boldsymbol{U}$ are all real and the eigenvectors are complete. The water depth and the *normal* velocity are both constant across the shear wave, while the *tangential* velocity component changes discontinuously (see Toro (1997) for details about Riemann problem).

By solving the IVP of Riemann (eq. 2.1), the desired outward flux $\boldsymbol{F}(\boldsymbol{U})$ which is at the origin of local axes $x = 0$ and the time $t = 0$ can be obtained.

2.2.1.3 Exact Riemann Solvers

An algorithm, which solves the Riemann initial-value problem is called Riemann solver. The idea of Riemann solver application in numerical methods was used for the first time by Godunov (1959). He presented a shock-capturing method, which has the ability to resolve strong wave interaction and flows including steep gradients such as bores and shear waves. The so called Godunov type upwind methods originate from the work of Godunov. These methods have become a mature technology in the aerospace industry and in scientific disciplines, such as astrophysics. The Riemann solver application to SWE is more recent. It was first attempted by Glaister (1988) as a pioneering attack on shallow water flow problems in 1-D cases.

In the algorithm pioneered by Godunov, the initial data in each cell on either side of an interface is presented by piecewise constant states with a discontinuity at the cell interface (Figure 2.5). At the interface the Riemann problem is solved exactly. The exact solution in each cell is then replaced by new piecewise constant approximation. Godunov's method is conservative and satisfies an entropy condition (Delis et al., 2000). The solution of Godunov is an exact solution of Riemann problem; however, the exact solution is related to a simplified problem since the initial data is approximated in each cell.

To compute numerical solutions by Godunov type methods, the exact Riemann solver or approximate Riemann solver can be used. The choice between the exact and approximate Riemann Solvers depends on:

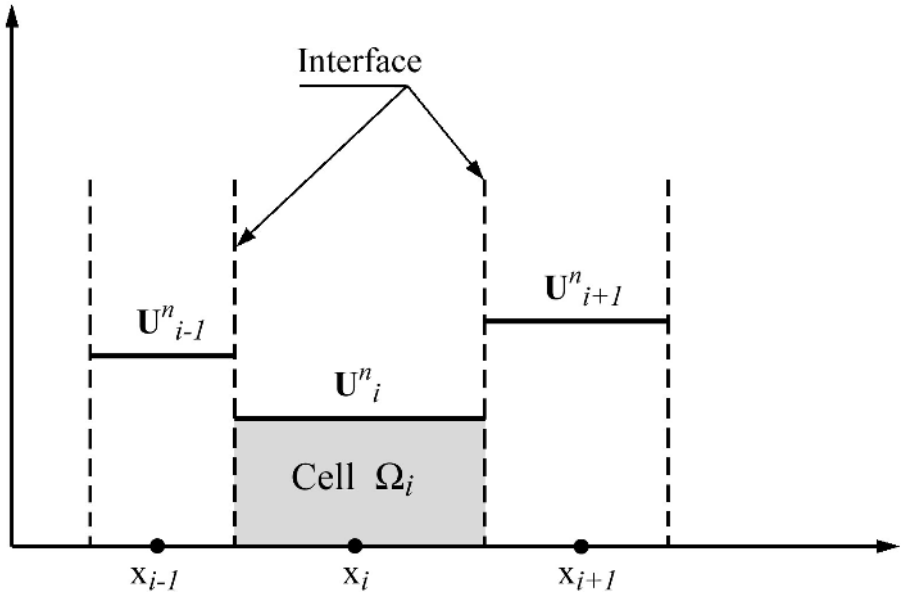

Figure 2.5 *Piecewise constant data of Godunov upwind method*

- Computational cost
- Simplicity and applicability
- Correctness

Correctness seems to be the overriding criterion; however the applicability can be also very important. Toro argued that for the shallow water equations, the argument of computational cost is not as strong as for the Euler equations. For the SWE approximate Riemann solvers may lead to savings in computation time of the order of 20%, with respect to the exact Riemann solvers (Toro, 2001). However, due to the iterative approach of the exact Riemann solver on SWE, its implementation of this will be more complicated if some extra equations, such as dispersion and turbulence equations, are solved together with SWE. Since for these new equations new Riemann solvers are needed, which include new iterative approaches, complications seem to be inevitable. Therefore, an approximate solution which retains the relevant features of the exact solution is desirable. This led to the implementation of approximate Riemann solvers which are non-iterative and therefore, in general, more efficient than the exact solvers.

2.2.1.4 Approximate Riemann Solvers

Several researchers in aerodynamics have developed approximate Riemann solvers for the Euler equations, such as Flux Difference Splitting (FDS) by Roe (1981), Flux Vector Splitting (FVS) by van Leer (1982) and approximate Riemann Solver by Harten et al. (1983); Osher and Solomon (1982). The first two approximate Riemann solvers have been frequently used in aerodynamics as well as in hydrodynamics.

In addition to the exact Riemann solver, the HLL and HLLC approximate Riemann solvers have been implemented in the code.

2.2.1.4.1 HLL Riemann Solver

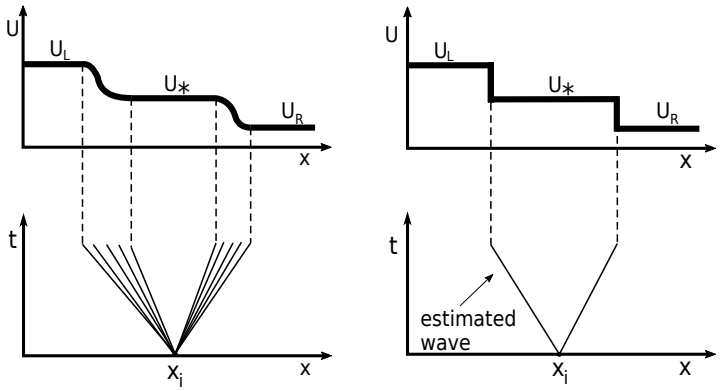

Figure 2.6 *Principle of the HLL Riemann Solver. The analytical solution (left) is replaced by an approximate one with a constant state U_* separated by waves with estimated wave speeds (right)*

The HLL (Harten, Lax and van Leer) approximate Riemann solver devised by Harten et al. (1983) is used widely in shallow water models. It is a Godunov-type scheme based on the two-wave assumption. This approach assumes estimates for the wave speeds of the left and right waves. The solution of the Riemann problem between the two waves is thereby approximated by a constant state as indicated in Figure 2.6. This two-wave assumption is only strictly valid for the one dimensional case. When applied to two dimensional cases, the intermediate waves are neglected in this approach.

The HLL solver is very efficient and robust for many inviscid applications such as SWE.

By applying the integral form of the conservation laws in appropriate control volumes the HLL-flux is derived. The numerical flux over an edge is sampled between three different cases separated by the left and right waves. The indices L and R stand for the left and right states of the local Riemann problem.

$$\boldsymbol{F}_{i+1/2} = \begin{cases} \boldsymbol{F}_L & if \quad 0 \leq S_L, \\ \boldsymbol{F}^{hll} = \dfrac{S_R\boldsymbol{F}_L - S_L\boldsymbol{F}_R + S_RS_L(\boldsymbol{U}_R - \boldsymbol{U}_L)}{S_R - S_L} & if \quad S_L \leq 0 \leq S_R, \\ \boldsymbol{F}_R & if \quad 0 \geq S_R. \end{cases} \tag{2.2}$$

Furthermore, the left and right wave speed velocities are estimated as

$$S_L = u_L - \sqrt{gh_L}q_L \; ; \; S_R = u_R + \sqrt{gh_R}q_R \tag{2.3}$$

where $q_K (K = L, R)$ are

$$q_K = \begin{cases} \sqrt{\frac{1}{2}\left[\frac{(h_*+h_K)h_*}{h_K^2}\right]} & if \quad h_* > h_K, \\ 1 & if \quad h_* \leq h_K. \end{cases} \tag{2.4}$$

The quantity h_* is an estimate for the exact solution of the water depth in the star region

obtained using the depth positivity condition. It reads as

$$h_* = \frac{1}{2}(h_L + h_R) - \frac{1}{4}(u_R - u_L)(h_L - h_R)/(\sqrt{gh_L} + \sqrt{gh_R}) \tag{2.5}$$

In case of dry-bed conditions, the wave speed estimations are modified as follow:

$$\begin{aligned} S_L &= \begin{cases} u_R - 2\sqrt{gh_R} & if \quad h_L = 0, \\ usualestimate & if \quad h_L > 0, \end{cases} \\ S_R &= \begin{cases} u_L + 2\sqrt{gh_L} & if \quad h_R = 0, \\ usualestimate & if \quad h_R > 0. \end{cases} \end{aligned} \tag{2.6}$$

2.2.1.4.2 HLLC Riemann Solver

A modification and improvement of the HLL approximate solver was proposed by Toro (1994). This so called HLLC approximate Riemann solver also accounts for the impact of intermediate waves, such as shear waves and contact discontinuities, in two dimensional problems. In addition to the estimates of left and right wave speeds, the HLLC solver also requires an estimate for the speed of the middle wave. This middle wave than divides the region between the left and right waves into two constant states.

The numerical flux over an edge is sampled regarding four different cases as

$$\boldsymbol{F}_{i+1/2} = \begin{cases} \boldsymbol{F}_L & if \quad 0 \leq S_L, \\ \boldsymbol{F}_{*L} = \boldsymbol{F}_L + S_L(\boldsymbol{U}_{*L} - \boldsymbol{U}_L) & if \quad S_L \leq 0 \leq S_*, \\ \boldsymbol{F}_{*R} = \boldsymbol{F}_R + S_R(\boldsymbol{U}_{*R} - \boldsymbol{U}_R) & if \quad S_* \leq 0 \leq S_R, \\ \boldsymbol{F}_R & if \quad 0 \geq S_R. \end{cases} \tag{2.7}$$

The states $\boldsymbol{U}_{*L}, \boldsymbol{U}_{*R}$ are obtained, as proposed by Toro (1997), from the relations

$$\boldsymbol{U}_{*L} = h_L \left(\frac{S_L - u_L}{S_L - S_*} \right) \begin{bmatrix} 1 \\ S_* \\ \nu_L \end{bmatrix} \quad ; \quad \boldsymbol{U}_{*R} = h_R \left(\frac{S_R - u_R}{S_R - S_*} \right) \begin{bmatrix} 1 \\ S_* \\ \nu_R \end{bmatrix} \tag{2.8}$$

S_L, S_* and S_R are the estimated wave speeds for the left, middle and right waves. S_L and S_R are estimated according to eq. 2.3 or eq. 2.6 for the dry bed case. with h_* given by eq. 2.5.

The middle wave speed S_* is calculated as proposed by Toro (1997) in a suitable way for taking into account dry-bed problems as

$$S_* = \frac{S_L h_R(u_R - S_R) - S_R h_L(u_L - S_L)}{h_R(u_R - S_R) - h_L(u_L - S_L)} \tag{2.9}$$

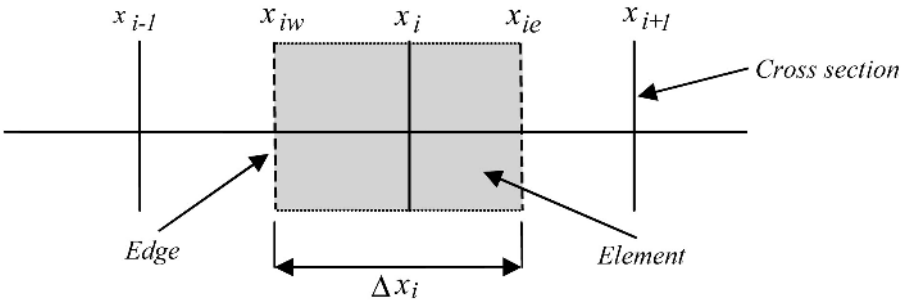

Figure 2.7 *Definition sketch*

2.2.2 Saint-Venant Equations

2.2.2.1 Spatial Discretisation

The time Discretisation is based on the explicit Euler schema, where the new values are calculated considering only values from the precedent time step. The spatial Discretisation of the Saint Venant equations is carried out by the finite volume method, where the differential equations are integrated over the single elements.

It is assumed that values, which are known at the cross section location, are constant within the element. Throughout this section it therefore can be stated that:

$$\int_{x_{iL}}^{x_{iR}} f(x)\, dx \approx f(x_i)(x_{iR} - x_{iL}) = f_i \Delta x_i \tag{2.10}$$

where x_{iR} and x_{iL} are the positions of the edges at the east and the west side of element i, as illustrated in Figure 2.7.

2.2.2.2 Discrete Form of Equations

2.2.2.2.1 Continuity Equation

The eq. 2.10 is integrated over the element:

$$\int_{x_{iL}}^{x_{iR}} \left(\frac{\partial A}{\partial t} + \frac{\partial Q}{\partial x} - q_l \right) \mathrm{d}x = 0 \tag{2.11}$$

The different parts of the equation are discretized as follows:

$$\int_{x_{iL}}^{x_{iR}} \frac{\partial A_i}{\partial t}\, \mathrm{d}x \approx \frac{\partial A_i}{\partial t}\, \Delta x_i \approx \frac{A_i^{t+1} - A_i^t}{\Delta t}\, \Delta x_i \tag{2.12}$$

$$\int_{x_{iL}}^{x_{iR}} \frac{\partial Q_i}{\partial x}\, \mathrm{d}x = Q(x_{iR}) - Q(x_{iL}) = \Phi_{c,iR} - \Phi_{c,iL} \tag{2.13}$$

$$\int_{x_{iL}}^{x_{iR}} q_l \, \mathrm{d}x \approx q_{iR}(x_{iR} - x_i) + q_{iL}(x_i - x_{iL}) \tag{2.14}$$

$\Phi_{c,iR}$ and $\Phi_{c,iL}$ are the continuity fluxes calculated by the Riemann solver and q_{iR} and q_{iL} the lateral sources in the corresponding river segments.

For the explicit time discretisation the new value of A will be:

$$A_i^{t+1} = A_i^t - \frac{\Delta t}{\Delta x_i}(\Phi_{c,iR} - \Phi_{c,iL}) - \frac{\Delta t}{\Delta x_i}(q_{iR}(x_i - x_{i,R}) + q_{iL}(x_{iL} - x_i)) \tag{2.15}$$

2.2.2.2.2 Momentum Equation

Assuming that the lateral in- and outflows do not contribute to the momentum balance, thus neglecting the last term of eq. 1.9 and integrating over the element, the momentum equation becomes:

$$\int_{x_{iL}}^{x_{iR}} \left(\frac{\partial Q}{\partial t} + \frac{\partial}{\partial x}\left(\beta \frac{Q^2}{A_{red}}\right) + \sum Sources \right) \mathrm{d}x = 0 \tag{2.16}$$

The different parts of the equation are discretized as follows:

$$\int_{x_{iL}}^{x_{iR}} \frac{\partial Q_i}{\partial t} \, \mathrm{d}x \approx \frac{\partial Q_i}{\partial t} \, \Delta x_i \approx \frac{Q_i^{t+1} - Q_i^t}{\Delta t} \, \Delta x_i \tag{2.17}$$

$$\int_{x_{iL}}^{x_{iR}} \frac{\partial Q_i}{\partial x} \, \mathrm{d}x = \beta \frac{Q^2}{A_{red}}\bigg|_{x_{iR}} - \beta \frac{Q^2}{A_{red}}\bigg|_{x_{iL}} = \Phi_{m,iR} - \Phi_{m,iL} \tag{2.18}$$

$\Phi_{m,iR}$ and $\Phi_{m,iL}$ are the momentum fluxes calculated by the Riemann solver.

For the explicit time Discretisation the new value of Q will be:

$$Q_i^{t+1} = Q_i^t - \frac{\Delta t}{\Delta x_i}(\Phi_{m,iR} - \Phi_{m,iL}) + \sum Sources \tag{2.19}$$

2.2.2.3 Discretisation of Source Terms

2.2.2.3.1 Bed Slope Source Term

The bed slope source term:

$$W = gA\frac{\partial z_S}{\partial x} \tag{2.20}$$

is discretized as follows:

$$\int_{x_{iL}}^{x_{iR}} gA_{red}\frac{\partial z_S}{\partial x}\,dx \approx gA_{redi}\frac{\partial z_S}{\partial x}\bigg|_{x_i}\Delta x_i \approx gA_{redi}\left(\frac{z_{S,i+1}-z_{S,i-1}}{x_{i+1}-x_{i-1}}\right)\Delta x_i \tag{2.21}$$

With the subtraction of the bed slope source term, eq. 2.19 becomes

$$Q_i^{t+1} = Q_i^t - \frac{\Delta t}{\Delta x_i}(\Phi_{m,ir}-\Phi_{m,il}) - \Delta t\; gA_{redi}\left(\frac{z_{S,i+1}-z_{S,i-1}}{x_{i+1}-x_{i-1}}\right) \tag{2.22}$$

2.2.2.3.2 Friction Source Term

The friction source term:

$$Fr = gA_{red}S_f$$

is simply calculated with the local values:

$$\int_{x_{iL}}^{x_{iR}} gA_{red}S_{fi}\,\mathrm{d}x \approx gA_{redi}S_{fi}\Delta x_i \tag{2.23}$$

and

$$S_{fi} = \frac{Q_i^t|Q_i^t|}{(K_i^t)^2} \tag{2.24}$$

This computation form however leads to problems if the element was dry in the precedent time step, because in this case A , and thus K , become very small, and S_{fi} very large. This leads to numerical instabilities. For this reason a semi-implicit approach has been applied, which considers the discharge of the present time step:

$$S_{fi} = \frac{Q_i^{t+1}|Q_i^t|}{(K_i^t)^2} \tag{2.25}$$

Consequently instead of simply subtracting the source term from eq. 2.22, the following operation is executed on the new discharge Q_i^{t+1} :

$$Q_i^{t+1} = \frac{Q_i^{t+1}}{1+\dfrac{\Delta t|Q_i^t|gA_i^t}{(K_i^t)^2}} \tag{2.26}$$

With this approach the discharge tends to zero for small conveyances.

2.2.2.3.3 Hydraulic Radius / Conveyance

The hydraulic radius and the conveyance of a cross section are calculated by different ways for different types of cross sections, depending on the geometry which is specified by the user. The cross section can be simple or composed by a main channel and flood plains. Additionally it can have a bed bottom.

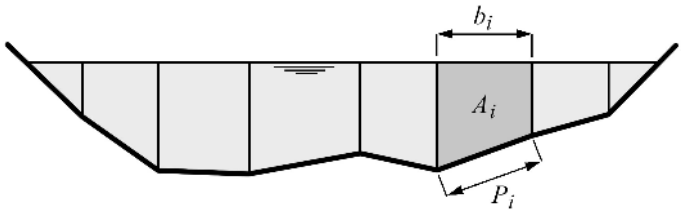

Figure 2.8 *Simple cross section without definition of bed*

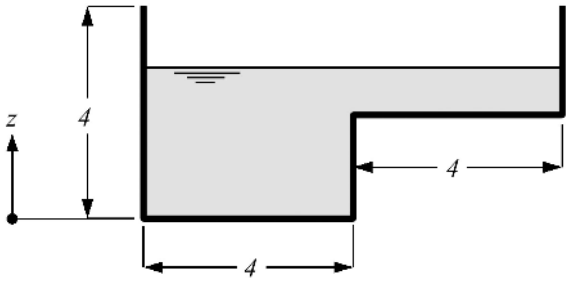

Figure 2.9 *Conveyance computation of a channel with a flat zone*

A simple cross section is used when only a range for the main channel is defined and no flood plain or bottom is specified (Figure 2.8). For an arbitrary simple cross section and a given water surface elevation, the corresponding hydraulic radius R is calculated by the total wetted area A divided by the total wetted perimeter P.

In order to get the conveyance K, a representative friction coefficient c_f for the wetted part of the cross section needs to be determined. This is done by averaging the raw friction values k_i (e.g. Strickler, Manning, Chezy, etc.) over the wetted part of the cross section, weighted with the wetted perimeter. The averaged friction value $\bar{k}$ is then used to calculate the friction coefficient dependent on the function of the friction type. In general form, $c_f = f(\bar{k})$.

$$R = \frac{\sum A_i}{\sum P_i} \tag{2.27}$$

$$K = c_f \sqrt{gR} A \tag{2.28}$$

If there are slices with nearly horizontal ground, such as flood plains for example, this computation mode can lead to jumps in the water level-conveyance graph (see Figure 2.9 and Figure 2.10 for a dimensionless example). It is dangerous however to store the conveyance in a table, from which values will be read by interpolation. If the conveyance is calculated by adding the conveyances of the single slices, the jump can be avoided, but this method leads to an underestimation of the conveyance for water levels higher than the step.

In order to overcome this problem and deal with such cross sections, there is the possibility to define a main channel and (right and left) flood plains, which will be treated differently. Such a cross section is illustrated in Figure 2.11. In this case the conveyance and the discharge are calculated separately for each part of the cross section. The total conveyance results by summation.

Cross section with definition of bed (Figure 2.12)

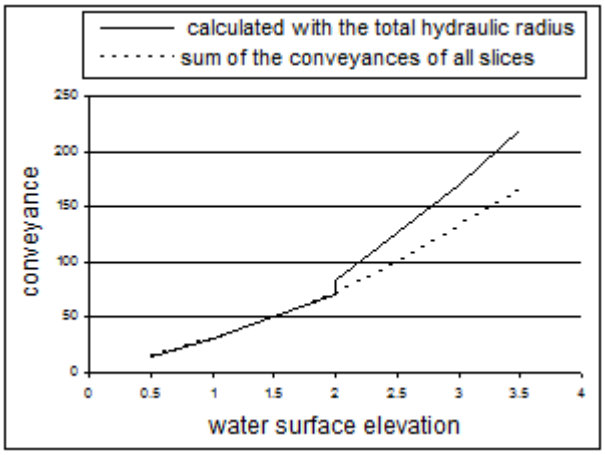

Figure 2.10 *Conveyance computation of a channel with a flat zone*

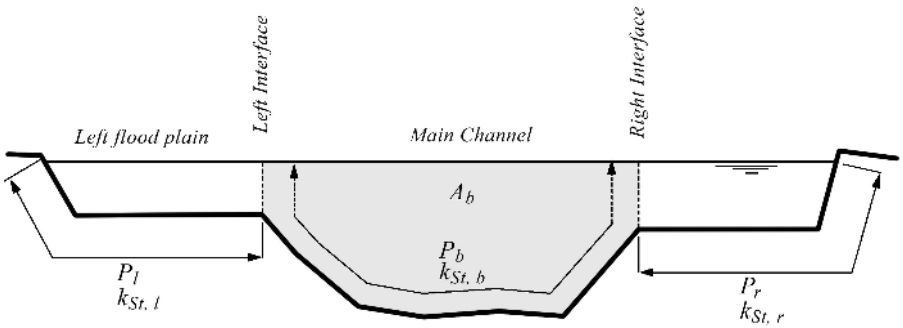

Figure 2.11 *Cross section with flood plains and main channel*

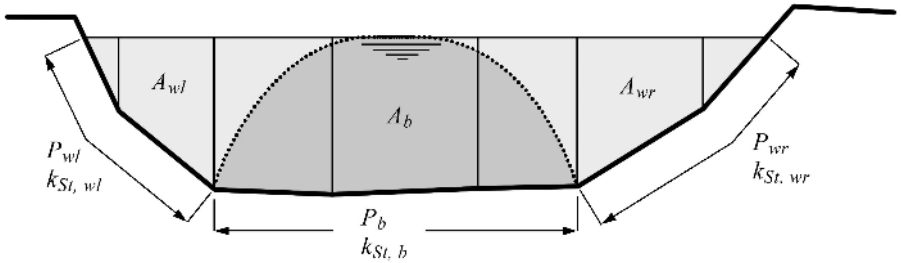

Figure 2.12 *Cross section with definition of a bed*

Additionally to the distinction of flood plains and main channel, a bed bottom can be specified for both simple and composed cross sections. In this case for the computation of the hydraulic radius of the main channel are considered the distinct influence areas of bottom, walls and, if existing, interfaces to the flood plains. In Figure 2.12 is illustrated the case without flood plains or a water level below them.

The conveyance in this case is calculated by the following steps:

$$A_b = R_b P_b \tag{2.29}$$

$$A_{tot} = A_{wl} + A_{wr} + A_b \tag{2.30}$$

$$R_b = \frac{A_{tot}}{k_{stb}^{3/2}\left(\frac{P_{wl}}{k_{StWl}^{3/2}} + \frac{P_b}{k_{Stb}^{3/2}} + \frac{P_{wr}}{k_{StWr}^{3/2}}\right)} \tag{2.31}$$

$$K_b = cf\sqrt{gR_b}A_b \tag{2.32}$$

$$U_{mb} = \frac{K_b}{A_b}\sqrt{S} \tag{2.33}$$

$$Q_b = U_{mb}A_b \tag{2.34}$$

$$Q_w = U_{mb}\left(\frac{A_{tot}}{1.05} - R_b P_b\right) \tag{2.35}$$

$$Q = Q_b + Q_w \tag{2.36}$$

$$K = Q/\sqrt{S} \tag{2.37}$$

$$K = K_b + K_w = \frac{Q_b}{\sqrt{S}} + \frac{Q_w}{\sqrt{S}} = \frac{K_b}{A_b}R_b P_b + \frac{K_b}{A_b}\left(\frac{A_{tot}}{1.05} - R_b P_b\right) = K_b + K_b\left(\frac{A_{tot}}{1.05A_b} - 1\right) \tag{2.38}$$

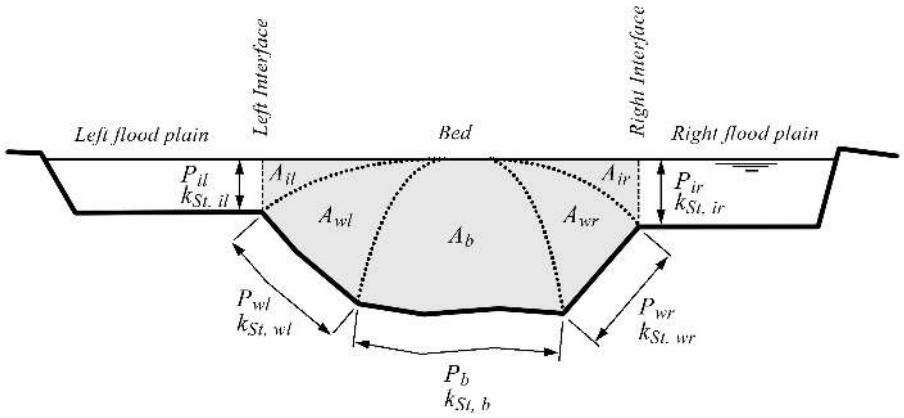

Figure 2.13 *Cross section with flood plains and definition of a bed bottom*

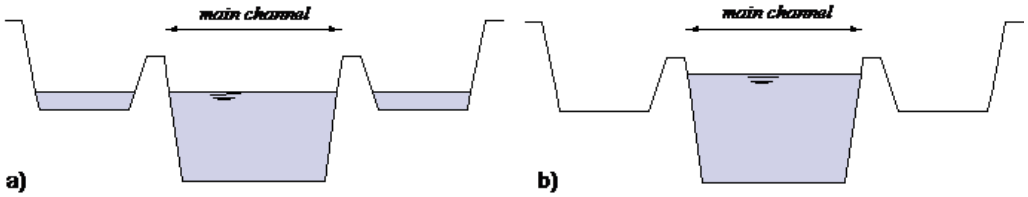

Figure 2.14 *Water level in a cross section with internal levees: a) without consideration of the levees, b) with consideration of the levees*

Figure 2.13 shows the case of a water level higher than the flood plains.

In this case two more partial areas are distinguished for the computation of the hydraulic radius of the bed and:

$$R_b = \frac{A_{tot}}{k_{Stb}^{3/2}\left(\frac{P_{il}}{k_{Stil}^{3/2}} + \frac{P_{wl}}{k_{Stwl}^{3/2}} + \frac{P_b}{k_{Stb}^{3/2}} + \frac{P_{wr}}{k_{Stwr}^{3/2}} + \frac{P_{ir}}{k_{Stir}^{3/2}}\right)} \tag{2.39}$$

2.2.2.3.4 Simple approach for consideration of internal levees

From the wetted surface A provided by the equation solution, the corresponding water surface elevation z has to be determined. All further hydraulic variables in the cross section are computed from this value. A special problem occurs if there are levees in the channel. The very simple 1-D approach leads to the situation in illustration a) of Figure 2.14. The reality however would correspond more to illustration b).

The first approach can lead to problems i.e. for the computation of bed load, as part of the shear stress is lost. For this reason the regions out of the main channel are considered only when the water level exceeds the top level of the levees. When the whole main channel is full and the wetted area increases, the water surface elevation remains constant until the flood plains are “filled”. Only then the water surface elevation will continue to rise, like illustrated in Figure 2.15. The second approach is used as default, but it can be switched-off.

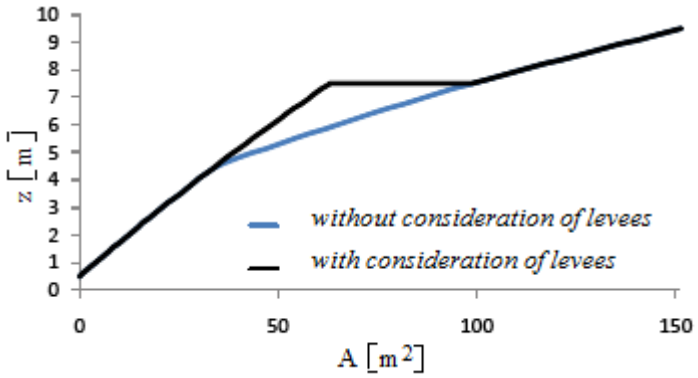

Figure 2.15 *Function $z(A)$ with and without consideration of the levees*

2.2.2.4 Discretisation of Boundary conditions

While normally the edges are placed in the middle between two cross sections, which are related to the elements, at the boundaries the left edge of the first upstream element and the right edge of the last downstream element are situated at the same place as the cross sections themselves. Thus there is no distance between the edge and the cross section.

2.2.2.4.1 Inlet Boundary

The boundary condition is applied to the left edge of the first element, where it serves to determine the fluxes over the element side. If there is no water coming in, these fluxes are simply set to 0.

If there is an inlet flux it must be given as a hydrograph. The given discharge is directly used as the continuity flux, whereas for the computation of the momentum flux, A_{red} and β are determined in the first cross section (which has the same location).

$$\Phi_{c,1R} = Q_{bound} \tag{2.40}$$

$$\Phi_{m,1R} = \beta_1 \frac{(Q_{bound})}{A_{red1}} \tag{2.41}$$

For the computation of the bed source term in the first cell, the values in the cell are used instead of the lacking upstream values:

$$W_1 = A_{red1} \left(\frac{z_{S,2} - z_{S,1}}{x_2 - x_1} \right) \tag{2.42}$$

2.2.2.4.2 Outlet Boundary

- weir and gate:

  The wetted area A_N^{n-1} of the last cross section at the previous time step is used to determine the water surface elevation $z_{S,N}$. With $z_{S,N}$, the wetted area of the weir or gate and finally the out flowing discharge Q are calculated, which are used for the computation of the flux over the outflow edge:

$$\Phi_{c,NL} = Q_{weir} \tag{2.43}$$

$$\Phi_{m,NL} = \frac{(Q_{weir})^2}{A_{weir}} \tag{2.44}$$

- z(t) and z(Q):

  If the given boundary condition is a time evolution of the water surface elevation or a rating curve, the discharge Q is taken from the last cell and time step. In the case of a rating curve it is used to determine the water surface elevation z_S . The given elevation is used to calculate the target A and β in the last cross section.

  To satisfy the desired water level, the required inflow from the reservoir into the simulation domain is calculated from:

$$Q_{res}(t) = Q_{in}(t) - \frac{\Delta x}{\tau}(A_{target} - A(t)) \tag{2.45}$$

  This approach converges to the target water surface elevation within the characteristic time τ.

$$\Phi_{c,NL} = Q_{res} \tag{2.46}$$

$$\Phi_{m,NL} = \beta_{bound}\frac{(Q_{res})^2}{A_{bound}} \tag{2.47}$$

- In/out:

  With the boundary condition in/out the flux over the outflow edge is just equal to the inflow flux of the last cell:

$$\Phi_{c,Ll} = \Phi_{c,NR} \tag{2.48}$$

$$\Phi_{m,NL} = \Phi_{m,NR} \tag{2.49}$$

  For the computation of the bed source term in the last cell, the values in the cell are used instead of the lacking downstream values:

$$W_N = A_{redN}\left(\frac{z_{S,N} - z_{S,N-1}}{x_N - x_{N-1}}\right) \tag{2.50}$$

2.2.2.4.3 Inner Boundaries

- Inner Weir:

  The inner weir uses a slightly other approach than the boundary weir. If the weir crest is higher than the water surface elevation in the neighbouring elements, the weir acts as a wall.

If one or both of the neighbouring water surface elevations are above the weir crest, the weir formula for discharge

$$Q = \frac{2}{3}\mu\sigma_{uv}w\sqrt{2g(z_{upstream} - z_{weir})^3} \tag{2.51}$$

is used. This is the classical Poleni formula for a sharp crested weir with an additional factor σ_{uv} which accounts for the reduction in discharge due to incomplete weir flow. If only one side of the weir has a water surface elevation above the weir crest, then a complete weir flow is given with $\sigma_{uv} = 1$. w is the width of the weir.

As soon as the water surface elevation tops the weir crest level on both sides of the weir, the incomplete case is active and the reduction factor σ is calculated according to the Diagram Figure 2.32.

As for the momentum, there is no momentum due to velocity accounted for in the downstream direction. This behaviour acts as if all kinetic energy is dissipated over a weir.

2.2.2.4.4 Moving Boundaries

Boundaries are always considered to be on an edge. A moving boundary appears if one of the cells, limited by the edge, is dry. In this case some changes have to be considered for the computations:

- Flux over an internal edge:

  If in one of the cells the water depth at the lowest point of the cross section is lower than the dry depth h_{min} , the energy level in the other cell is computed. If this is lower than the water surface elevation in the dry cell the flow over the edge is 0. Otherwise it is calculated normally.

- Bed source:

  For the computation of the bed source term in the case of the upstream or downstream cell being dry, the local values are used as in the following example with an upstream dry cell:

$$W_i = A_{red,i}\left(\frac{z_{S,i+1} - z_{S,i}}{x_{i+1} - x_i}\right) \tag{2.52}$$

2.2.2.5 Solution Procedure

a) General solution procedure of BASEchain in detail (Figure 2.16 and Figure 2.17)
b) Time loop (Figure 2.18)
c) Hydrodynamic equations (Figure 2.19)
d) Morphodynamic equations (Figure 2.20)
e) Suspended load equations (Figure 2.21)

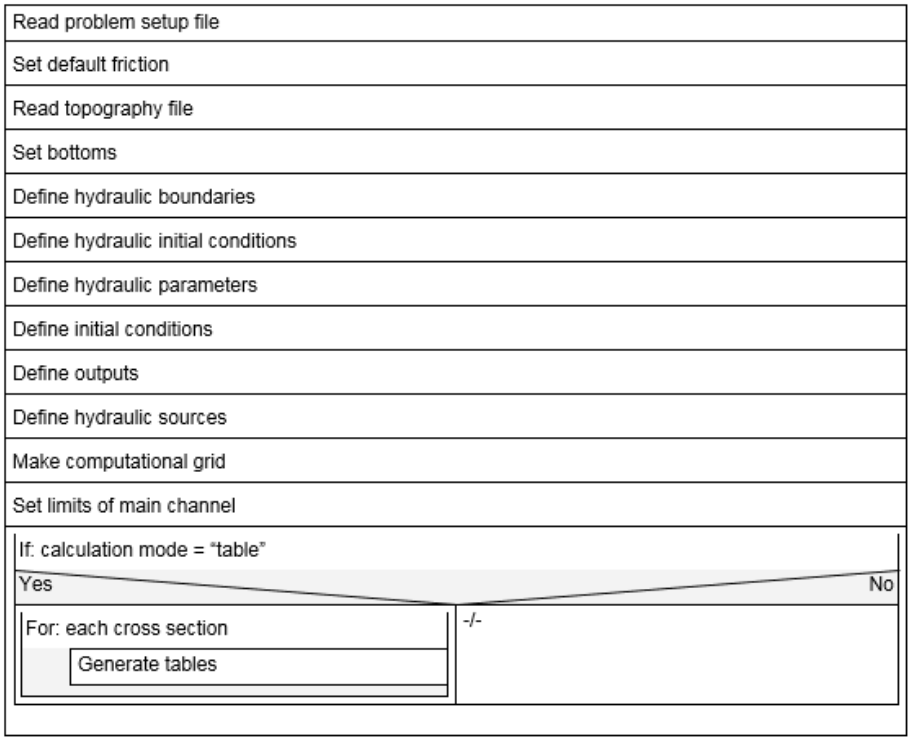

Figure 2.16 *General solution procedure of BASEchain*

2.2.3 Shallow Water Equations

2.2.3.1 Discrete Form of Equations

Numerical methods are used to transform the differential and the integral equations into discrete algebraic equations. Based on the mentioned reasons, the FV method has been used in the present work for the discretisation of SWE. The eq. 1.36 can be rewritten in the following integral form:

$$\int_{\Omega} \boldsymbol{U}_t \, \mathrm{d}\Omega + \int_{\Omega} \nabla \cdot (\boldsymbol{F}, \boldsymbol{G}) \, \mathrm{d}\Omega + \int_{\Omega} \boldsymbol{S} \, \mathrm{d}\Omega = 0 \tag{2.53}$$

in which Ω equals the area of the calculation cell (Figure 2.1) Using the Gauss' relation eq. 2.53 becomes:

$$\int_{\Omega} \boldsymbol{U}_t \, \mathrm{d}\Omega + \int_{\partial\Omega} (\boldsymbol{F}, \boldsymbol{G}) \cdot \boldsymbol{n}_s \, \mathrm{d}l + \int_{\Omega} \boldsymbol{S} \, \mathrm{d}\Omega = 0 \tag{2.54}$$

Assuming U_t and S are constant over the domain for first order accuracy, it can be written:

$$\boldsymbol{U}_t + \frac{1}{\Omega} \int_{\partial\Omega} (\boldsymbol{F}, \boldsymbol{G}) \cdot \boldsymbol{n}_s \, \mathrm{d}l + \boldsymbol{S} = 0 \tag{2.55}$$

The eq. 2.54 can be discretized by a two-phase scheme namely predictor corrector scheme as follows:

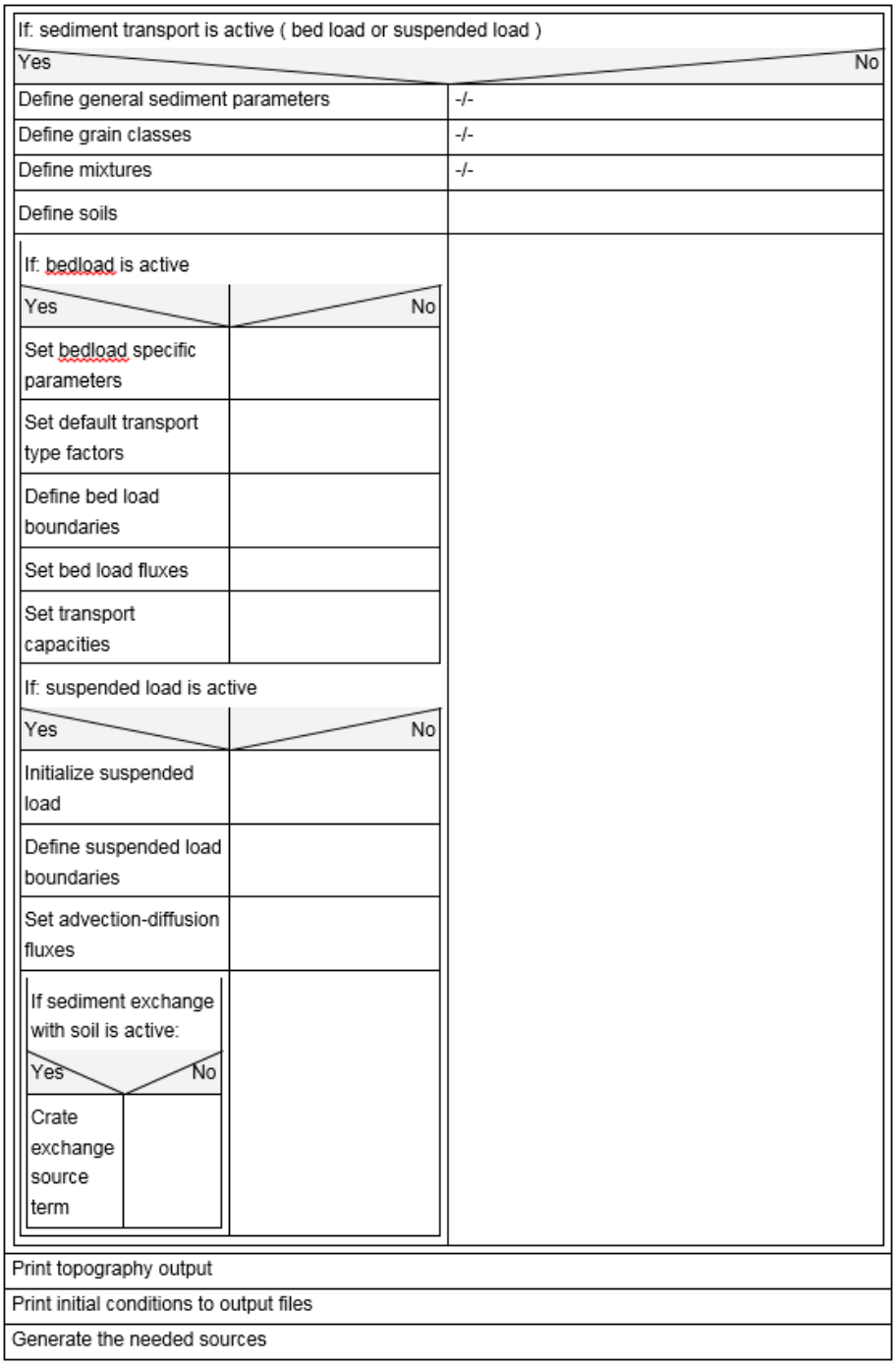

Figure 2.17 *General solution procedure of BASEchain*

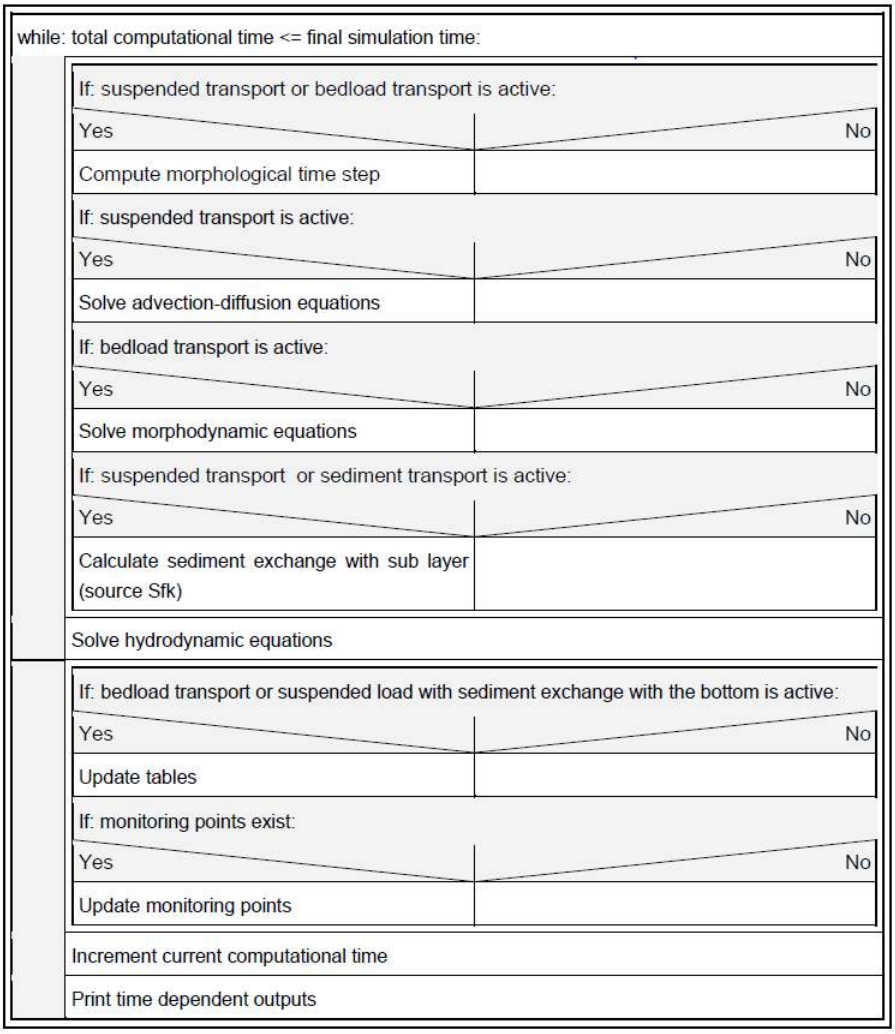

Figure 2.18 *Time loop*

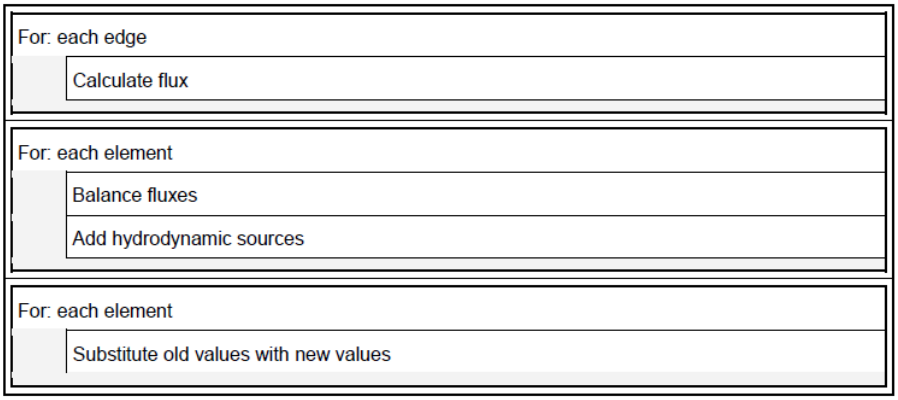

Figure 2.19 *Hydrodynamic equations*

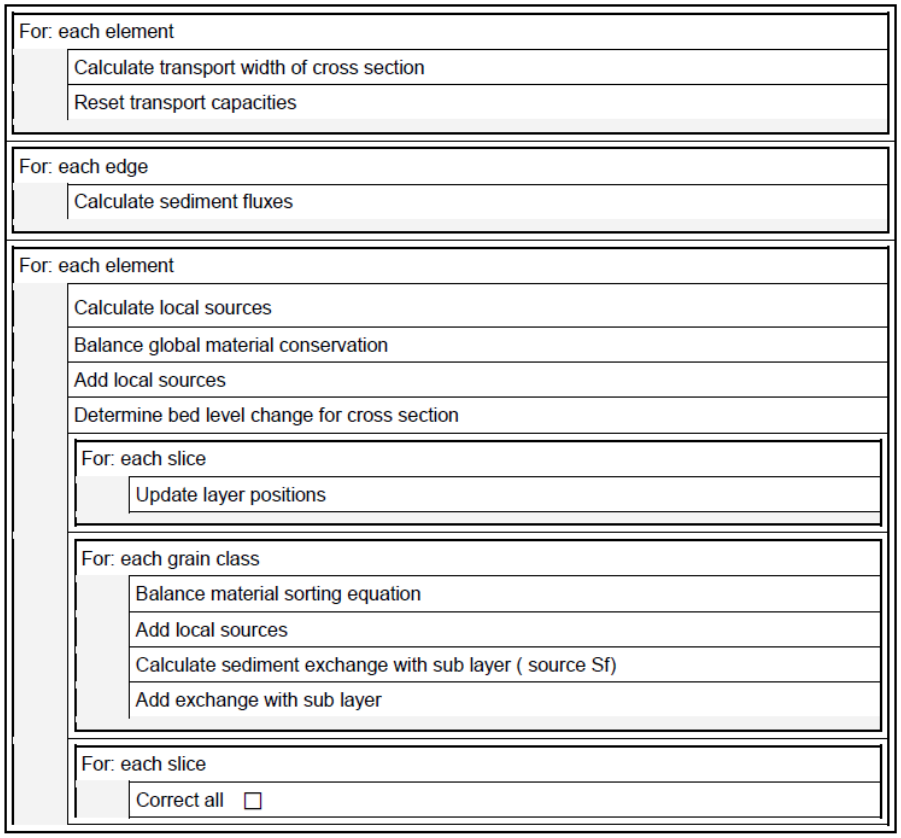

Figure 2.20 *Morphodynamic equations*

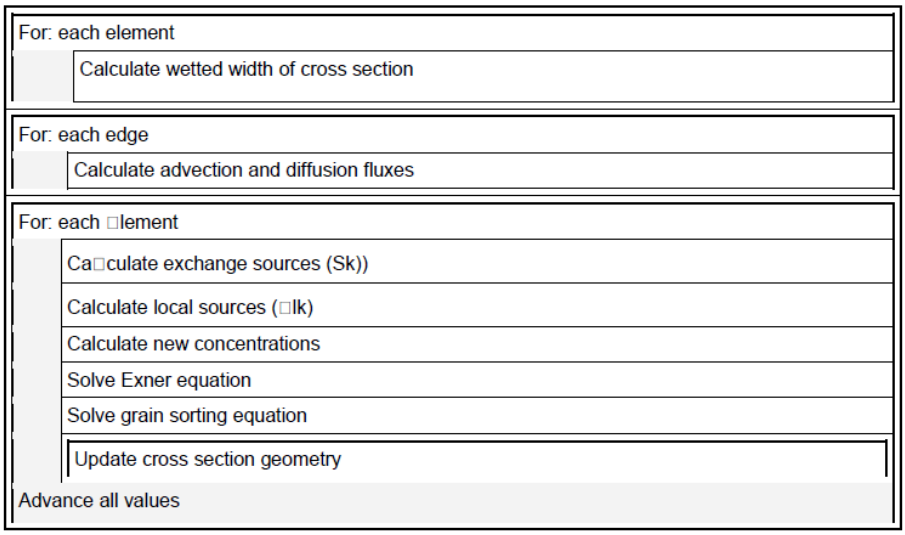

Figure 2.21 *Suspended load equations*

$$\boldsymbol{U}_i^{n+1} = \boldsymbol{U}_i^n - \frac{\Delta t}{\Omega} \sum_{j=1}^{3} (\boldsymbol{F}, \boldsymbol{G})_{i,j}^n \times \boldsymbol{n}_j l_j - \Delta t \boldsymbol{S}_i \tag{2.56}$$

where

m	= number of cell or element sides
$(\boldsymbol{F}, \boldsymbol{G})_{i,j}$	= numerical flux through the side of cell
$n_{s,i}$	= unit vector of cell side

The advantage of two-phase scheme is the second order accuracy in time marching. In the FV method, the key problem is to estimate the normal flux through each side of the domain, namely $((\boldsymbol{F}, \boldsymbol{G}) \cdot \boldsymbol{n}_s)$. There are several algorithms to estimate this flux. The set of SWE is hyperbolic and, therefore, it has an inherent directional property of propagation. For instance, in 1-D unsteady flow, information comes from both, upstream and downstream, in sub critical cases, while information only comes from upstream in supercritical cases. Algorithms to estimate the flux should appropriately handle this property. The *Riemann solver*, which is based on characteristics theory, is such an algorithm. It is the solution of Riemann Problem. The Riemann solver under the FV method formulation is especially suitable for capturing discontinuities in sub critical or supercritical flow, e.g. a dam break wave or flood propagation in a river.

2.2.3.1.1 Flux Estimation

Considering the integral term of flux in eq. 2.55, it can be written:

$$\int_{\partial\Omega} (\boldsymbol{F}(\boldsymbol{U}), \boldsymbol{G}(\boldsymbol{U})) \cdot \boldsymbol{n}_s \, \mathrm{d}l = \int_{\partial\Omega} (\boldsymbol{F}(\boldsymbol{U}) \cos\theta + \boldsymbol{G}(\boldsymbol{U}) \sin\theta) \, \mathrm{d}l \tag{2.57}$$

in which $\boldsymbol{n}_s = (\cos\theta, \sin\theta)$ is the outward unit vector to the boundary of domain Ω_i (see Figure 2.22). Based on the rotational invariance property for $\boldsymbol{F}(\boldsymbol{U})$ and $\boldsymbol{G}(\boldsymbol{U})$ on the boundary of the domain, it can be written according to Toro (1997):

$$(\boldsymbol{F}(\boldsymbol{U}), \boldsymbol{G}(\boldsymbol{U})) = \boldsymbol{T}^{-1}(\theta) \boldsymbol{F}(\boldsymbol{T}(\theta)\boldsymbol{U}) \tag{2.58}$$

where θ is the angle between the vector $\boldsymbol{n}_s$ and x-axis, measured counter clockwise from the x-axis (see Figure 2.22).

$$\boldsymbol{T}(\theta) = \begin{pmatrix} 1 & 0 & 0 \\ 0 & \cos\theta & \sin\theta \\ 0 & -\sin\theta & \cos\theta \end{pmatrix} \tag{2.59}$$

$\boldsymbol{T}^{-1}(\theta)$ = inverse of $\boldsymbol{T}(\theta)$

Using eq. 2.58, eq. 2.55 can be rewritten as:

$$\boldsymbol{U}_t + \frac{1}{\Omega} \int_{\partial\Omega} \boldsymbol{T}^{-1}(\theta) \boldsymbol{F}(\boldsymbol{T}(\theta)\boldsymbol{U}) \, \mathrm{d}l + \boldsymbol{S} = 0 \tag{2.60}$$

The quantity $\boldsymbol{T}(\theta)\boldsymbol{U}$ is transformed of $\boldsymbol{U}$, with velocity components in the normal and tangential direction. For each cell in the computational domain, the quantity $\boldsymbol{U}$, thus

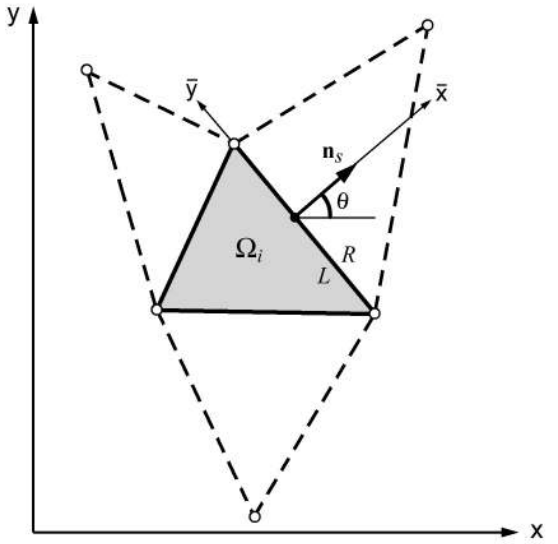

Figure 2.22 *Geometry of a Computational Cell* Ω_i *in FV*

$\boldsymbol{T}(\theta)\boldsymbol{U}$ may have different values, which results in a discontinuity across the interface between cells. Therefore, the two-dimensional problem in eq. 2.53 or eq. 2.55 can be handled as a series of local Riemann problems in the normal direction to the cell interface ($\bar{x}$) by the eq. 2.60.

Applying the foregoing, the flux computations over the edges are preformed in three successive steps:

- First, the vector of conserved variables $\boldsymbol{U}$ is transformed into the local coordinate system at the edge with the operation $\boldsymbol{T}(\theta)\boldsymbol{U}$.
- A one-dimensional, local Riemann problem is formulated and solved in the normal direction of the edge. From this calculation results the new flux vector over the edge $\boldsymbol{F}[\boldsymbol{T}(\theta)\boldsymbol{U}]$.
- The flux vector, formulated in the local coordinate system at the edge, is transformed back to Cartesian coordinates with $\boldsymbol{T}^{-1}\boldsymbol{F}[\boldsymbol{T}(\theta)\boldsymbol{U}]$. The Sum of the fluxes of all edges of an element gives the total fluxes in x- and y directions.

2.2.3.1.2 Flux Correction

When the solution is advanced and the continuity and momentum equations are updated in each cell, there may be occurring situations in which more water is removed from an element than is actually stored in the element (overdraft). Such overdraft is mostly experienced in situations with strongly varying topography and low water depths, e.g. near wet-dry interfaces on irregular beds. To guarantee positive depths in all elements, a correction of the depths and volumetric fluxes is applied in such situations following an approach based on Begnudelli and Sanders (2006). However, in some rare cases the overdraft cannot be corrected and therefore mass continuity is not guaranteed.

The overdraft element i having a negative water depth receives water from its surrounding element k if two conditions are fulfilled. The element k must previously have taken water from the overdraft element and it must have water available. The corrections of the depths and volumetric fluxes of the neighbouring elements k are then calculated as

$$\begin{aligned} h_k^{corr} &= h_k + \omega_k h_i \frac{A_i}{A_k} \\ Flux_k^{corr} &= Flux_k + \omega_k h_i \frac{A_i}{\Delta t} \end{aligned} \tag{2.61}$$

where h_k is the water depth and $Flux_k$ is the volumetric Flux of the neighbouring element. h_i is the (negative) water depth of the overdraft element and ω_k is a weighting factor which is obtained by weighting the volumetric fluxes of all corrected neighbouring elements k.

$$\omega_k = \frac{Flux_k}{\sum_k Flux_k} \tag{2.62}$$

In case of element k does not have enough water available the overdraft is partly compensated. Subsequently all the weights have to be recalculated and a new correction attempt is made. After the correction of the neighbouring elements, the water depth of the overdraft element is set to zero.

2.2.3.2 Discretisation of Source Terms

In eq. 2.56 there are different possibilities for the evaluation of the source term $\boldsymbol{S}_i$. It can be evaluated either with the variables of the old time step as $\boldsymbol{S}_i(\boldsymbol{U}_i)$, which is often referred to as unsplitted scheme, or it can be evaluated with the advanced values $\boldsymbol{U}_i^{n+1/2}$, which already include changes due to the numerical fluxes computed during this time step as $\boldsymbol{S}_i(\boldsymbol{U}_i^{n+1/2})$. The use of the advanced values for the source term calculation is chosen here because it gives better results (Toro, 2001). Therefore eq. 2.56 is split in following way

$$\begin{aligned} \boldsymbol{U}_i^{n+1/2} &= \boldsymbol{U}_i^n - \frac{\Delta t}{\Omega} \sum_{j=1}^{3} (\boldsymbol{F}, \boldsymbol{G})_{i,j}^n \cdot \boldsymbol{n}_j \mathrm{d}l_j \\ \boldsymbol{U}_i^{n+1} &= \boldsymbol{U}_i^{n+1/2} + \Delta t \boldsymbol{S}_i(\boldsymbol{U}_i^{n+1/2}) \end{aligned} \tag{2.63}$$

But, as explained in the following, the friction source term $\boldsymbol{S}_{i,fr}$ receives a special treatment.

2.2.3.2.1 Friction Source Term

When treating the friction source terms, a simple explicit Discretisation may cause numerical instabilities if the water depth is very small, because the water depth is in the denominator. Such problematic situations may occur in particular at drying-wetting interfaces. To circumvent the numerical instabilities, the frictions terms are treated in a semi-implicit way. Therefore the friction source term is calculated with the unknown value $\boldsymbol{U}_i^{n+1}$ at the new time level as

$$\boldsymbol{U}_i^{n+1} = \boldsymbol{U}_i^{n+1/2} + \Delta t \boldsymbol{S}_{i,fr}(\boldsymbol{U}_i^{n+1}) \tag{2.64}$$

Considering the generalized c_f friction coefficient and after some algebraic manipulations, one obtains:

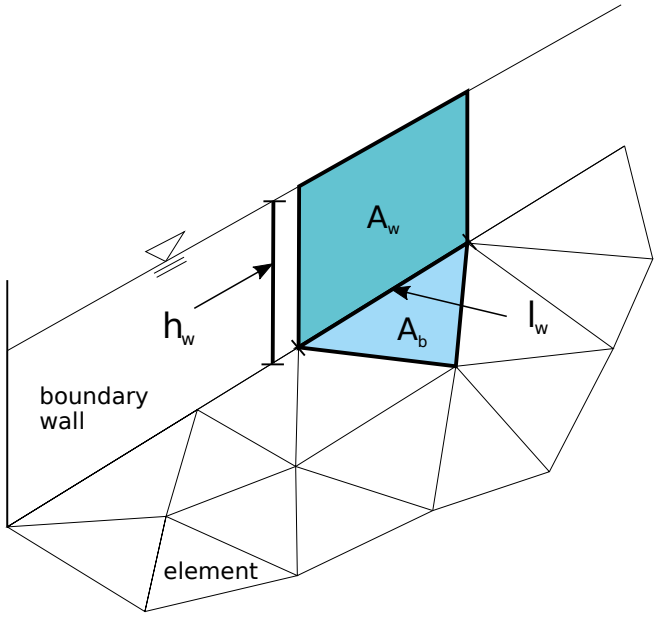

Figure 2.23 *Wetted perimeter of a boundary element with wall friction*

$$\boldsymbol{U}_i^{n+1} = \frac{\boldsymbol{U}_i^{n+1/2}}{1 + \Delta t \frac{\sqrt{(u_i^n)^2 + (\nu_i^n)^2}}{c_{fi}^2 R_i}} \tag{2.65}$$

Hydraulic Radius

The calculation of the friction source term requires a definition of the hydraulic radius $\boldsymbol{R}_i$ in the element i. The hydraulic radius is defined here as water depth in the element ($\boldsymbol{R}_i = \boldsymbol{h}_i$).

Wall friction

In cases where an element is situated at a boundary wall of the domain, the influence of the additional wall friction on the flow can optionally be considered, as illustrated in Figure 2.23. The friction slope is extended to include additional wall friction effects. The method is similar to the approach of Brufau and Garcia-Navarro and Vazquez-Cendon (2000) but differs in the type the different friction parts are added together. In this implementation the friction values of the bed c_f and the wall c_{fw} can be chosen differently.

The friction slope in x-direction is calculated as

$$S_{i,fr,x} = \frac{u\sqrt{u^2 + \nu^2}}{g} \left(\frac{1}{\bar{c}_f^2 R_w} \right) \tag{2.66}$$

with R_w being the hydraulic radius of the wall friction at the boundary edge w. The first term in eq. 2.66 defines the friction losses due to bed friction and the second term defines the additional friction losses due to the flow along the boundary wall. The friction slope in y-direction is derived in an analogous way.

The hydraulic radius R_w at the wall boundary edge i is calculated as

$$R_w = \frac{V_{water}}{A_w} = \frac{A_b h}{A_b + \sum_i l_{w,i} h} \tag{2.67}$$

where I_w is the length of the element's edge located at the wall boundary, A_b is bottom area of the element and A_w is the wetted area of the wall. The average friction coefficient $\bar{c}_f$ at the boundary edge is calculated as

$$\bar{c}_f = \frac{c_f A_b + c_{fw} \sum_i A_{w,i}}{A_b + \sum_i A_{w,i}}$$

with c_{fw} as the friction coefficient of the wall and $\sum_i A_{w,i}$ as the sum of all wetted wall areas. For the determination of the bottom shear stress for sediment transport computations, this additional wall friction component is not taken into account.

2.2.3.2.2 Source Term for viscous and turbulent Stresses

The kinematic and turbulent stresses are treated as source term. For the derivatives, the divergence theorem from Gauss is used similarly to the ordinary fluxes. This approach allows a derivative to be calculated as a sum over averaged values on an edge. A potential division by zero cannot occur. In the following, a cantered scheme for diffusive fluxes on an unstructured grid based on the approach of Mohamadian et al. (2005) is described.

For the Finite Volume Method, the diffusive source terms are integrated over an element:

$$\iint_\Omega \boldsymbol{S}_d \, \mathrm{d}\Omega = \iint_\Omega \frac{\partial \boldsymbol{F}^d}{\partial x} + \frac{\partial \boldsymbol{G}^d}{\partial y} \, \mathrm{d}\Omega \tag{2.68}$$

By using the divergence theorem, the diffusive flux integrals are becoming boundary integrals

$$\iint_\Omega \frac{\partial \boldsymbol{F}^d}{\partial x} + \frac{\partial \boldsymbol{G}^d}{\partial y} \, \mathrm{d}\Omega = \oint_{\partial\Omega} \boldsymbol{F}^d \cdot \boldsymbol{n} + \boldsymbol{G}^d \cdot \boldsymbol{n} \, \mathrm{d}s \tag{2.69}$$

The boundary integral is discretized by a summation over the element edges (index e)

$$\oint_{\partial\Omega} \boldsymbol{F}^d \cdot \boldsymbol{n} + \boldsymbol{G}^d \cdot \boldsymbol{n} \, \mathrm{d}s = \sum_e (\boldsymbol{F}_e^d \cdot \boldsymbol{n}_e + \boldsymbol{G}_e^d \cdot \boldsymbol{n}_e) \, \mathrm{d}s_e \tag{2.70}$$

The diffusive fluxes $\boldsymbol{F}_e^d$ and $\boldsymbol{G}_e^d$ on the element edges are calculated by a centred scheme

$$\boldsymbol{F}_e^d = \frac{1}{2}(\boldsymbol{F}_R^d + \boldsymbol{F}_L^d), \quad \boldsymbol{G}_e^d = \frac{1}{2}(\boldsymbol{G}_R^d + \boldsymbol{G}_L^d) \tag{2.71}$$

where R and L stand for a value right and left of the edge. The diffusive fluxes on the edges read then as

$$\boldsymbol{F}_e^d = \frac{1}{2}\begin{pmatrix} 0 \\ \left(\nu h \frac{\partial u}{\partial x}\right)_R + \left(\nu h \frac{\partial u}{\partial x}\right)_L \\ \left(\nu h \frac{\partial v}{\partial x}\right)_R + \left(\nu h \frac{\partial v}{\partial x}\right)_L \end{pmatrix} \tag{2.72}$$

and

$$\boldsymbol{G}_e^d = \frac{1}{2}\begin{pmatrix} 0 \\ \left(\nu h \frac{\partial u}{\partial y}\right)_R + \left(\nu h \frac{\partial u}{\partial y}\right)_L \\ \left(\nu h \frac{\partial v}{\partial y}\right)_R + \left(\nu h \frac{\partial v}{\partial y}\right)_L \end{pmatrix} \tag{2.73}$$

where $\nu = \nu_m + \nu_t$ is the sum of the molecular (kinematic) and turbulent eddy viscosity. For this approach, the velocity derivatives at the element canters are used as right and left approximation near the edge. The values for the water depth h right and left of an edge are reconstructed using the water surface elevation of the adjacent elements. The turbulent eddy viscosity ν_t can be either set to a constant value or calculated dynamically for each element. Using the dynamic case, the values for ν_t are taken from the right and left element of an edge.

All that remains is to calculate the derivatives of the velocity components at the element centres. For Finite Volume Methods, this is an easy task using again the divergence theorem. The derivative of a general scalar variable φ on an arbitrary element is given by

$$\left(\frac{\partial \varphi}{\partial x}\right)_{Elem} = \frac{1}{\Omega}\int_\Omega \frac{\partial \varphi}{\partial x}\,\mathrm{d}\Omega \approx \frac{\sum_e \varphi_e \Delta y_e}{\Omega} \tag{2.74}$$

$$\left(\frac{\partial \varphi}{\partial y}\right)_{Elem} = \frac{1}{\Omega}\int_\Omega \frac{\partial \varphi}{\partial y}\,\mathrm{d}\Omega \approx \frac{\sum_e \varphi_e \Delta x_e}{\Omega} \tag{2.75}$$

where Ω is the area of the element and e stands for an edge. φ_e is a value on the edge. As in finite volume methods, most variables are defined on an element, φ_e has to be calculated as average of the neighbouring elements:

$$\varphi_e = \frac{1}{2}(\varphi_R + \varphi_L) \tag{2.76}$$

The spatial differences Δy_e and Δx_e are the differences of the edge's node-coordinates in x and y direction. For this method to work, it is important to have the same direction of integration along the elements edges either clockwise or counter-clockwise.

As a result, a viscous term from eq. 2.72 is computed as

$$\left(\nu h \frac{\partial u}{\partial x}\right)_L \approx \nu_L h_L \frac{\sum_e u_e \Delta y_e}{\Omega_L} \tag{2.77}$$

with $u_e = 0.5(u_{eL} + u_{eR})$.

The depth-averaged turbulent viscosity ν_t can either be set to a constant value or it is calculated for every element using the formula

$$\nu_t = \frac{\kappa}{6} u_* h \tag{2.78}$$

Where $\kappa = 0.4$ is the von Karman constant and u_* is the shear velocity which is defined as

$$u_* = \sqrt{c_f(u^2 + v^2)} \tag{2.79}$$

Where c_f is the bed friction coefficient derived from the same Manning- or Strickler-value as defined for bed friction.

2.2.3.2.3 Bed Slope Source Term and Bed Slope Calculation

The irregularity of the topography plays an important role in real world applications and often can have great impacts on the final accuracy of the results. A Discretisation scheme with the elevations defined in the nodes of a cell leads to an accurate representation of the topography. Special attention thereby is needed with regard to the C-property which is discussed in Section 2.2.3.3.

The numerical treatment of the bed slope source term here is formulated based on Komaei's method (Komaei and Bechteler, 2004). Regarding eq. 2.55, it is required to compute the integral of the bed slope source term over a element Ω_i .

$$\iint_\Omega \boldsymbol{S}_B \, \mathrm{d}\Omega = \iint_\Omega \begin{pmatrix} 0 \\ ghS_{Bx} \\ ghS_{By} \end{pmatrix} \mathrm{d}\Omega = g \iint_\Omega h \begin{pmatrix} 0 \\ -\dfrac{\partial z_B(x,y)}{\partial x} \\ -\dfrac{\partial z_B(x,y)}{\partial y} \end{pmatrix} \mathrm{d}\Omega \tag{2.80}$$

Assuming that the bed slope values are constant over a cell, eq. 2.80 can be simplified to:

$$\iint_\Omega \boldsymbol{S}_B \, \mathrm{d}\Omega = g \left(\iint_\Omega h \, \mathrm{d}\Omega \right) \begin{pmatrix} 0 \\ S_{Bx} \\ S_{By} \end{pmatrix} = g Vol_{water} \begin{pmatrix} 0 \\ S_{Bx} \\ S_{By} \end{pmatrix} \tag{2.81}$$

In order to evaluate the above integral, it is necessary to compute the bed slope of a cell and the volume of the water over a cell. Since the numerical model allows the use of triangular cells as well as quadrilateral cells in hybrid meshes, these both cases need to be distinguished.

Triangular cells

The bed slope of a triangular cell can be computed by using the finite element formulation as given by Hinton and Owen (1979). It is assumed that z_b varies linearly over the cell (Figure 2.24):

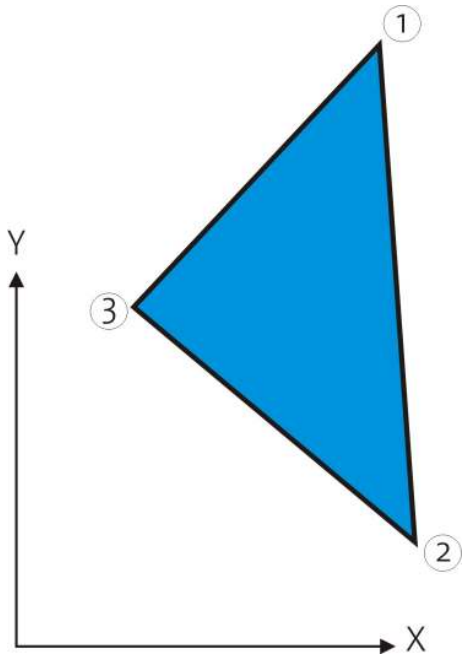

Figure 2.24 *A Triangular Cell*

$$z_B(x,y) = \alpha_1 + \alpha_2 x + \alpha_3 y \tag{2.82}$$

in which $\alpha_2 = \dfrac{\partial z_B}{\partial x}$; $\alpha_3 = \dfrac{\partial z_B}{\partial y}$

The constants α_1 ,α_2 and α_3 can be determined by inserting the nodal coordinates and equating to the corresponding nodal values of z_B. Solving for α_1 , α_2 and α_3 finally gives

$$z_B(x,y) = \frac{1}{2\Omega}\left[(a_1 + b_1 x + c_1 y)z_{b,1} + (a_2 + b_2 x + c_2 y)z_{b,2} + (a_3 + b_3 x + c_3 y)z_{b,3}\right] \tag{2.83}$$

where

$$\left.\begin{aligned} a_1 &= x_2 y_3 - x_3 y_2 \\ b_1 &= y_2 - y_3 \\ c_1 &= x_3 - x_2 \end{aligned}\right\} \tag{2.84}$$

With the other coefficients given by cyclic permutation of the subscripts in the order 1,2,3. The area Ω of the triangular element is given by

$$2\Omega = \begin{vmatrix} 1 & x_1 & y_1 \\ 1 & x_2 & y_2 \\ 1 & x_3 & y_3 \end{vmatrix} \tag{2.85}$$

One can compute the bed slopes in x- and y-direction in each cell as

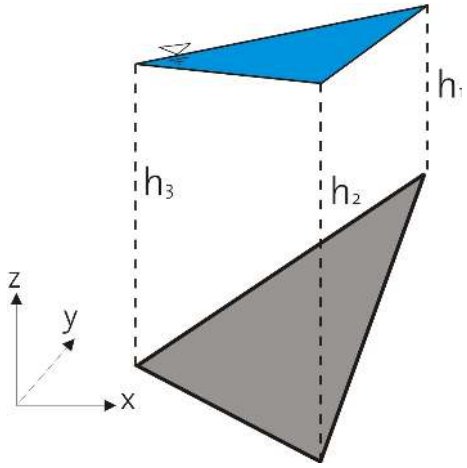

Figure 2.25 *Water volume over a cell*

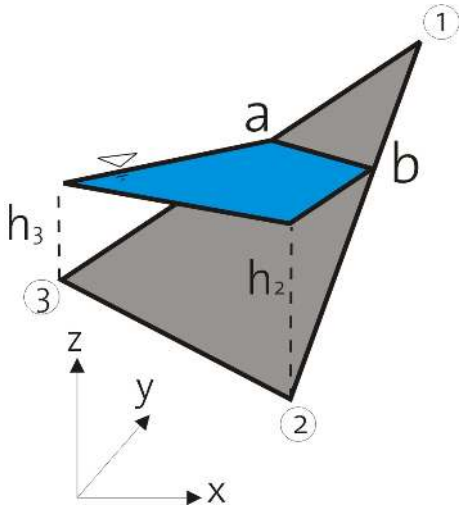

Figure 2.26 *Partially wet cell*

$$\left.\begin{aligned} S_{Bx} &= -\frac{\partial z_B(x,y)}{\partial x} = -\frac{1}{2\Omega}(b_1 z_{B,1} + b_2 z_{B,2} + b_3 z_{B,3}) \\ S_{By} &= -\frac{\partial z_B(x,y)}{\partial y} = -\frac{1}{2\Omega}(c_1 z_{B,1} + c_2 z_{B,2} + c_3 z_{B,3}) \end{aligned}\right\} \tag{2.86}$$

The water volume over a cell can also be computed by using the parametric coordinates of the Finite Element Method.

$$Vol_{water} = \left(\frac{h_1 + h_2 + h_3}{3}\right)\Omega \tag{2.87}$$

where h_1 , h_2 and h_3 are the water depths at the nodes 1, 2 and 3 respectively (Figure 2.25).

In the case of partially wet cells (Figure 2.26) the location of the wet-dry line (a and b) has to be determined, where the water surface plane intersects the cell surface.

Using the coordinates of a and b, the water volume over the cell can be calculated as:

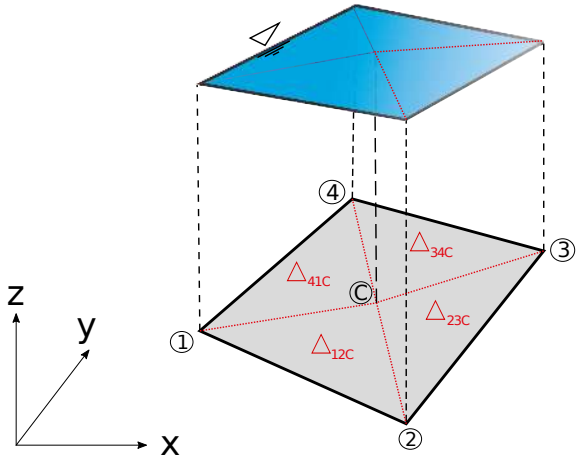

Figure 2.27 *Quadrilateral element and its division into four triangles (Δ_{12C}, Δ_{23C}, Δ_{34C}, Δ_{41C})*

$$Vol_{water} = \Omega_{a32}\frac{h_2 + h_3}{3} + \Omega_{2ba}\frac{h_2}{3} \tag{2.88}$$

In the computation of the fluxes through the edges (1-2) and (1-3), the modified lengths are used. The modified length is computed under the assumption that the water elevation is constant over a cell.

Quadrilateral cells

The numerical treatment of the bed source term calculation greatly increases in complexity if one has to deal with quadrilateral elements with four nodes. In the common case these nodes do not lie on a plane and therefore the slope of the element is not uniquely determined and not trivially computed. Even if the nodes initially lie on a plane, this situation can change if morphological simulations with mobile beds are performed.

To prevent complex geometric algorithms and to avoid the problematic bed slope calculation, the quadrilateral element is divided up into four triangles. Then the calculations outlined before for triangular cells can be applied separately on each triangle.

The four triangles are obtained by connecting each edge with the centroid C of the element. The required bed elevation of this centroid C is thereby estimated by a weighted distance averaging of the nodal elevations as proposed by Valiani et al. (2002):

$$z_C = \frac{\sum_{k=1}^{4} z_k \sqrt{(x_k - x_C)^2 + (y_k - y_C)^2}}{\sum_{k=1}^{4} \sqrt{(x_k - x_C)^2 + (y_k - y_C)^2}} \tag{2.89}$$

where z_C is the interpolated bed elevation of the centroid and k is the index of the four nodes of the quadrilateral element. Following this procedure the water volumes and bed slopes are calculated in the same way as outlined before for each of the triangles. Finally the bed slope term of the quadrilateral element is obtained as sum over the values of the corresponding four triangles.

$$\iint_{\Omega} \boldsymbol{S}_B \, \mathrm{d}\Omega = g \left(\iint_{\Omega} h \, \mathrm{d}\Omega \right) \begin{pmatrix} 0 \\ S_{Bx} \\ S_{By} \end{pmatrix} = g \sum_{k=1}^{4} \left[Vol_{water,\Delta_k} \begin{pmatrix} 0 \\ S_{Bx,k} \\ S_{By,k} \end{pmatrix} \right] \tag{2.90}$$

This calculation method circumvents the problematic bed slope determination for the quadrilateral element during the calculation of the bed source term.

But for other purposes, like for morphological simulations with bed load transport, a defined bed slope within the quadrilateral element may be needed. For such situations the bed slope is determined by an area-weighting of the slopes of the k triangles. Replacing ϕ with the x- or y-coordinate, one obtains the bed slopes as follows:

$$\frac{\partial z_B(x,y)}{\partial \phi} \approx \frac{1}{A_{Quad}} \sum_{k=1}^{4} \left(\frac{\partial z_{B,k}(x,y)}{\partial \phi} A_{\Delta,k} \right) \quad , \quad \phi = x, y \tag{2.91}$$

2.2.3.3 Conservative property (C-Property)

The usually applied shock capturing schemes were originally designed for hyperbolic systems without source terms. Such schemes do not guarantee the C-property in the presence of source terms like the bed source term in the shallow water equations. At stagnant conditions, when simulating still water above an uneven bed, unphysical fluxes and oscillations may result from an unbalance between the flux gradients and the bed source terms. In order to guarantee the C-property following condition, the reduced momentum equation for stagnant conditions, must hold true:

$$\begin{aligned} \oint_{d\Omega} \left(\frac{1}{2} g h^2 \right) n_x \, \mathrm{d}l &= g \iint_{\Omega} h S_{Bx} \, \mathrm{d}\Omega|_{\zeta=const} \\ \oint_{d\Omega} \left(\frac{1}{2} g h^2 \right) n_y \, \mathrm{d}l &= g \iint_{\Omega} h S_{By} \, \mathrm{d}\Omega|_{\zeta=const} \end{aligned} \tag{2.92}$$

Therefore it is necessary to guarantee conservation by an appropriate treatment and discretisation of the flux gradients and the bed source terms. Recent studies provide several approaches for proper source term treatment, but are often either computationally complex or cannot be easily transferred to unstructured meshes. Following the approach of Komaei, the left hand terms $0.5gh^2_{mod}$ are calculated with a modified depth at the edges. This modified depth is calculated as integral over the linearly varying water depth at an edge.

$$h^2_{mod} = \frac{1}{L} \int_0^L h^2(x) \, \mathrm{d}x = \frac{h_i^2 + h_i h_j + h_j^2}{3} \tag{2.93}$$

h_i and h_j are the water depths at the edge's left and right nodes, as shown in Figure 2.28.

It can be easily proved that using h_{mod} in the determination of the flux gradients guarantees the C-property on unstructured grids, if the bed source terms are discretized as product of the water volume with the bed slope as shown before. This is exemplified here for a completely wetted triangle in x-direction:

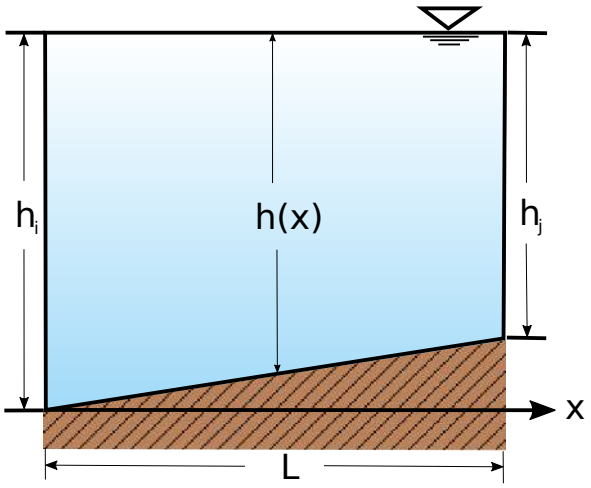

Figure 2.28 *Edge with linearly varying water depth*

$$
\begin{aligned}
& g \iint_{\Omega} h S_{Bx} \, \mathrm{d}\Omega|_{\zeta=const} = g Vol_{water} S_{Bx} = g \frac{1}{3}(h_1+h_2+h_3)\frac{1}{2}[b_1 z_{B,1} + b_2 z_{B,2} + b_3 z_{B,3}] \\
& = \frac{g}{6}(h_1+h_2+h_3)[b_1(\zeta - h_1) + b_2(\zeta - h_2) + b_3(\zeta - h_3)] \\
& = \frac{g}{6}(h_1+h_2+h_3)\left[\zeta \underbrace{(b_1+b_2+b_3)}_{=0} - b_1 h_1 - b_2 h_2 - b_3 h_3\right] \\
& = -\frac{g}{6}(h_1+h_2+h_3)[b_1 h_1 + b_2 h_2 + b_3 h_3]
\end{aligned}
$$

$$
\begin{aligned}
& -\oint_{d\Omega} \left(\frac{1}{2} g h^2\right) n_x \, \mathrm{d}l = -\frac{1}{2} g \sum_{k=1}^{n} \left[\int_{x=0}^{l} h(x) \, \mathrm{d}x\right] \\
& = -g\frac{1}{2}\left[\frac{1}{3}(h_1^2 + h_1 h_2 + h_2^2) b_3 + \frac{1}{3}(h_2^2 + h_2 h_3 + h_3^2) b_1 + \frac{1}{3}(h_3^2 + h_3 h_1 + h_1^2) b_2\right] \\
& = -\frac{g}{6}(h_1+h_2+h_3)[b_1 h_1 + b_2 h_2 + b_3 h_3]
\end{aligned}
\tag{2.94}
$$

Both terms lead to the same result and therefore balance exactly for stagnant flow conditions.

2.2.3.4 Discretisation of Boundary Conditions

The hydrodynamic model uses the essential boundary conditions, i.e. velocity and water surface elevation are to be specified along the computational domain. The theoretical background of the boundary condition has already been already discussed in book one "Physical Models". In this part the numerical treatment of the two most important boundary types, namely inlet and outlet will be discussed separately.

2.2.3.4.1 Inlet Boundary

- Hydrograph:

The hydrograph boundary condition is applied to a user defined inlet section which is defined by a list of boundary edges. The velocity vectors are assumed to be perpendicular

to these boundary edges and the inlet section is assumed to be a straight line with uniform water elevation (1-D treatment). If there is an incoming discharge it must be given as hydrograph. Both steady and unsteady discharges can be specified along the inlet section, where water surface elevation and the cross-sectional area are allowed to change with time. For an unsteady discharge, the hydrograph is digitized in a data set of the form:

$$\begin{array}{cc} t^1 & Q^1 \\ \cdots & \\ t^n & Q^n \\ \cdots & \\ t^{end} & Q^{end} \end{array}$$

where Q^n is the total discharge inflow at time t^n. The hydrograph specified in this way, can be arbitrary in shape. The total discharge is interpolated, based on the corresponding time.

The water elevation at the inlet section is determined by the values of the old time step at the adjacent elements. In case of dry conditions or supercritical flow at the inlet section, the water elevation is calculated according the known discharge. For these iterative h-Q calculations normal flow is assumed and an average bed slope, perpendicular to the inlet section, must be given.

The calculated total inflow discharge is distributed over the inflow boundary edges and the according momentum component is calculated. Thereby only the edges below the water surface elevation receive a discharge. If some edges lie above the water elevation they are treated as walls. To distribute the inflow discharge over the wetted inflow boundary edges following approach is implemented.

The discharge Q_i for each edge i is calculated as fraction of the total discharge Q_{in} using a weighting factor K_i as

$$Q_i = K_i Q_{in} \tag{2.95}$$

This weighting factor K_i can be calculated based on its local conveyance as

$$K_i = \frac{c_{fi}\sqrt{R_i}\sqrt{g}A_i}{\sum_{j=1}^{n}(c_{fj}\sqrt{R_j}\sqrt{g}A_j)} \tag{2.96}$$

where K_i is the discharge at edge i and the index j ranges from the first to the last wetted edge of the inflow boundary edges. R_i , A_i and c_{fi} are the hydraulic radius, the wetted area and the friction factor of the corresponding elements respectively.

Alternatively, the weighting factor K_i can be calculated based on the local wetted areas at the edge i, which finally results in equal inflow velocities over all edges.

$$K_i = \frac{A_i}{\sum_{j=1}^{n} A_j} \tag{2.97}$$

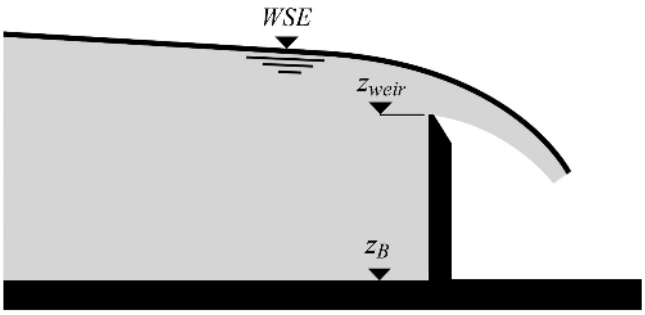

Figure 2.29 *Flow over a weir*

2.2.3.4.2 Outlet Boundary

- Free surface elevation boundary:

As is mentioned in Table 1.2, just one outlet boundary condition is necessary to be defined. This could be the flux, the water surface elevation or the water elevation-discharge curve at the outflow section. There is often no boundary known at the outlet. In this situation, the boundary should be modelled as a so-called free surface elevation boundary. A zero gradient assumption at the outlet could be a good choice. This could be expressed as follows:

$$\frac{\partial}{\partial \mathbf{n}} = 0 \tag{2.98}$$

Although this type of boundary condition has a reflection problem, numerical experiences have shown that this effect is limited just to five to ten grid nodes from the boundary. Therefore it has been suggested to slightly expand the calculation domain in the outlet region to use this type of outlet boundary (Nujić, 1998).

- Weir:

In the other possibility of outlet boundary condition namely defining a weir (Figure 2.29), the discharge at the outlet is computed based on the weir function (Chanson, 1999)

$$q = \frac{2}{3} C \sqrt{2g(h_{up} - h_{weir})^3}$$

where

$$C = 0.611 + 0.08 \frac{h_{up} - h_{weir}}{h_{weir}} \quad ; \quad h_{up} = WSE - z_B \quad and \quad h_{weir} = z_{weir} - z_B$$

Alternatively, instead of calculating the factor C automatically, a constant Poleni factor can be set.

The hydraulic and geometric parameters such as WSE, z_B are the calculated variables on the adjacent elements of the outlet boundary. Here it is assumed that the water surface elevation is constant within the element. The weir elevation z_{weir} is a time dependent parameter. Based on the weir elevation (Figure 2.30) some edges of the outlet are considered as a weir and the others have free surface elevation boundary condition. In order to avoid

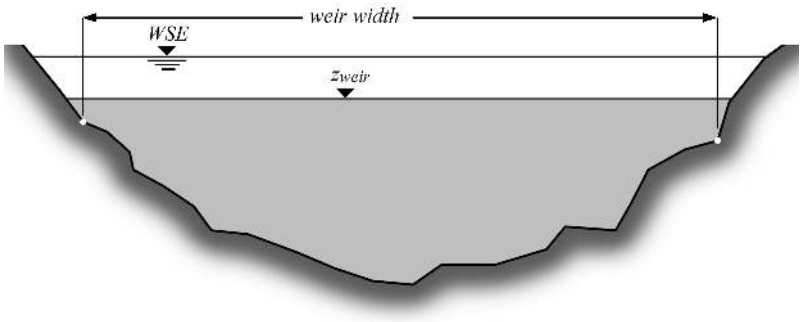

Figure 2.30 *Outlet cross section with a weir*

instabilities due to the water surface fluctuations, the following condition are adopted in the program

if $(h_{up}(t) \leq h_{weir}(t) + kh_{dry}) \Rightarrow$ edge is a wall

if $(h_{up}(t) > h_{weir}(t) + kh_{dry}) \Rightarrow$ edge acts as weir or a free surface elevation boundary

k is a numerical factor and has been set to 3 in this version. Figure 2.30 also shows the effective computational width of a weir in a natural cross section.

- Gate:

The discharge over a gate boundary condition is computed according to

$$q = \mu h_{gate}\sqrt{2gh_0} \tag{2.99}$$

Within this formula, h_0 is the water depth upstream of the gate. h_{gate} denotes the difference between gate level and soil elevation at the gate's location. The factor μ can be defined by the user (constant value or dynamical). According to Bernoullis' equation and assuming the upstream water is at rest, the discharge coefficient is

$$\mu = \frac{\delta}{\sqrt{1 + \frac{\delta h_{gate}}{h_0}}} \tag{2.100}$$

where δ is the contraction coefficient of the outflow jet. Assuming a sharp-edged sluice gate the contraction coefficient is calculated by Voigt (1971).

$$\delta = \frac{1}{1 + 0.64\sqrt{1 - (h_{gate}/h_0)^2}} \tag{2.101}$$

The value of μ is usually around 0.6.

The gate formula is only active if the water surface elevation in the element belonging to the boundary edge is higher than the gate elevation. Other possible states of the gate are wall (in case of gate elevation lower than the soil elevation) and zero-gradient (in all other cases).

- h-Q-relation:

A water elevationdischarge relation can be applied as outflow boundary condition. Several outflow boundary edges are therefore defined in a list. The outflow velocity vectors are assumed to be perpendicular to the outflow boundary edges and the outflow section is assumed to be a straight line with a uniform water elevation (1-D treatment). A relation must be given between the outflow water surface elevation and the total outflow discharge. This h-Q relation is digitized in a data set of the form

$$\begin{matrix} h^1 & Q^1 \\ \dots & \\ h^n & Q^n \end{matrix}$$

where Q^n is the total outflow discharge for a given water surface elevation h^n. The h-Q-relation specified in this way, can be arbitrary in shape. The total outflow discharge is interpolated, based on the corresponding water surface elevation.

The water surface elevation at the outflow section is determined from the values of the elements adjacent to the boundary edges at the last time step. With this water elevation a total outflow discharge is interpolated using the given h-Q relation. Alternatively, if no h-Q-relation is given, the outflow discharge is calculated under the assumption of normal flow at the outflow section. In this case an average bed slope perpendicular to the outflow cross section must be given.

The calculated total outflow discharge is then distributed over all wetted outflow boundary edges according to a weighting factor based on the local conveyance or the wetted area (see Section 2.2.3.4.1). In contrast, cells which are not fully wetted are set to wall boundary.

- Z-Hydrograph:

Another outflow boundary condition is to specify the time evolution of the water surface at the outflow location. This boundary conditions aims to control the water elevation at the outlet, e.g. at outflows to reservoirs with known water elevations.

A time evolution of the water surface elevation must be given in the form

$$\begin{matrix} t^1 & WSE^1 \\ \dots & \\ t^n & WSE^n \end{matrix}$$

If the actual outlet water elevation lies below the desired reservoir elevation, than a wall boundary is set at the outflow. On the other hand, if the actual water elevation lies above the reservoir water elevation, a Riemann solver is applied. The Riemann problem is defined between the outflow edges and a ghost cell outside of the domain with the reservoir water level. (But be aware that the outlet water level is not guaranteed to be identical to the specified water elevation.)

2.2.3.4.3 Inner Boundaries

Inner boundary conditions are used to model hydraulic structures like a weir or a gate within a model domain. Since the Saint Venant equations are not applicable for calculating the flux at these structures, an empirical approach is implemented in BASEMENT.

For the inner boundary in BASEchain a definition of a reference cross section which is located upstream of the weir/gate is mandatory. The reference cross section is the cross section where the water surface is just not affected by the flow acceleration at the weir (Figure 2.31).

In the 1-D model only one weir field with the width of all weir fields can be set up. Thus, an empirical formula for the effective width w_{eff} is implemented to take the reduction of the width due to head losses at piers and abutments into account,

$$w_{eff} = w - 2(n_p c_p + c_a)H_{ref} \tag{2.102}$$

where w is the total width of all the weir fields, n_p is the number of piers, c_p is a coefficient depending on the shape of the piers, c_a is a coefficient depending on the shape of the abutment and H_{Ref} is the energy height above the bottom level at the reference cross section.

- Inner Weir:

The inner weir uses a slightly other approach than the boundary weir. If the weir crest is higher than the water surface elevation in the neighbouring elements, the weir acts as a wall. If one or both of the neighbouring water surface elevations are above the weir crest (1, Figure 2.31), this weir formula is used

$$q = \frac{2}{3}\mu\sigma_{uv}\sqrt{2g(z_{Ref} - z_{weircrest})^3} \tag{2.103}$$

where q is the specific discharge related to the effective width w_{eff}. This formula is the classical POLENI formula for a sharp crested weir with an additional factor σ_{uv} which accounts for the reduction in discharge due to incomplete weir flow. If only one side of the weir has a water surface elevation above the weir crest, then a complete weir flow is given with $\sigma_{uv} = 1$ (Figure 2.31). As soon as the water surface elevation tops the weir crest level on both sides of the weir, the incomplete case is active and the reduction factor σ_{uv} is calculated according to the Diagram in Figure 2.32. z_{Ref} is the water surface elevation at the reference cross section. The weir bottom level (2) is the lowest possible weir crest level (Figure 2.31).

The momentum flux at the weir is a function of the wetted area A_{Weir} above the weir crest. In BASEchain two options of calculation types are implemented:

I) "Standard": The wetted area above the weir crest is calculated as

$$A_{Weir} = (z_{Ref} - z_{weircrest})w_{eff}$$

II) "Critical": It is assumed that the critical flow depth is at the weir crest. The critical flow depth is calculated as $h_{crit} = 2/3[z_{Ref}\text{-}z_{weircrest}]$. The wetted area above the weir crest is calculated as $A_{Weir} = h_{crit}w_{eff}$. For a model calibration the water surface elevation z_{crit} of the critical flow depth above the weir crest can be adjusted by the calibration factor f_{crit}. $z_{correction} = z_{crit} + f_{crit}(z_{Ref} - z_{crit})$. The formula for the calculation of the factor f_{crit} is $f_{crit} = a + bh_{crit}$.

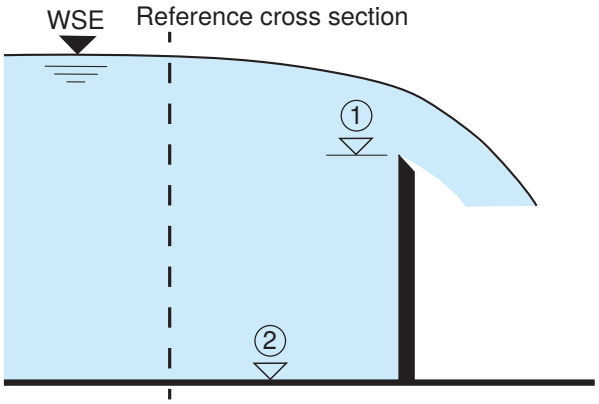

Figure 2.31 *Inner weir with a complete weir flow. (1) weir crest level, (2) weir bottom level, Reference cross section where water surface in unaffected by the flow acceleration at the weir*

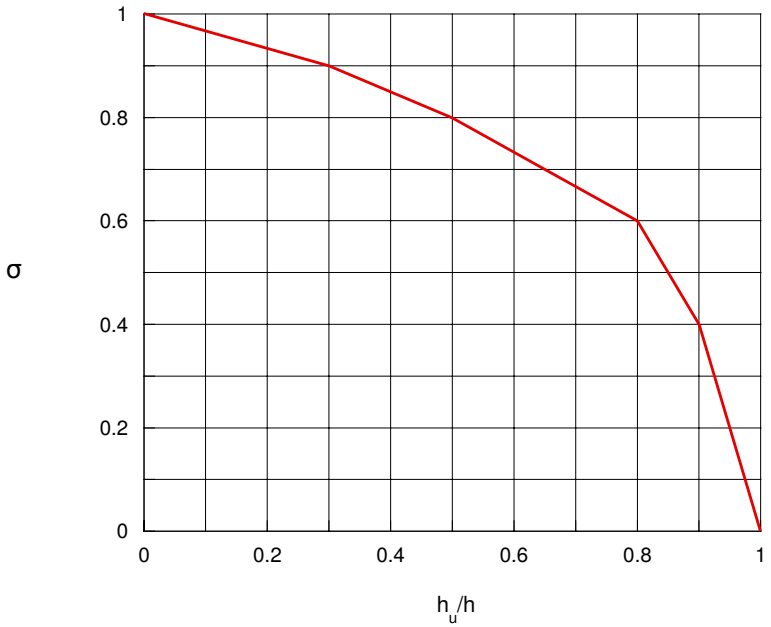

Figure 2.32 *Reduction factor σ_{uv} for an incomplete flow over the weir. h_u is the downstream water depth over the weir crest and h denotes the upstream flow depth over the weir crest*

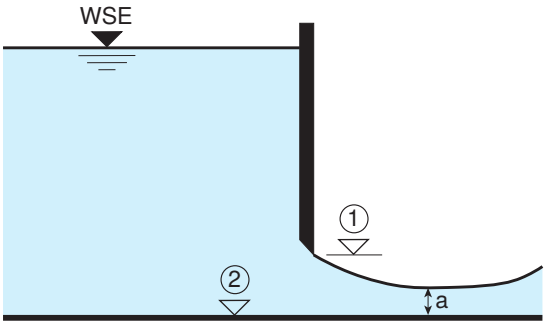

Figure 2.33 *Inner sluice gate. (1) gate level, (2) gate bottom level, a = water depth at vena contracta*

- Inner Gate:

In BASEchain three types of gates are implemented: sluice gate, gate with flap and radial gate with flap. The simplest gate type is the sluice gate which has three modes. Either the gate level (1) is equal or less than the gate bottom level (2, Figure 2.33). The gate is then closed and acts as a wall.

If the gate level is above the gate bottom level, the gate is considered as open. As long as the water surface elevation near the gate is below the gate level, the flux at the inner boundary is calculated as a weir flux with, where the weir level is equal to the gate bottom level. The gate is active as soon as one of the neighbouring water surface elevations is above the gate level (Figure 2.33). Similar to the gate boundary condition, the calculation of the specific discharge is

$$q = \mu h_{gate} \sqrt{2gh_0} \tag{2.104}$$

The gate opening is defined as h_{gate} = gate level (1) - gate botom level (2) (Figure 2.33), h_0 denotes the water depth at the cross section upstream of the gate. The discharge coefficient μ depends on the contraction factor δ which is the ratio of the water depth a at the vena contracta to the gate opening h_{gate} and is calculated as

$$\mu = \delta / \sqrt{1 + \frac{\delta h_{gate}}{h_0}} \tag{2.105}$$

Derived from the conjugate depths at a hydraulic jump the criterion for considering the backwater effect at the gate is defined as

$$\frac{h_d}{h_{gate}} > \frac{\delta}{2} \left(\sqrt{1 + \frac{16}{\delta \left(1 + \frac{\delta h_{gate}}{h_0}\right)} \frac{h_0}{h_{gate}}} - 1 \right) \tag{2.106}$$

where h_d is the water depth downstream of the gate. When the backwater effect has to be considered the discharge coefficient depends also on the water depth downstream of the gate (Bollrich, 2000).

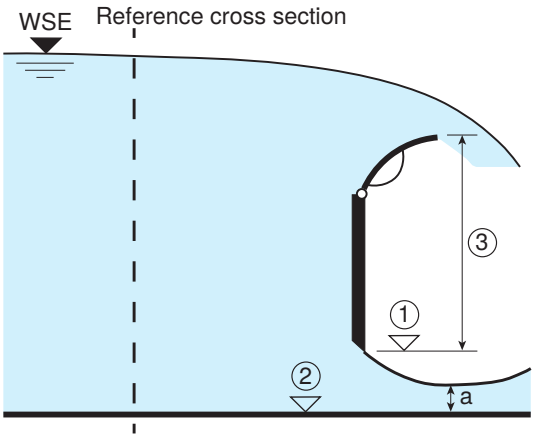

Figure 2.34 *Inner gate with flap. (1) gate level, (2) gate bottom level, (3) gate size which is defined as the difference between flap level and gate level, a = water depth at the vena contracta*

$$\mu = \delta\sqrt{\left[1-2\frac{\delta h_{gate}}{h_0}\left(1-\frac{\delta h_{gate}}{h_d}\right)\right]-\sqrt{\left[1-2\frac{\delta h_{gate}}{h_0}\left(1-\frac{\delta h_{gate}}{h_d}\right)\right]^2+\left(\frac{h_d}{h_0}\right)^2-1}} \tag{2.107}$$

As for the momentum, the velocity through the gate is taken into account in both, downstream and upstream direction.

The second gate type is the gate with flap. Three modes are equal to the sluice gate:

I) The gate is closed and the water surface elevation is lower than the flap level. The inner boundary acts as a wall.

II) The water surface elevation is lower than the gate level. Then the exact Riemann solver is used.

III) The gate is active. This means the water surface elevation is higher than the gate level but lower than the flap level. In this case the gate flow is calculated by the gate formula.

In case of a closed gate an overflow at the flap is possible. Then the inner boundary acts as a weir and the weir level corresponds to the flap level. The flux calculation complies with the flux calculation of the inner weir. For the weir flow a discharge coefficient depending on the shape of the flaps must be defined. If the gate is active and the water surface elevation is higher than the flap level, the flux is calculated as the sum of the gate flow and the weir flow (Figure 2.34).

The third gate type in BASEchain is the radial gate with flap. The specific discharge at a radial gate is calculated with this formula (Knapp, 1960)

$$q = \psi h_{gate}\sqrt{2g\left(H_{Ref}-\frac{h_{gate}}{2}\right)} \tag{2.108}$$

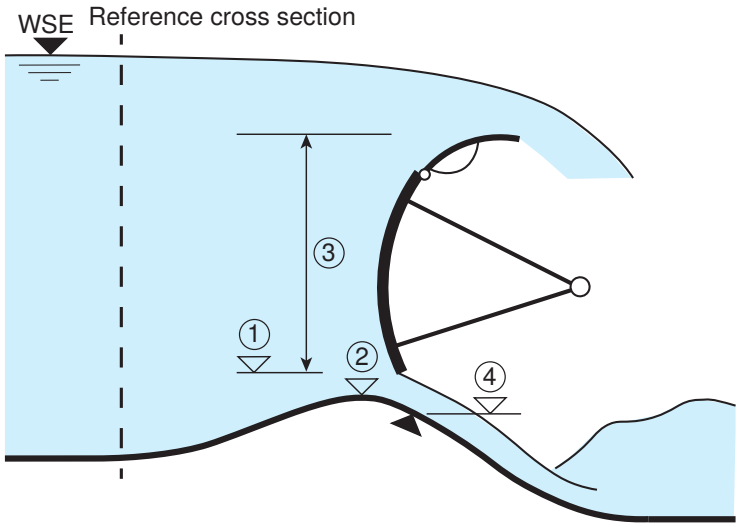

Figure 2.35 *Radial gate with flap at a Jambor sill: (1) gate level, (2) weir bottom level, (3) gate height which is the difference between flap level and gate level, (4) gate bottom level which is the level of the closed gate*

where H_{Ref} is the energy height at the reference cross section above the bottom level and ψ is the discharge coefficient which is defined as $\psi = \alpha(h_{gate}/H_{Ref})^{\beta}$. The user has to define the calibration parameters α and β. The gate is active, when the gate level is higher than the gate bottom level. The gate height h_{gate} is the difference between gate level (1) and gate bottom level (4) (Figure 2.35).

A radial gate is often combined with a weir sill, a so called Jambor sill. Due to various operational conditions for this gate type several parameters have to be defined. The gate is closed, if the gate level is equal or less than the gate bottom level at the Jambor sill (4, Figure 2.35). In this case the inner boundary acts either as a wall or a as a weir with the overfall at the flaps. This depends on the water surface elevation, whether it is higher or lower than the flap level.

If the water surface elevation is higher than the flap level, the flux is calculated in the same way as the gate with flap, namely as the sum of the gate flow and the weir flow. If the gate is closed and the water surface exceeds the flap level, the inner boundary acts as a weir.

As soon as the radial gate is open and the water surface elevation is lower than the gate level the inner boundary acts as a weir with the weir bottom level (2, Figure 2.35). For the calculation of the weir flux the energy height above the bottom elevation at the reference cross section is used.

- Inner HQ-relation:

The inner HQ-Relation boundary acts similar to the inner gate boundary condition. However, instead of applying the gate-formula to determine the discharge over the inner structure, a water surface discharge relation is applied. By specifying a self-determined HQ-relation for the inner structure, a lot of flexibility is offered for the implementation. The HQ-relation may be used e.g. to simulate a culvert, a bridge or a pipe flow. The quality of the results depends strongly on the provided HQ-table!

For each edge of the upstream stringdef, the water level is taken from the adjacent cell and the HQ-relation is used to determine the corresponding discharge over the edge (scaled to the edge length). The water flows through the inner structure and re-enters the domain at the downstream corresponding edge. The HQ relation is digitized in a data set as

$$\begin{matrix} h^1 & Q^1 \\ \dots & \\ h^n & Q^n \end{matrix}$$

where Q^n is the total outflow discharge and h^n is the water surface elevation.

Differing from other inner boundaries, this boundary operates only in a given direction from upstream to downstream (stringdef1 = upstream, stringdef = downstream) and cannot deal with changing flow directions! Furthermore, please note that the inner HQ-relation does not depend upon the z-elevations of the boundary cells and, hence, may be used to act over large distances with arbitrary height differences, as e.g. a long pipe within the domain. At the moment, however, it is not feasible to incorporate information of the downstream water surface elevation, what limits the applicability to culvert or pipe modelling in some scenarios.

If inner boundaries and sediment transport computations are combined, the problem arises that sediment masses are not transported over the inner boundary but stop in front of the inner boundary structure. This behaviour is undesired in some scenarios. A solution to overcome this problem, allowing for sediment continuity, is the use of 'dredge sources' which can be used to let the sediments pass the inner boundary (see Section 2.3.3.3.2).

2.2.3.4.4 Moving Boundaries

Dry, partial wet and fully wet elements

Natural rivers and streams are highly irregular in both plan form and topography. Their boundaries change with the time varying water level. The FV-based model with moving boundary treatment is capable of handling these complex and dynamic flow problems conveniently. The computational domain expands and contracts as the water elevation rises and falls. Obviously, the governing equations are solved only for wet cells in the computational domain. An important step of this method is to determine the water edge or the instantaneous computational boundary. A criterion, h_{min} , is used to classify the following two types of nodes:

1. A node is considered dry, if $z_S \leq z_B + h_{min}$
2. A node is considered wet, if $z_S > z_B + h_{min}$

The determination of h_{min} is tricky, which can vary between 10^{-6} m and 0.1 m. Based on the flow depth at the centre of the element we defined three different element categories (Figure 2.36):

1. dry cells where the flow depth is below h_{min},
2. partial wet cells where the flow depth above h_{min} but not all nodes of the cell are under water and
3. fully wet cells where all nodes included cell centre are under water.

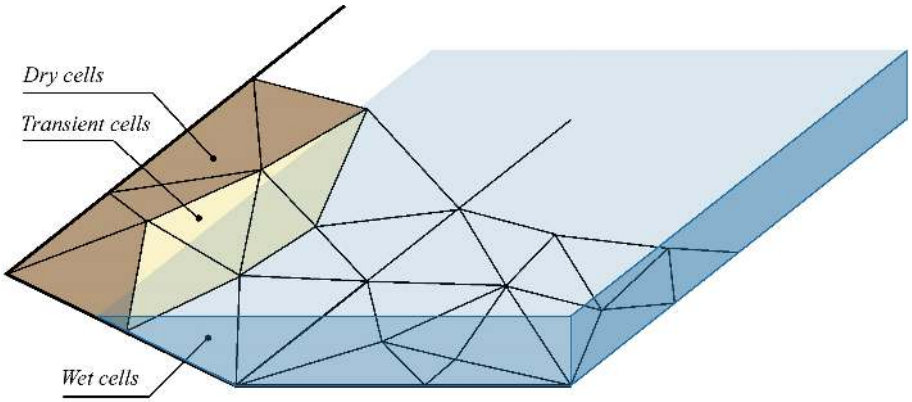

Figure 2.36 *Schematic representation of a mesh with dry, partial wet and wet elements*

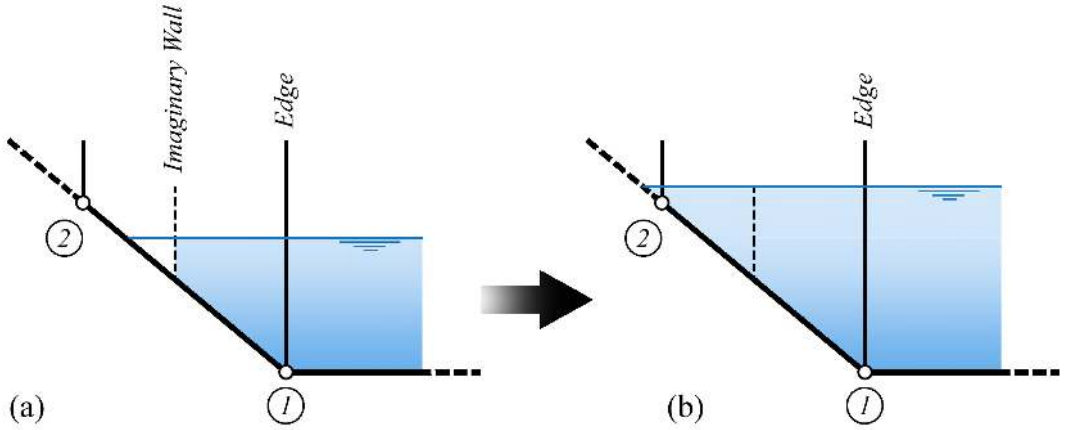

Figure 2.37 *Wetting process of an element*

By comparing the water surface elevation of two adjacent elements (Figure 2.37) and determining which cell is dry it was decided whether there were or not a flux through the edge.

Although the determination of h_{min} is tricky, as it mentioned above, it has been successfully used in the past, has in the range of 0.05 ~ 0.1 m for natural rivers. It can be adjusted to optimize the solution for particular flow and boundary conditions. It is suggested to consider it close to $min(0.1h, 0.1)$.

Another problem related to partially wetted elements is the determination of the final velocities at the end of the time step from the vector of the conserved variables $\mathbf{U}$. To calculate the velocities the conserved variables must be divided by the flow depth as indicated below.

$$\begin{aligned} \nu_x &= \frac{(\nu_x h)}{h} \\ \nu_y &= \frac{(\nu_y h)}{h} \end{aligned} \tag{2.109}$$

For an element situated at the wetting and drying interface, the outflow of water amounts may lead to very small water depths. Because the water depths are in the denominator,

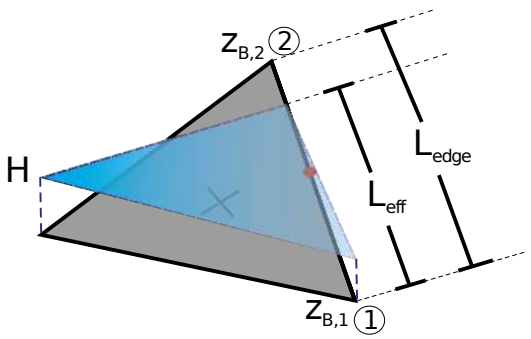

Figure 2.38 *Definition of effective length at partially wetted edge*

instabilities can arise when updating the new velocities. To prevent these instabilities it is checked if the water depth is smaller than the residual h_{min} . In such a case the velocities are set to zero, since the water will not move in such a practical situation.

Flux computations at dry-wet interfaces

When solving the shallow water equations along dry-wet interfaces, special attention is needed and different situations must be distinguished. Some models solve the complete equations only for completely wetted elements, where all nodes are under water. Here, in contrast, the flux computations are also performed for partially wetted elements. This procedure is computationally more costly and has larger programming efforts, but it leads to more accurate results in some situations and it can reduce problems related to the wetting-drying process.

The complete flux computation is performed over a partially wetted edge if two conditions are fulfilled:

- At least one of the both elements adjacent to the edge must be wetted, i.e. its water depth must be above h_{min} .
- At least at one side of the edge, the element's water surface elevation must be above the average edge elevation.

The flux computations over partially wetted edges need to take into account that the flux takes not place over the whole length of the edge (see Figure 2.38). The actually over flown effective length L_{eff} is calculated as follows assuming a constant water level.

$$L_{eff} = \left(\frac{H - z_{B,1}}{z_{B,2} - z_{B,1}} \right) L_{edge} \tag{2.110}$$

Here H is the water surface elevation in the partially wetted element and $z_{B,1}$, $z_{B,2}$ are the nodal elevations of the edge

In Figure 2.39 several possible configurations at dry-wet interfaces are illustrated which need to be treated appropriately. Attention must be paid to correctly reproduce the physics and to preserve the C-property for stagnant flow conditions.

The first case a) shows a wetted left element adjacent to a dry right element, where the left water surface elevation H_L is above the center elevation $z_{B,R}$ of the right element. Here, no

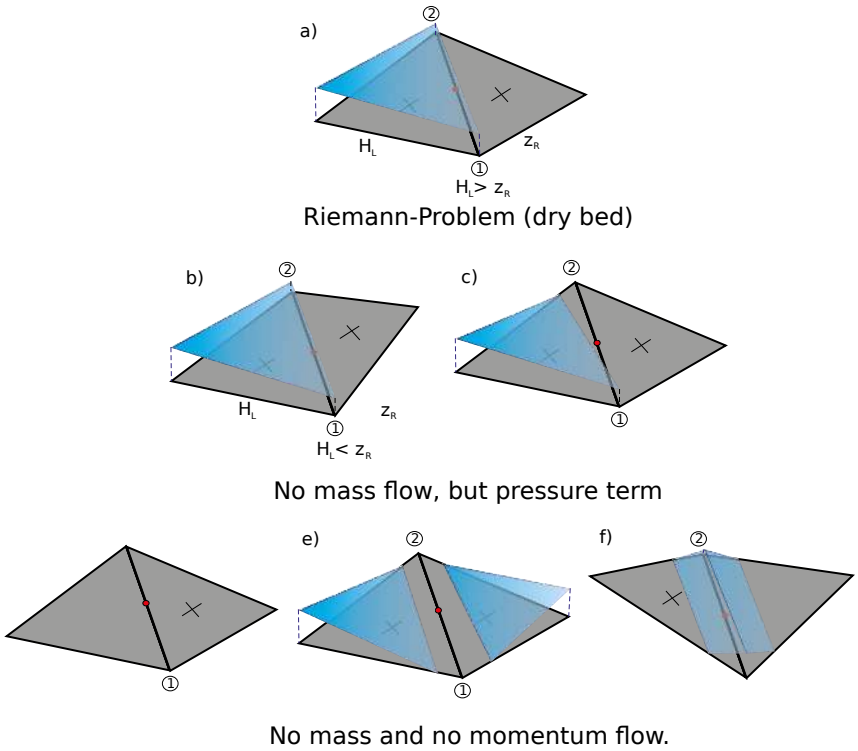

Figure 2.39 *Different cases for flux computations over an edge at wet-dry interfaces*

special treatment is needed and a Riemann problem can be formulated. But the Riemann solver must be capable of treating dry bed conditions in an appropriate way.

Case b) corresponds to an adverse slope at the right, dry element, where the left water surface elevation H_L is below the right bed elevation $z_{B,R}$. This case has recently received attention in the literature, as e.g. by Brufau et al. (2002). It requires a special treatment because applying the Riemann solver in a situation with adverse slopes can produce incorrect results. Some authors suggest to treat the dry-wet interface as a wall or to set the velocities to zero. But these treatments are problematic because they do not always preserve the C-property. Here a simple method is adopted whereas no Riemann problem is formulated at the edge. But instead, only the pressure terms are evaluated which exactly balance the bed source terms, thus guaranteeing a correct behaviour for stagnant flow conditions.

In case c) the water elevation H_L at the left element is below the average edge elevation. In such a situation no Riemann problem is formulated as stated above. But again the pressure term is evaluated here to preserve the C-property.

Finally, in cases d), e) and f) either both elements are dry or the edge is completely dry. In these cases neither mass fluxes nor momentum fluxes need to be evaluated.

2.2.3.5 Solution Procedure

The logical flow of data through BASEplane from the entry of input data to the creating of output files and the major functions of the program is illustrated in Figure 2.40, Figure 2.41 and Figure 2.42 shows the data flow through the hydrodynamic and morphodynamic routines respectively. Program main control data is read first, and then the mesh file,

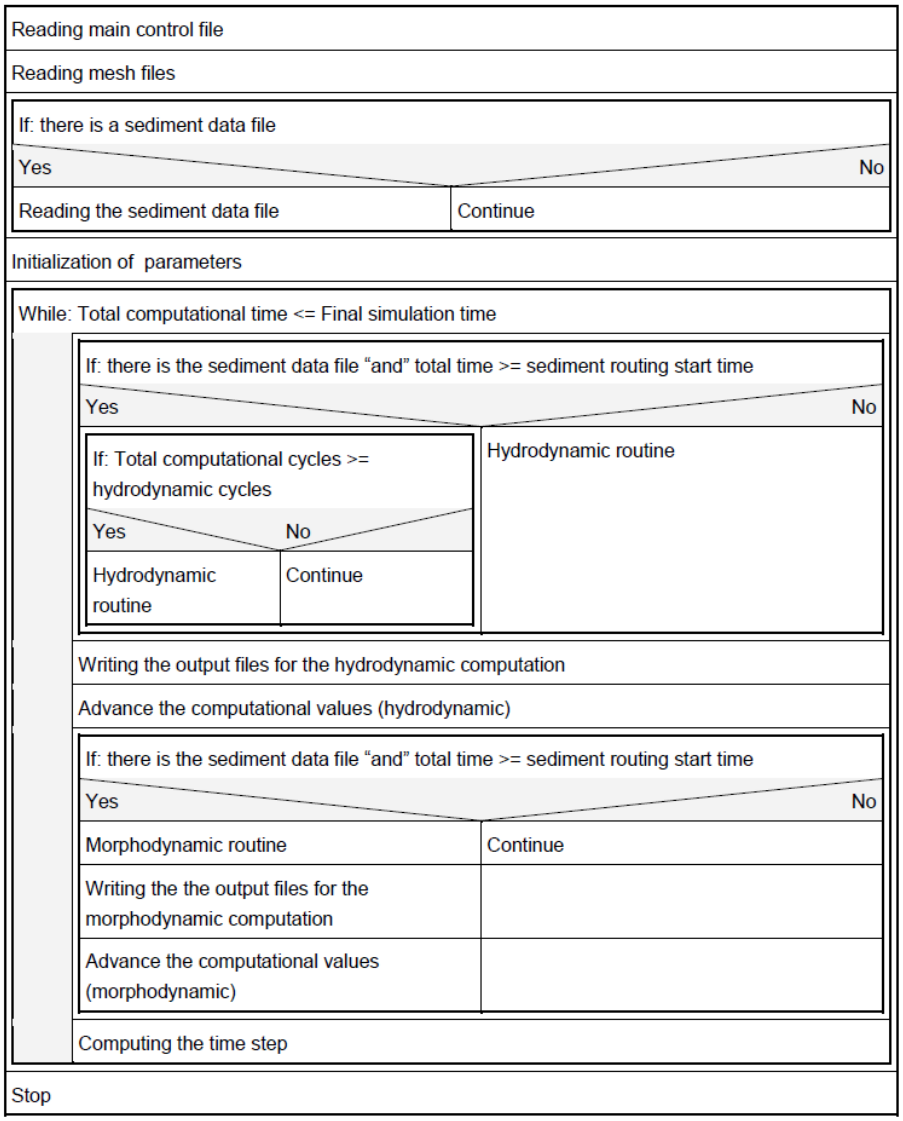

Figure 2.40 *The logical flow of data through BASEplane*

and then the sediment data file if there is one. Initialization of the parameters and computational values is made next. If the sediment movement computation is requested, the hydrodynamic routine will be started in cycle steps defined by user, otherwise the hydrodynamic routine is run. After the hydrodynamic routine, the morphodynamic routine is carried out next, if it is requested. Results can be printed at the end of every time steps or only at the end of selected time steps.

a) General solution procedure of BASEplane (Figure 2.40)
b) Hydrodynamic routine in detail (Figure 2.41)
c) Morphodynamic routine in detail (Figure 2.42)

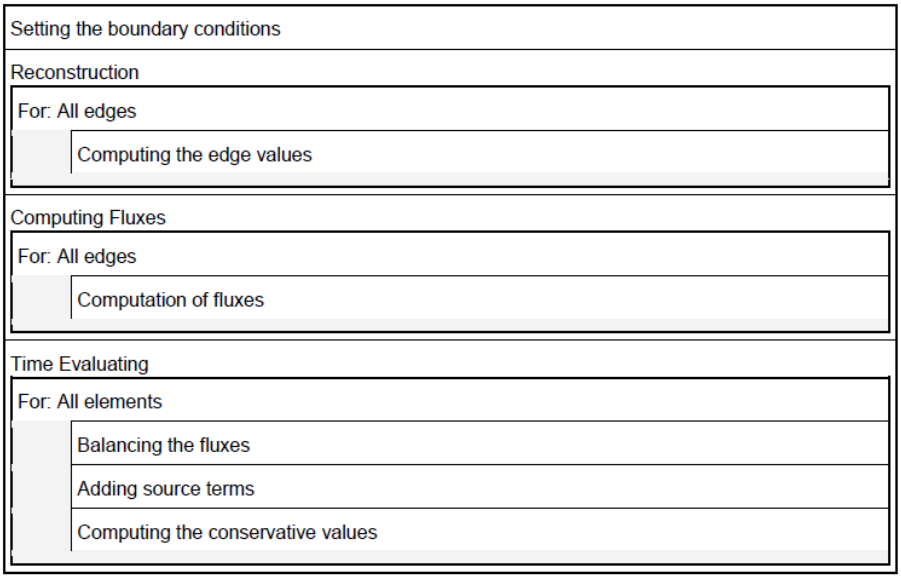

Figure 2.41 *Data flow through the hydrodynamic routine*

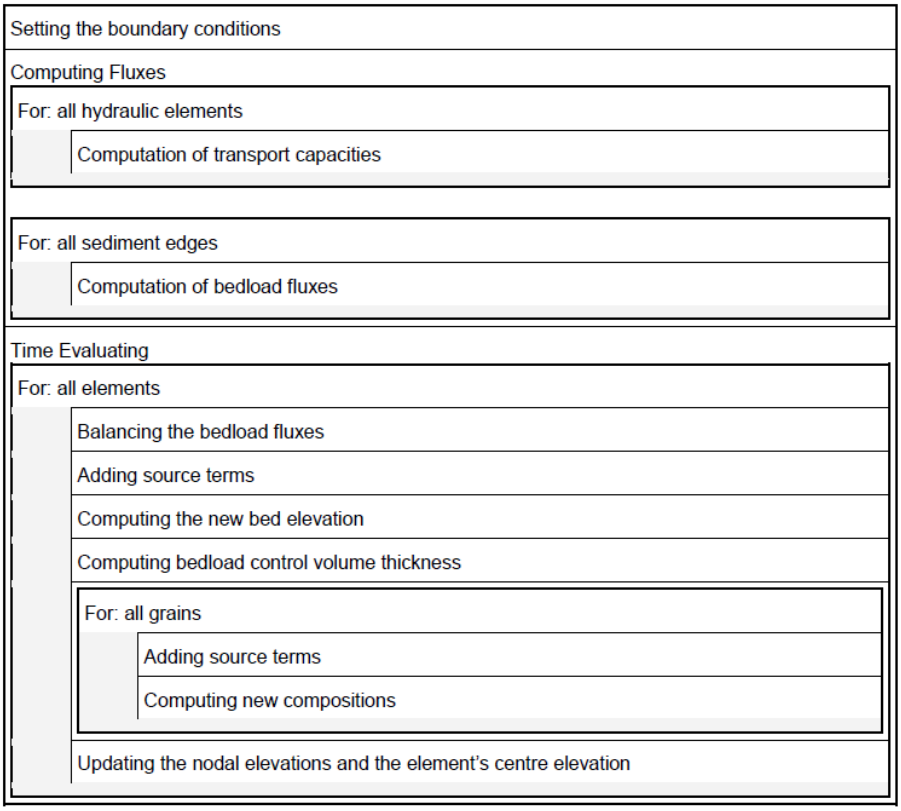

Figure 2.42 *Data flow through the morphodynamic routine*

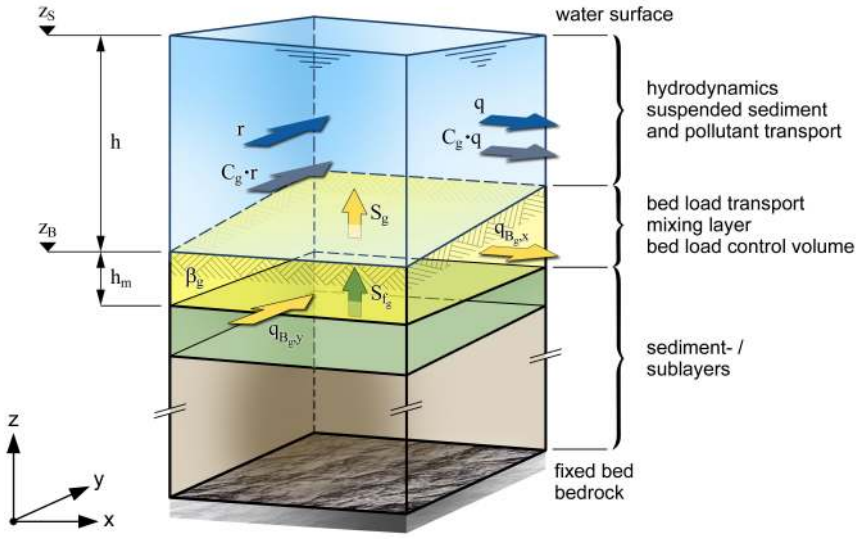

Figure 2.43 *Vertical Discretisation of a computational cell*

2.3 Solution of Sediment Transport Equations

2.3.1 Vertical Discretisation

2.3.1.1 General

A two phase system (water and solids) in which the sediment mixture can be represented by an arbitrary number of different grain size classes is formulated. The continuous physical domain has to be horizontally and vertically divided into control volumes to numerically solve the governing equations for the unknown variables. Figure 2.43 shows a single cell of the numerical model with vertical partition into the three main control volumes: the upper layer for momentum and suspended sediment transport, the active layer for bed load sediment transport as well as bed material sorting and sub layers for sediment supply and deposition.

The primary unknown variables of the upper layer are the water depth h and the specific discharge q and r in directions of Cartesian coordinates x and y. In the active layer, $q_{B_g,x}$ and $q_{B_g,y}$ are describing the specific bed load fluxes (index refers to the g-th grain size class). A change of bed elevation z_B can be gained by a combination of balance equations for water and sediment and corresponding exchange terms (source terms) between the vertical layers.

2.3.1.2 Determination of Mixing Layer Thickness

The bed load control volume is the region where bed load transport occurs and it is assumed to have a uniform grain distribution over the depth. Its extension is well-defined by the bed surface at level z_B and its thickness h_m , which plays an important role for grain sorting processes during morphological simulations with multiple grain classes.

Different methods are implemented for the determination of this thickness h_m . It can be determined either dynamically during the simulation (at the moment only for 2-D

simulations) or it can be given a priori as a constant value for the whole simulation. The latter is used by default with an active layer thickness of 0.1 m.

Borah's approach

With this approach the active layer thickness h_m is different for degradation and for aggradation. In case of deposition, h_m corresponds to the thickness of the current deposition stratum. In case of degradation, h_m is proportional to the bed level decrase with a limitation to account for the situation of an armoured bed (Borah et al. (1982)).

If the bed level increases ($\Delta z_B > 0$):

$$h_m^{n+1} = h_m^n + \Delta z_B \tag{2.111}$$

If the bed level decreases ($\Delta z_B < 0$):

$$h_m = 20\Delta z_B + \frac{d_l}{\sum \beta_{nm}(1-p)} \tag{2.112}$$

where d_l is the smallest non-mobile grain size and $\sum \beta_{nm}$ is the sum of the non-mobile sediment fractions, and p is porosity.

Calculation based on mean diameter d_{90}

Following this approach the new thickness h_m is determined proportional to the characteristic grain size diameter d_{90} in the bed load control volume. The factor of proportionality can be chosen freely.

$$h_m^{n+1} = factor \cdot d_{90} \tag{2.113}$$

But this simple approach does not take into account influences of present bottom shear stresses or present erosion rates. Typically, the factor is between 1 and 3.

2.3.2 One Dimensional Sediment Transport

2.3.2.1 Spatial Discretisation

2.3.2.1.1 Soil Segments

For each cross section slice a different composition of the soil can be specified. A variable number of sediment layers can be defined. Figure 2.44 illustrates by example a possible distribution of soil types in a cross section. Each colour represents for a different grain class mixture. Usually however one soil type will cover several cross section slices, like in Figure 2.46.

The modification of the geometry of the cross section due to sediment transport it is illustrated in Figure 2.46. This can lead to the elimination of layers or to the creation of new ones. The grain class mixture of deposition will be the same over the whole wetted width.

The elevation changes will modify the soil elements which are considered to be wetted, but it is not always obvious when this is the case. For this reason the user can define

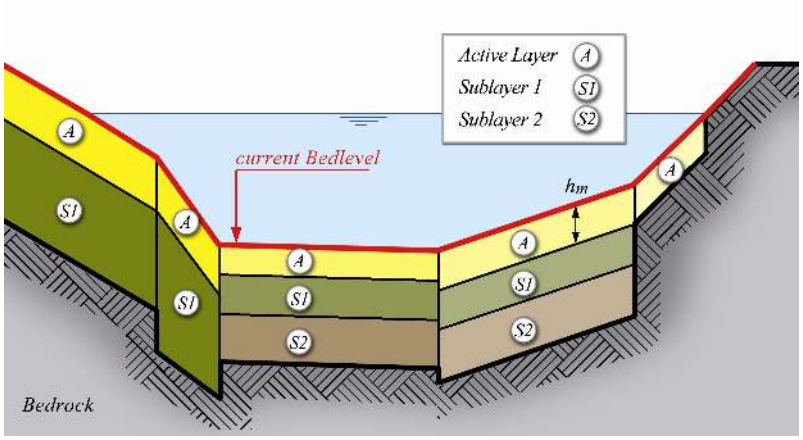

Figure 2.44 *Soil Discretisation in a cross section*

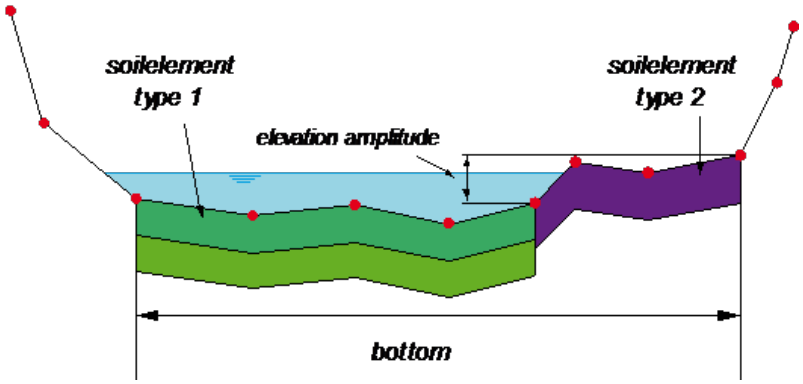

Figure 2.45 *Soil Discretisation in a cross section*

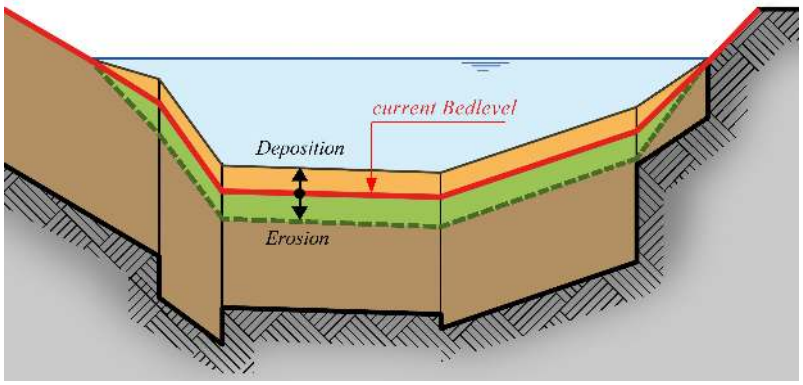

Figure 2.46 *Effect of bed load on cross section geometry*

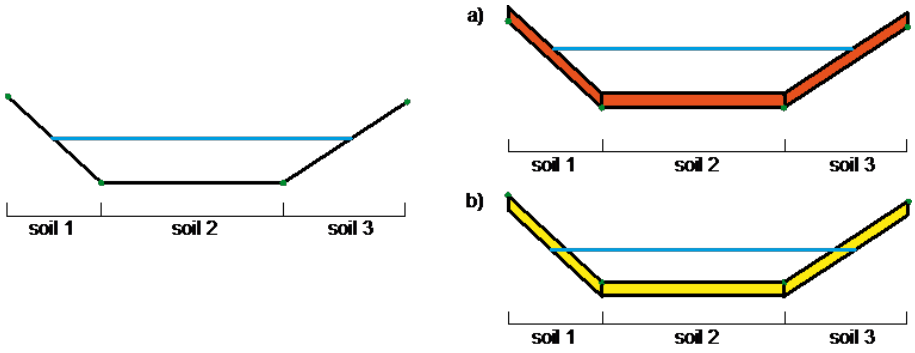

Figure 2.47 *Deposition a) and erosion b) due to suspended load with a wetting fraction of 0.9.*

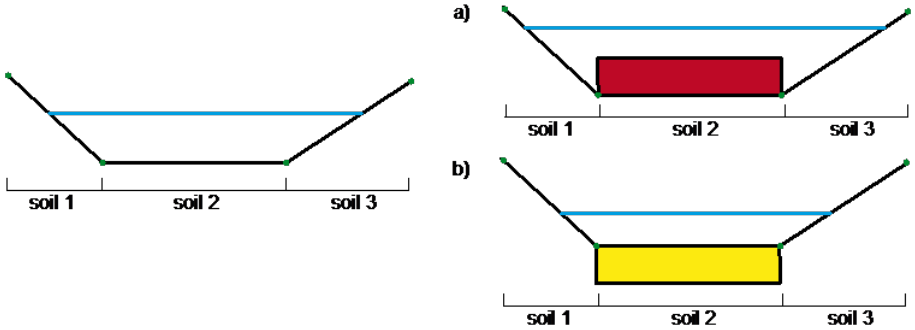

Figure 2.48 *Deposition a) and erosion b) due to suspended load with a wetting fraction of 0.1.*

which fraction of the elevation amplitude of the soil has to be below the water level by a parameter called *wetting_fraction*. In the example in Figure 2.45 the soil element of type 2 would be moved with a *wetting_fraction* of 0.3 but not with a *wetting_fraction* of 1. All points of a wetted soil element are affected by the same elevation change.

Figure 2.47, Figure 2.48, Figure 2.49, Figure 2.50, Figure 2.51 and Figure 2.52 give some simple examples of bedlevel changes to illustrate the mechanisms.

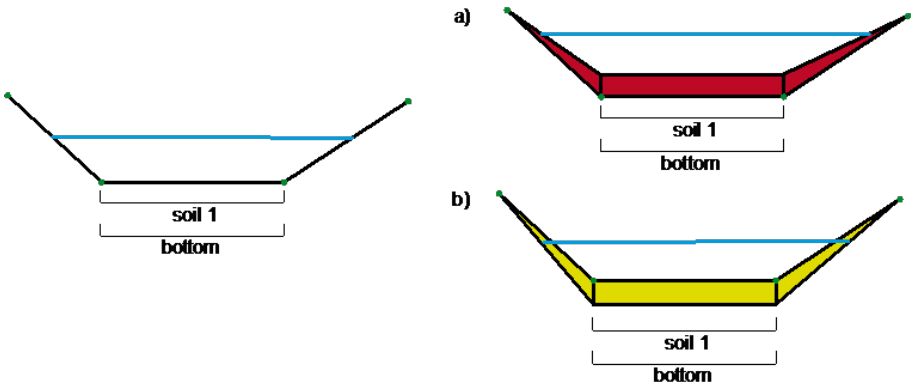

Figure 2.49 *Deposition a) and erosion b) due to bed load without cross section points on embankments.*

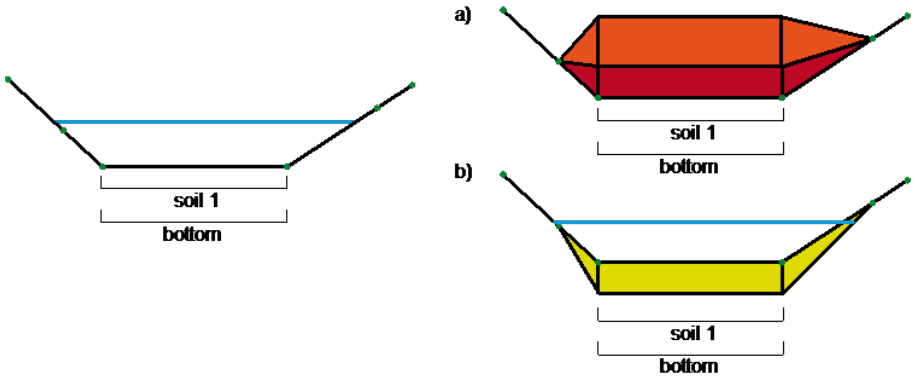

Figure 2.50 *Deposition a) and erosion b) due to bed load with cross section points on embankments.*

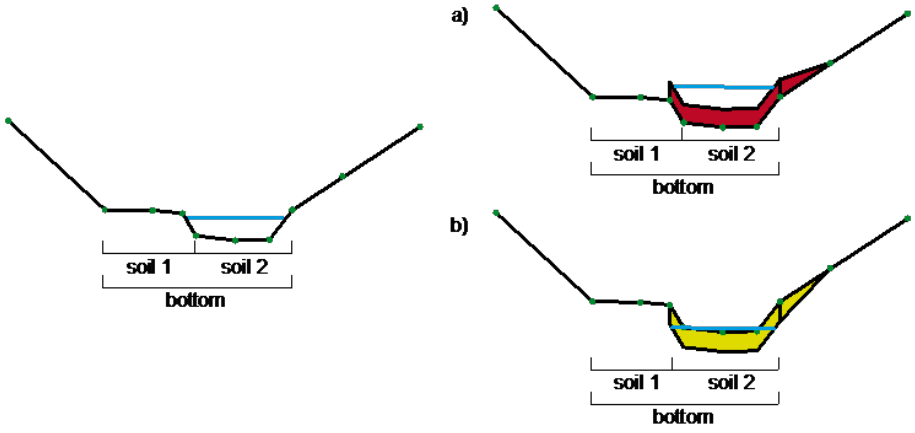

Figure 2.51 *Deposition a) and erosion b) due to bed load with 2 soils defined on the bottom.*

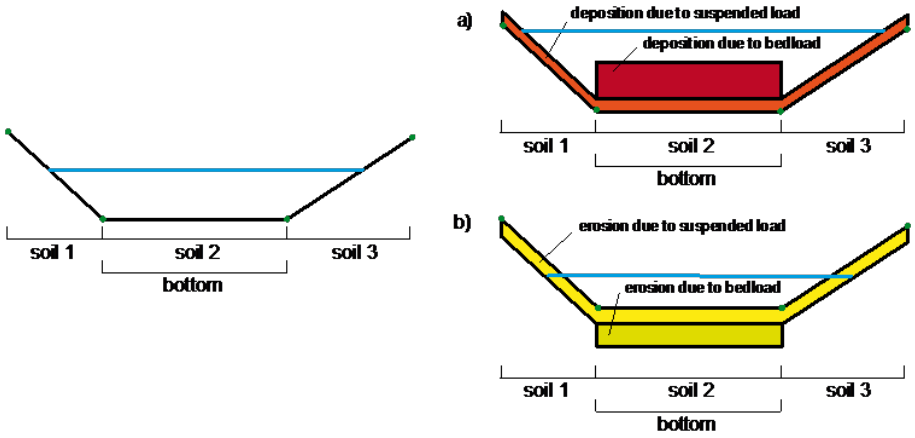

Figure 2.52 *Deposition a) and erosion b) due to bed load and suspended load.*

2.3.2.2 Discrete Form of Equations

2.3.2.2.1 Advection-Diffusion Equation

The one dimensional suspended sediment or pollutant transport in river channels is described by eq. 1.66 in the Mathematical Models section. This equation has to be solved for each grain class g in the same manner. For this reason in this section g is omitted and the equation becomes:

$$A\frac{\partial C}{\partial t} + Q\frac{\partial C}{\partial x} - \frac{\partial}{\partial x}\left(A\Gamma\frac{\partial C}{\partial x}\right) - S = 0 \tag{2.114}$$

C is the concentration of transported particles averaged over the cross-section.

For the moment the sources S, which vary for different types of transport, will be set to 0.

The eq. 2.114 is integrated over the element (see Figure 2.7)

$$\int_{x_{iL}}^{x_{iR}} \left(A\frac{\partial C}{\partial t} + Q\frac{\partial C}{\partial x} - \frac{\partial}{\partial x}\left(A\Gamma\frac{\partial C}{\partial x}\right)\right) \mathrm{d}x = 0 \tag{2.115}$$

and the different parts are calculated as follows:

$$\int_{x_{iL}}^{x_{iR}} A\frac{\partial C_i}{\partial t}\,\mathrm{d}x = A_i \int_{x_{iL}}^{x_{iR}} \frac{\partial C}{\partial t}\,\mathrm{d}x \approx A_i\frac{\partial C_i}{\partial t}\Delta x_i \approx A_i\frac{C_i^{n+1} - C_i^n}{\Delta t}\Delta x_i \tag{2.116}$$

$$\int_{x_{iL}}^{x_{iR}} Q\frac{\partial C}{\partial x}\,\mathrm{d}x = Q_i \int_{x_{iL}}^{x_{iR}} \frac{\partial C}{\partial x}\,\mathrm{d}x = Q_i(C(x_{iR}) - C(x_{iL})) = (\Phi_{a,iR} - \Phi_{a,iL}) \tag{2.117}$$

$$\int_{x_{iL}}^{x_{iR}} \frac{\partial}{\partial x}\left(A\Gamma\frac{\partial C}{\partial x}\right)\mathrm{d}x = \left(A\Gamma\left.\frac{\partial C}{\partial x}\right|_{x_{iR}} - A\Gamma\left.\frac{\partial C}{\partial x}\right|_{x_{iL}}\right) = \Phi_{d,iR} - \Phi_{d,iL} \tag{2.118}$$

The concentration at the new time is:

$$C_i^{n+1} = C_i^n - \frac{\Delta t}{\Delta x_i A_i}(\Phi_{a,iR} - \Phi_{a,iL} - \Phi_{d,iR} + \Phi_{d,iL}) \tag{2.119}$$

2.3.2.2.2 Computation of Diffusive Flux

The diffusive flux is calculated by finite differences.

$$\Phi_{d,iR} = A_{iR}\Gamma\frac{C_{i+1} - C_i}{x_{i+1} - x_i} \tag{2.120}$$

For the interpolation on the edge of the wetted area, known only in the cross sections, the geometric mean is used:

$$A_{iR} = \sqrt{A_{i+1}A_i} \tag{2.121}$$

If Γ is not given by the user it is calculated as follows:

$$\Gamma = \frac{\sqrt{\nu_L \nu_R}}{\sigma} \tag{2.122}$$

σ is generally assumed to be 0.5 (Celik and Rodi 1984).

The eddy viscosity averaged over the depth can be calculated by (Fäh, 1997):

$$\nu = uh\kappa/6 \tag{2.123}$$

2.3.2.2.3 Computation of Advective Flux

A general problem of the computation of the advective flux is that it leads to strong numerical diffusion. Several schemes can be used, four of them are implemented.

The first possibility to compute he advective flux over the edge (element boundary) is to interpolate the concentration values from the neighbouring elements, considering the flow direction, and multiply it with the water discharge over the edge.

a) QUICK-Scheme

For a positive flow from left to right the quick scheme determines the concentration due to advection at the upstream edge of element i by:

$$\begin{aligned} C_{a,iL} = &\frac{(x_{iL} - x_{i-1})(x_{iL} - x_{i-2})}{(x_i - x_{i-1})(x_i - x_{i-2})}C_i + \frac{(x_{iL} - x_{i-2})(x_{iL} - x_i)}{(x_{i-1} - x_{i-2})(x_{i-1} - x_i)}C_{i-1} \\ &+\frac{(x_{iR} - x_{i-1})(x_{iR} - x_i)}{(x_{i-2} - x_{i-1})(x_{i-2} - x_i)}C_{i-2} \end{aligned} \tag{2.124}$$

More in general the concentration is:

$$C_{a,iL} = \begin{cases} C_i + g_1(C_{i+1} - C_i) + g_2(C_i - C_{i-1}) \rightarrow u > 0 \\ C_{i+1} + g_3(C_i - C_{i+1}) + g_4(C_{i+1} - C_{i+2}) \rightarrow u < 0 \end{cases} \tag{2.125}$$

Between the velocities u_i and u_{i+1} the one with the larger absolute value is determinant.

$$g_1 = \frac{(x_{iR} - x_i)(x_{iR} - x_{i-1})}{(x_{i+1} - x_i)(x_{i+1} - x_{i-1})} \tag{2.126}$$

$$g_2 = \frac{(x_{iR} - x_i)(x_{i+1} - x_{iR})}{(x_i - x_{i-1})(x_{i+1} - x_{i-1})} \tag{2.127}$$

$$g_3 = \frac{(x_{iR} - x_{i+1})(x_{iR} - x_{i+2})}{(x_i - x_{i+1})(x_i - x_{i+2})} \tag{2.128}$$

$$g_4 = \frac{(x_{iR} - x_{i+1})(x_i - x_{iR})}{(x_{i+1} - x_{i+2})(x_i - x_{i+2})} \tag{2.129}$$

The QUICK scheme tends to get instable, especially for the pure advection-equation with explicit solution (Chen and Falconer, 1992). For this reason the more stable QUICKEST scheme (Leonard, 1979) is often used:

b) QUICKEST-Scheme

$$C_{iR,QUICKEST} = C_{iR,QUICK} - \frac{1}{2} Cr_{iR}(C_{i+1} - C_i) + \frac{1}{8} Cr_{iR}(C_{i+1} - 2C_i + C_{i-1}) \tag{2.130}$$

with

$$Cr_{iR} = \frac{u_{i+1} + u_i}{2} \frac{\Delta t}{\Delta x} \tag{2.131}$$

c) Holly-Preissmann

The QUICKEST-scheme still leads to an important diffusion. For this reason the HollyPreissmann scheme (Holly and Preissmann, 1977), which gives better results, is also implemented. This scheme is based on the properties of characteristics and can not be applied directly for the present Discretisation.

To find $C(x_{iR})$ of eq. 2.117 the properties of characteristics or finite differences are used, placing the edges on a new grid so that $C(x_{iR})$ becomes C_j and $C(x_{iL}) = C_{j-1}$. Considering only the advection part of the eq. 2.114 and dividing by the cross section area A:

$$\frac{\partial C}{\partial t} + \frac{u \partial C}{\partial x} = 0 \tag{2.132}$$

and

$$\frac{C_j^{n+1} - C_j^n}{\Delta t} = -u \frac{C_j^n - C_{j-1}^n}{x_j - x_{j-1}} \tag{2.133}$$

Thus the new concentration is

$$C_j^{n+1} = \left(1 - u\frac{\Delta t}{x_j - x_{j-1}}\right) C_j^n + u\frac{\Delta t}{x_j - x_{j-1}} C_{j-1}^n \tag{2.134}$$

for a courant number $CFL = u(dt/dx) = 1 : C_j^{n+1} = C_{j-1}^n$. This means that the solute travels from one side of the cell to the other during the time step.

The Holly-Preissmann scheme calculates the values in function of CFL and the upstream value.

$$Y(Cr) = ACr^3 + BCr^2 + DCr + E \tag{2.135}$$

$Y(0) = C_j^n$; $Y(1) = C_{j-1}^n$

$\dot{Y}(0) = \frac{\partial C_j^n}{\partial x}$; $\dot{Y}(1) = \frac{\partial C_{j-1}^n}{\partial x}$

$$C_j^{n+1} = a_1 C_{j-1}^n + a_2 C_j^n + a_3 \frac{\partial C_{j-1}^n}{\partial x} + a_4 \frac{\partial C_j^n}{\partial x} \tag{2.136}$$

$$a_1 = Cr^2(3 - 2Cr) \tag{2.137}$$

$$a_2 = 1 - a_1 \tag{2.138}$$

$$a_3 = Cr^2(1 - Cr)\Delta x \tag{2.139}$$

$$a_4 = -Cr(1 - Cr)^2 \tag{2.140}$$

and

$$\frac{\partial C_j^{n+1}}{\partial x} = b_1 C_{j-1}^n + b_2 C_j^n + b_3 \frac{\partial C_{j-1}^n}{\partial x} + b_4 \frac{\partial C_j^n}{\partial x} \tag{2.141}$$

$$b_1 = 6Cr(Cr - 1)/\Delta x \tag{2.142}$$

$$b_2 = -b_1 \tag{2.143}$$

$$b_3 = Cr(3Cr - 2) \tag{2.144}$$

$$b_4 = (Cr - 1)(3Cr - 1) \tag{2.145}$$

However this form is only valid for a constant velocity u. If u is not constant the velocities in the different cells and at different times have to be considered. The velocity u_* is determined by interpolation of u_{j-1}^n ,u_j^n ,u_j^{n+1} .

$$\bar{u}_j = \frac{1}{2}(u_j^n + u_j^{n+1}) \tag{2.146}$$

$$\bar{u}^n = (u_{j-1}^n \theta) + (1-\theta) u_{j+1}^n \tag{2.147}$$

with

$$\theta = u_i^n \frac{\Delta t}{x_{j-1} - x_j} \tag{2.148}$$

$$\hat{u} = \frac{1}{2}(\bar{u}_j + \bar{u}^n) \tag{2.149}$$

$$Cr = \hat{u}\frac{\Delta t}{\Delta x} = \frac{u_j^{n+1} + u_j^n}{2\frac{x_{j-1} - j}{\Delta t} - u_{j-1}^n + u_j^n} \tag{2.150}$$

The Holly-Preissmann scheme gives good results for the pure advection-diffusion equation. But if a sediment exchange with the bed takes place, because of the shifted grid, it does not react to the influence of the source term.

For the last 3 schemes the advective flux is computed multiplying the concentration on the edge with the discharge over the edge:

$$\Phi_{a,iR} = Q_{iR} C_{iR}$$

d) Modified Discontinuous Profile Method (MDPM)

The MDPM method presented by Badrot-Nico et al. (2007) is like a transposing of the Holly-Preissmann scheme from a finite difference to a finite volume context and thus much more adapted for the use within BASEMENT.

In this method the advective flux is calculated directly as a sediment discharge:

$$\Phi_{iR} = \frac{1}{\Delta t} A_i \int_{t^n}^{t^{n+1}} u(t) C(x_{iR}, t) dt \tag{2.151}$$

Using the invariance property along a characterstic line (Figure 2.53) this equation can be transformed to

$$\Phi_{iR} = \frac{1}{\Delta t} A_i \int_{x_{iL}}^{x_{iR}} C(x, t^n)\, dx \tag{2.152}$$

The function $C_i^n(x)$ is reconstructed from the mean concentration in the cell C_i^n and the concentration values on the edges C_{iL}^n and C_{iR}^n (Figure 2.54) by satisfying mass conservation in the cell.

$$\tilde{C}_i^n(x) = \begin{cases} U_{iL}^n & if \quad x \leq x_{i-1/2} + \alpha_i \Delta x_i \\ U_{iR}^n & if \quad x > x_{i-1/2} + \alpha_i \Delta x_i \end{cases} \tag{2.153}$$

with

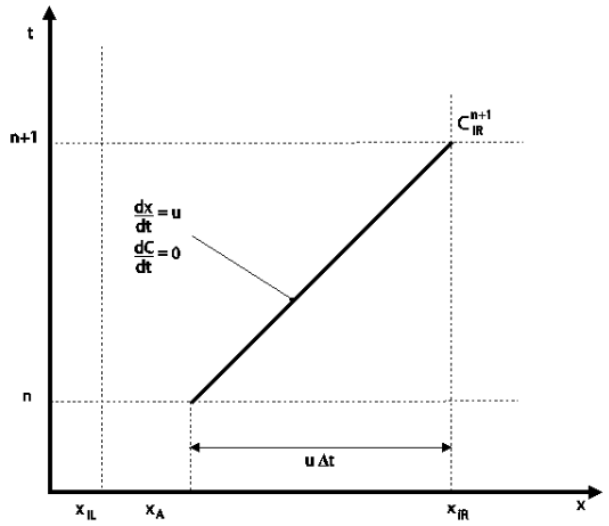

Figure 2.53 *Invariance of C along the characteristic line y*

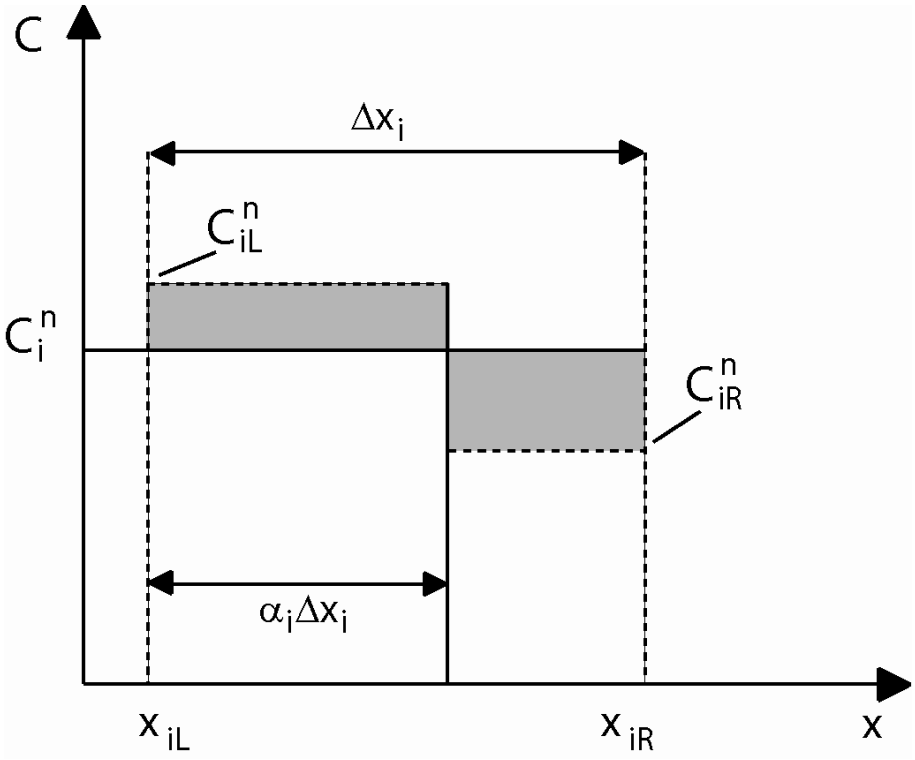

Figure 2.54 *Function* $\tilde{C}_i^n(x)$

$$\alpha_i = \frac{C_i^n - C_{iR}^n}{C_{iL}^n - C_{ir}^n} \tag{2.154}$$

and $\alpha_i \in [0,1]$.

If $C_{iL}^n = C_{iR}^n$ or $(C_{iL}^n - C_i^n)(C_i^n - C_{iR}^n) < 0$ the following values are set:

$$\left.\begin{array}{l} C_{iL}^n = C_i^n \\ C_{iR}^n = C_i^n \\ \alpha_i = \varepsilon \end{array}\right\}$$

ε is an arbitrary value between 0 and 1.

If the velocity is the flux of suspended load per unity of depth and width can now be determined as follows:

$$h_i = C_{iL}^n \, max(x_{i+1/2} - x - (1-\alpha_i)\Delta x_i, 0) + C_{iR}^n \, min(x_{i+1/2} - x, (1-\alpha_i)\Delta x_i) \tag{2.155}$$

If the velocity is negative respectively:

$$g_i = -C_{iL}^n min(x - x_{i+1/2}, \alpha_{i+1}\Delta x_{i+1}) - C_{iR}^n max(x - x_{i+1/2} - \alpha_{i+1}\Delta x_{i+1}, 0) \tag{2.156}$$

The abscissa of the foot of the characteristic is given by $x_A = x_{i+1/2} - u_{i+1/2}^n(t)\Delta t$.

Finally the advective flux is:

$$\Phi_{i+1/2} = \begin{cases} \dfrac{1}{\Delta t} h_i(x_A) & if \quad u_{x_{i+1/2}}^n > 0 \\ \dfrac{1}{\Delta t} g_{i+1}(x_A) & if \quad u_{x_{i+1/2}}^n < 0 \end{cases} \tag{2.157}$$

Furthermore the new concentrations on the edges have to be prepared for the computations of the next time step:

$$C_{i+1/2}^{n+1} = \begin{cases} C_{iL}^n & if \quad u_{x_{i+1/2}}^n(t) > 0 \quad and \quad Cr_x \geq 1 - \alpha_i \\ C_{iR}^n & if \quad u_{x_{i+1/2}}^n(t) > 0 \quad and \quad Cr_x < 1 - \alpha_i \\ C_{i+1L}^n & if \quad u_{x_{i+1/2}}^n(t) < 0 \quad and \quad Cr_x \geq -\alpha_i \\ C_{i+1R}^n & if \quad u_{x_{i+1/2}}^n(t) < 0 \quad and \quad Cr_x < -\alpha_i \end{cases} \tag{2.158}$$

The required Courant number is

$$Cr_x = \begin{cases} u_x(t)\dfrac{\Delta t}{\Delta x_i} & u_x(t) > 0 \\ u_x(t)\dfrac{\Delta t}{\Delta x_{i+1}} & u_x(t) < 0 \end{cases} \tag{2.159}$$

2.3.2.2.4 Global Bed Material Conservation Equation

As the y-direction is not considered, in the one dimensional case the mass conservation equation (Exner-equation) becomes:

$$(1-p)\frac{\partial z_B}{\partial t} + \left(\sum_{k+1}^{ng}\frac{\partial q_B}{\partial x} + s_g - sl_{B_g}\right) = 0 \tag{2.160}$$

q_B is the sediment flux per unit channel width. Integrating eq. 2.160 over the channel width, hence multiplying everything by the channel width, the following equation is obtained:

$$(1-p)\frac{\partial A_{Sed}}{\partial t} + \left(\sum_{k=1}^{ng}\frac{\partial Q_B}{\partial x} + S_g - Sl_{B_g}\right) = 0 \tag{2.161}$$

The discretisation is effected exactly in the same way as for the hydraulic mass conservation. The eq. 2.161 is integrated over the element (Figure 2.7):

$$\int_{x_{iL}}^{x_{iR}}\left((1-p)\frac{\partial A_{Sed}}{\partial t} + \left(\sum_{k=1}^{ng}\frac{\partial Q_B}{\partial x} + S_g - Sl_{B_g}\right)\right)\mathrm{d}x = 0 \tag{2.162}$$

The parts of the eq. 2.162 are discretized as follows:

$$(1-p)\int_{x_{iL}}^{x_{iR}}\frac{\partial A_{Sed,i}}{\partial t}\,\mathrm{d}x = (1-p)\frac{A_{Sed,i}^{n+1} - A_{Sed,i}^{n}}{\Delta t}\Delta x \tag{2.163}$$

$$\int_{x_{iL}}^{x_{iR}}\frac{\sum_{k=1}^{ng} Q_{B,i}}{\partial x}\,\mathrm{d}x = \sum_{k=1}^{ng} Q_B(x_{iR}) - \sum_{k=1}^{ng} Q_B(x_{iL}) = \Phi_{B,iR} - \Phi_{B,iL} \tag{2.164}$$

$$\int_{x_{iL}}^{x_{iR}}\sum_{k=1}^{ng}(S_g - Sl_{B_g})\,\mathrm{d}x = \sum_{k=1}^{ng} S_g - \sum_{k=1}^{ng} Sl_{B_g} \tag{2.165}$$

$\Phi_{B,iL}$ and $\Phi_{B,iR}$ are the bed load fluxes through the west and east side of the cell. Their determination will be discussed later (Section 2.3.2.3.1).

The change of the sediment area is thus calculated by:

$$\Delta A_{Sed} = A_{Sedi}^{n+1} - A_{Sedi}^{n} = \frac{\Delta t}{\Delta x_i}(\Phi_{B,iR} - \Phi_{B,iL}) - \frac{\Delta t}{\Delta x_i}\left(\sum_{k=1}^{ng} S_g - \sum_{k=1}^{ng} Sl_{B_g}\right) \tag{2.166}$$

As the result of the sediment balance is an area, the deposition or erosion height Δz_b has yet to be determined. The erosion or deposition is distributed over the wetted part of the cross section. If a bed bottom is defined the deposition height is equal and constant for all wetted slices. Only in the exterior slices the bed level difference is 0 where the cross section becomes dry. The repartition of the soil level change is illustrated in Figure 2.55.

The change of the bed level is calculated as follows:

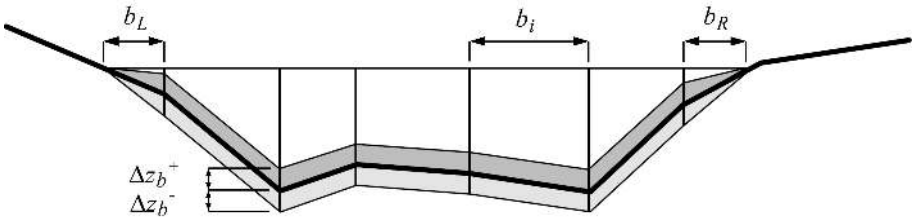

Figure 2.55 *Distribution of sediment area change over the cross section*

$$\Delta z_B = \frac{\Delta A_{Sed}}{\frac{b_r}{2} + \frac{b_l}{2} + \sum b_i} \tag{2.167}$$

As the sediments transported by bed load can be deposed only on the bed bottom, whilst the sediments transported by suspended load can be deposed on the whole wetted section, two separate values of ΔA_{Sed} and Δz_B are calculated for the two processes by splitting eq. 2.166 in two parts.

The change of bed level due to bed load is:

$$\Delta A_{Sed,bl} = \frac{\Delta t}{\Delta x_i}(\Phi_{B,iR} - \Phi_{B,iL}) - \frac{\Delta t}{\Delta x_i}\left(\sum_{k=1}^{ng} Sl_{B_g}\right) \tag{2.168}$$

The change of bed level due to suspended load accordingly:

$$\Delta A_{Sed,bl} = -\frac{\Delta t}{\Delta x_i}\left(\sum_{k=1}^{ng} S_g - \sum_{k=1}^{ng} Sl_g\right) \tag{2.169}$$

2.3.2.2.5 Bed material sorting equation

For the 1-D computation the bed material sorting equation computation is:

$$(1-p)\,\frac{\partial}{\partial t}(\beta_g h_B) + \frac{\partial q_{B_g}}{\partial x} + s_g - sf_g - sl_{B_g} = 0 \tag{2.170}$$

Considering the whole width of the cross section and introducing an active layer area A_B , eq. 2.170 becomes:

$$(1-p)\,\frac{\partial}{\partial t}(\beta_g A_B) + \frac{\partial Q_{B_g}}{\partial x} + S_g - Sf_g - Sl_{B_g} = 0 \tag{2.171}$$

The eq. 2.171 is integrated over the length of the control volume:

$$\int_{x_{iL}}^{x_{iR}} \left((1-p)\frac{\partial}{\partial t}(\beta_g A_B) + \frac{\partial Q_{B_g}}{\partial x} + S_g - Sf_g - Sl_{B_g}\right) dx = 0 \tag{2.172}$$

The different parts are discretized as follows:

$$(1-p)\int_{x_{iL}}^{x_{iR}} \frac{\partial}{\partial t}(\beta_g A_B)\,\mathrm{d}x = (1-p)\frac{\beta_g^{n+1}A_B^{n+1} - \beta_g^n A_B^n}{\Delta t}\Delta x \tag{2.173}$$

$$\int_{x_{iL}}^{x_{iR}} \frac{\partial Q_{B_g}}{\partial x}\,\mathrm{d}x = Q_B(x_{iR}) - Q_B(x_{iL}) = \Phi_{g,iR} - \Phi_{g,iL} \tag{2.174}$$

Then the new β_g at time $n+1$ can be calculated for every element i by:

$$\beta_{g_i}^{n+1} = \left((1-p)\beta_{gi}^n A_{B_i}^n - \frac{\Delta t}{\Delta x_i}(\Phi_{iR}^k - \Phi_{iL}^k) - (S_g - Sf_g - Sl_{B_g})\frac{\Delta t}{\Delta x_i}\right)/((1-p)A_{B_i}^{n+1}) \tag{2.175}$$

As for the global bed material conservation equation the bed material sorting equation is also solved twice: once for the bed load and once for the suspended load.

$$\beta_{g_i,bl}^{n+1} = \left((1-p)\beta_{gi}^n A_{B_i}^n - \frac{\Delta t}{\Delta x_i}(\Phi_{iR}^k - \Phi_{iL}^k) - (-Sf_g - Sl_{B_g})\frac{\Delta t}{\Delta x_i}\right)/((1-p)A_{B_i}^{n+1}) \tag{2.176}$$

and

$$\beta_{g_i,susp}^{n+1} = \left((1-p)\beta_{gi}^n A_{B_i}^n - (-Sf_g - Sl_g)\frac{\Delta t}{\Delta x_i}\right)/((1-p)A_{B_i}^{n+1}) \tag{2.177}$$

2.3.2.2.6 Interpolation

To solve the eq. 2.164 and eq. 2.174 the total bed load fluxes over the edges ($\Phi_{B,iL}$,$\Phi_{B,iR}$) and the fluxes for the single grain classes ($Q_{B_g,iL}$, $Q_{B_g,iR}$) are needed, but the data for the computation of bed load are available only in the cross sections. For this reason the values on the edges are interpolated from the values calculated for the cross sections, depending on a weight choice of the user (θ):

$$\Phi_{B,iL} = (\theta)Q_{B,i-1} + (1-\theta)Q_{B,i} \tag{2.178}$$

If all values for the computation of Q_B by a bed load formula are taken from the cross section, the results of sediment transport tend to generate jags, as some effects of discretisation accumulate instead of being counterbalanced. For this reason it has been preferred not to take all values from the same location. The local discharge Q is substituted by a mean discharge for the edge, computed with the discharges in the upstream and downstream elements of the edge. This means that the bed load in a cross section will be calculated twice with different values of Q.

2.3.2.3 Discretisation of Source Terms

2.3.2.3.1 External Sediment Sources and Sinks

The discretisation of external sediment sources and sinks is analogous to BASEplane. Please see Section 2.3.3.3.1

2.3.2.3.2 Sediment Flux through Bottom of Bed Load Control Volume

The discretisation of the sediment flux through the bottom of the bed load control volume is analogous to BASEplane. Please see Section 2.3.3.3.3

2.3.2.3.3 Source Term for Sediment Exchange between Water and Bottom

The source term S_g from eq. 1.72 is computed in different ways depending on the scheme used for the solution of the advection equation.

a) With MDPM scheme

The source term S_g is calculated for the concentration value on the left and the concentration value on the right according to eq. 1.72 :

$$S_{g,L} = f(C_{iL}^n)$$
$$S_{g,R} = f(C_{iR}^n)$$

The volume exchanged with the bottom during Δt is given by the sum of the exchange on the left and the exchange on the right:

$$E_{L1} = \alpha S_{g,L} B \Delta x \Delta t \tag{2.179}$$

$$E_{L2} = \alpha_2 S_{g,L} B \Delta x \Delta t / 2 \tag{2.180}$$

$$E_L = E_{L1} + E_{L2} \tag{2.181}$$

$$E_{R1} = \alpha_2 S_{g,R} B \Delta x \Delta t / 2 \tag{2.182}$$

$$E_{R2} = \alpha_3 S_{g,R} B \Delta x \Delta t \tag{2.183}$$

$$E_R = E_{R1} + E_{R2} \tag{2.184}$$

Where α is defined like in eq. 2.154, $\alpha_2 = min(Cr_x, 1-\alpha)$ and $\alpha_3 = max(1-\alpha-Cr_x, 0)$

The final mean source term is then:

$$S_g = \frac{(E_L + E_R)}{B \Delta t \Delta x} \tag{2.185}$$

The exchange values on the right and left side are used to adjust the concentration values on the edges. The new concentrations on the edges after deposition or erosion in the left and right part of the cell are calculated by:

$$C_{iL}^{n+1} = \frac{C_{iL}^n A_i \alpha \Delta x + E_{L1}}{A_i \alpha \Delta x} \tag{2.186}$$

$$C_{iR}^{n+1} = \frac{C_{iR}^n A_i \alpha_3 \Delta x + E_{R2}}{A_i \alpha_3 \Delta x} \tag{2.187}$$

b) With QUICK and QUICKEST scheme

S_g is calculated for each cross section according to eq. 1.72 .

c) With Holly-Preissmann scheme

The Holly-Preissmann scheme should not be used with material erosion and deposition.

2.3.2.3.4 Splitting of Bed Load and Suspended Load Transport

The same size of particles can be transported by bed load as well as by suspended load. van Rijn (1984b) found a parameter which describes the relation between the two transport modes depending on the shear velocity u_* and the sink velocity w_k determined in eq. 1.60 - eq. 1.62.

$$\begin{aligned} \varphi_k &= 0 && if \quad \left(\frac{u_*}{w_k}\right) < 0.4 \\ \varphi_k &= 0.25 + 0.325 ln\left(\frac{u_*}{w_k}\right) && if \quad 0.4 \leq \left(\frac{u_*}{w_k}\right) \leq 10 \\ \varphi_k &= 1 && if \quad \left(\frac{u_*}{w_k}\right) > 10 \end{aligned} \tag{2.188}$$

The computation of bed load flux and the computation of the exchange flux between suspended load and bed (eq. 1.71) have to be modified as follows:

$$Q_{B_g} = (1 - \varphi_g) Q_{B_g} \tag{2.189}$$

$$S_g = w_g(\varphi_g \beta_g C_{e_g} - C_{d_g}) \tag{2.190}$$

2.3.2.3.5 Abrasion

As BASEMENT always works with volumes, the abrasion after Sternberg (eq. 1.117 in the Mathematical Models section) is applied as follows:

$$V(x) = V_0 e^{-c(x - x_0)} \tag{2.191}$$

For the sediment balance in the element, the incoming sediment flux over the upstream edge is reduced by the factor:

$$f = e^{-c(x - x_0)}$$

where the x is the position of the present element and x_0 the position of the upstream element. The factor f is constant for an edge and is computed at the beginning of the computation.

2.3.2.4 Solution Procedure

The solution procedure for the one dimensional sediment transport is described in chapter Section 2.2.2.5.

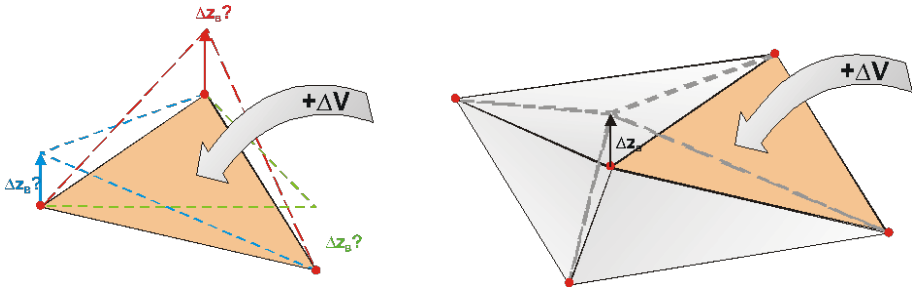

Figure 2.56 *Schematic illustration of problems related to the update of bed elevations*

2.3.3 Two Dimensional Sediment Transport

2.3.3.1 Spatial Discretisation

The finite volume method is applied to discretise the morphodynamic equations, slightly different from that of the hydrodynamic section. In the hydrodynamic discretisation a cell-centered approach is applied (see Figure 2.2). Thereby, the bed elevations are defined in the cell vertexes (nodes) of each cell. This arrangement, with bed elevations defined in the nodes, enables a more accurate representation of the topography compared to an approach with bed elevations defined in the cell centres. A further advantage of the chosen approach is that the slope within each cell is clearly defined by its nodal bed elevations.

But applying the same Discretisation approach for the sediment transport leads to several problematic aspects, which can be summarized briefly as follows.

- The change of a cell's sediment volume ΔV would have to be distributed on all nodes of the cell, where the bed elevations are defined. But it is not obvious by which criteria the sediment volume must be divided upon these nodes (see left part of Figure 2.56).
- If a nodal elevation would be changed due to a sediment inflow into a cell, this change in bed elevation would not only affect the sediment volume of this cell, but also the sediment volumes of all neighbouring cells (see right part of Figure 2.56). This situation is problematic regarding the conservation properties of the numerical scheme and it induces numerical fluxes into the neighbouring cells which cause undesired numerical diffusion.

To circumvent these problematic aspects and to ensure a fully conservative numerical scheme, a separate mesh is used for the spatial discretisation for the sediment transport. Because the hydraulic and sediment simulations are performed on different meshes, this approach is called "dual mesh morphodynamics" (DMMD) from here on. Both meshes, with its cells and edges, are illustrated in Figure 2.57 .

The cells of the sediment mesh are constructed around the nodes of the hydraulic mesh by connecting the midpoints of the edges and the centres of the hydraulic cells. This procedure results in the generation of median dual cells. Following this dual mesh approach all conservative variables of the sediment transport (z_b ,β_g ,C_g) are defined within the centres of the sediment cells, thus forming a standard finite volume approach regarding the sediment transport. Changes in bed elevation of a node do not influence the neighbouring sediment elements, as it is illustrated in Figure 2.58. Therefore this Discretisation approach is conservative and no diffusive fluxes into the neighbouring cells do occur.

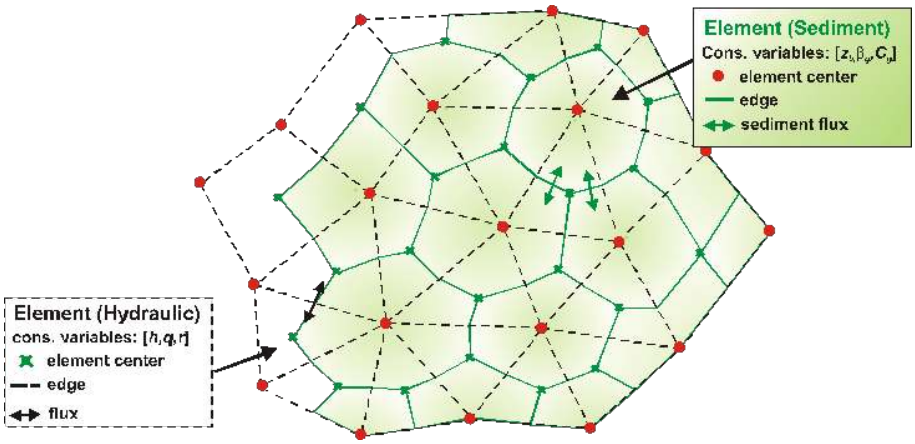

Figure 2.57 *Dual mesh approach with separate meshes for hydrodynamics (black) and sediment transport (green). Sediment cells have the bed elevations defined in their cell centers.*

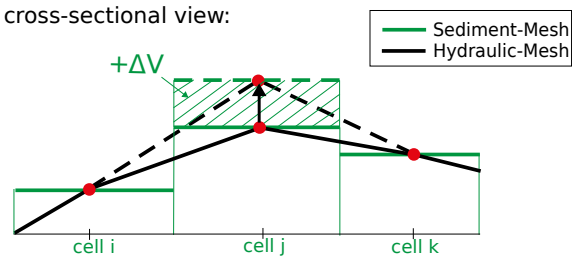

Figure 2.58 *Cross sectional view of dual mesh approach. Changes in sediment volume ΔV do not affect the neighboring cells' sediment volumes.*

The sediment mesh is generated automatically during the program start from the hydraulic mesh without the need of any additional information.

2.3.3.2 Discrete Form of Equations

2.3.3.2.1 Global Bed material Conservation Equation - Exner Equation

Considering the Exner equation (eq. 1.86) and applying the FVM, it can be written in the following integral form

$$(1-p)\int_{\Omega}\frac{\partial z_B}{\partial t}\,\mathrm{d}\Omega+\int_{\Omega}\sum_{g=1}^{ng}\left(\frac{\partial q_{B_g,x}}{\partial x}+\frac{\partial q_{B_g,y}}{\partial y}\right)\mathrm{d}\Omega=\int_{\Omega}\sum_{g=1}^{ng}(sl_g-s_{Bg})\,\mathrm{d}\Omega \tag{2.192}$$

In which Ω is the same computational area as defined in hydrodynamic model (Figure 2.22). Using the Gauss' theory and assuming $\partial z_B/\partial t$ is constant over the element, one obtains

$$(1-p)\frac{z_B^{n+1}-z_B^n}{\Delta t}+\frac{1}{\Omega}\sum_{g=1}^{ng}\int_{\partial\Omega}(q_{B_g,x}n_x+q_{B_g,y}n_y)\,\mathrm{d}l=\frac{1}{\Omega}\sum_{g=1}^{ng}(Sl_g-S_{Bg}) \tag{2.193}$$

Where n_x and n_y are components of the unit normal vector of the edge in x and y direction respectively.

2.3.3.2.2 Computation of Bed Load Fluxes

Direction of bed load flux

The direction of the bed load flux equals the direction of the velocity in near bed region and is a 2-D vector in a 2-D simulation. It is assumed here that this direction equals the direction of the depth-averaged velocity, although this assumption may become invalid in particular in curved channels with significant secondary flow motions. A correction of this flux direction is performed on sloped bed surfaces due to the gravitational induced lateral bed load flux component. The lateral transport component is perpendicular to the direction of flow velocity and therefore the resulting bed load flux vector is determined as

$$\overrightarrow{q}_{B_{res}}=\overrightarrow{q}_B+\overrightarrow{q}_{B_{lateral}}=q_B\begin{pmatrix}\cos\theta\\ \sin\theta\end{pmatrix}+q_{B_{lateral}}\begin{pmatrix}\sin\theta\\ -\cos\theta\end{pmatrix} \tag{2.194}$$

where θ is the angle between the velocity vector and the x-axis.

Computation of bed load flux

The bed load transport capacity $\overrightarrow{q}_B$ and the lateral transport $\overrightarrow{q}_{B_{lateral}}$ are calculated using the transport formulas outlined in the Mathematical Models section. Different empirical transport formulas can be used and also fractional transport for multiple grain classes can be considered. These formulas require the flow variables and the soil compositions as data input.

As a consequence of the discretisation of the sediment elements as median dual cells, each sediment edge lies completely within a hydraulic element (see Figure 2.59, where sediment edges are indicated in green color). Therefore an obvious approach is to determine the

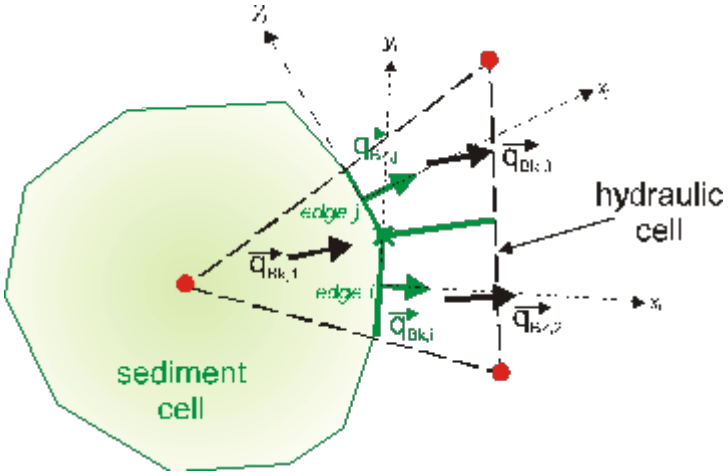

Figure 2.59 *Determination of bed load flux over the sediment cell edges i,j*

bed load fluxes over a sediment edge with the flow variables and the bottom shear stress defined in this hydraulic element. This eases the computations since no interpolations of hydraulic variables onto the sediment edges are necessary. Furthermore, it can be made use of the clearly defined bed slope within this hydraulic element, derived from its nodal elevations.

Following this approach the transport capacity is calculated with the flow variables defined in the centre of the hydraulic element. But since the transport capacity calculations also depend on the bed materials and grain compositions, this computation is repeated for every sediment element which partially overlaps the hydraulic element. Thus, one obtains multiple transport rates within the hydraulic element, as illustrated in Figure 2.59. (In case of single grain simulations, the bed material is the same over the hydraulic element and therefore the transport calculation must only be done once.) From these multiple transport rates an averaged transport rate over the sediment cell is determined by areal weighting.

Finally, the flux over the sediment cell edge is determined from the calculated transport capacities to its left and right sediment elements as

$$q_{B,edge} = \left[(\theta_{up})\overrightarrow{q}_{B,res,L} + (1-\theta_{up})\overrightarrow{q}_{B,res,R}\right]\overrightarrow{n}_{edge} \tag{2.195}$$

where θ_{up} is the upwind factor and $\overrightarrow{n}_{edge}$ is the normal vector of the edge.

Treatment of partially wetted elements

Per default no sediment transport is calculated within partially wetted hydraulic elements. This behaviour seems favourable in most situations. For example, in some cases it prevents upper parts of a river bank, which are not over flown, from automatically being eroded by sediment erosion which takes place only at the toe of the bank. But this default behaviour can be changed for special situations.

2.3.3.2.3 Flux Correction

When bed load fluxes are summed up over an element k, there may occur situations in which more sediment mass leaves the element than is actually available. Such situations

are observed for example when the bed level reaches a fixed bed elevation or bed armour where no further erosion can take place.

To guarantee sediment mass conservation over the whole domain a correction of the bed load fluxes which leave the element is applied in such situations. All the outgoing computed bed load fluxes of such an overdraft element k are reduced proportionally by a factor $\omega_{k,g}$. This factor is determined in a way that limits the overall outflow to the available sediment mass $V_{sed,k,g}$.

$$\omega_{k,g} = \begin{cases} \dfrac{\sum_{j=1}^{ng} Flux_{out,j,g} - V_{sed,k,g}}{\sum_{j=1}^{ng} Flux_{out,j,g}} & if \quad V_{sed,k,g} < \sum_{j=1}^{ng} Flux_{out,j,g} \\ 0 & if \quad V_{sed,k,g} \geq \sum_{j=1}^{ng} Flux_{out,j,g} \end{cases} \tag{2.196}$$

$$Flux^{corr}_{out,k,g} = (1 - \omega_{k,g}) Flux_{out,k,g}$$

2.3.3.2.4 Bed Material Sorting Equation

The global bed material conservation eq. 2.193 has to be solved first, because its results are needed to solve the bed material sorting equation. The bed material sorting equation (eq. 1.78) is also discretized using FVM. The discretized form is

$$(1-p)\frac{(h_m\beta_g)^{n+1} - (h_m\beta_g)^n}{\Delta t} + \frac{1}{\Omega}\int_{\partial\Omega} \left(q_{B_g,x} n_x + q_{B_g,y} n_y\right) \mathrm{d}l + \frac{1}{\Omega} S_g - \frac{1}{\Omega} S l^n_{B_g} - s f^*_g = 0 \tag{2.197}$$

The bed load control volume thickness h_m has to be determined before the new values of fractions are calculated through the eq. 2.197. The determination of h_m is detailed in Section 2.3.1.2. The solution of the bed material sorting equation finally yields the grain factions β^{n+1}_g at the new time level.

2.3.3.2.5 Advection-Diffusion Equation

The two dimensional suspended sediment or pollutant transport in river channels is described by eq. 1.68 in the Mathematical Models section. This equation has to be solved for each grain class g in the same manner. For this reason g is omitted in this section as well as the source terms. This yields to the following equation:

$$\frac{\partial}{\partial t} Ch + \frac{\partial}{\partial x}\left(Cq - h\Gamma\frac{\partial C}{\partial x}\right) + \frac{\partial}{\partial y}\left(Cr - h\Gamma\frac{\partial C}{\partial y}\right) = 0 \tag{2.198}$$

C is the concentration of transported suspended material averaged over flow depth.

The eq. 2.114 also can be written as follows.

$$(Ch)_t + \nabla(Cq, Cr) - \nabla(h\Gamma C_x, h\Gamma C_y) = 0 \tag{2.199}$$

It is integrated over the area of the hydraulic element Ω :

$$\int_{\Omega} ((Ch)_t + \nabla(Cq, Cr) - \nabla(h\Gamma C_x, h\Gamma C_y))\,\mathrm{d}\Omega = 0 \tag{2.200}$$

Applying the Gauss theorem, eq. 2.200 becomes:

$$\int_{\Omega} (Ch)_t \mathrm{d}\Omega + \oint_{\partial\Omega} (Cq, Cr)\,\overrightarrow{n}\,\mathrm{d}l - \oint_{\partial\Omega} (h\Gamma C_x, h\Gamma C_y)\,\overrightarrow{n}\,\mathrm{d}l = 0 \tag{2.201}$$

the different parts are calculated as follows:

$$\int_{\Omega} (C_i h_i)_t \mathrm{d}\Omega = h_i \int_{\Omega} \frac{\partial C_i}{\partial t}\mathrm{d}\Omega \approx h_i \frac{\partial C_i}{\partial t}\Omega \approx h_i \frac{C_i^{n+1} - C_i^n}{\Delta t}\Omega \tag{2.202}$$

the advective flux is:

$$\oint_{\partial\Omega} (Cq, Cr)\,\overrightarrow{n}\,\mathrm{d}l = \sum_j C_j(q_j, r_j)\overrightarrow{n_j} l_j = \sum_j \Phi_{a,j} \tag{2.203}$$

and the diffusive flux:

$$\oint_{\partial\Omega} (h\Gamma C_x, h\Gamma C_y)\,\overrightarrow{n}\,\mathrm{d}l = \sum_j h_j\Gamma(C_x, C_y)\overrightarrow{n_j} l_j = \sum_j \Phi_{d,j} \tag{2.204}$$

The concentration at the new time $n+1$ is:

$$C_i^{n+1} = C_i^n - \frac{\Delta t}{\Omega_i h_i} \sum_j (\Phi_{a,j} - \Phi_{d,j}) \tag{2.205}$$

2.3.3.2.6 Computation of Diffusive Flux

The diffusive flux over the edge is computed by the derivatives of the concentration over the edge multiplied with the vector normal to the edge, the edge length, the water depth on the edge and the diffusivity:

$$\Phi_{d,j} = h_j\Gamma \begin{pmatrix} \frac{\partial C_j}{\partial x} \\ \frac{\partial C_j}{\partial y} \end{pmatrix} \overrightarrow{n}_i l_j$$

The derivatives of the concentration are given by the mean value of the derivatives in the left and the right element of the edge:

$$\begin{pmatrix} \frac{\partial C_j}{\partial x} \\ \frac{\partial C_j}{\partial y} \end{pmatrix} = \frac{1}{2} \left[\begin{pmatrix} \frac{\partial C_L}{\partial x} \\ \frac{\partial C_L}{\partial y} \end{pmatrix} + \begin{pmatrix} \frac{\partial C_R}{\partial x} \\ \frac{\partial C_R}{\partial y} \end{pmatrix} \right] \tag{2.206}$$

The mean value of the derivatives of the concentration in an element can be transformed on a sum over the edges by the Gauss theorem:

$$\left(\frac{\partial C}{\partial x}\right)_i = \frac{1}{\Omega}\int_\Omega \frac{\partial C}{\partial x}\,\mathrm{d}\Omega \approx \frac{1}{\Omega}\sum_j C_j \Delta y_j \tag{2.207}$$

$$\left(\frac{\partial C}{\partial y}\right)_i = \frac{1}{\Omega}\int_\Omega \frac{\partial C}{\partial y}\,\mathrm{d}\Omega \approx \frac{1}{\Omega}\sum_j C_j \Delta x_j \tag{2.208}$$

2.3.3.2.7 Computation of Advective Flux using the Upwind Scheme

The Upwind Scheme is the simplest possible method to calculate the advective flux in eq. 2.203. The hydraulic discharges q and r over the edge are known from the hydraulic computation (eq. 2.53). The only challenge is the choice of the edge concentration C.

For the Finite Volume Method, the concentration is regarded as constant over every computation element. Instead of averaging element concentrations in order to get an edge concentration, the upwind scheme simply uses the concentration from the upwind element. The upwind element for an edge is the one element from which the hydraulic discharge originates.

Upwind schemes are computationally not expensive. However, their side effect is an increased numerical diffusion which flattens strong gradients within the concentration. If it was important to detect a sharp front in the concentration, a more accurate and more time-expensive scheme like the MDP-method should be used.

2.3.3.2.8 Computation of Advective Flux using the MDPM scheme

The computation of the advective flux with the MDP-method (Badrot-Nico et al., 2007), is described for the one dimensional case in Section 2.3.2.2.3 d). Because of the unstructured grid used in BASEMENT the MDP-method is not used separately in x and y-direction but directly in the direction of the local velocity.

The advective flux is calculated directly as a sediment discharge:

$$\Phi_{a,j} = C_j \begin{pmatrix} q_j \\ r_j \end{pmatrix} \vec{n}_j l_j$$

The discharge of water over the edge $\begin{pmatrix} q_j \\ r_j \end{pmatrix} \vec{n}_j$ is known from the hydraulic computation (eq. 2.53). As the concentration on the edge in the MDPM scheme is not constant in time, the flux is integrated over the time step.

The flux from the element i over the edge j can be described as:

$$\Phi_j = \frac{1}{\Delta t} h_j l_j \int_{t^n}^{t^{n+1}} u_i(t) C_j(t)\,\mathrm{d}t \tag{2.209}$$

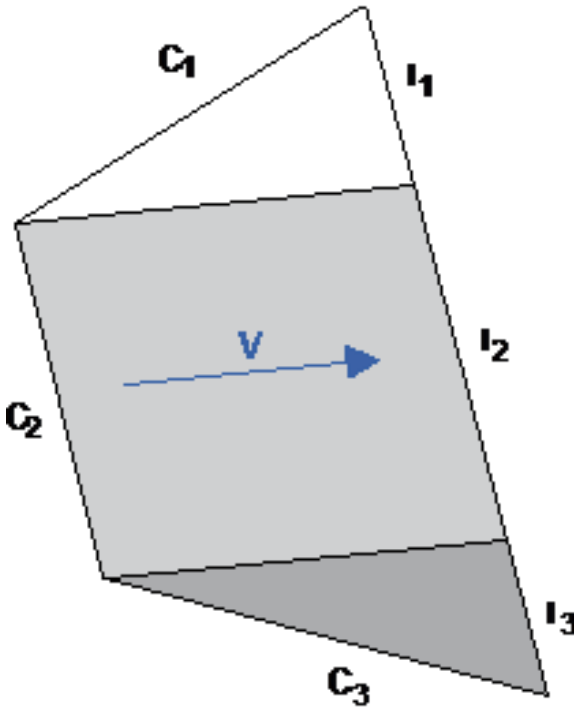

Figure 2.60 *Division of element and edge j in segments which receive the water from different upstream edges.*

The velocity u_i in the element is constant and its multiplication with the depth h_i on the edge gives the specific discharge q_i over the edge, which is known from the hydraulics. Hence the flux is:

$$\Phi_j = \frac{1}{\Delta t} q_j l_j \int_{t^n}^{t^{n+1}} C_j(t)\, \mathrm{d}t \tag{2.210}$$

or:

$$\Phi_j = q_j l_j C_j(t) \tag{2.211}$$

Now the concentration $C_i(t)$ hast to be determined on the edge. It changes not only with time. If the edge is not perpendicular to the velocity, it is not constant over the whole length of the edge at one moment. It depends on the concentration on the edge from which the water comes. For an unstructured grid with triangular or quadrilateral elements these can be up to 3 different edges. For this reason the edge j is divided in k segments for which the fluxes Φ_k are computed separately and then summed up:

$$\Phi_j = \sum_{1}^{k} \Phi_k \tag{2.212}$$

This procedure is illustrated in figure Figure 2.60.

From now on only a segment concerned by one upstream edge will be considered. The concentration on the upstream edge is C_L and the one on the downstream edge C_R. The

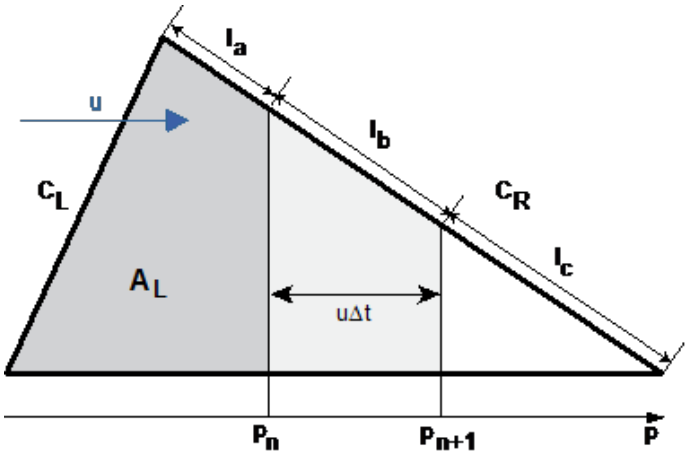

Figure 2.61 *Position of the front between the upstream and the downstream concentration at the beginning and at the end of the time step.*

part of the segment which is over flown with concentration C_L or C_R changes while the concentration front between the two concentrations advances.

The position of the front is determined in an analogous way to 1D with eq. 2.154. But instead of representing the fraction of the distance behind the front, α now represents the fraction of the area. The area which is behind the front therefore becomes:

$$A_L = \alpha_i A_i \tag{2.213}$$

The position of the front at the beginning of the time step p_n, can now be determined from the area A_L .

The position at the end of time step p_{n+1} is obtained by adding the distance covered during the time step $u\Delta t$. l_a indicates concentration C_L during the whole time step and l_c with concentration C_R. For l_b the fractions with C_L and C_R have to be integrated over time. It holdes:

$$\Phi_k = (C_L l_a + C_R l_c + (0.5C_L + 0.5C_R) l_b) q \tag{2.214}$$

Finally the concentrations on the edge j have to be replaced:

The value used as C_L, when the edge lies upstream, is replaced with C_L if the edge is partially behind the concentration front at the end of the time step. The value used asC_R, when the edge lies downstream, is replaced with C_L if the edge at the end of the time step lies completely behind the concentration front.

2.3.3.3 Discretisation of Source Terms

2.3.3.3.1 External Sediment Sources and Sinks

The source term Sl_B can be used, for example, to describe a local input or removal of sediment masses into a river or mass inflow due to slope failures. This source term can be added directly to the equations. It is specified as mass inflow with a defined grain mixture.

2.3.3.3.2 Dredge sources and sediment continuity at inner boundaries

A special subset of external sediment sinks is the so-called 'dredge source'. This source type allows for the definition of a constant dredge-level. Using the 'dredge source', sediment is removed from a cell if its bed elevation exceeds the specified dredge-level due to sediment deposition. The exceeding sediment is then removed by dredging. Additional parameters, like the maximum dredge rate, may be used to adjust the model to realistic scenarios.

This type of 'dredge source' can also be applied to achieve sediment continuity at inner boundary conditions, as e.g. an inner weir structure. It is possible to set dredge sources at the upstream region of the inner boundary, to prevent large sediment deposits and to hold a constant bed elevation. To achieve sediment continuity, one can add the removed sediment (due to dredging) to other elements, situated downstream of the inner structure. Thereby the sediments can pass the inner boundary.

2.3.3.3.3 Sediment Flux through Bottom of Bed Load Control Volume

The source term sf_g describes the change in volume of material of grain class g which enters or leaves the bed load control volume. The term sf_g is a time dependent source term and a function of grain fractions and the bed load control volume thickness. Therefore it has been handled in a special form in order to consider the time variation of the parameters. A two step method is applied, where in the first step the fractions are updated without the sf_g source term. Then, in the second step, this source term is computed with the advanced grain fractions values. The first step can be written as

$$\beta_g^{n+1/2} = \frac{1}{h_m^{n+1}} \left((h_m \beta_g)^n - \frac{\Delta t}{(1-p)\Omega} \int_{\partial\Omega} (q_{B_g,x} n_x + q_{B_g,y} n_y)^n \, \mathrm{d}l + \frac{\Delta t}{(1-p)\Omega} S l_{B_g}^n \right) \tag{2.215}$$

After this predictor step, the advanced value $\beta_g^{n+1/2}$ is used for the calculation of the fractions of the new time level β_g^{n+1} by adding the $sf_g(\beta_g^{n+1/2})$ source term as

$$\beta_g^{n+1} = \beta_g^{n+1/2} + \frac{\Delta t}{h_m^{n+1}(1-p)} sf_g \tag{2.216}$$

And the sf_g source term, which describes the material which enters or leaves the bedload control volume, is finally discretized as given below.

$$sf_g = -(1-p) \frac{\beta_g^{n+1/2}(z_F^{n+1} - z_{sub}) - \beta_g^n (z_F^n - z_{sub})}{\Delta t} \tag{2.217}$$

In the calculation of this expression for the sf_g term, cases of erosion and deposition must be considered separately.

Erosion

In case of erosion the bottom of the bed load control volume z_F moves down and the fractions of the underneath layer enter the control volume. The fractions of this underneath layer are constant over time, i.e. $\beta_g = \beta_{g_{sub}}^n = \beta_{g_{sub}}^{n+1/2}$, and the source term therefore calculates as:

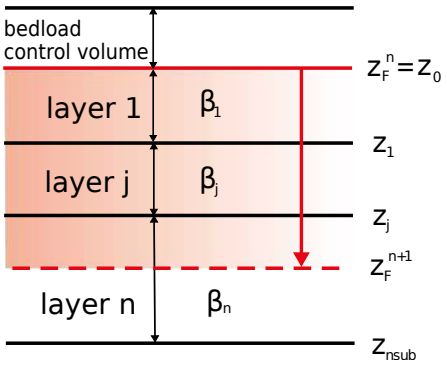

Figure 2.62 *Definition of mixed composition $\beta_{g_{mix}}$ for the eroded volume (red)*

$$sf_g = -(1-p)\beta_g \frac{(z_F^{n+1} - z_F^n)}{\Delta t} \tag{2.218}$$

Implementing this source term it must be paid attention to situations where the eroded bed volume comprises more than the first underneath sub layer. In such a situation the exchanged sediment does not exactly have the composition $\beta_{g_{sub}}^n$ of this first underneath layer, but a mixture $\beta_{g_{mix}}$ of the different compositions of all affected underneath sublayers (see Figure 2.62). In this implementation the number of the affected layers n_{sub} can be arbitrary.

The mixed grain composition $\beta_{g_{mix}}$ is determined by weighting the grain fractions with the layer thicknesses as

$$\beta_{g_{mix}} = \frac{1}{z_F^n - z_F^{n+1}} \sum_{j=1}^{nsub} \left[\beta_{g_j}(z_{j-1} - max(z_j, z_F^{n+1}))\right] \tag{2.219}$$

Deposition

In case of deposition, the bottom of the bed load control volume z_F moves up and material with the updated composition $\beta_g^{n+1/2}$ leaves the bed load control volume and enters the underneath layer. The source term therefore calculates as:

$$sf_g = -(1-p)\beta_g^{n+1/2} \frac{(z_F^{n+1} - z_F^n)}{\Delta t} \tag{2.220}$$

And a likewise term is used to update the grain compositions of the first underneath layer.

2.3.3.3.4 Sediment Exchange between Water and Bottom

The source term S_g describes the exchange between the suspended load in the water column and the sediment surface.

2.3.3.4 Gravitational Transport

2.3.3.4.1 Basic concepts

The erosion and deepening of stream leads to a steepening of the stream banks which finally can result in discontinuous mass collapses from time to time into the stream. The slope failures thereby are a main mechanism for the lateral widening of the stream. The occurrence of slope failures depends strongly on the soil characteristics and pore pressures present in the bank material. Furthermore, this gravitational induced transport type also plays a significant role in modelling dike or dam breaches due to overtopping.

The main idea of this geometrical approach is to assume that a slope failure takes place if the slope becomes steeper than a critical slope. If the critical value is exceeded, sediment material moves from the upper regions in direction of the slope and finally deposits in the lower region. This corresponds to a rotation of the cell in a way that its slope is flattened until the critical angle is reached. In order to be able to better represent the complex geotechnical aspects, it is distinguished here between three different critical failure angles in this approach:

1. A critical failure angle γ_{dry} , for partially saturated material at the bank which is not over flown. This angle may largely exceed the material's angle of repose γ_{rep} in small-grained materials due to stabilizing effects of negative pore pressures.
2. A critical failure angle γ_{wet} , for fully saturated material below the water surface. This angle can be assumed to be in the range of the material's angle of repose.
3. A deposition angle, γ_{dep} , for the deposited and not compacted material resulting from the slope collapse. This angle determines the sliding of the collapsed masses into the stream after the failure. It should be smaller than γ_{wet} and is supposed here to be in the range of about half the material's angle of repose.

These different critical angles thereby should fulfil the criteria $\gamma_{dry} > \gamma_{wet} > \gamma_{dep}$.

The idea of using different critical failure angles above and below the water surface already was successfully applied by previous numerical models for dike breaches (e.g. Faeh (2007)). In addition, recent laboratory tests of Soares-Frazão et al. (2007) clearly showed a formation of different side wall angles above and below the water surface in their experimental flume.

Algorithm of geometrical slope failure modelling

The geometrical approach is applied on the original mesh which is used for the hydraulic calculations (see Figure 2.63). This is advantageous because the slopes of the hydraulic cells are clearly defined by the elevations of their nodes. A similar approach of a 2D bank-failure operator applied on unstructured meshes was recently presented by Swartenbroekx et al. (2010). But due to the use of the dual-mesh approach the computation here differs significantly from their method. The computational algorithm consists of five successive computational steps:

(1) In a first step the steepness of a hydraulic cell's slope is used as an indicator if a slope failure has to be assumed. The appropriate critical failure angle is selected depending upon the water elevation. It is checked if the cell is wetted or dry and if the present sediment in the control volume was previously deposited or not.

(2) Then for each sediment edge i a volume V_i is calculated which must flow over the sediment edge in order to flatten the slope of the cell in a way that it no longer exceeds the critical value. Using Median-Dual cells for the sediment transport, this is easily possible since each sediment edge is situated completely within a hydraulic

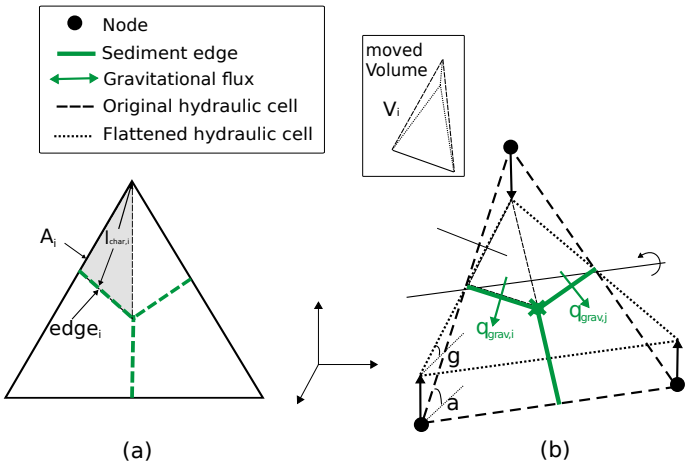

Figure 2.63 *Gravitational transport for an element with a slope angle larger than the critical slope angle (dashed = original situation, dotted = flattened slope after collapse)*

cell. The size of the volume V_i depends on the difference between the present slope in the cell and the critical slope which shall be set. The present slope and the critical slope in the cell are projected on the normal vector of this sediment edge i and the pyramidal volume is then determined as:

$$V_i = \frac{1}{3} A_i l_{char,i} (\boldsymbol{n}_i \boldsymbol{S}_i - \boldsymbol{n}_i \boldsymbol{S}_{crit,i})$$

with A_i = area above the sediment edge, $l_{char,I}$ = characteristic length, $\boldsymbol{S}_i$ = slope vector of the cell, $\boldsymbol{S}_{crit,i}$ = critical slope vector, $\boldsymbol{n}_i$ = normal vector of sediment edge and h_i = height of pyramidal volume. If γ_{dep} is set, then V_i is limited to the deposited material present in the cell.

(3) Finally the gravitational flux $q_{B_g,ngrav}$ over the edge is obtained by dividing this volume V_i by the time step size Δt. This flux leads to mass transport from the upper to the lower sediment cell which results in a flattening of the cell's slope.

$$q_{B_g,ngrav} = \frac{V_i}{\Delta t}$$

(4) The balancing of the gravitational fluxes and the determination of the new soil elevations z_B is achieved by applying and solving the Exner equation using the same numerical approaches as outlined for the bed load transport. This procedure ensures that fixed bed elevations or surface armouring layers are taken into account and the mass continuity is fulfilled.

(5) The modification of the slope of a cell in turn influences the slopes of all adjacent cells. For this reason the algorithm can be applied in an iterative manner also for the affected adjacent cells until finally no more slope angle is found which exceeds the critical value.

2.3.3.4.2 Fractional transport

The presented algorithm can be applied in this form for single grain computations only. For fractional transport additional aspects must be taken into account. In fractional transport

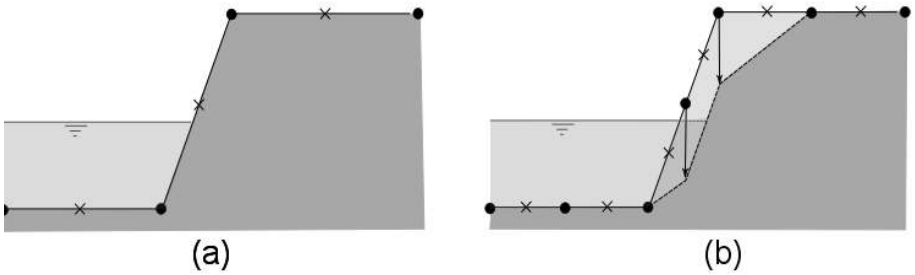

Figure 2.64 *Influence of grid resolution on the slope failures. (a) No slope failure with a coarse mesh at the indicated water level. (b) Slope failure at the same water level using a fine mesh.*

simulations, the failed slope may be composed of multiple soil layers with different grain compositions. If the slope fails, collapsed material from different soil layers with different grain compositions will be mixed and finally deposit at the toe of the slope. A detailed modelling of these mixing processes would require tracking the particles' individual motions and interactions, which cannot be achieved using the geometrical approach. Instead, a simple procedure is chosen to cope with this situation by applying the sorting equations to consider some mixing and the continuity of the failed masses. The moved material volume V_i is now limited to the available material within the bed load control volume. And because this control volume typically is rather small, with a height in the order of few grain diameters, the moved material in one computational step will be usually not sufficient to establish the critical slope. Therefore, the algorithm needs large number of iterations to establish the critical failure slopes.

2.3.3.4.3 Influence of grid resolution

Using the geometrical approach the side walls of a channel typically will collapse as soon as the water level wets at least one of the steep cells. If the cell becomes wetted the critical angle γ_{wet} is applied on this cell resulting in a collapse of the side wall. But in case of coarse discretization, the water level must be rather high until the critical angle γ_{wet} is applied. The slope failure therefore takes place slowly and may be underestimated. In contrast, in case of a finer grid resolution, the slope failure will take place earlier at a lower water level. Hence, the accuracy of the geometrical approach depends strongly on the grid resolution and a rather fine discretization should be applied at the areas of interest.

2.3.3.5 Management of Soil Layers

In case of sediment erosion, the bottom of the bed load control volume can sink below the bottom of the underneath soil layer. In such a situation the soil layer is completely eroded and consequently the data structure is removed. If the eroded layer was the last soil layer, than fixed bed conditions are set.

In case of sediment deposition, the uppermost soil layer grows in its thickness. And such an increase in layer thickness can continue up to large values during prolonged aggradation conditions. But very thick soil layers can be problematic, because the newly deposited sediments are completely mixed with the sediment materials over the whole layer thickness. Therefore a dynamic creation of new soil layers in multiple grain simulations should be enabled, which allows the formation of new soil layers.

Finding suitable general criteria for the creation of new soil layers is a difficult task. Here, two main conditions are identified and implemented:

- The thickness h_{sl} of the existing soil layer must exceed a given maximum layer thickness h_{max} before a new layer is created. Generation of a new soil layer: $h_{sl} > h_{max}$
- The grain composition of the depositing material must be different from the present grain composition of the soil layer. It is assumed here in a simple approach that this condition is fulfilled if the mean diameters of the grain compositions differ more than a given percentage P .

$$\left| \frac{d_{m,deposition} - d_{layer}}{d_{layer}} \right| > P/100$$

2.3.3.6 Solution Procedure

The manner - uncoupled, semi coupled or fully coupled - to solve eq. 1.34, eq. 1.77 and eq. 1.84 from the section Mathematical Models or appropriate derivatives with minor corrections has been often discussed over the last decade. A good overview is given by Kassem and Chaudhry (1998) or Cao et al. (2002). Uncoupled models are often blamed for their lacking of physical and numerical considerations. Vice versa coupled models are said to be very inefficient in computational effort and accordingly inapplicable for practical use. Kassem and Chaudhry (1998) showed that the difference of results calculated by coupled and semi coupled models is negligible. In addition Belleudy (2000) found that uncoupled solutions have nearly identical performance to coupled solutions even near critical flow conditions. Furthermore, the increasing difficulties and stability problems of coupled models that have to be expected when applying complicated sediment transport formulas or simulating multiple grain size classes are to be mentioned.

According to the preliminary state of this project the model with uncoupled solution of the water and sediment conservation equations has been chosen. This requires the assumption that changes in bed elevation and grain size distributions at the bed surface during one computational time step have to be slow compared to changes of the fluid variables, which dictates an upper limit on the computational time step. Consequently, the asynchronous solution procedure as depicted in Figure 2.65 and described in Figure 2.40 is justified: flow and sediment transport equations are solved uncoupled throughout the entire simulation period, i.e. with calculation of the flow field at the beginning of a given time step based on current bed topography and ensuing multiple sediment transport calculations based on the same flow field until the end of the respective time step. Thus the given duration of a calculation cycle Δt_{seq} (overall time step) consists of one hydraulic time step Δt_h and a resulting number of time steps Δt_s for sediment transport (see Figure 2.66).

By default, the mobile bed equations for sediment and suspension are solved using the current hydraulic time step with one cycle. For BASEplane, in case of quasi-stationary conditions where the changes in the hydraulic are small, the number of cycle step can be increased. The shallow water equations are solved using the hydraulic time step. The resulting water levels and velocities are then used to solve the mobile bed equations until they have been calculated for the number of cycle steps. This leads to a considerable speedup, reducing the calculation time as the hydraulic equations are solved only occasionally. The

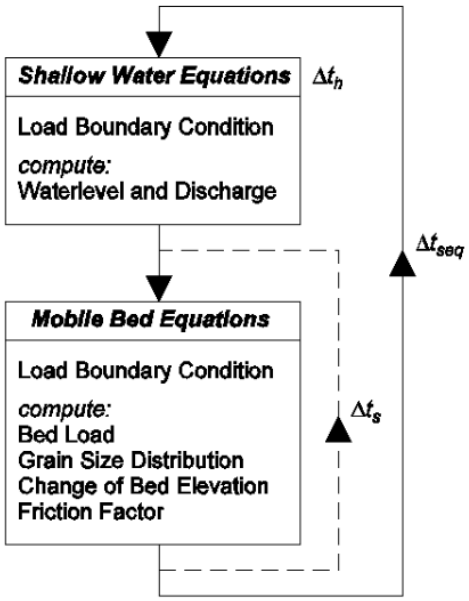

Figure 2.65 *Uncoupled asynchronous solution procedure consisting of sequential steps*

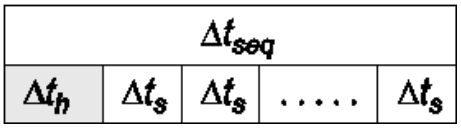

Figure 2.66 *Composition of the given overall calculation time step* Δt_{seq}

determination of the time step for the mobile bed equations depends on the model being used. For suspension transport, a time step size Δt_s is calculated to satisfy the numerical stability.

2.4 Time Discretisation and Stability Issues

2.4.1 Explicit Schemes

2.4.1.1 Euler First Order

The explicit time discretisation method implemented in BASEMENT is based on Euler first order method. According the method the full discretized equations are

$$\boldsymbol{U}_i^{n+1} = \boldsymbol{U}_i^n + RES(\boldsymbol{U})$$

$$z_B^{n+1} = z_B^n + RES(\boldsymbol{U}, d)$$

$$\beta_g^{n+1} = \beta_g^n + RES(\boldsymbol{U}, d_g, hm)$$

Where the $RES(\dots)$ is the summation of fluxes and source terms.

2.4.2 Determination of Time Step Size

2.4.2.1 Hydrodynamic

For explicit schemes, the hydraulic time step is determined according the restriction based on the Courant number. In case of the 2-D model the Courant number is defined as follows:

$$CFL = \frac{(\sqrt{u^2 + \nu^2} + c)\Delta t}{L} \leq 1 \tag{2.221}$$

Where L is the length of an edge with corresponding velocities of the element u, ν and $c = \sqrt{gh}$. In general, the CFL number has to be smaller than unity.

2.4.2.2 Bedload Transport

For the sediment transport another condition $c >> c_3$ holds true, which states that the wave speed of water c is much larger than the expansion velocity c_3 of a bottom discontinuity (eg. de Vries (1966)). Since the value of c_3 depends on multiple processes like bed load, lateral and gravity induced transport, its definitive determination is not obvious. Therefore the global time steps have been adopted based on the hydrodynamic condition.

2.4.2.3 Suspension Transport

For the suspension transport, the time step Δt_s is calculated similar to the hydraulic time step. However, the wave velocity $c = \sqrt{gh}$ is not taken into account, leading to slightly higher time step sizes. This time step is only active if a cycle step larger than 1 has been defined. By default, the cycle step is set to 1 and all mobile bed equations use the hydraulic time step.

2.4.3 Implicit Scheme

2.4.3.1 Introduction

In addition to the explicit scheme, BASEchain supports implicit calculations. To evaluate the evolution of the geometry of a channel as an effect of sediment transport, often long term computations are necessary. Additionally the calibration of a model with sediment transport is particularly laborious and needs many simulations. With the explicit solution of the hydraulics the needed simulation time becomes very large. This is because the explicit method uses a small time step, limited by the CFL-Number. The implicit method is needed to avoid this problem, allowing much larger time steps.

This chapter describes the implicit solution of the hydrodynamics in detail. The system of equations to solve is formed by eq. 1.3 and eq. 1.9 and applied to each cross section.

2.4.3.2 Time Discretisation

For the time discretisation of the differential equation $\partial u/\partial t = f(u)$ the θ-method is used:

$$\frac{u^{n+1} - u^n}{\Delta t} = \theta f(u^{n+1}) + (1-\theta) f(u^n)$$

with $0 \leq \theta \leq 1$.

If $\theta = 0$ the explicit Euler method results: the values at time n+1 are computed solely from the old values at time n with limitation of the time step by the CFL-number. For $\theta = 0.5$ the scheme is second-order accuracy in time.

On the contrary, if $\theta = 1$ the solution is fully implicit. The equations are solved with the values at the new time n+1. As they are not known, initial values are assumed and the solution is approached to the exact solution by iteration. BASEchain uses the Newton-Raphson method, which has the quality to converge rapidly. However this is only the case if the initial values are sufficiently close to the exact solution. Here the values of the last time step are used as initial values for the iterations. This means that the more distant the new time from the old one and the bigger the change of the hydraulic state, the higher is the possibility that the solution cannot be found.

For the present implementation, the recommended value of θ is between 0.5 and 1.

2.4.3.2.1 Continuity Equation

The integration of the continuity equation

$$\int_{x_{iw}}^{x_{ie}} \left(\frac{\partial A_{si}}{\partial t} + \frac{\partial Q}{\partial x} - q \right) dx = F_{\hat{\imath}}^n + F_{\hat{\imath}}^{\Phi} + F_{\hat{\imath}}^q = 0$$

gives the following integral terms.

$$F_{\hat{\imath}}^n = \int_{x_{iw}}^{x_{ie}} \frac{\partial A_{si}}{\partial t}\, dx$$

$$F_{\hat{\imath}}^{\Phi} = \int_{x_{iw}}^{x_{ie}} \frac{\partial Q}{\partial x}\, dx$$

$$F_{\hat{\imath}}^q = -\int_{x_{iw}}^{x_{ie}} q\, dx$$

Applying the θ -method:

$$F_{\hat{\imath}}^{n+1} = F_{\hat{\imath}}^n + \theta(F_{\hat{\imath}}^{\Phi} + F_{\hat{\imath}}^q) + (1-\theta)(F_{\hat{\imath}}^{\Phi 0} + F_{\hat{\imath}}^{q0}) \tag{2.222}$$

2.4.3.2.2 Momentum Equation

The integration of the momentum equation:

$$\int_{x_{iw}}^{x_{ie}} \left(\frac{\partial Q}{\partial t} + \frac{\partial}{\partial x} \left(\beta \frac{Q^2}{A_{red}} \right) + g A_{red} \frac{\partial z}{\partial x} + g A_{red} S_f \right) dx = G_i^n + G_i^\Phi + G_i^{sz} + G_i^{sf} = 0$$

leads to the following integral terms:

$$G_i^n = \int_{x_{iw}}^{x_{ie}} \frac{\partial Q}{\partial t}\, dx$$

$$G_i^\Phi = \int_{x_{iw}}^{x_{ie}} \frac{\partial}{\partial x} \left(\beta \frac{Q^2}{A_{red}} \right) dx$$

$$G_i^{sz} = \int_{x_{iw}}^{x_{ie}} g A_{red} \frac{\partial z}{\partial x}\, dx$$

$$G_i^{sf} = \int_{x_{iw}}^{x_{ie}} g A_{red} S_f\, dx$$

Applying the θ-method:

$$G_i^{n+1} = G_i^n + \theta(G_i^\Phi + G_i^{sz} + G_i^{sf}) + (1-\theta)(G_i^{\Phi 0} + G_i^{sz0} + G_i^{sf0}) \tag{2.223}$$

2.4.3.3 Solution

The equation system is

$$F(x) = 0$$

with

$$F = (F_1, G_1, F_2, G_2, \ldots, F_{n-1}, G_{n-1}, F_n, G_n)$$

and

$$x = (A_1, Q_1, A_2, Q_2, \ldots, A_{n-1}, Q_{n-1}, A_n, Q_n)$$

The system is solved by the Newton-Raphson method. Starting from an approximated solution x^k, the corresponding improved solution x^{k+1} is determined by the linear equation system.

$$Ax^{k+1} - c = 0 \tag{2.224}$$

with

$$c = Ax^k - F$$

and

$\mathcal{A} =$

$$\begin{bmatrix}
\frac{\partial F_1}{\partial A_{red,1}} & \frac{\partial F_1}{\partial Q_1} & \frac{\partial F_1}{\partial A_{red,2}} & \frac{\partial F_1}{\partial Q_2} & & & & & & & & & & \\
\frac{\partial G_1}{\partial A_{red,1}} & \frac{\partial G_1}{\partial Q_1} & \frac{\partial G_1}{\partial A_{red,2}} & \frac{\partial G_1}{\partial Q_2} & & & & & & & & & & \\
\frac{\partial F_2}{\partial A_{red,1}} & \frac{\partial F_2}{\partial Q_1} & \frac{\partial F_2}{\partial A_{red,2}} & \frac{\partial F_2}{\partial Q_2} & \frac{\partial F_2}{\partial A_{red,3}} & \frac{\partial F_2}{\partial Q_3} & & & & & & & & \\
\frac{\partial G_2}{\partial A_{red,1}} & \frac{\partial G_2}{\partial Q_1} & \frac{\partial G_2}{\partial A_{red,2}} & \frac{\partial G_2}{\partial Q_2} & \frac{\partial G_2}{\partial A_{red,3}} & \frac{\partial G_2}{\partial Q_3} & & & & & & & & \\
 & & \frac{\partial F_3}{\partial A_{red,2}} & \frac{\partial F_3}{\partial Q_2} & \frac{\partial F_3}{\partial A_{red,3}} & \frac{\partial F_3}{\partial Q_3} & \frac{\partial F_3}{\partial A_{red,4}} & \frac{\partial F_3}{\partial Q_4} & & & & & & \\
 & & \frac{\partial G_3}{\partial A_{red,2}} & \frac{\partial G_3}{\partial Q_2} & \frac{\partial G_3}{\partial A_{red,3}} & \frac{\partial G_3}{\partial Q_3} & \frac{\partial G_3}{\partial A_{red,4}} & \frac{\partial G_3}{\partial Q_4} & & & & & & \\
 & & & & & & \cdot & \cdot & & & & & & \\
 & & & & & & \cdot & \cdot & & & & & & \\
 & & & & & & \frac{\partial F_{n-2}}{\partial A_{red,n-3}} & \frac{\partial F_{n-2}}{\partial Q_{n-3}} & \frac{\partial F_{n-2}}{\partial A_{red,n-2}} & \frac{\partial F_{n-2}}{\partial Q_{n-2}} & \frac{\partial F_{n-2}}{\partial A_{red,n-1}} & \frac{\partial F_{n-2}}{\partial Q_{n-1}} & & \\
 & & & & & & \frac{\partial G_{n-2}}{\partial A_{red,n.3}} & \frac{\partial G_{n-2}}{\partial Q_{n-3}} & \frac{\partial G_{n-2}}{\partial A_{red,n-2}} & \frac{\partial G_{n-2}}{\partial Q_{n-2}} & \frac{\partial G_{n-2}}{\partial A_{red,n-1}} & \frac{\partial G_{n-2}}{\partial Q_{n-1}} & & \\
 & & & & & & & & \frac{\partial F_{n-1}}{\partial A_{red,n-2}} & \frac{\partial F_{n-1}}{\partial Q_{n-2}} & \frac{\partial F_{n-1}}{\partial A_{red,n-1}} & \frac{\partial F_{n-1}}{\partial Q_{n-1}} & \frac{\partial F_{n-1}}{\partial A_{red,n}} & \frac{\partial F_{n-1}}{\partial Q_n} \\
 & & & & & & & & \frac{\partial G_{n-1}}{\partial A_{red,n-2}} & \frac{\partial G_{n-1}}{\partial Q_{n-2}} & \frac{\partial G_{n-1}}{\partial A_{red,n-1}} & \frac{\partial G_{n-1}}{\partial Q_{n-1}} & \frac{\partial G_{n-1}}{\partial A_{red,n}} & \frac{\partial G_{n-1}}{\partial Q_n} \\
 & & & & & & & & & & \frac{\partial F_n}{\partial A_{red,n-1}} & \frac{\partial F_n}{\partial Q_{n-1}} & \frac{\partial F_n}{\partial A_{red,n}} & \frac{\partial F_n}{\partial Q_n} \\
 & & & & & & & & & & \frac{\partial G_n}{\partial A_{red,n-1}} & \frac{\partial G_n}{\partial Q_{n-1}} & \frac{\partial G_n}{\partial A_{red,n}} & \frac{\partial G_n}{\partial Q_n}
\end{bmatrix}$$

2.4.3.4 Integral Terms

2.4.3.4.1 Continuity Equation

The integral terms of the continuity equation are approximated as follows. For a general cross section i:

$$F_i^{n+1} = F_i^n + F_i^\Phi + F_i^q$$

$$F_i^n = \frac{A_{si} - A_{si}^0}{\Delta t} \Delta x_i$$

$$F_i^\Phi = \Phi_{ie}^c - \Phi_{iw}^c$$

$$F_i^q = -q_i^- \Delta x_i^- - q_i^+ \Delta x_i^+$$

For the first cross section i = 1:

$$F_1^n = \frac{A_1 - A_1^0}{\Delta t} \Delta x_1$$

$$F_1^{\Phi} = \Phi_{1e}^{c} - Q_{in}$$

$$F_1^{q} = -q_1^{+}\Delta x_1$$

For the last cross section i = N

$$F_n^{n} = \frac{A_n - A_n^0}{\Delta t}\Delta x_n$$

$$F_n^{\Phi} = Q_{out} - \Phi_{nw}^{c}$$

$$F_n^{q} = -q_n^{-}\Delta x_n$$

2.4.3.4.2 Momentum Equation

The integral terms of the continuity equation are approximated as follows. For a general cross section i:

$$G_i^{n} = \frac{Q_i - Q_i^0}{\Delta t}\Delta x_i$$

$$G_i^{\Phi} = \Phi_{ie}^{m} - \Phi_{iw}^{m}$$

$$G_i^{sz} = gA_{red,i}\frac{z_{i+1} - z_{i-1}}{2}$$

$$G_i^{sf} = gA_{red,i}S_{fi}\Delta x_i \qquad S_{fi} = \frac{Q_i|Q_i|}{K_i^2}$$

For the first cross section i = 1:

$$G_1^{n} = \frac{Q_{in} - Q_{in}^0}{\Delta t}\Delta x_1$$

$$G_1^{\Phi} = \Phi_{1e}^{m} - \frac{\beta_1 Q_{in}^2}{A_{red,in}}$$

$$G_1^{sz} = gA_{red,1}\frac{z_2 - z_1}{2}$$

$$G_1^{sf} = gA_{red,1}S_{f1}\Delta x_1 \qquad S_{f1} = \frac{Q_1|Q_1|}{K_1^2}$$

For the last cross section i = n

$$G_n^n = \frac{Q_{out} - Q_{out}^0}{\Delta t} \Delta x_n$$

$$G_n^\Phi = \frac{\beta_n Q_{out}^2}{A_{red,out}} - \Phi_{nw}^m$$

$$G_n^{sz} = g A_n \frac{z_n - z_{n-1}}{2}$$

$$G_n^{sf} = g A_n S_{fn} \Delta x_n \qquad S_{fn} = \frac{Q_n |Q_n|}{K_n^2}$$

2.4.3.5 General Description of the Derivatives for the Matrix A

2.4.3.5.1 Derivatives of the Continuity Equation

For a general cross section i:

$$\frac{\partial F_i}{\partial A_{red,i-1}} = \frac{\partial \Phi_{ie}^c}{\partial A_{red,i-1}} - \frac{\partial \Phi_{iw}^c}{\partial A_{red,i-1}}$$

$$\frac{\partial F_i}{\partial A_{red,i}} = \frac{\Delta x_i}{\Delta t} \frac{dA_i}{dA_{red,i}} + \frac{\partial \Phi_{ie}^c}{\partial A_{red,i}} - \frac{\partial \Phi_{iw}^c}{\partial A_{red,i}}$$

$$\frac{\partial F_i}{\partial A_{red,i+1}} = \frac{\partial \Phi_{ie}^c}{\partial A_{red,i+1}} - \frac{\partial \Phi_{iw}^c}{\partial A_{red,i+1}}$$

$$\frac{\partial F_i}{\partial Q_{i-1}} = \frac{\partial \Phi_{ie}^c}{\partial Q_{i-1}} - \frac{\partial \Phi_{iw}^c}{\partial Q_{i-1}}$$

$$\frac{\partial F_i}{\partial Q_i} = \frac{\partial \Phi_{ie}^c}{\partial Q_i} - \frac{\partial \Phi_{iw}^c}{\partial Q_i}$$

$$\frac{\partial F_i}{\partial Q_{i+1}} = \frac{\partial \Phi_{ie}^c}{\partial Q_{i+1}} - \frac{\partial \Phi_{iw}^c}{\partial Q_{i+1}}$$

For the first cross section i = 0:

$$\frac{\partial F_1}{\partial A_{red,1}} = \frac{\Delta x_1}{\Delta t} \frac{dA_1}{dA_{red,1}} + \frac{\partial \Phi_{1e}^c}{\partial A_{red,1}} - \frac{\partial Q_{in}}{\partial A_{red,1}}$$

$$\frac{\partial F_1}{\partial A_{red,2}} = \frac{\partial \Phi_{1e}^c}{\partial A_{red,2}} - \frac{\partial \Phi_{in}^c}{\partial A_{red,2}}$$

$$\frac{\partial F_1}{\partial Q_1} = \frac{\partial \Phi_{1e}^c}{\partial Q_{1=in}} - \frac{\partial Q_{in}}{\partial Q_{1=in}}$$

$$\frac{\partial F_1}{\partial Q_2} = \frac{\partial \Phi_{1e}^c}{\partial Q_2} - \frac{\partial Q_{in}}{\partial Q_2}$$

For the last cross section i = n:

$$\frac{\partial F_n}{\partial A_{red,n-1}} = \frac{\partial Q_{out}}{\partial A_{red,n-1}} - \frac{\partial \Phi^c_{nw}}{\partial A_{red,n-1}}$$

$$\frac{\partial F_n}{\partial A_{red,n}} = \frac{\Delta x_n}{\Delta t}\frac{dA_n}{dA_{red,n}} + \frac{\partial Q_{out}}{\partial A_{red,n}} - \frac{\partial \Phi^c_{nw}}{\partial A_{red,n}}$$

$$\frac{\partial F_n}{\partial Q_{n-1}} = \frac{\partial Q_{out}}{\partial Q_{n-1}} - \frac{\partial \Phi^c_{nw}}{\partial Q_{n-1}}$$

$$\frac{\partial F_n}{\partial Q_n} = \frac{\partial Q_{out}}{\partial Q_{n=out}} - \frac{\partial \Phi^c_{nw}}{\partial Q_{n=out}}$$

2.4.3.5.2 Derivatives of the Momentum Equation

For a general cross section i:

$$\frac{\partial G_i}{\partial A_{red,i-1}} = \frac{\partial \Phi^m_{ie}}{\partial A_{red,i-1}} - \frac{\partial \Phi^m_{iw}}{\partial A_{red,i-1}} + \frac{gA_{red,i}}{2}\frac{dz_{i-1}}{dA_{red,i-1}}$$

$$\frac{\partial G_i}{\partial A_{red,i}} = \frac{\partial \Phi^m_{ie}}{\partial A_{red,i}} - \frac{\partial \Phi^m_{iw}}{\partial A_{red,i}} + \frac{g}{2}(z_{i+1} - z_{i-1}) + g\Delta x_i S_{fi}\left(1 - 2\frac{A_{red,i}}{K_i}\frac{dK_i}{dA_i}\right)$$

$$\frac{\partial G_i}{\partial A_{red,i+1}} = \frac{\partial \Phi^m_{ie}}{\partial A_{red,i+1}} - \frac{\partial \Phi^m_{iw}}{\partial A_{red,i+1}} + g\frac{A_{red,i}}{2}\frac{dz_{i+1}}{dA_{red,i+1}}$$

$$\frac{\partial G_i}{\partial Q_{i-1}} = \frac{\partial \Phi^m_{ie}}{\partial Q_{i-1}} - \frac{\partial \Phi^m_{iw}}{\partial Q_{i-1}}$$

$$\frac{\partial G_i}{\partial Q_i} = \frac{\Delta x_i}{\Delta t} + \frac{\partial \Phi^m_{ie}}{\partial Q_i} - \frac{\partial \Phi^m_{iw}}{\partial Q_i} + 2gA_{red,i}\Delta x_i\frac{Sf_i}{Q_i}$$

$$\frac{\partial G_i}{\partial Q_{i+1}} = \frac{\partial \Phi^m_{ie}}{\partial Q_{i+1}} - \frac{\partial \Phi^m_{iw}}{\partial Q_{i+1}}$$

For the first cross section i = 1:

$$\frac{\partial G_1}{\partial A_{red,1}} = \frac{\partial \Phi^m_{1e}}{\partial A_{red,1}} - \frac{\partial \Phi^m_{in}}{\partial A_{red,1}} + \frac{g}{2}(z_2 - z_1) + g\Delta x_1 S_{f1}\left(1 - 2\frac{A_1}{K_1}\frac{dK_1}{dA_{red,1}}\right)$$

$$\frac{\partial G_1}{\partial A_{red,2}} = \frac{\partial \Phi^m_{1e}}{\partial A_{red,2}} - \frac{\partial \Phi^m_{in}}{\partial A_{red,2}} + g\frac{A_1}{2}\frac{dz_2}{dA_2}$$

$$\frac{\partial G_1}{\partial Q_1} = \frac{\Delta x_1}{\Delta t} + \frac{\partial \Phi^m_{1e}}{\partial Q_{in}} - \frac{\partial \frac{\beta_1 Q^2_{in}}{A_{red,in}}}{\partial Q_{in}} + 2gA_{red,1}\Delta x_1\frac{Sf_1}{Q_{in}}$$

$$\frac{\partial G_1}{\partial Q_2} = \frac{\partial \Phi_{1e}^m}{\partial Q_2} - \frac{\partial \frac{\beta_1 Q_{in}^2}{A_{red,in}}}{\partial Q_2}$$

For the last cross section i = n:

$$\frac{\partial G_n}{\partial A_{red,n-1}} = \frac{\partial \Phi_{out}^m}{\partial A_{red,n-1}} - \frac{\partial \Phi_{nw}^m}{\partial A_{red,n-1}} + g\frac{A_{red,n}}{2}\frac{dz_{n-1}}{dA_{red,n-1}}$$

$$\frac{\partial G_n}{\partial A_{red,n}} = \frac{\partial \Phi_{out}^m}{\partial A_{red,n}} - \frac{\partial \Phi_{nw}^m}{\partial A_{red,n}} + \frac{g}{2}(z_n - z_{n-1}) + g\Delta x_n S_{fn}\left(1 - 2\frac{A_n}{K_n}\frac{dK_n}{dA_{red,n}}\right)$$

$$\frac{\partial G_n}{\partial Q_{n-1}} = \frac{\partial \Phi_{out}^m}{\partial Q_{n-1}} - \frac{\partial \Phi_{nw}^m}{\partial Q_{n-1}}$$

$$\frac{\partial G_n}{\partial Q_n} = \frac{\Delta x_n}{\Delta t} + \frac{\partial \Phi_{out}^m}{\partial Q_n} - \frac{\partial \Phi_{nw}^m}{\partial Q_n} + 2gA_{red,n}\Delta x_n \frac{Sf_n}{Q_n}$$

2.4.3.6 Determination of the Derivatives with Upwind Flux Determination

With the upwind method the flux is defined as follows:

$$f(x_{ie}) = \Gamma_i^{ie} f_i + \Gamma_{i+1}^{ie} f_{i+1} \tag{2.225}$$

with

$$\begin{array}{llll} \Gamma_i^{ie} = 1 & and & \Gamma_{i+1}^{ie} = 0 & if \quad Q_i + Q_{i+1} \geq 0 \\ \Gamma_i^{ie} = 0 & and & \Gamma_{i+1}^{ie} = 1 & if \quad Q_i + Q_{i+1} < 0 \end{array}$$

2.4.3.6.1 Derivatives of the Continuity Equation

For a general cross section:

$$\frac{\partial F_i}{\partial A_{red,i-1}} = 0$$

$$\frac{\partial F_i}{\partial A_{red,i}} = \frac{\Delta x_i}{\Delta t}\frac{\partial A_i}{\partial A_{red,i}}$$

$$\frac{\partial F_i}{\partial A_{red,i+1}} = 0$$

$$\frac{\partial F_i}{\partial Q_{i-1}} = -\theta \Gamma_{i-1}^{i-0.5}$$

$$\frac{\partial F_i}{\partial Q_i} = \theta(\Gamma_i^w - \Gamma_i^e)$$

$$\frac{\partial F_i}{\partial Q_{i+1}} = \theta \Gamma^e_{i+1}$$

For cross section i =1:

$$\frac{\partial F_1}{\partial A_{red,1}} = \frac{\Delta x_1}{\Delta t} \frac{\partial A_1}{\partial A_{red,1}}$$

$$\frac{\partial F_1}{\partial Q_1} = \theta(\Gamma^e_1 - 1)$$

$$\frac{\partial F_1}{\partial Q_2} = \theta \Gamma^e_2$$

For cross section i =n:

$$\frac{\partial F_n}{\partial A_n} = \frac{\Delta x_n}{\Delta t} \frac{\partial A_n}{\partial A_{red,n}}$$

$$\frac{\partial F_n}{\partial Q_{n-1}} = -\theta \Gamma^w_{n-1}$$

$$\frac{\partial F_n}{\partial Q_n} = \theta(1 - \Gamma^w_n)$$

2.4.3.6.2 Derivatives of the Momentum Equation

For a general cross section i:

$$\frac{\partial G_i}{\partial A_{red,i-1}} = \theta \left(\Gamma^w_{i-1} \left[\beta \frac{Q^2}{A_{red}} \right] \left(\frac{1}{A_{red,i-1}} - \frac{1}{\beta_{i-1}} \frac{d\beta_{i-1}}{dA_{red,i-1}} \right) \right) - g \frac{A_{red,i}}{2} \frac{dz_{i-1}}{dA_{red,i-1}}$$

$$\frac{\partial G_i}{\partial A_{red,i}} = \theta \left((\Gamma^w_i - \Gamma^e_i) \left[\beta \frac{Q^2}{A_{red}} \right]_i \left(\frac{1}{A_{red,i}} - \frac{1}{\beta_i} \frac{d\beta_i}{dA_{red,i}} \right) + \frac{g}{2}(z_{i+1} - z_{i-1}) \right) + \theta \left(g \Delta x_i S_{fi} \left(1 - 2 \frac{A_{red,i}}{K_i} \frac{dK_i}{dA_{red,i}} \right) \right)$$

$$\frac{\partial G_i}{\partial A_{red,i+1}} = \theta \left(-\Gamma^e_{i+1} \left[\beta \frac{Q^2}{A_{red}} \right]_{i+1} \left(\frac{1}{A_{red,i+1}} - \frac{1}{\beta_{i+1}} \frac{d\beta_{i+1}}{dA_{red,i}} \right) + g \frac{A_{red,i}}{2} \frac{dz_{i+1}}{dA_{red,i+1}} \right)$$

$$\frac{\partial G_i}{\partial Q_{i-1}} = -2\theta \Gamma^w_{i-1} \frac{1}{Q_{i-1}} \left[\beta \frac{Q^2}{A_{red}} \right]_{i-1}$$

$$\frac{\partial G_i}{\partial Q_i} = \frac{\Delta x_i}{\Delta t} + 2\theta \left((\Gamma^e_i - \Gamma^w_i) \frac{1}{Q_i} \left[\beta \frac{Q^2}{A_{red}} \right]_i + 2 g A_{red,i} \Delta x_i \frac{Sf_i}{Q_i} \right)$$

$$\frac{\partial G_i}{\partial Q_{i+1}} = 2\theta\Gamma^e_{i+1}\frac{1}{Q_{i+1}}\left[\beta\frac{Q^2}{A_{red}}\right]_{i+1}$$

For cross section i =1:

$$\frac{\partial G_1}{\partial A_{red,1}} = \theta\left((1-\Gamma^e_1)\left[\beta\frac{Q^2}{A_{red}}\right]_1\left(\frac{1}{A_{red,1}} - \frac{1}{\beta_1}\frac{d\beta_1}{dA_{red,1}}\right) + \frac{g}{2}\left(z_2 - z_1 - A_{red,1}\frac{dz_1}{dA_{red,1}}\right)\right) + \theta\left(g\Delta x_1 S_{f1}\left(1 - 2\frac{A_{red,1}}{K_1}\frac{dK_1}{dA_{red,1}}\right)\right)$$

$$\frac{\partial G_1}{\partial A_{red,2}} = \theta\left(-\Gamma^e_2\left[\beta\frac{Q^2}{A_{red}}\right]_2\left(\frac{1}{A_{red,2}} - \frac{1}{\beta_2}\frac{d\beta_2}{dA_{red,2}}\right) + g\frac{A_{red,2}}{2}\frac{dz_2}{dA_{red,2}}\right)$$

$$\frac{\partial G_1}{\partial Q_1} = \frac{\Delta x_1}{\Delta t} + 2\theta\left((\Gamma^e_1 - 1)\frac{1}{Q_1}\left[\beta\frac{Q^2}{A_{red}}\right]_1 + 2gA_{red,1}\Delta x_1\frac{Sf_1}{Q_1}\right)$$

$$\frac{\partial G_1}{\partial Q_2} = 2\theta\Gamma^e_2\frac{1}{Q_2}\left[\beta\frac{Q^2}{A_{red}}\right]_2$$

For cross section i =n:

$$\frac{\partial G_n}{\partial A_{red,n-1}} = \theta\left(\Gamma^w_{n-1}\left[\beta\frac{Q^2}{A_{red}}\right]_{n-1}\left(\frac{1}{A_{n-1}} - \frac{1}{\beta_{n-1}}\frac{d\beta_{n-1}}{dA_{n-1}}\right)\right) - g\frac{A_n}{2}\frac{dz_{n-1}}{dA_{red,n-1}}$$

$$\frac{\partial G_n}{\partial A_{red,n}} = \theta\left((\Gamma^w_n - 1)\left[\beta\frac{Q^2}{A_{red}}\right]_n\left(\frac{1}{A_n} - \frac{1}{\beta_n}\frac{d\beta_n}{dA_n}\right) + \frac{g}{2}\left(z_n - z_{n-1} + A_n\frac{dz_n}{dA_n}\right)\right) + \theta\left(g\Delta x_n S_{fn}\left(1 - 2\frac{A_n}{K_n}\frac{dK_n}{dA_n}\right)\right)$$

$$\frac{\partial G_n}{\partial Q_{n-1}} = -2\theta\Gamma^w_{n-1}\frac{1}{Q_{n-1}}\left[\beta\frac{Q^2}{A}\right]_{n-1}$$

$$\frac{\partial G_n}{\partial Q_n} = \frac{\Delta x_n}{\Delta t} + 2\theta\left((1-\Gamma^w_n)\frac{1}{Q_n}\left[\beta\frac{Q^2}{A}\right]_n + gA_n\Delta x_n\frac{Sf_n}{Q_n}\right)$$

2.4.3.7 Determination of the Derivatives with Roe Flux Determination

Fluxes and derivatives of the fluxes of the continuity equation:

$$\Phi^c_{ie} = Q(ie) = \frac{1}{2}(Q_i + Q_{i+1}) - R_{cA}(A_{i+1} - A_i) - R_{cQ}(Q_{i+1} - Q_i) \tag{2.226}$$

$$\begin{array}{lll} \frac{\partial \Phi^c_{ie}}{\partial A_{i-1}} = 0 & \frac{\partial \Phi^c_{ie}}{\partial A_i} = R^{ie}_{cA} & \frac{\partial \Phi^c_{ie}}{\partial A_{i+1}} = -R^{ie}_{cA} \\ \frac{\partial \Phi^c_{ie}}{\partial Q_{i-1}} = 0 & \frac{\partial \Phi^c_{ie}}{\partial Q_i} = 0.5 + R^{ie}_{cQ} & \frac{\partial \Phi^c_{ie}}{\partial Q_{i+1}} = 0.5 - R^{ie}_{cQ} \end{array}$$

$$\Phi^c_{iw} = Q(iw) = 0.5(Q_{i-1} + Q_i) - R_{cA}(A_i - A_{i-1}) - R_{cQ}(Q_i - Q_{i-1}) \tag{2.227}$$

$$\begin{array}{lll} \frac{\partial \Phi^c_{iw}}{\partial A_{i-1}} = R^{iw}_{cA} & \frac{\partial \Phi^c_{iw}}{\partial A_i} = -R^{iw}_{cA} & \frac{\partial \Phi^c_{iw}}{\partial A_{i+1}} = 0 \\ \frac{\partial \Phi^c_{iw}}{\partial Q_{i-1}} = 0.5 + R^{iw}_{cQ} & \frac{\partial \Phi^c_{iw}}{\partial Q_i} = 0.5 - R^{iw}_{cQ} & \frac{\partial \Phi^c_{iw}}{\partial Q_{i+1}} = 0 \end{array}$$

Fluxes and derivatives of the fluxes of the momentum equation:

$$\Phi^m_{ie} = \beta \left.\frac{Q^2}{A}\right|_{ie} = 0.5\left(\beta_i \frac{Q_i^2}{A_i} + \beta_{i+1}\frac{Q_{i+1}^2}{A_{i+1}}\right) - R_{mA}(A_{i+1} - A_i) - R_{mQ}(Q_{i+1} - Q_i) \tag{2.228}$$

$$\begin{array}{lll} \frac{\partial \Phi^m_{ie}}{\partial A_{i-1}} = 0 & \frac{\partial \Phi^m_{ie}}{\partial A_i} = -0.5\beta_i \frac{Q_i^2}{A_i^2} + R^{ie}_{mA} & \frac{\partial \Phi^m_{ie}}{\partial A_{i+1}} = -0.5\beta_{i+1}\frac{Q_{i+1}^2}{A_{i+1}^2} - R^{ie}_{mA} \\ \frac{\partial \Phi^m_{ie}}{\partial Q_{i-1}} = 0 & \frac{\partial \Phi^m_{ie}}{\partial Q_i} = \beta_i \frac{Q_i^2}{A_i^2} + R^{ie}_{mQ} & \frac{\partial \Phi^m_{ie}}{\partial Q_{i+1}} = \beta_{i+1}\frac{Q_{i+1}^2}{A_{i+1}^2} - R^{ie}_{mQ} \end{array}$$

$$\Phi^m_{iw} = \beta \left.\frac{Q^2}{A}\right|_{iw} = 0.5\left(\beta_i \frac{Q_{i-1}^2}{A_i - 1} + \beta_i \frac{Q_i^2}{A_i}\right) - R_{mA}(A_i - A_{i-1}) - R_{mQ}(Q_i - Q_{i-1}) \tag{2.229}$$

$$\begin{array}{lll} \frac{\partial \Phi^m_{iw}}{\partial A_{i-1}} = -0.5\beta_{i-1}\frac{Q_{i-1}^2}{A_{i-1}^2} + R^{iw}_{mA} & \frac{\partial \Phi^m_{iw}}{\partial A_i} = -0.5\beta_i \frac{Q_i^2}{A_i^2} - R^{iw}_{mA} & \frac{\partial \Phi^m_{ie}}{\partial A_{i+1}} = 0 \\ \frac{\partial \Phi^m_{iw}}{\partial Q_{i-1}} = \beta_{i-1}\frac{Q_{i-1}}{A_{i-1}} + R^{iw}_{mQ} & \frac{\partial \Phi^m_{iw}}{\partial Q_i} = \beta_i \frac{Q_i}{A_i} - R^{iw}_{mQ} & \frac{\partial \Phi^m_{iw}}{\partial Q_{i+1}} = 0 \end{array}$$

2.4.3.7.1 Derivatives of the Continuity Equation:

For a general cross section i:

$$\frac{\partial F_i}{\partial A_{red,i-1}} = -R^{iw}_{cA}$$

$$\frac{\partial F_i}{\partial A_{red,i}} = \frac{\Delta x_i}{\Delta t}\frac{\partial A_i}{\partial A_{red,i}} + R^{ie}_{cA} + R^{iw}_{cA}$$

$$\frac{\partial F_i}{\partial A_{red,i+1}} = -R^{ie}_{cA}$$

$$\frac{\partial F_i}{\partial Q_{i-1}} = -\frac{1}{2} - R_{cQ}^{iw}$$

$$\frac{\partial F_i}{\partial Q_i} = R_{cQ}^{ie} - R_{cQ}^{iw}$$

$$\frac{\partial F_i}{\partial Q_{i+1}} = \frac{1}{2} - R_{cQ}^{ie}$$

For the first cross section i=1:

$$\frac{\partial F_1}{\partial A_{red,1}} = \frac{\Delta x_1}{\Delta t}\frac{\partial A_1}{\partial A_{red,1}} + R_{cA}^{ie} - \frac{\partial Q_{in}}{\partial A_{red,1}}$$

$$\frac{\partial F_1}{\partial A_{red,2}} = -R_{cA}^{ie}$$

$$\frac{\partial F_1}{\partial Q_{1=in}} = R_{cQ}^{ie} - 0.5$$

$$\frac{\partial F_1}{\partial Q_2} = \frac{1}{2} - R_{cQ}^{ie}$$

For the last cross section i=n:

$$\frac{\partial F_n}{\partial A_{n-1}} = -R_{cA}^{iw}$$

$$\frac{\partial F_n}{\partial A_n} = \frac{\Delta x_n}{\Delta t}\frac{\partial A_n}{\partial A_{red,n}} + R_{cA}^{iw} + \frac{\partial Q_{out}}{\partial A_{red,n}}$$

$$\frac{\partial F_n}{\partial Q_{n-1}} = -\frac{1}{2} - R_{cA}^{iw}$$

$$\frac{\partial F_n}{\partial Q_n} = 0.5 + R_{cQ}^{iw}$$

2.4.3.7.2 Derivatives of the Momentum Equation

For a general cross section i:

$$\frac{\partial G_i}{\partial A_{red,i-1}} = \frac{1}{2}\beta_{i-1}U_{i-1}^2 - R_{mA}^{iw} + g\frac{A_{red,i}}{2}\frac{dz_{i-1}}{dA_{red,i-1}}$$

$$\frac{\partial G_i}{\partial A_{red,i}} = -\frac{1}{2}\beta_i U_i^2 + R_{mA}^{ie} + \frac{1}{2}\beta_i U_i^2 + R_{mA}^{iw} + \frac{g}{2}(z_{i+1} - z_{i-1}) + g\Delta x_i S_{fi}\left(1 - 2\frac{A_{red,i}}{K_i}\frac{dK_i}{dA_{red,i}}\right)$$

$$\frac{\partial G_i}{\partial A_{red,i+1}} = -\frac{1}{2}\beta_{i+1}U_{i+1}^2 - R_{mA}^{ie} + g\frac{A_{red,i}}{2}\frac{dz_{i+1}}{dA_{red,i+1}}$$

$$\frac{\partial G_i}{\partial Q_{i-1}} = \beta_{i-1}U_{i-1} - R_{mQ}^{iw}$$

$$\frac{\partial G_i}{\partial Q_i} = \frac{\Delta x_i}{\Delta t} + R_{mQ}^{ie} + R_{mQ}^{ie} + 2gA_{red,i}\Delta x_i\frac{Sf_i}{Q_i}$$

$$\frac{\partial G_i}{\partial Q_{i+1}} = \beta_{i+1}U_{i+1} - R_{mQ}^{ie}$$

For the first cross section i=1:

$$\frac{\partial G_1}{\partial A_{red,1}} = -\frac{1}{2}\beta_1 U_1^2 + R_{mA}^{1e} - \frac{\partial \Phi_{in}^m}{\partial A_{red,1}} + \frac{g}{2}(z_2 - z_1) + g\Delta x_1 S_{f1}\left(1 - 2\frac{A_{red,1}}{K_1}\frac{dK_1}{dA_{red,1}}\right)$$

$$\frac{\partial G_1}{\partial A_{red,2}} = -\frac{1}{2}\beta_2 U_2^2 + R_{mA}^{1e} + g\frac{A_{red,1}}{2}\frac{dz_2}{dA_{red,2}}$$

$$\frac{\partial G_1}{\partial Q_1} = \frac{\Delta x_1}{\Delta t} + \beta_1 U_1 + R_{mQ}^{1e} - \frac{\partial \Phi_{in}^m}{\partial Q_{1=in}} + 2gA_1\Delta x_1\frac{Sf_1}{Q_1}$$

$$\frac{\partial G_1}{\partial Q_2} = \beta_2 U_2 - R_{mQ}^{1e}$$

For the last cross section i=n

$$\frac{\partial G_n}{\partial A_{red,n-1}} = \frac{1}{2}\beta_{n-1}U_{n-1}^2 - R_{mA}^{nw} + g\frac{A_{red,n}}{2}\frac{dz_{n-1}}{dA_{red,n-1}}$$

$$\frac{\partial G_n}{\partial A_{red,n}} = -\frac{1}{2}\beta_n U_n^2 + R_{mA}^{ne} + \frac{1}{2}\beta_n U_n^2 + R_{mA}^{nw} + \frac{g}{2}(z_n - z_{n-1}) + g\Delta x_n S_{fn}\left(1 - 2\frac{A_{red,n}}{K_n}\frac{dK_n}{dA_{red,n}}\right)$$

$$\frac{\partial G_n}{\partial Q_{n-1}} = \beta_{n-1}U_{n-1} - R_{mQ}^{nw}$$

$$\frac{\partial G_n}{\partial Q_n} = \frac{\Delta x_n}{\Delta t} + \beta_n U_n + R_{mQ}^{ne} - \beta_n U_n + R_{mQ}^{nw} + 2gA_n\Delta x_n\frac{Sf_n}{Q_n} = \frac{\Delta x_n}{\Delta t} + R_{mQ}^{ne} + R_{mQ}^{ne} + 2gA_n\Delta x_n\frac{Sf_n}{Q_n}$$

2.4.3.8 Derivatives of the fluxes for an inner Weir

w is the weir width and p the Poleni factor

2.4.3.8.1 Derivatives for the continuity flux

$$\frac{\partial \Phi^c_{ie}}{\partial A_i} = wp\sqrt{2g(z_i - z_{weir})}\frac{dz_i}{dA_i} \quad \frac{\partial \Phi^c_{iw}}{\partial A_i} = 0$$
$$\frac{\partial \Phi^c_{ie}}{\partial A_{i-1}} = 0 \quad \frac{\partial \Phi^c_{iw}}{\partial A_{i-1}} = wp\sqrt{2g(z_{i-1} - z_{weir})}\frac{dz_{i-1}}{dA_{i-1}}$$
$$\frac{\partial \Phi^c_{ie}}{\partial A_{i+1}} = 0 \quad \frac{\partial \Phi^c_{iw}}{\partial A_{i+1}} = 0$$

$$\frac{\partial \Phi^c_{ie}}{\partial Q_{i-1}} = 0 \quad \frac{\partial \Phi^c_{iw}}{\partial Q_{i-1}} = 1$$
$$\frac{\partial \Phi^c_{ie}}{\partial Q_i} = 1 \quad \frac{\partial \Phi^c_{iw}}{\partial Q_i} = 0$$
$$\frac{\partial \Phi^c_{ie}}{\partial Q_{i+1}} = 0 \quad \frac{\partial \Phi^c_{iw}}{\partial Q_{i+1}} = 0$$

2.4.3.8.2 Derivatives of the momentum flux

$$\frac{\partial \Phi^m_{ie}}{\partial A_{i-1}} = 0 \quad \frac{\partial \Phi^m_{iw}}{\partial A_{i-1}} = \frac{8gp^2w^2(z_{i-1} - z_{weir})^2}{3A_{weir}}\frac{dz_{i-1}}{dA_{i-1}}$$
$$\frac{\partial \Phi^m_{ie}}{\partial A_i} = \frac{8gp^2w^2(z_{i-1} - z_{weir})^2}{3A_{weir}}\frac{dz_i}{dA_i} \quad \frac{\partial \Phi^m_{iw}}{\partial A_i} = 0$$
$$\frac{\partial \Phi^m_{ie}}{\partial A_{i+1}} = 0 \quad \frac{\partial \Phi^m_{iw}}{\partial A_{i+1}} = 0$$
$$\frac{\partial \Phi^m_{ie}}{\partial Q_{i-1}} = 0 \quad \frac{\partial \Phi^m_{iw}}{\partial Q_{i-1}} = \frac{2Q_{i-1}}{A_{i-1}}$$
$$\frac{\partial \Phi^m_{ie}}{\partial Q_i} = \frac{2Q_i}{A_i} \quad \frac{\partial \Phi^m_{iw}}{\partial Q_i} = 0$$
$$\frac{\partial \Phi^m_{ie}}{\partial Q_{i+1}} = 0 \quad \frac{\partial \Phi^m_{iw}}{\partial Q_{i+1}} = 0$$

2.5 Numerical Solution of Sub-surface Flow

2.5.1 Introduction

The numerical solution of the Richard's equation is a challenging task due to strong non-linearities introduced by the constitutive models. Additionally, at the interfaces between different soils in heterogeneous embankments, steep jumps and abrupt changes in the variables may occur. Many models were presented in the past solving the Richard's equation based on Finite-Difference or Finite-Element methods and showed good results. A novel application of the Lattice-Boltzmann method on the Richard's equation was recently presented by Ginzburg et al. (2004) and Ginzburg (2006), basing on a LBM approach for generic anisotropic advection-dispersion equations. The application of the LBM has some advantages which can make it an interesting alternative choice compared to classical continuum approaches. The method is simple and easy to implement and it allows for

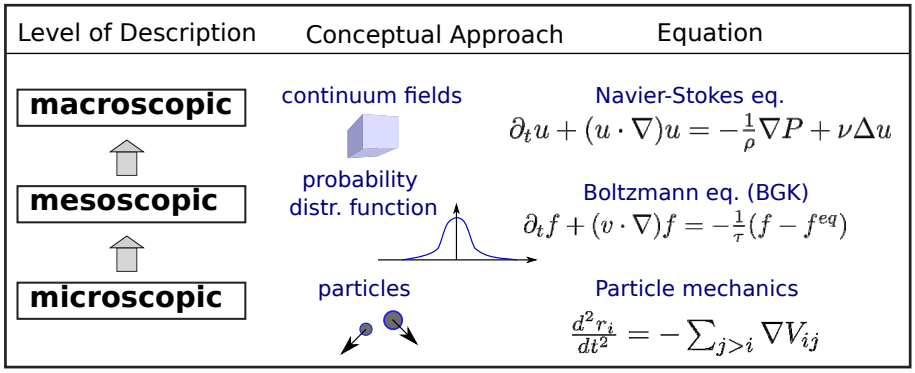

Figure 2.67 *Comparison of different levels of description and conceptual approaches applied to determine fluid motion.*

the modeling of complex geometries using bounce-back boundaries. Also, the method is local and therefore suited well for parallelization. Ginzburg adapted solution strategies for advection-diffusion problems to different formulations of the Richard's equation, like the moisture θ formulation and mixed moisture-pressure head $\theta - h$ formulation. This method of Ginzburg is applied and adapted here to simulate the 3-D sub-surface flow in the saturated and partially-saturated zone.

2.5.2 Lattice-Boltzmann Method

The LBM is a mesoscopic modelling approach which is positioned in between microscopic, particle-based dynamics and macroscopic continuum approaches. The underlying theory bases on the Boltzmann equation from kinetic theory which was derived by the Austrian physicist and philosopher L. Boltzmann.

The Boltzmann equation is formulated for a probability distribution function $f(\overrightarrow{r}, t)$ of particles in the 6-D phase-space $\overrightarrow{r}(\overrightarrow{x}, \overrightarrow{v})$. This phase-space is formed by the three spatial coordinates and the three velocity components. The distribution function may be seen as a representation of particles at time t with locations and velocities in between $\overrightarrow{r}$ and $\overrightarrow{r} + \Delta\overrightarrow{r}$. The integration of the distribution function over the phase-space results in the macroscopic fluid density. Since the LBM is used here to solve the macroscopic Richard's equation, the function $f(\overrightarrow{r}, t)$ may be interpreted as a directional saturation density, whereas the integration over the phase-space results in the macroscopic water saturation. The Boltzmann equation for the scalar distribution function $f(\overrightarrow{r}, t)$ can be written in 1D as (Mohamad, 2011)

$$\frac{\partial f(\overrightarrow{r}, t)}{dt} + v\frac{\partial f(\overrightarrow{r}, t)}{dx} = \Omega \tag{2.230}$$

with Ω as the collision operator, which describes the mutual influences of distribution functions $f(\overrightarrow{r}, t)$ on each other. This partial differential equation has the simple form of a single linear transport equation, even in higher dimensions. The main problem for solving the Boltzmann equation, however, is the treatment of its complex collision operator. The single relaxation time BGK (Bhatnagar et al., 1954) approach is often applied and treats the collision as simple relaxation of the distribution function f towards its equilibrium state, characterized by the local equilibrium distribution function f^{eq}. The collision operator then results to $\Omega = \omega(f - f^{eq})$ with the relaxation parameter ω.

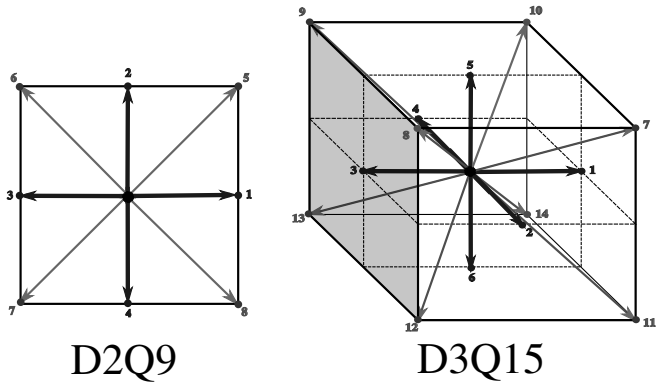

Figure 2.68 *2D lattice with 9 directions (left), 3D lattice with 15 directions (right).*

The LBM solves the Boltzmann equation in a discrete form on a uniform mesh. The discrete Boltzmann equation for the spatial mesh directions q reads

$$\underbrace{f_q(\overrightarrow{r}+\Delta t\overrightarrow{c}_q,t+\Delta t)=f_q(\overrightarrow{r},t)}_{\text{advection step}}+\underbrace{\omega[f_q(\overrightarrow{r},t)-f_q^{eq}(\overrightarrow{r},t)]}_{\text{collision step}}+\underbrace{Q_q/c_m}_{\text{source}} \quad q=1\ldots n_q \tag{2.231}$$

with a single time relaxation parameter ω being determined as a function of the diffusivity D as $\omega=-1.0/(D/c_s^2+0.5)$. The diffusivity is determined as

- $D=k_r(\theta)k_f\partial h/\partial\theta$ for the θ formulation, and
- $D=k_r(\theta)k_f$ for the mixed $\theta-h$ formulation.

The variable Q_q on the right hand side is an external source for modelling water infiltration into the embankment. The parameter c_s^2 is determined as c/ϑ with the free adjustable constant ϑ.

The uniform mesh is constructed with cubic cells using a set of q discrete velocities c_q which connect the grid cells with each other. Overall, n_q =15 different directions are used (3DQ15). The directions of the q discrete velocities (compare Figure 2.68) are set as

$$c_q=c_m\begin{cases}(0,0,0),(1,0,0),(0,1,0),(-1,0,0),(0,-1,0),(0,0,1),(0,0,-1) & q=0\ldots6\\(1,1,1),(-1,1,1),(-1,-1,1),(1,-1,1) & q=7\ldots10\\(1,1,-1),(-1,1,-1),(-1,-1,-1),(1,-1,-1) & q=11\ldots14\end{cases} \tag{2.232}$$

2.5.3 Solution procedure

Mainly three explicit computational steps are applied to solve the discrete Boltzmann equation. The first two steps are hereby analogous to particle based approaches, whereas the third step reflects the handling with particle distribution functions instead of single particles.

2.5.3.1 Advection step

At the advection step, the distribution functions are just moved along the discrete lattice directions from each cell to its adjacent cells. At the lattice boundaries special treatments are required as described below.

2.5.3.2 Collision step

The collision operator is approximated using the BGK approach which assumes a simple relaxation of f towards its equilibrium distribution function f^{eq} , i.e. the solution approaches the equilibrium over time according to the single time relaxation parameter w.

The equilibrium distribution function hereby is the key element of the collision step where the main physics of the problem is included. The solution strategy in the LBM stays largely the same even for different physical problems, like e.g. fluid motion governed by the Navier-Stokes equation, whereas mainly the equilibrium distribution function has to be replaced. The equilibrium distribution function is here applied only in first order accuracy as provided in a general formulation by Ginzburg et al. (2004). It is outlined in the next section in detail.

2.5.3.3 Update of macroscopic variables

Using the relationships given above and the empirical constitutive model, the discrete Boltzmann equation is solved in each direction q by applying the propagation and collision steps mentioned above. The macroscopic variables of interest can finally be derived from the computed distribution functions f_q at the new time level.

The effective water saturation θ is simply obtained by summing up the distribution functions of all directions of a cell, which corresponds to an integration of f over phase-space. Afterwards, the pore-water pressure head h can be derived using the water retention curve. According to Ginzburg et al. (2004) one obtains:

$$\theta = \sum_{q=0}^{n} f_q$$

$h = f(\theta)$

$$\overrightarrow{v}_f = (\theta_s - \theta_r) \cdot \left[\sum_{q=0}^{n} \overrightarrow{c} f_q^{eq} + \begin{pmatrix} c_{x0} & \cdots & c_{xn} \\ c_{y0} & \cdots & c_{yn} \end{pmatrix} \cdot \begin{pmatrix} f_0^{eq} - f_0 \\ \vdots \\ f_n^{eq} - f_n \end{pmatrix} \right] \tag{2.233}$$

2.5.4 Equilibrium functions

The equilibrium distribution function for the θ formulation is given in first order accuracy in all mesh directions by

$$f_q^{eq} = \begin{cases} \left(1.0 - \frac{7}{3}c_s^2\right) \cdot \theta & q = 0 \\ t_q \theta c_s^2 & q = 1,2,3,4 \\ t_q \cdot (\theta c_s^2 + \overrightarrow{I} \cdot \overrightarrow{c}) & q = 5,7,8,9,10 \\ t_q \cdot (\theta c_s^2 - \overrightarrow{I} \cdot \overrightarrow{c}) & q = 6,11,12,13,14 \end{cases} \tag{2.234}$$

where $c_s^2 = c/\vartheta$ with ϑ being a free constant. The method is local because the equilibrium function needs no information from neighbouring cells.

Accordingly, the equilibrium distribution function for the mixed $\theta - h$ formulation is obtained in all mesh directions as

$$f_q^{eq} = \begin{cases} \theta - 7/3c_s^2 \cdot h & q = 0 \\ t_q \cdot (hc_s^2) & q = 1,2,3,4 \\ t_q \cdot (hc_s^2 + \overrightarrow{I} \cdot \overrightarrow{c}) & q = 5,7,8,9,10 \\ t_q \cdot (hc_s^2 - \overrightarrow{I} \cdot \overrightarrow{c}) & q = 6,11,12,13,14 \end{cases} \tag{2.235}$$

In contrast to the θ formulation, the mixed $\theta - h$ formulation is able to reproduce the continuous transition of the pressure head at the interface of different soils correctly. Therefore, the mixed $\theta - h$ formulation should be applied in cases of heterogeneous embankments with core and filter zones. The θ formulation, however, has advantageous stability conditions for imbibition problems (Ginzburg, 2006) and as such is recommended for use in case of homogeneous embankments. The weighting factors t_q for the lattice directions q can be derived for the chosen lattice configuration. The values for the 3DQ15 model are:

q	t_q (D3Q15)
1-6	1/3
7-14	1/24

To calculate the equilibrium functions given above, the advective, gravitational term $\overrightarrow{I}$, which acts in vertical downward direction, is needed and is evaluated as

$$\overrightarrow{I} = -k_r(\theta) k_s \overrightarrow{e}_z \tag{2.236}$$

2.5.5 Boundary and initial conditions

At the mesh boundaries the values of the distribution function f_q in the incoming directions are unknown and must be provided.

- For solid walls standard bounce-back boundaries are used. The unknown incoming distribution functions f_q thereby are set equal to the outgoing, anti-symmetric values to simulate wall reflection. Using this type of boundary condition allows incorporating even complex boundaries.
- A water column above the embankment is modelled using a pressure boundary, thereby presuming a hydrostatic pressure distribution. Equilibrium conditions are

assumed at the boundary which allows for computing the values for the incoming directions ($f_q = f_q^{eq}$). For the mixed $\theta - h$ formulation, the water depth can be directly used as pore-water pressure head. For the θ formulation, the water saturation θ is needed instead and can be derived from the inverse water retention curve $\theta = f(h)$.

- The seepage flow out of the embankment is modelled with a combined approach. In the saturated zone ($q \geq 1.0$) a constant saturation of 1.0 is set at the boundary cells. In the unsaturated zone ($q < 1.0$) a bounce-back boundary is set.

The exact treatment of sloped or curved boundaries may become difficult, especially in 3D. Here, for simplicity, the sloped embankment faces are approximated using a series of steps using reflection angles of 0°, 45° or 90°. These simplifications can reduce the numerical accuracy in the vicinity of the embankment faces.

As initial conditions, the pore pressures or saturations in the domain can be given. The initial distribution functions are then set equal to the corresponding equilibrium values ($f_q = f_q^{eq}$) assuming equilibrium conditions.

3

References

Agoshkov, V.I., Quarteroni, A... and Saleri, F. (1994). Recent Developments in the Numerical-Simulation of Shallow-Water Equations. 1. Boundary-Conditions. *Applied Numerical Mathematics [Peer Reviewed Journal]*, 15(2): 175–200.

Ashida, K. and Michiue, M. (1971). An investigation over river bed degradation downstream of a dam. *Proceedings of the 14th congress of IAHR*, No. 3: 247–256. Paris, France.

Badrot-Nico, F., Brissaud, F. and Guinot, V. (2007). A finite volume upwind scheme for the solution of the linear advection-diffusion equation with sharp gradients in multiple dimensions. *Advances in Water Resources*, 30: 2002–2025.

Bechteler, W., Nujić, M. and Otto, A. (1993). Program Package "FLOODSIM" and its Application. *Proceedings of the international conference on hydroscience & engineering*, No. 1: 762–767. Washington DC, USA.

Beffa, C.J. (1994). Praktische Lösung der tiefengemittelten Flachwassergleichungen. *VAW-Mitteilung* 133, Versuchsanstalt für Wasserbau, Hydrologie und Glaziologie (VAW), ETH Zürich.

Begnudelli, L. and Sanders, B. (2006). Unstructured Grid Finite-Volume Algorithm or Shallow-Water Flow and Scalar Transport with Wetting and Drying. *Journal of Hydraulic Engineering*, 132(4): 371–384.

Belleudy, P. (2000). Modelling of deposition of sediment mixtures, part 1: analysis of a flume experiment. *Journal of Hydraulic Research, IAHR*, 38(6).

Bennett, J. and Nordin, C. (1977). Simulation of Sediment Transport and Armouring. (XXII, Ed.) *Hydrological Sciences Bulletin*, 22(4): 555–569.

Bertoldi, W., Siviglia, A., Tettamanti, S., Toffolon, M., Vetsch, D. and Francalanci, S. (2014). Modeling vegetation controls on fluvial morphological trajectories. *Geophysical Research Letters*, 41(20): 7167–7175.

Bezzola, G.R. (2002). Fliesswiederstand und Sohlenstabilität natürlicher Gerinne [PhD thesis]: Eidgenössische Technische Hochschule Zürich.

Bhatnagar, P., Gross, E. and Krook, M. (1954). A Model for Collision Processes in Gases. I. Small Amplitude Processes in Charged and Neutral One-Component Systems. *Physical review*, 94(3): 511–525.

Blanckaert, K. (2011). Hydrodynamic processes in sharp meander bends and their morphological implications. *Journal of Geophysical Research: Earth Surface*, 116(F1): F01003.

Bollrich, G. (2000). Technische Hydromechanik 1. *Beuth Verlag GmbH*, Berlin.

Borah, D.K., Alonso, C.V. and Prasad, S.N. (1982). Routing Graded Sediments in Streams - Formulations. *Journal of the Hydraulics Division-Asce*, 108: 1486–503.

Brooks, R.H. and Corey, A.T. (1964). Hydraulic Properties of Porous Media. *Hydrology papers* 3, Colorado State University; Colorado State University.

Brufau, P., Garcia-Navarro, P., Playán, E. and Zapata, N. (2002). Numerical Modeling of Basin Irrigation with an Upwind Scheme. *Journal of Irrigation and Drainage Engineering*, 128(4): 212–223.

Cao, Y., Williams, D. and Larsen, D.P. (2002). Comparison of Ecological Communities: The Problem of Sample Representativeness. *Ecological Monographs*, 72(1): 41–56.

Chanson, H. (1999). The Hydraulics of Open Channel Flow: An Introduction. *Edward Arnold*, London, UK.

Chaudhry, M.H. (1993). Open-Channel Flow. *Prentice Hall*, Englewood Cliffs, New Jersey.

Chen, Y. and Falconer, R.A. (1992). Advection-diffusion modelling using the modified QUICK scheme. *International Journal for Numerical Methods in Fluids*, 15: 1171–1196.

Chen, X., Ma, J. and Dey, S. (2010). Sediment transport on arbitrary slopes: Simplified model. *Journal of Hydraulic Engineering-ASCE*, 136(5): 311–317.

Cunge, J.A., Holly, F.M. and Verwey, A. (1980). Practical aspects of computational river hydraulics. *Pitman Advanced Pub*, Boston.

de Vries, M. (1966). Application of luminophores in sandtransport-studies. Meinema, TU Delft.

Delis, A., Skeels, C. and Ryrie, S. (2000). Evaluation of Some Approximate Riemann Solvers for transient Open Channel Flows. *Journal of Hydraulic Research.*, 38(3): 217–231.

Engelund, F. (1974). Flow and bed topography in channel bends. *Journal of the Hydraulics Division ASCE*, 100(11): 1631–1648.

Engelund, F. and Hansen, E. (1972). A monograph on sediment transport in alluvial streams. *Teknisk Forlag, Copenhagen*,

Faeh, R. (2007). Numerical Modeling of Breach Erosion of River Embankments. *Journal of Hydraulic Engineering*, 133(9): 1000–1009.

Fäh, R. (1997). Numerische Simulation der Strömung in offenen Gerinnen mit beweglicher Sohle. *VAW-Mitteilung* 153, Versuchsanstalt für Wasserbau, Hydrologie und Glaziologie(VAW), ETH Zürich.

Garcia-Navarro, P. and Vazquez-Cendon, M. (2000). On numerical treatment of the source terms in the shallow water equations. *Computers & Fluids*, 29(8): 951–979.

Ginzburg, I. (2006). Variably saturated flow described with the anisotropic Lattice Boltzmann methods. *Computers & Fluids*, 35: 831–848.

Ginzburg, I., Carlier, J. and Kao, C. (2004). Lattice Boltzmann approach to Richard's equation. *Proceedings of the CMWR XV, CT Miller*, 583–597. Chapel Hill, NC, USA.

Glaister, P. (1988). Approximate Riemann solutions of the shallow water equations. *Journal of Hydraulic Research*, 26: 293–306.

Godunov, S.K. (1959). A difference method for numerical calculation of discontinuous solutions of the equations of hydrodynamics. *Matematicheskii Sbornik*, 89(3): 271–306.

Harten, A., Lax, P. and van Leer, B. (1983). On Upstream Differencing and Godunov-Type Schemes for Hyperbolic Conservation Laws. *Siam Review*, 25(1): 35–61.

Hinton, E. and Owen, D.R.J. (1979). An introduction to finite element computations. *Pineridge Press Ltd*, Swansea, UK.

Holly, F.M. and Preissmann, A. (1977). Accurate calculation of transport in two dimensions. *Journal of Hydraulic Div. Am. Soc. Civ. Engineering*, 103(11): 1259–1277.

Hunziker, R.P. (1995). Fraktionsweiser Geschiebetransport [PhD thesis]: Eidgenössische Technische Hochschule Zürich.

Hunziker, R.P. and Jaeggi, M.N.R. (2002). Grain sorting processes. *Journal of Hydraulic Engineering-Asce*, 128(12): 1060–1068.

Ikeda, S. (1982). Lateral Bed-Load Transport on Side Slopes. *Journal of the Hydraulics Division-Asce*, 108(11): 1369–1373.

Jäggi, M. (1995). Vorlesung: Flussbau. ETH Abt. II, VIII, und XC. ETH Zürich.

Kassem, A.A. and Chaudhry, M.H. (1998). Comparison of Coupled and Semicoupled Numerical Models for Alluvial Channels. *Journal of Hydraulic Engineering-Asce*, 124(8): 794–802.

Knapp, F. (1960). Ausfluss, Überfall und Durchfluss im Wasserbau. *Verlag G. Braun*, Karlsruhe.

Komaei, S. and Bechteler, W. (2004). An improved, robust implicit solution for the two-dimensional shallow water equations on unstructured grids. *Proc., 2nd Int. Conf. on Fluvial Hydraulics*, Greco, M. ed., No. 2: 1065–1072. Balkema, Rotterdam, The Netherlands.

Lam, L., Fredlund, D.G. and Barbour, S.L. (1987). Transient seepage model for saturated-unsaturated soil systems: a geotechnical engineering approach. *Canadian Geotechnical Journal*, 24: 565–580.

Leonard, B.P. (1979). A Stable and Accurate Conservative Modelling Procedure Based on Quadratic Upstream Interpolation. *Comput. Methods Appl. Mech. Eng.*, 19(1): 59–98.

Li, S. and Millar, R. (2011). A two-dimensional morphodynamic model of gravel-bed river with floodplain vegetation. *Earth Surface Processes and Landforms*, 36(2): 190–202.

Lin, B. (1984). Current Study of Unsteady Transport of Sediment in China. *Proceedings of Japan-China Bilateral Seminar on River Hydraulics and Engineering Experiences*, *Proceedings of Japan-China Bilateral Seminar on River Hydraulics; Engineering Experiences, Tokyo-Kyoto –Sapporo.*, Tokyo-Kyoto-Sapporo.

Lu, G.Y. and Wong, D.W. (2008). An adaptive inverse-distance weighting spatial interpolation technique. *Computers & geosciences*, 34(9): 1044–1055.

Malcherek, A. (2001). Sedimenttransport und Morphodynamik. Vorlesungsskript der Universität der Bundeswehr München, München.

Marti, C. (2006). Morphologie von verzweigten Gerinnen: Ansätze zur Abfluss-, Geschiebetransport und Kolktiefenberechnung [PhD thesis]: ETH Zürich, Versuchsanstalt für Wasserbau, Hydrologie und Glaziologie -VAW-.

Meyer-Peter, E. and Müller, R. (1948). Formulas for Bed-Load Transport, 2nd Meeting IAHR, Stockholm, Sweden.

Minh Duc, B. (1998). Berechnung der Strömung und des Sedimenttransports in Flüssen mit einem tiefengemittelten numerischen Verfahren [PhD thesis]: Karlsruhe University, Germany.

Mohamad, A.A. (2011). Lattice Boltzmann Method – Fundamentals and Engineering Applications with Computer codes. *Springer-Verlag*, London.

Mohamadian, A., Le Roux, D.Y., Tajrishi, M. and Mazaheri, K. (2005). A mass conservative scheme for simulating shallow flows over variable topographies using unstructured grid. *Advances in Water Resources*, 28(5): 523–539.

Mualem, Y. (1976). A New Model for Predicting the Hydraulic Conductivity of Unsaturated Porous Media. *Water Resources Research*, 12(3): 513–552.

Nujić, M. (1998). Praktischer Einsatz eines hochgenauen Verfahrens für die Berechnung von tiefengemittelten Strömungen. Institut für Wasserwesen. Universität der Bundeswehr München. Institut für Wasserwesen. Universität der Bundeswehr München.

Osher, S. and Solomon, F. (1982). Upwind Difference-Schemes for Hyperbolic Systems of Conservation-Laws. *Mathematics of Computation*, 38: 339–374.

Parker, A.J., G.; Sutherland (1990). Fluvial armor. *Journal of Hydraulic Reasearch*,

Parker, G. (1990). Surface-based bedload transport relation for gravel rivers. *Journal of Hydraulic Reasearch*, 28(4): 417–436.

Parker, G. (2008). Transport of Gravel and Sediment Mixtures. *Sedimentation engineering: Processes, measurements, modeling and practice*, No. 110: 165–252. *ASCE*, Virginia.

Parker, G., Klingeman, P.C. and McLean, D.G. (1982). Bedload and Size Distribution in Paved Gravel-Bed Streams. *Journal of Hydraulic Division, ASCE*, 108(4): 544–571.

Rickenmann, D. (1990). Bedload transport capacity of slurry flows at steep slopes [PhD thesis]: Versuchsanstalt für Wasserbau, Hydrologie und Glaziologie (VAW), ETH Zürich.

Rickenmann, D. (1991). Hyperconcentrated Flow and Sediment Transport at Steep Slopes. *Journal of Hydraulic Engineering*, 117(11): 1419–1439.

Roe, P.L. (1981). Approximate Riemann Solvers, Parameter Vectors and Difference Schemes. *Journal of computational physics*, 43: 357–372.

Rozovskii, I.L. (1957). Flow of Water in Bends of Open Channels. *Academy of Science of the Ukrainian S.S.R, Institute of Hydrology; Hydraulic Engineering*,

Shields, A. (1936). Anwendungen der Ähnlichkeitsmechanik und der Turbulenzforschung auf die Geschiebebewegungen. Mitteilung der Preussischen Versuchsanstalt für Wasserbau und Schiffbau. Berlin, Deutschland.

Smart, G. and Jaeggi, M. (1983). Sediment Transport on Steep Slopes. *VAW-Mitteilung* 64, Versuchsanstalt für Wasserbau,Hydrologie und Glaziologie (VAW). Zürich, ETH Zürich.

Soares-Frazão, S., Le Grelle, N., Spinewine, B. and Zech, Y. (2007). Dam-break induced morphological changes in a channel with uniform sediments: measurements by a laser-sheet imaging technique. *Journal of Hydraulic Research*, 45: 87–95.

Sternberg, H. (1875). Untersuchungen über Längen- und Querprofil geschiebeführender Flüsse. (p. 4.-5. Zeitschrift für Bauwesen 25, Ed.) *Zeitschrift für Bauwesen, Wien*, 25: 483–506.

Sun, Z. and Donahue, J. (2000). Statistically Derived Bedload Formula for any Fraction of Nonuniform Sediment. *Journal of Hydraulic Engineering-Asce*, 126(2): 105–111.

Swartenbroekx, C., Soares-Frazão, S., Staquet, R. and Zech, Y. (2010). Two-dimensional operator for bank failures induced by water-level rise in dam-break flows. *Journal of Hydraulic Research*, 48(3): 302–314.

Talmon, A., Struiksma, N. and van Mierlo, M. (1995). Laboratory measurements of the direction of sediment transport on transverse alluvial-bed slopes. *Journal of Hydraulic Research*, 33(4): 495–517.

Toro, S., E. F. (1994). Restoration of the contact surface in the HLL-Riemann solver. *Shock Waves*, 4: 25–34.

Toro, E.F. (1997). Riemann Solvers and Numerical Methods for Fluid Dynamics. *Springer-Verlag*, Berlin.

Toro, E.F. (2001). Shock-Capturing Methods for Free-Surface Shallow Flows. *John Wiley*, Chichester, New York.

Valiani, A., Caleffi, V. and Zanni, A. (2002). Case Study: Malpasset Dam-Break Simulation using a Two-Dimensional Finite Volume Method. *Journal of Hydraulic Engineering*, 128(5): 460–472.

van Genuchten, M.T. (1980). A Closed-form Equation for Predicting the Hydraulic Conductivity of Unsaturated Soils. *Soil Science Society of America Journal*, 44(5): 892–898.

van Leer, B. (1982). Flux-Vector Splitting for the Euler Equations. *In Proceedings of the 8th International Conference on Numerical Methods in Fluid Dynamics*, No. 170: 507–512.

van Rijn, L.C. (1989). Handbook Sediment Transport by Current and Waves. *Delft Hydraulics Laboratory*, Delft, The Netherlands.

van Rijn, L.C. (1984a). Sediment Transport, Part I: Bed Load Transport. *Journal of Hydraulic Engineering, ASCE*, 110(10): 1431–1456.

van Rijn, L.C. (1984b). Sediment Transport, Part II: Suspended Load Transport. *Journal of Hydraulic Engineering, ASCE*, 110(11): 1613–1641.

Voigt, H. (1971). Abflussberechnung gleichzeitig über- und unterströmter Stauelemente. *Dissertation* TU Dresden.

Westrich, B. and Juraschek, M. (1985). Flow transport capacity for suspended sediment. *XXIth IAHR Congress*, No. 3: 590–594. Melbourne, Australia.

Wilcock, P.T.C.J.C. (2003). Surface-based transport model for mixed-size sediment. *Journal of Hydraulic Engineering*,

Wong, M. and Parker, G. (2006). Reanalysis and correction of bed-load relation of meyer-peter and mã¼ller using their own database. *Journal of Hydraulic Engineering*, 132(11): 1159–1168.

Wu, W. (2007). Computational River Dynamics. *Taylor & Francis Ltd*, London, UK.

Wu, W., Wang, S.S.Y. and Jia, Y. (2000). Non-Uniform Sediment Transport in Alluvial Rivers. *Journal of Hydraulic Research*, 38(6): 427–434.

Xu, Y. (1998). Numerical Modeling of Suspended Sediment Transport in Rivers [PhD thesis]: Mitteilung 98, Institut für Wasserbau, Universität Stuttgart.

Yalin, M. and Silva, A. da (2001). Fluvial processes. *International Association of Hydraulic Engineering; Research (IAHR), Delft, The Netherlands*,

Zen, S., Zolezzi, G., Toffolon, M. and Gurnell, A.M. (2016). Biomorphodynamic modelling of inner bank advance in migrating meander bends. *Advances in water resources*, 93: 166–181.

Zhang, R. (1961). River Dynamics. *Industry Press*, Beijing, China.

Zyserman, J. and Fredsøe, J. (1994). Data Analysis of Bed Concentration of Suspended Sediment. *Journal of Hydraulic Engineering, ASCE*, 120(9): 1021–1042.